Study of serial markers of biological response in rectal cancer patients receiving preoperative chemoradiotherapy with or without biological agents

Aftab Alam Khan

University College London

Doctor of Medicine (Research)

DECLARATION

I, **Aftab Alam Khan**, confirm that the work presented in this thesis is my own. Where information has been derived from other sources, I confirm that this has been indicated in the thesis.'

DEDICATION

I would like to dedicate the work presented in this thesis to my dear mother, Mrs Shahwar Alam Khan (Ammi), who dedicated her life to us. She has been a life-long source of inspiration and motivation. Thank you Ammi for your prayers and endless support that made completion of this work possible.

I would like to express a very special thanks to Dr. Glynne-Jones, Prof. Vicky Goh and Prof. John Hartley for their kind words, support and advice throughout the project and critical appraisal of the manuscript.

ABSTRACT

The key to understanding the heterogeneous behaviour of similar stage locally advance rectal cancer lies in the understanding of tumour biology. The aim of this project was to investigate the biological behaviour of rectal cancers and its alterations in response to neoadjuvant chemoradiotherapy, by studying the intrinsic radiosensitivity, pathophysiology and angiogenesis of rectal cancers. It was intended to provide information that may help risk-stratify patients for individualised treatments including optimal timing of surgery after chemoradiotherapy.

Consecutive patients with locally advanced, non-metastatic rectal cancer, who were considered suitable for long-course neoadjuvant chemoradiotherapy, were prospectively recruited. Radiosensitivity was studied by investigating the timing of DNA repair analysis with single cell gel electrophoresis (comet assay). The tumour pathophysiology and angiogenesis was investigated in vivo by novel functional imaging techniques (multiparametric magnetic resonance imaging and dynamic contrast enhanced computed tomography).

It is demonstrated that rectal cancer tissue consists of cells with heterogeneous radiosensitivities and functional microvascularity. Until six weeks after NCRT, the DNA repair remains inhibited with progressive devascularisation and increasing hypoxic blood volume resulting in loss of tumour cells. Thereafter, variable fractions of cancer cell may continue to perish or survive with corresponding changes in vascularity. Therefore, the period between the sixth and eleventh weeks after neoadjuvant therapy is a critical time when surviving cells from rectal cancers may develop aggressive traits with long-term consequences. Hence, biological assessment of locally advance rectal cancers

after six weeks post-NCRT may help risk-stratify patients for individualised therapy.

CONTENTS

CONTENTS

CONTENTS

CONTENTS

CONTENTS

CONTENTS

CONTENTS

CONTENTS

LIST OF TABLES

LIST OF TABLES

LIST OF TABLES

LIST OF TABLES

LIST OF FIGURES

LIST OF FIGURES

LIST OF FIGURES

GLOSSARY

AC	Adenocarcinoma
ADC	Apparent diffusion coefficient
AIF	Arterial input function
bCV	Between-subject coefficient of variation
BER	Base excision repair
BF	Blood flow
BOLD	Blood oxygen level dependent
BV	Blood volume
bVAR	Between-subject variance component
CI	Confidence interval
CI Cohort	95% Confidence interval of dSD of a group
CRM	Circumferential resection margin
CRT	Chemoradiotherapy
CT	Computed tomography
DCE	Dynamic contrast enhance
DDR	DNA damage response
DFS	Disease free survival
DIS	Distal intramural spread
DM	Distant metastasis
DNA	Deoxyribonucleic acid
DSB	Double strand breaks
dSD	Mean squared difference
DW	Diffusion weighted
EAUS	Endoanal ultrasound
ECVAG	The European comet assay validation group
EGFR	Epidermal growth factor receptor
ELAPE	Extralevator abdominoperineal excision (of rectum)
EMVI	Extramural venous invasion
F	Variance ratio
Gd-DTPA	Gadolinium with diethylenetriaminepentacetate
Gy	Gray (unit of irradiation)
HR	Hazard ratio
HRc	Homologous recombination
$IAUGC_{60}$	Initial area under the gadolinium curve
ICC	Interc-class correlation coefficient
ISW	Intrinsic susceptibility weighted
k_{ep}	Rate constant
K^{trans}	Volume transfer contant or Extraction fraction

GLOSSARY

LARC	Locally advance rectal cancer
LoA	Bland-Altman limits of agreement
LR	Local recurrence
MC	Mucinous carcinoma
MDCT	Multidetector computed tomography
MMR	Mismatch repair
MPG	Motion probing gradients
MR	Magnetic resonance
MRI	Magnetic resonance Imaging
MVD	Microvascular density
NCRT	Neoadjuvant chemoradiotherapy
NER	Nucleotide excision repair
NHEJ	Non-homologous end joining
OR	Odds ratio
pCR	Pathological complete response
PET	Positron emission tomography
PNI	Perineural invasion
PS	Permeability surface area
r	Repeatability coefficient
R_2*	Transverse relaxation rate
RECIST	Response evaluation criteria in solid tumours
RNA	Ribonucleic acid
ROI	Region of interest
SCPRT	Short-course pre-operative radiotherapy
SD	Standard deviation
SE	Standard error
SF*X*	Surviving fraction (*X* –denotes number)
sm	submucosal (classification of carcinoma)
SSB	Single strand breaks
TGF	Tumour growth factor
TM	Tail moment
TME	Total mesorectal excision
TNM	Tumour, Node, Metastasis classification
TRG	Tumour regression grade
UICC	Union for international cancer control
VDA	Vascular disruptive agents
v_e	Interstitial volume fraction per volume of tissue
VEGF	Vascular endothelial growth factor
VEGFR	Vascular endothelial growth factor receptor

GLOSSARY

VOI	Volume of interest
wCV	Within-subject coefficient of variation
wSD	Within-subject stadard deviation
wVAR	Within-subject variance component
ymr	Post neoadjuvant chemoradiotherapy magnetic resonance imaging staging
yp	Post neoadjuvant chemoradiotherapy pathological staging

1 CHAPTER 1: INTRODUCTION

Colorectal cancers are the third most common cancer in the United Kingdom. About one-third occur in the rectum and anus (36%) [1]. The risk of bowel cancer increases with age with a peak incidence of rectal cancer at 65 years of age and over. Men are more commonly affected (60%). The majority are classified as adenocarcinoma (AC) but mucinous carcinoma (MC) is a distinct form of CRC, which occurs in 10-15% of patients. It differs from AC in both clinical and histopathological appearance and is associated with a poorer response to therapies.

Locally advanced rectal cancer (LARC) has significant risks for both local recurrence and distant metastases. The evidence-based management of LARC involves fluoropyrimidine-based neoadjuvant chemoradiotherapy (NCRT) followed by total mesorectal excision (TME) of the residual tumour [2] after an interval of 6-12 weeks. NCRT has an accepted role in reducing the risk of local recurrence in LARC, particularly when the circumferential resection margin (CRM) is breached or threatened, according to magnetic resonance imaging (MRI). NCRT can obtain a significant downsizing response and a curative resection can then be achieved in >80% of cases. NCRT may also facilitate sphincter sparing [3]. However, despite advances in imaging, staging, surgical technique, chemotherapy and radiotherapy, population studies show there has been only a small improvement in overall survival, treatment related morbidity and quality of life (see Figure 1.1).

CHAPTER 1: INTRODUCTION

Figure 1.1: Bowel Cancer, age-standardised one-year net survival, Adult (Aged 15-99), England and Wales, 1971-2011

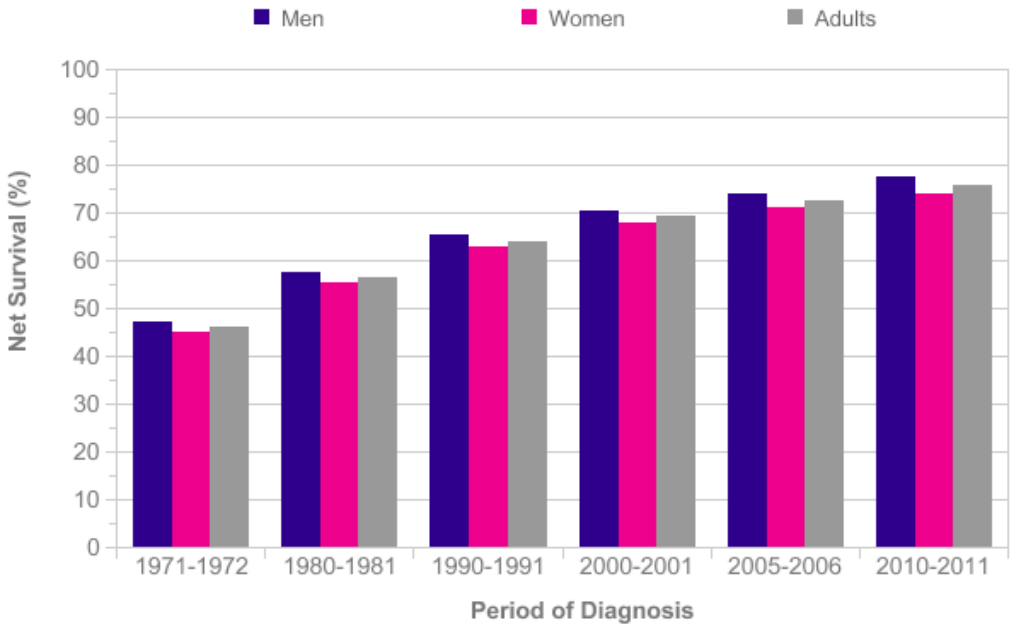

1.1 Exclusive clinical behaviour of rectal cancers

The unique clinical course of rectal cancer disease observed is a cumulative effect of innate tumour biology and management strategy [4]. There is a high incidence of lymph node and/or distant metastasis at the time of diagnosis of rectal cancer [5]. The tumour biology depends on tumour location, histopathology and molecular profiles.

1.1.1 Tumour location versus biological behaviour

The UK Royal College of Pathologist [6] classify rectal cancer as (Figure 1.2):

(i) Entirely above the level of peritoneal reflection anteriorly

(ii) Astride (or at) the level of peritoneal reflection anteriorly

(iii) Entirely below the level of peritoneal reflection anteriorly

Lopez-Kostner et al [7] showed differential long-term prognosis according to the location of tumour within the rectum: for sigmoid (>15cm; n=225), upper rectum (10-15 cm; n=229) and lower rectum (<10 cm; n = 437), the five-year local recurrence rates were 2.0%, 2.8% and 8.6%; the five-year local and distance recurrence rate were 3.9%, 4.7% and 12.9%; the five-year cancer related mortality were 13.5%, 12.7% and 25.6%, respectively. Tumours below the peritoneal reflection have the highest local recurrence rates [8].

Figure 1.2: Diagrammatic illustration of rectal tumours in relation to peritoneal reflection [6]).

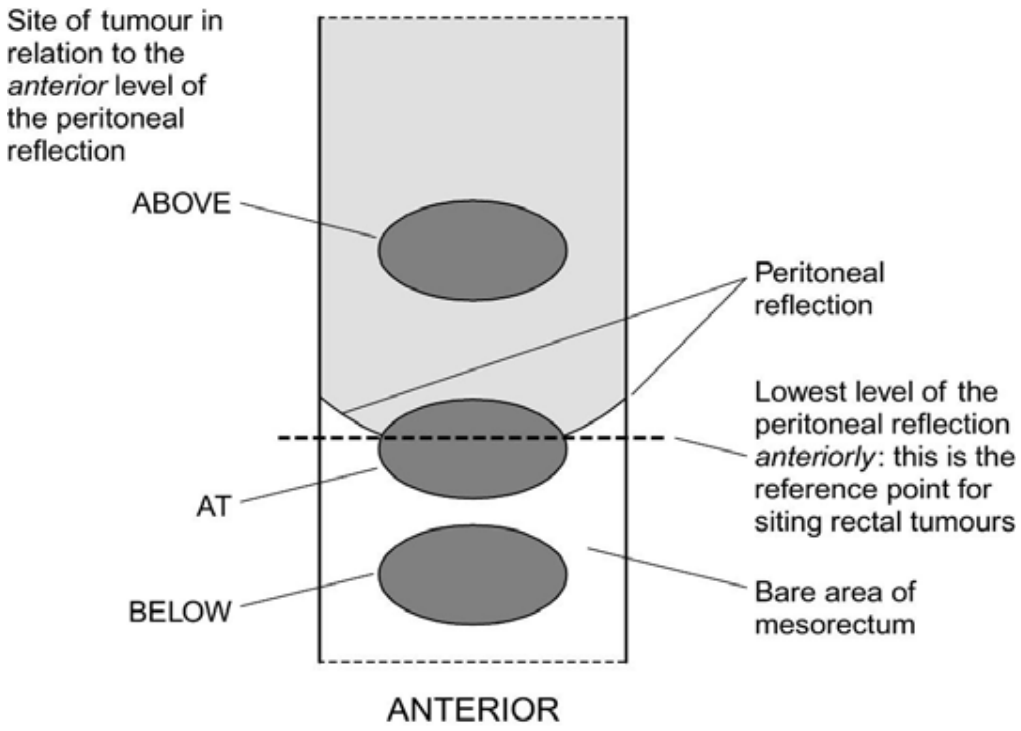

Tumour location within the rectum directly affects the pattern of tumour spread. The three recognised means of disease progression include:

(i) Contiguous spread

(ii) Lymphatic spread

(iii) Haematogenous spread

1.1.1.1 Contiguous Spread

The lower part of rectum lies in a funnel shaped extra-peritoneal cavity where its muscularis propria is in direct contact with the surrounding lymph node embedded in a cushion of fatty tissue called ‘mesorectum’. Hwang et al [8] and others [9, 10] reported that rectal tumours located in the non-peritonealised part of rectum (up to 5 cm from anal verge) were an independent risk factor for recurrence-poor-survival. Posterior and lateral low rectal cancers that penetrate the rectal wall directly invade the mesorectum and may produce micrometastases in the mesorectum. Anteriorly, any extension of tumour results in penetration into either prostate and/or bladder in males or the vagina in females and such tumours are also technically challenging for surgical excision. Thus the majority of local recurrences may arise from contiguous spread [11] and occur either at the base of bladder, prostrate, vagina or sacrum [12].

1.1.1.2 Lymphatic spread

The initial spread is principally through mesenteric drainage to perirectal nodes within the mesorectum. The majority of the perirectal lymph nodes reside in the proximal two-thirds of the posterior mesorectum [13]. The subsequent spread is preferentially alongside superior haemorrhoidal vessels towards the base of inferior mesenteric artery. About 10-15% of locally advanced low rectal cancer spread to iliac and obturator lymph nodes (middle

and inferior haemorrhoidal arteries) [14]. Subsequently, proximal spread occur alongside iliac vessels and para-aortic lymph nodes [15].

1.1.1.3 Haematogenous spread

Distant metastasis is to liver by means of portal circulation common in upper rectal cancers (superior haemorrhoidal vein), whereas low rectal cancer have a higher incidence of pulmonary metastasis via systemic circulation (middle and inferior haemorrhoidal vein) [8, 16].

1.1.2 Histopathological features versus biological behaviour

1.1.2.1 Staging of rectal cancer

The stage of the disease is an effective prognostic indicator. There are two histopathological staging systems include (see appendix I, page 372):

(i) Dukes Classification

(ii) Tumour, Node, Metastases (TNM) classification and staging

The Dukes' staging system is based on the depth of mural invasion and lymph node involvement of the tumour [17]. The TNM classification is based on anatomic disease extent and published by the Union for International Cancer Control (UICC) [18]. There are limitations in the accuracy of risk prediction by staging systems and rectal cancers at identical stages may show heterogeneous prognosis. There is a general tendency to over-stage nodes when using size criteria alone. Mixed signal intensity and irregular borders of the nodes are supporting features of involvement, but one third of involved rectal cancer nodes are often <5mm and many may not even be visualized.

There are features of rectal cancer disease with prognostic significance not incorporated into the aforementioned staging systems. For example, the important relationship of rectal tumour to mesorectal fascia that has been highlighted by Heald et al [19] and its significance in staging has been further established in several later studies [20].

1.1.2.2 Tumour histology type

The following histopathological features are established markers predicting biological behaviour:

- **Poorly differentiated adenocarcinomas** - are associated with reduced survival (independent of the disease stage) [21-25], lymph node metastasis [23, 26] and poor response to NCRT [27].
- **Mucinous tumours** - rectal adenocarcinoma is considered mucinous when >50% of the tumour volume consists of extracellular mucus, where malignant epithelium can be found in clumps or as single cells. The mucin produced by tumours is able to dissect through the gut wall and facilitate tumour extension [28].
- **Infiltrative border configuration** – is an independent risk factor of poor prognosis in several studies [29, 30]. A comprehensive analysis of 1420 colorectal cancer blocks (39.2% rectum) by Zlobec et al. [31], reported a significant drop in 5 year survival from 80% to 62.7% for patients with stage II disease how had ‘pushing border’ and ‘infiltrative growth pattern’, respectively.

- **Tumour budding** – is the presence of small cluster of undifferentiated tumour cells ahead of the invasive front of the lesion [32]. It corresponds to the initial phase of tumour invasion and represents a biological index of tumour aggressiveness confirmed in several studies showing increasing severity of tumour budding to be associated with nodal metastases and extramural vascular invasion, more aggressive malignant behaviour [33-35], early metastasis [36], poor local control and survival [37, 38]. In patients who receive NCRT, the morphology of post irradiation tumour budding depends on the histologic response to radiation. For radiation insensitive rectal tumours (moderate tumour regression grade - TRG 2 or 3), post irradiation budding intensity help stratify risk of recurrence and survival [39].

1.1.2.3 The depth of tumour invasion

Prior to the standard use of NCRT, Jass et al. [40] demonstrated that ≥5mm of invasion into perirectal fat significantly increases the local recurrence rate of rectal adenocarcinoma. Subsequent studies propose a depth of tumour invasion border greater that 4-6 mm beyond the muscularis propria to be associated with higher rates of local recurrence and diminished disease-free survival over five years [41-45].

About 10% of submucosal (pT1) rectal tumour spread to lymphatics. Within the pT1 group, tumour limited to superficial-third submucosa (sm1) show 2% lymph node involvement, tumours involving the middle-third submucosa (sm2) show 8% lymph node involvement and tumour involving the deepest-third

submucosa (sm3) show 23% lymph node involvement [46]. The simultaneous lymphatic spread is around 30% in tumours invading muscularis propria and increases to 50% in tumours invading out into peri-rectal tissue [40].

Rectal cancers classified under pT3 (cancers cells beyond muscularis propria), show wide prognostic heterogeneity and further subdivision according to the depth of mesorectal extension give more specific estimates of long-term prognosis [47]. Recent European Society of Medical Oncology consensus guidelines [48] recommend the penetration of the tumour into the mesorectal fat should be described in millimetres to define T3 subgroups. The T3 stage includes minimal invasion (0.5-1mm) beyond the muscularis propria i.e. T3a (which carries a prognosis almost as good as stage T2N0) ranging to gross invasion into the mesorectum or peritoneum >10mm [44]. Hence cancers at opposite ends of this T3 spectrum have completely different risks of lymph node involvement and hence different prognostic implications. Patients with pT3b compared to pT3c (extramural invasion <5 vs >5mm; see appendix I, page 372) had 5 year survival rates of 85% and 54%, respectively [44]. The prognostic difference between tumours with different depth of invasion remains even after NCRT - as shown by different outcomes for ypT3a (defined as 5 mm or less) and ypT3b staged tumours (defined as more than 5mm)in terms of local recurrence (7% vs 18%, p 0.04), distant metastasis (20% vs 41%; p 0.03), disease-free survival (73% vs 47%; p 0.01), overall survival (79% vs 74%; p 0.03) and cancer-related survival (81% vs 74%; p 0.007) over 5 years [49].

1.1.2.4 Circumferential Resection Margin and Distal Intramural Spread

The radial or circumferential resection margin (CRM) is the distance between the outer lateral aspect of the tumour and the fascia propria recti or mesorectal fascia (see Figure 1.3). So the distance between the edge of the surgical specimen that should lay on the mesorectal fascia and the closest tumour satellite is taken as the CRM and measured in millimetres. The CRM is considered involved if the tumour extends to within 1mm or less of the excision margin and historically was seen in 20% of resected specimen [50]. The modes of this involvement include direct spread, tumour satellite, lymph node spread and vascular spread. The CRM involvement increases rates of local recurrence [50] and is regarded as the most important indicator of local failure after surgery.

Figure 1.3: Circumferential resection margin [51]

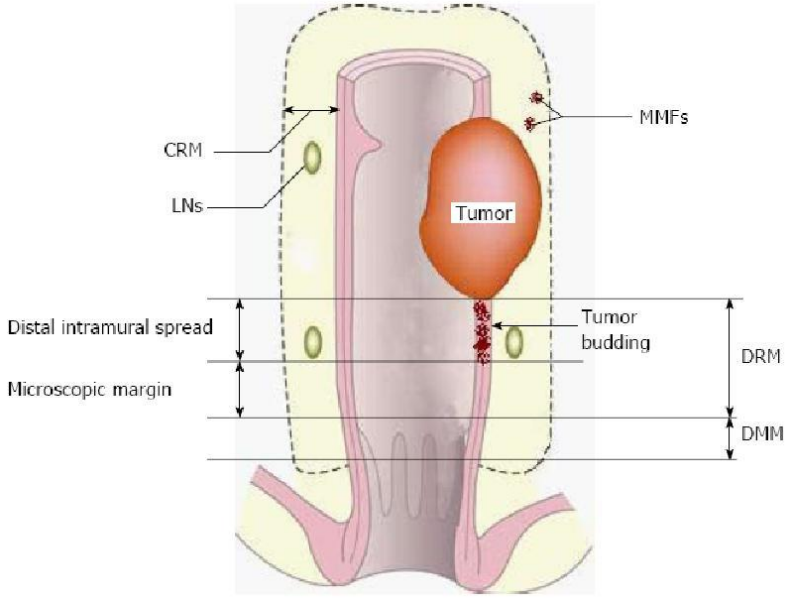

(*Circumferential resection margin; DRM: Distal resection margin. DMM: Distal mesorectal margin; LNs: Lymph nodes; MMF: Mesorectal microfoci*)

CHAPTER 1: INTRODUCTION

Wibe et al [52] from the Norwegian rectal cancer project showed an exponential increase in local recurrence, metastasis and death with a decreasing CRM. The risk factors for CRM involvement include lymph node positive tumour and abdominoperineal excision of rectum [53, 54]. The later may be explained by rectal anatomy: at the level of levator muscles the mesorectum tapers sharply; consequently the distance between the outer muscularis propria and the mesorectal fascia decreases, which increases the likelihood of tumour being in close proximity or breaching the distal TME plane[55]. Hence, presence of tumour at CRM may be an indicator of advance disease [56] or due to surgical failure to remove all tumour [57], and proven to be a powerful prognostic marker of rectal cancer recurrence, distant metastasis and survival [52, 58-62]. In a pooled analysis of 17,500 patients, Quirke et al [63] reported a significantly better predictive value of CRM for local recurrence in patients receiving NCRT than when no preoperative therapy was given (HR 6.3 vs 2.0, respectively, $p < 0.05$), distant metastasis (HR 2.8; 95% CI, 1.9 to 4.3) and survival (HR 1.7; 95% CI, 1.3 to 2.3). Analysis of CRM involvement in participants from a Dutch nationwide randomised multicentre trial [64], a trial comparing preoperative radiotherapy followed by surgical excision of rectal cancer against surgery alone, has shown that tumour that extend to within <2mm from CRM in non-irradiated patients increased risk of local recurrence to 16% compared to 5.8% with no CRM involvement [65]. Furthermore, in the patients with CRM ≤ 1mm, neither neoadjuvant nor adjuvant radiotherapy improve the local recurrence rates [66, 67].

The microscopic 'distal intramural spread (DIS)' of cancer cells has also shown to predict prognosis and a spread of >1 cm in patients not receiving NCRT is associated with decreased disease free survival (DFS) [68] and high incidence of local lymph node [69, 70] and distant metastasis [68, 71]. A later study investigating DIS in patients treated with NCRT, found that vast majority of their study sample had no DIS beyond 1 cm (sample size=20; DIS ≤1 cm=10; DIS >1cm = 1) and there was no significant effect of DIS on survival [72]. A study by Vernava et al [73] showed that even 1cm tumour free distal intramural margin is sufficient to prevent local recurrence, distant metastasis and prolong 5-year survival rates (Distal resection margin > 0.8 cm, n=219 Vs < 0.8 cm, n=20; LR 8.7 / 5.0 %, p >0.05, DM 14.2 / 10.0%, p> 0.05 and 5-year-survival 67.3 / 49.3%, p 0.01).

1.1.2.5 Lymphatic involvement

Lymphatic invasion is a strong predictor of lymph node metastases as recently shown in a meta-analysis analysis of 42 histopathological markers from 72 studies. Glasgow et al [23] have shown lymphatic invasion (OR 8.62) significantly outperformed tumour depth (T2 Vs T1; OR 2.62) and overall differentiation (OR 2.38) in predicting nodal spread in early cancers. The 'lymph node involvement' is present in 30-40% of patients with new diagnosis of rectal cancer [74] and proved to be a powerful prognostic marker of recurrence in several longitudinal studies involving retrospective multivariate analysis [75]. About 15-42% of patients with rectal cancer have small (<5mm) mesorectal lymph nodes that contain a tumour [76] . The incidence of small lymph node involvement increases by 10% in the lower mesorectum. The

increasing ‘quantity of lymph nodes’ involved correlate to worsening outcomes [77-80]. In patients treated with NCRT, the presence of lymph node metastasis in postoperative specimen confers poor survival [78, 81, 82]. The ‘total number of lymph node retrieved’ from postoperative specimen also plays a crucial role in forecasting prognosis [83, 84]. In patient achieving pCR after NCRT, residual nodal positivity may still exit [85], and therefore, the status of lymph node is the most relevant independent prognostic factor for distant metastasis and survival [86].

1.1.2.6 Extramural Vascular and Perineural Invasion

Extramural venous invasion (EMVI) is an independent marker of prognosis [87] and is present in 30-40% of specimens resected. Knudsen et al [88] demonstrated a proportional increase in extramural venous and perineural invasion with higher Duke’s stages. Multivariate analyses have shown strong links between EMVI and synchronous metastatic disease [89-92], local recurrence , disease free survival [93-95] and overall survival [88, 96]. In an analysis of 682 rectal cancer specimens, the likelihood of developing liver metastasis at the time of death was three times higher in cases with venous invasion than when no invasion was seen in surgically resected specimen[88]. The presence of EMVI is also a strong predictor of lymph node involvement in T1/T2 rectal cancer [97]. Perineural invasion (PNI) is present in 24 – 35 % of resected specimen and is shown to be a predictive marker of local recurrence [98, 99]. Both venous and neural invasion can predict significantly reduced actuarial survivals in patients with node-negative tumours [100].

The presence of PNI is also associated with decreased survival [88] even after curative management in rectal cancer disease (Stage I, II [101] and III [102, 103]).

1.1.2.7 Pathological Tumour Regression Grade

After NCRT, varying degree of fibrosis or fibro-inflammatory tissue may develop at the site of the tumour. This was first described in rectal cancers by Dworak [104], who proposed a pathological tumour regression grading system (TRG) based on the proportion of residual tumour left in fibrotic stroma after NCRT; the grading system ranges from no response to complete response (see table 1.1). A pathological complete response (pCR) is defined as no residual viable tumour cells within the specimen. A similar grading system was described for oesophageal cancer by Mandard et al.[105] previously and has been applied for rectal cancer response in some studies. TRG is observer dependent and poorly reproducible. Hence, TRG has failed to demonstrate any independent prognostic value in large randomised trials and should not be considered as a surrogate endpoint.

MRI based TRG has been examined in 3 separate datasets (Mercury, CORE, LOREC) and although it does not correlate very well with ultimate histology it does with response / down-staging and more importantly with outcome (see below, section 1.4.2).

Table 1.1: Pathological Tumour Regression Grading (pTRG)

Dworak	Mandard	Definition
0	TRG 5	No regression
1	TRG 4	Dominant tumour mass with obvious fibrosis and/or vasculopathy
2	TRG 3	Dominantly fibrotic changes with few tumour cells or groups (easy to find)
3	TGR 2	Very few (difficult to find microscopically) tumour cells in fibrotic tissue with or without mucous substance
4	TRG 1	No tumour cells, only fibrotic mass

1.1.3 Molecular profiles versus biological behaviour

The molecular markers can be broadly divided in to those that predict: (i) Response to neoadjuvant treatment and (ii) long-term survival. The details are presented in table 1.2.

Table 1.2: Molecular Markers shown to have prognostic significance in rectal cancer

Molecular Marker	Normal function	Prognostic importance
p53 gene and protein	Tumour suppressor gene that encodes for DNA-binding phosphoprotiens that eliminates DNA damaged cell from cell cycle	Abnormal p53 related with increased risk of death (RR 1.32; CI 1.23 –1.42) and high failure rates to radiotherapy (RR 1.49; CI 1.25-1.77) [106]; wild type p53 in rectal cancer patient was associated with 5-year survival benefit for those receiving Fluoropyrimidine based chemotherapy with or without radiotherapy [107]
p21 protein	The p21 is cyclin-dependent kinase inhibitor that is activated by wild-type p53 and its activation induces G1 arrest when cells are exposed to DNA damaging agents.	Some studies have shown p21 expression as a useful predictor of radiosensitivity and long-term prognosis [108-110], whereas, other have not shown any useful role [111-114].
Bcl–2 and Bax	Integral part in cell apoptosis in response to cytotoxic signal from chemo- and/or radiotherapy	Bcl-2 expression is associated with complete response rates [115], metastasis free survival [116] and overall survival [117]. High Bax expression is seen in responders [112, 118-120] and disease–free survivors [121], whereas, there are many studies where neither Bcl-2 nor Bax has shown any prognostic significance [111, 122-124].

Molecular Marker	Normal function	Prognostic importance
Ki-67 (Proliferation Index)	The Ki-67 and its epitope MIB-1, are nuclear protein found in proliferating cells except during G0 and early G1 phase	Proliferative index can potentially predict treatment sensitive tumour. Cancers with low proliferative index can be radioresistant [125]. Ki-67 expression predicts response to NRCT [126] [127]. However, earlier studies failed to show any relation between presence of Ki-67 in pre-treatment biopsy and response to treatment [128-131].
Cyclo-oxygenase 2 (COX-2)	Enzyme that catalyses the conversion of arachidonic acid to prostaglandins [132]	High level of COX-2 in pre-treatment biopsy respond poorly to neoadjuvant therapy as compared to those with normal COX-2 levels [111, 133-135] [136]. In multivariate analysis, COX-2 positivity was an independent predictor of distant-metastasis free survival, DFS and OS, and combination of COX-2 and VEGF positivity showed a strong correlation with decreased DFS (p=0.007) [137].
Survivin	Blocks apoptosis by inhibiting activation of Caspase-3 and Caspase-7 regulating cell cycle in G2/M phase	There is a potential role of survivin in predicting rectal tumour aggressiveness [138], lack of response to neoadjuvant treatment [139, 140] and long-term prognosis [141, 142]. Failure of survivin downregulation after NCRT is related with poor DFS and survival [141].

Molecular Marker	Normal function	Prognostic importance
Thymidylate synthase	Enzyme in folate metabolism that converts deoxyuridine monophosphate to deoxythymidine monophosphate providing the de novo sole source of thymidine required for DNA synthesis and repair during cell cycle and proliferation [143]	Fluorouracil (FU) works by primarily targeting TS enzyme initiating cell cycle arrest and cell death [144]. Hence, the polymorphism of TS gene may indicate sensitivity of rectal tumour cells to fluoropyrimidines [145]. However, studies investigating LARC treated with neoadjuvant 5-FU have shown conflicting results; both low [146, 147] and high [113, 126, 148, 149] TS expression have shown higher response rate in separate settings. Similar contradictory report exist on the level of TS expression in pre-treatment biopsies and long-term prognosis; whilst some studies have shown early disease recurrence and shortened survival in patients with high TS levels [150], others have shown similar unfavourable effects with low TS expression in pre-treatment rectal cancer tissue [151].
RAS Proto-oncogenes (KRAS, NRAS and HRAS)	Control signalling pathway that are key regulators of several aspects of normal cell growth [152]	NRAS mutation occurs in less than 5% of colorectal cancers and is associated with rectal tumours and distant metastasis. HRAS mutation has been observed in bladder and oesophageal cancers. A recent retrospective review of 1519 cases did not show any association between NRAS or HRAS and clinicopathological features of colorectal cancers [152].

Molecular Marker	Normal function	Prognostic importance
KRAS	Involved in growth transduction and cellular differentiation by activating protein kinase receptors [153]	KRAS mutation provides an effective indicator of tumour sensitivity to anti-EGFR chemotherapy. Several clinical studies support the positive correlation between KRAS mutation and lack of response to anti-EGFR chemotherapy in colorectal cancers [154-156]. KRAS status has no value in predicting response to standard fluoropyrimidine-based chemoradiation [157, 158] and its role as a marker of long-term outcomes also remains unclear [159-161].
Epidermal Growth Factor Receptor (EGFR)	Activates downstream effectors in gene expression, causing cellular proliferation, inhibition of apoptosis and angiogenesis [162]	High expression of EGFR in pre-treatment biopsies is associated with poor response to NCRT [148, 163-165]. Overexpression of EGFR show higher metastatic potential, [166], local recurrence [167], poor DFS [168], and survival [169]. The EGFR and its components are established molecular target for monoclonal antibody (Cetuximab; Erbitux, Merck Pharmaceuticals) and molecular blockade (Gefitinib) based novel chemotherapeutics.

1.1.4 Tumour pathophysiology versus biological behaviour

Tumour pathophysiology is critical for tumour survival, progression and response to treatment. The availability and uptake of nutrients including oxygen, disposal of waste, humoral functions and delivery of cytotoxic agents is mainly dependent on cancer microenvironment. The features with most impact on tumour microenvironment include:

(i) Angiogenesis

(ii) Tumour blood flow

1.1.4.1 Angiogenesis

Angiogenesis is a complex process of new blood vessel formation from pre-existing ones. It involves activation, proliferation and direct migration of endothelial cells to form new capillaries. Physiological angiogenesis occur during embryogenesis, wound healing and reproductive cycle in adults [170]. Pathological angiogenesis is characterized by persistent proliferation of endothelial cells and is a prominent feature of many diseases including rheumatoid arthritis, psoriasis, and proliferative retinopathy. Invasive cancers have the ability to stimulate angiogenesis from surrounding vessels and establish blood flow to support their nutrition, waste management, humoral activity and growth [171, 172].

1.1.4.1.1 The regulation of angiogenesis

There are endogenous pro-angiogenic stimulant factors that promote endothelial cells to dissolve their extracellular matrix, migrate towards tumour

cell and proliferate to form new vascular network. The most significant angiogenic promoters include a family of cytokines known as vascular endothelial growth factors (VEGF), their receptors (VEGFR) and TGF-β superfamily. There are also a variety of endogenous angiogenic inhibitor presumed to regulate angiogenesis and include thrombospondon-1, angiostatin (a fragment protein from cleavage of plasminogen within tumour [173]) and endostatin (derived from collagen XVIII [174]). The shift of fine balance between pro and anti-angiogenic factor levels, termed ‘angiogenic switch’, determines progression and pattern of angiogenesis.

1.1.4.1.2 Physiological versus neoplastic angiogenesis

Physiological angiogenesis results in organised microvascular architecture that maintains a homogenous density throughout tissue planes, vascular hierarchical pattern, endothelial cell spacing and vascular permeability. In neoplastic angiogenesis there is loss of fine balance of ‘angiogenic switch’ [175, 176] that results in structurally and functionally abnormal vascular networks. There is chaotic microvascular architecture, the vascular density is heterogeneous throughout tissue planes and the vessels formed are immature with small diameters that are permeable to large molecules [177]. In addition, the proliferating cancer cells also compress intra-tumoral blood and lymph vessels. These structural abnormalities contribute to high interstitial pressure equalling intra-capillary pressure resulting is heterogeneous blood flow within vascular networks and creates a microenvironment surrounding cancer cells that is characterised by interstitial hypertension, impaired blood supply, hypoxia and acidosis [178, 179].

1.1.4.1.3 The impact of neoplastic angiogenesis on rectal tumour behaviour

The cumulative effect of abnormal vascular structure and blood flow makes cancer tissue resistant to treatment by hindering drug and oxygen radical delivery. The hypoxic and acidic environment also compromise cytotoxic function of host immune cells and may induce genetic alteration within malignant cells leading to increased metastatic potential [178]. Rectal cancers with dominant angiogenesis are associated with aggressive behaviour, treatment resistance and recurrence [180, 181]. The degree of angiogenesis within resected rectal cancer specimen has been proposed as an independent marker of prognosis [182-184].

1.1.4.2 Tumour Vascular Morphology

The neovascularization in tumours usually originates from venules within the tissue mass or host tissue [185]. The tumour has two populations of blood vessels: (i) pre-existing host vessels incorporated into tumour tissue and (ii) tumour vessel from neoplastic angiogenesis. Neoplastic vessels have severe morphological defects (see table 1.3 by Vaupel et al [185]). The loss of vascular organization results in infinite number of different vessel type combination frequently resulting in arteriovenous shunting and veno-venous circulation [186]. Skinner et al [187] examined the structure of benign and malignant colorectal tumours and found increased density of microvessels resulting in formation of nodular clusters of capillaries, formation of sheets of frequent anastomosing capillaries and almost complete packing of the interstitial spaces of the tumour by capillaries.

Table 1.3: Structural and functional abnormalities of neoplastic angiogenesis [185]

A. Structural abnormalities ("vascular chaos")
1. Abnormal Vessel Wall
Incomplete or missing endothelial lining
Interrupted or absent basement membrane
Blood channels line by tumour cell cords
Lack of pericytes, contractile wall components and pharmacological/physiological receptors
2. Abnormal vascular structure
Contour irregularities (formation of lacuna-like sinusoidal and cystiform blood vessels)
Tortuosity (distortions, twisting, bending)
Elongation of vessels
Existence of arteriovenous shunts (global flow > nutritive flow)
Loss or hierarchy
3. Abnormal vascular density
Heterogeneous distribution of vascularization ("chaotic network", appearance of avascular areas)
Expansion of the intercapillary space (increase of diffusion distances)
B. Functional abnormalities ("circulatory chaos")
1. Consequence of altered morphology
Arteriovenous shunt perfusion (~30%)
Regurgitation and intermittent flow
Unstable speed and direction of flow
Absence of vasomotion
Increased vascular fragility
Obstruction of microvessels by WBC and tumour cells
High tumour vascular (geometric) resistance
2. Consequence of altered rheology
RBC sludging, leukocyte sticking
Platelet aggregation
Micro- and macrothrombosis
Increase of viscous resistance
3. Consequence of increased vascular permeability
Heterogeneous distribution of vascularization ("chaotic network", appearance of avascular areas)
Expansion of the intercapillary space (increase of diffusion distances)

1.1.4.3 Tumour Blood Flow

The tumour microcirculation supply nutrients and remove waste, provide a vehicle for cancer cells to metastasize, determine pharmacodynamics of chemotherapeutics and efficacy of radiotherapy dependant on local oxygen concentration. The vascular volume of colon carcinoma was shown to be significantly greater than adenoma and normal colon (23% ±12.2 vs. 16.3%±3.4 and 11% ± 4.2 respectively) [187]. Interestingly, Hinganu et al [188] studied neoangiogenesis of rectal adenocarcinoma of same grade (stage III) at different locations within the rectum, and reported an incremental rise in the length of neoplastic blood vessels and maximum neoangiogenesis area from inferior to middle and middle to upper rectal cancers.

The incorporated host vessels are reactive to physiological stimulus like hypoxia and therefore maximally dilated in areas of poor perfusion. Therefore, the global tumour blood flow in response to physiological stimulus (hypoxia / acidosis) depends on the ratio of host to neoplastic vasculature, which depend on tumour location, size, differentiation and stage, and keeps changing continuously. There is interstitial hypertension due to free water diffusion out of vessels tumour load and lack of lymphatic drainage causing luminal compression and nullifying perfusion pressures. There also considerable spatial and temporal heterogeneity of tumour microcirculation within individual vessels and different vascular micronetworks within one tumour and same tumour of different size, differentiation, grading and location [185].

1.1.4.4 Quantification of angiogenesis and tumour blood flow

There is no consensus method of quantifying tumour microvasculature. The method used in clinical studies include:

(i) VEGF and VEGFR assays

(ii) Microvascular Density (MVD)

Both methods use immunohistochemistry staining that involve use of monoclonal antibodies directed against antigens specific to VGEF, VGEFR and various endothelial antigens to assess MVD (factor VIII, CD31, CD34 and CD105) on resected and fixed histopathology specimen, but such staining may not reflect the extent of functional angiogenesis with the tumour [189].

The morphological appearance of tumour microvasculature does not necessarily correlate with its functional aspects. There are many functional elements of angiogenesis that also contribute to tumour biology and prognosis. Functional imaging is an emerging technology enabling in-vivo assessment of tumour tissue and its microenvironment. Studies investigating dynamic contrast enhanced magnetic resonance imaging (DCE-MRI) to measure functional angiogenesis have shown poor or inverse correlation between DCE parameters and VGEF/MVD static histological markers [190-192], further backing the independent role of functional angiogenesis in tumour biology.

CHAPTER 1: INTRODUCTION

1.2 Diagnostic imaging of rectal cancer

The imaging modalities use to investigate the extent of rectal cancer include:

1. Endoanal ultrasound
2. Magnetic Resonance Imaging

1.2.1 Endoanal ultrasound

Endoanal ultrasound (EAUS) is valuable in staging superficial rectal cancers (sensitivity 97%, specificity 96% for T1 tumours). It has a mean T- and N - stage accuracy of 85% and 75% respectively [193]. EAUS is of limited value for advance tumours as the depth of penetration for high frequency probes is limited to 5mm. Other limitations include availability of highly skilled operator and risk of understaging tumours [194].

1.2.2 Magnetic Resonance Imaging

Magnetic resonance imaging (MRI) of rectum and pelvis is currently the gold-standard imaging modality to assess mid-to-low rectal cancer disease. Technical advances and improved image resolution (high resolution MRI of rectum with phased array coils) provide detailed information on local disease extent and response to neoadjuvant treatment with valuable impact on clinical staging, treatment planning (defining surgical anatomy as well as prognostic markers for neoadjuvant and/or adjuvant treatment), response assessment and prognosis. The detailed rectal tumour morphology displayed by MRI is very close to histopathological findings. These results have been validated in multicentre studies showing excellent agreement between MRI and

histopathology assessment of rectal cancer [195, 196]. MRI is particularly useful in distinguishing between pT3b and pT3c disease extent. Controlled studies have shown MRI specificity for CRM involvement of 92% (CI 90-95%) [195, 197]. Histopathology remains gold standard to assess nodal involvement in rectal cancers; however, diseased nodes within mesorectum with irregular border or mixed intra-nodal signal can be seen on MRI (accuracy 85%). Morphologic MRI also displays the anatomic distribution of nodes both within and outside the mesorectum. The reported sensitivity and specificity of MRI in detecting EMVI is in the range of 62-100% and 88-89%, respectively [197-199]. The assessment of EMVI also provides critical insight into potential tumour response to neoadjuvant treatment. Yu et al [200] clearly demonstrated EMVI involvement on pre-treatment MRI as marker of poor response to NCRT on a multivariate analysis. Interestingly, MRI defined low rectal cancers (<5 cm from anal verge) were also shown to respond well to NCRT. Better response of low rectal cancers has been reported previously [201]. Despite the anatomical complexities, MRI remains a reliable modality in assessment of low rectal tumours. MRI based staging system for low rectal cancers has been recently developed and successfully validated in MERCURY II trial (see table 1.4) [202].

The MRI based markers of treatment response are shown in table 1.5 (adopted from review by Battersby et al). Studies comparing post-NCRT MRI staging (ymr) with histopathological staging (yp) have reported the following: ymrT-stage show good correlation and accuracy of 40–60% with ypT-stage

[203-205]; and ymrN-stage has reported accuracy of 87% with ypN-stage [205].

Table 1.4: MRI Stage for low rectal cancers [202]

MRI Stage	Definition
I	Tumour confined to bowel wall but not through full thickness
II	Tumour replaces the muscle coat but does not extend into the intersphincteric space
III	Tumour invades the intersphincteric space or lies within 1 mm of the levator muscle
IV	Tumour invades the external anal sphincter and is within 1 mm and beyond levators muscle with or without invading the adjacent structures

Table 1.5: MRI based markers of response to NCRT [55]

Pre-treatment MRI markers predicting response to NCRT
• Tumour Height – low rectal tumours are more likely to be 'good responders • EMVI – the presence of EMVI increases the likelihood of poor response
Post-NCRT MRI markers of response
• mrTRG • Tumour Height • EMVI (ymrEMVI) • CRM status • Depth of invasion (ymrT-stage) • Node status (ymrN-stage)

1.2.3 Assessment of tumour response to NCRT

1.2.3.1 Response Evaluation Criteria in Solid Tumours

The radiological assessment of tumour response to neoadjuvant treatments has been traditionally based on morphological criteria. The 'Response Evaluation Criteria in Solid Tumours (RECIST)' has been developed as standard criteria to assess response to neoadjuvant therapy (Table 1.6). There are few fundamental flaws with RECIST criteria: firstly it not specifically designed for rectal cancers, secondly the criteria is based on arbitrary figures not derived from outcome data, and non tumoural masses may persist without any impact on disease status, and finally, it does not take in account tumour biology which plays critical role in tumour behaviour.

Table 1.6: Response Evaluation Criteria in Solid Tumours (RECIST) [206]

Criteria	**Definition**
Complete Response	Disappearance of all target lesion
Partial response	30% decrease in the sum of the longest diameter of the target lesion
Progressive disease	20% increase in the sum of the longest diameter of the target lesion
Stable disease	Neither sufficient shrinkage nor increase

1.2.3.2 MRI based TRG

A more effective tool for assessment of rectal cancer response to NCRT has been the development of MRI tumour regression grading (mrTRG) in recent years, based on pathological tumour regression grade system [104, 105]. The entire tumour is assessed to determine if fibrosis signal intensity or if tumour signal intensity predominates (see table 1.7). In a prospective study of 111 patients, mrTRG independently predicted DFS (HR 3.28; 95%CI 1.22 to 8.8) and OS (HR 4.4; 95%CI 1.64 to 11.7), on multivariate analysis. Patients with mrTRG 1-3 (good response) had better five year DFS (72% vs 27%, $p<0.001$). In addition, mrTRG 1 and 2 were highly predictive of pCR [207].

Table 1.7: MRI Tumour regression grading

Grade	Definition
mrTRG1	Dominant low-signal intensity fibrosis with no tumour
mrTRG2	Low-signal intensity fibrosis with minimal residual tumour
mrTRG3	50% fibrosis/mucin and intermediate signal representing residual tumour.
mrTRG4	Predominance of tumour with minimal low-signal intensity fibrosis
mrTRG5	Tumour is unchanged from baseline

CHAPTER 1: INTRODUCTION

1.3 Management of locally advanced rectal cancers

The current management of patients with locally advanced rectal cancer includes three components:

1. Neoadjuvant chemoradiotherapy (NCRT)
2. Interval period
3. Total Mesorectal Excision (TME) of rectal cancer

1.3.1 The impact of radio-chemotherapy in the management of locally advance rectal cancers

The Swedish Rectal Cancer [208, 209], Dutch TME [64, 210, 211] and MRC CR07 trials [212] established the benefit of preoperative short-course radiotherapy in resectable rectal cancer, at least in terms of local recurrence even if this has not always resulted in a convincing survival. The largest possible gain has been seen in patients with extramural spread and node-positive disease. Preoperative radiotherapy has also been shown to be more beneficial than when given postoperatively [213]. The summary from these trial highlighted shortcomings in the management of patients including imprecise staging, sub-standard surgery and radiotherapy.

Two large trials specifically investigated the utility of fluoropyrimidine based chemotherapy with preoperative long-course radiotherapy, the EORTC 22921 [214, 215] and FFCD 9203 trials [216] showed reduction in local recurrence as well as increased rate of pathological complete response without any benefit in 5-year survival; but the trial were underpowered to show a 5%

difference in overall survival [2]. The German rectal trial [217] showed superiority of preoperative long course chemoradiation over postoperative treatment in terms of fewer local recurrences and less acute and late toxicity, but no survival benefit. The Polish [218, 219] and TROG trial [220] did not show any difference between short and long-course radiotherapy. A Cochrane systematic review has concluded that preoperative radiotherapy improves overall mortality and local control over surgery alone, and that preoperative chemoradiotherapy reduces local recurrence further without affecting overall mortality [221]. There were no difference recorded in local recurrence and survival in the two trials that's compared preoperative short-course and long-course radiotherapy in resectable cancers. The role of postoperative radio ± chemotherapy remains remains controversial because although some trials [222] and meta-analyses [223-225] showed survival benefit but toxicity is acknowledged to be worse post-operatively.

1.3.2 The impact of 'interval to surgery' in the management of locally advance rectal cancer

Francois et al [226, 227] is the only RCT exploring the interval between NCRT and surgery. They randomised 201 patients with lower to mid T2-3 rectal cancer to surgery within two weeks, or between six and eight weeks, following completion of 13 fractions of preoperative radiotherapy. Patients in the long-interval arm experienced greater clinical and pathological tumour responses, and their tumours were more likely to be down-staged according to the TNM classification. However, there were no differences between the two groups in

morbidity, anal function, local recurrence or survival at a median follow-up of 6.3 years.

Petterson et al [228] examined short-course pre-operative radiotherapy (SCPRT: 5Gy for 5 days). After SCPRT (5x5Gy) the current recommended interval to surgery is 3-7 days following radiation. Extension of the interval following SCPRT to surgery >6 weeks does demonstrate downstaging, but the optimal interval has not been defined [229]**.** Whether the same degree of tumour shrinkage and pCR can be achieved with SCPRT and extended interval to surgery is currently unclear until the final results of the Stockholm III trial [228] become available and hence this strategy still remains experimental.

1.3.3 The impact of surgery in the management of locally advance rectal cancer

Total mesorectal excision (TME) is the surgical technique for resection of rectum harbouring locally advanced cancer and involves removing rectal cancer together with mesorectal fat column, to minimise residual tumour overload (see figure 1.4) [230, 231]. The adaptation of TME of rectal cancer together with refined chemoradiotherapy techniques has decreased CRM rates and markedly improved rectal cancer recurrence [232]. The local relapse after TME alone for pT3-4 N1-2 of medium or low rectal cancer remains in the range of 15 – 20 % in randomised trials [210, 212]. The surgical training for TME has a major impact on the efficacy of treatment and prognosis of patient [233]. The CRM involvement was reported to be higher in

abdominoperineal excision than anterior resection of rectum in a national bowel cancer audit [234]. Hence, in the case of abdominoperineal resection for low rectal cancers, additional aim of the surgery is to prevent the waist in the specimen to prevent CRM involvement commonly seen at the level of anorectal junction [63, 235]. The recent adaptation of extralevator abdominoperineal excision (ELAPE) for low rectal cancer has shown less CRM involvement and intraoperative perforation than standard surgery [236].

Figure 1.4: The surgical planes of Total Mesorectal Excision and Extra-Levator Abdomino-Perineal Excision (ELAPE) surgery of rectum [237]

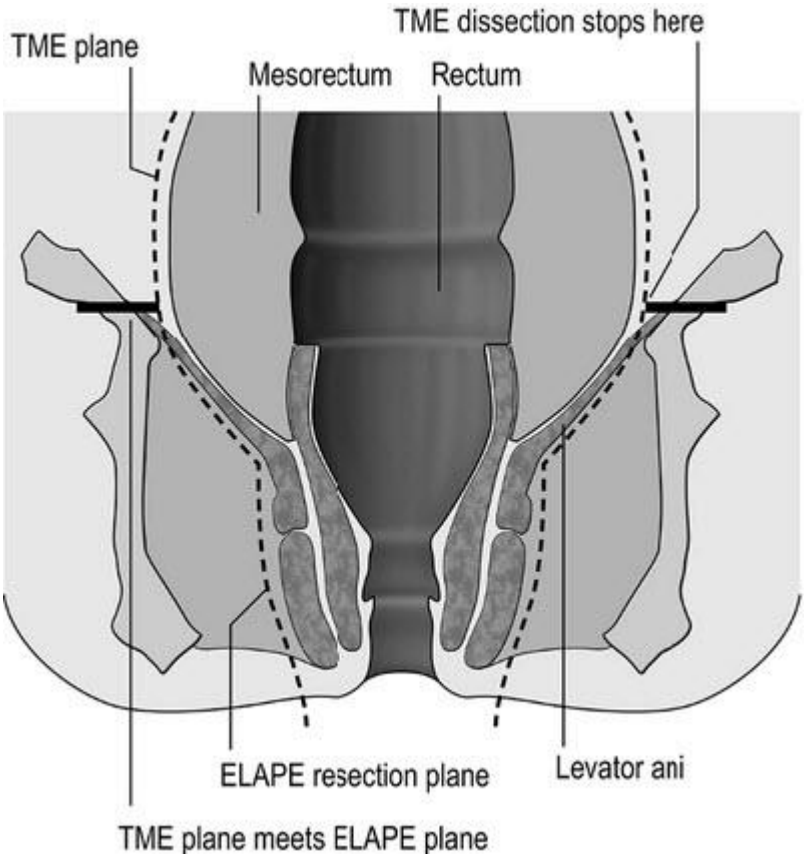

1.4 Basis for the current study and background of proposed experiments

The response to NCRT for similar staged locally advanced rectal cancers varies between patients: whilst in some patients the tumour completely disappears others show stable or progressive disease. A good response to NCRT improves long-term clinical outcomes as evidenced by lower recurrence rates and longer survival [238]. Mostly European trials report a clinical downstaging in the range of 50-60% including complete pathological response in 13-20% after NCRT. Hence a large cohort of patient is subjected to toxic NCRT without any benefit. To date, little is known about the molecular basis for such heterogeneous response to NCRT. Therefore, recent studies have focused on prognostic stratification based on rectal tumour biology and proposed the need for individualised treatment regimes. A simple measure, such as, increasing the interval to surgery after NCRT has shown to increase response rates in patients [239]. However, the exact duration of radiotherapy induced cell death after completion of NCRT remains unknown.

The radiosensitivity of tumour cell is based on several factors that can be broadly classified into either intrinsic or extrinsic factors. Intrinsic factors include cell DNA repair profiles, phase of cell cycle, balance between pro- and anti-apoptotic proteins, whilst, extrinsic factors include cell microenvironment including cellular density, tissue hypoxia, microvascular architecture and angiogenesis. A combination of these factors may result in heterogeneous radiosensitivities between cells within the same tumour tissue.

CHAPTER 1: INTRODUCTION

It may be hypothesised that rectal cancers differ from each other at a molecular level despite showing the same morphological features currently used to stage these tumours. The individual molecular characteristic of tumour cells possibly defines the disease course and response to therapy. The molecular characteristics are probably dynamic and may change in response to treatment. For example, previous studies have shown that a radiosensitive tumour tissue may become radioresistant by repopulating cells with upgraded DNA repair profiles between or after fractional radiotherapy [240], switch the mechanism angiogenesis to develop resistance [241] and/or even promote metastasis of any residual clonogens after curative surgery [242].

The focus of this project was to study the molecular features of rectal cancers that have shown to be crucial in other solid tumours and investigate any impact on clinical features, response to therapy and long-term prognosis. Experiments were designed to investigate serial molecular changes within tumour cells and their microenvironment at baseline and during the interval between NCRT and surgery.

The intrinsic factor studied included DNA damage and repair profiles, whilst extrinsic factors studied included tumour cellularity and necrosis, hypoxic foci, and functional vascularity.

1.4.1 Assessment of rectal cancer cell DNA damage and repair in response to radiotherapy

1.4.1.1 DNA damage and repair:

Radiotherapy-induced cellular cytotoxicity has long been attributed to the damage inflicted on DNA by ionising radiation. The DNA damage can manifest as single- or double–strand breaks, base damage, DNA or protein cross links, protein-protein cross links, and intra- or inter-strand cross links. Of the various specific lesions involved, the double-strand break (DSB) has been identified as being frequently responsible for the generation of lethal chromosomal abnormalities or the induction of apoptosis [243]. On the other hand, complex DNA repair mechanisms serve to limit the efficacy of radiotherapy, possibly having evolved as a means of protecting cells against lesser doses of naturally occurring radiation. The DNA damage response (DDR) is a coordinated cascade of events that sense the DNA damage, signals its presence, and mediates its repair or activates apoptosis. There are five major DNA repair mechanisms (see figure 1.5 and table 1.8):

1. Base excision repair
2. Mismatch repair
3. Nucleotide excision repair
4. Homologous Recombination for double-strand break repair
5. Non-homologous end joining for double-strand break repair

Figure 1.5: DNA damage and repair mechanisms [244]

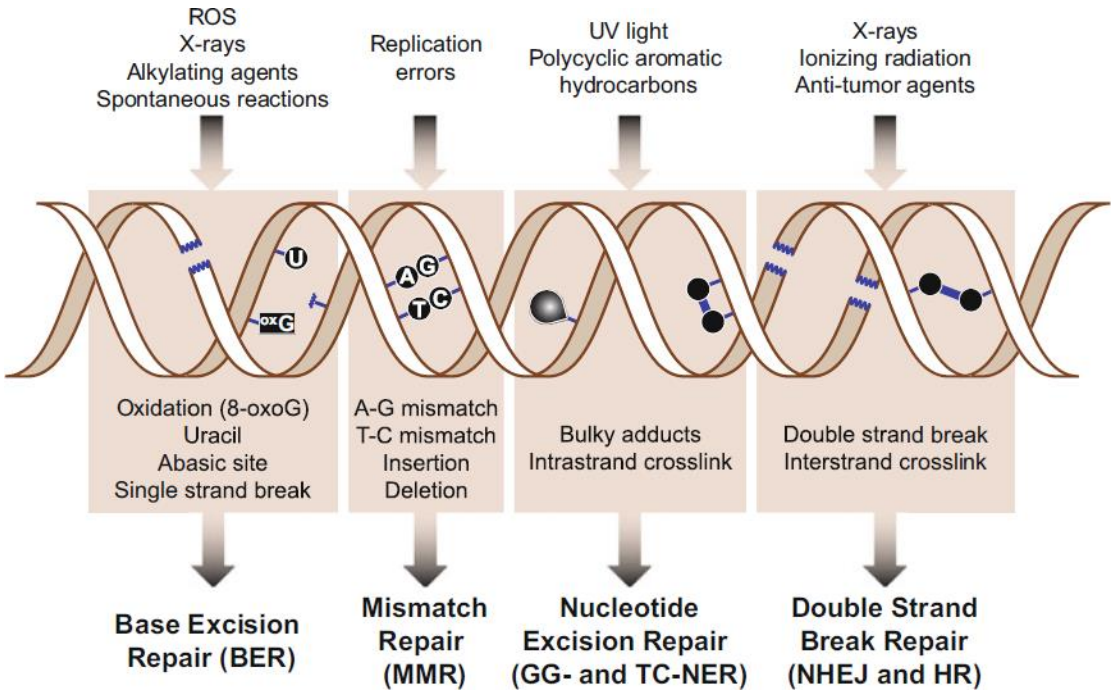

Table 1.8: DNA repair pathways:

Pathway	**Function**
Base Excision Repair	Repair of damaged DNA bases without significantly distorting the overall structure of DNA helix
Mismatch Repair	Post-replication repair of misincorporated bases that have escaped proofreading activity of replication polymerases
Nucleotide Excision repair	Recognise and remove a wide variety of bulky helix-distorting lesions of the DNA
Non-homologous end joining for DSB	Directly re-joins the two severed DNA ends in a sequence independent fashion (often error-prone) [245]
Homologous Recombination for DSB	Accurately re-synthesise damaged or missing sequence information at the break site by using a template located elsewhere in the genome [245]

1.4.1.2 Comet Assay - Measurement of DNA damage and repair

The single cell gel electrophoresis (Comet assay) has become an established technique for measuring DNA damage with wide spread applications in genotoxicity testing, human biomonitoring, molecular epidemiology, ecogenotoxicology, as well as fundamental research in DNA damage and repair [246]. It was first described by Ostling and Johanson [247] in 1984 followed by the most popular alkaline version described by Singh et al [248] . The assay is simple, economical and reproducible with high sensitivity.

1.4.1.2.1 Technology, Quantification and interpretation

The process involves lysis of cells with detergents and high salt after embedding in agarose so that the DNA is immobilised for subsequent electrophoresis. The detergents remove membranes, cytoplasm, and nucleoplasm and disrupt nucleosomes leaving behind nucleoids, consisting of nuclear matrix composed of ribonucleic acid (RNA), proteins and DNA. The DNA is negatively supercoiled as the double helix turns around the histones of the nucleosomes [246]. An alkaline variant (lysis of cells in a solution at pH>13) is favoured as this produces more pronounced comets in response to a given dose of radiation, reflecting more extensive DNA damage, including DSBs and SSBs. Hence, while it is technically no more sensitive at detecting the presence of DNA damage, it is able to discriminate more accurately between different levels of damage. Consequently, in order to demonstrate measurable differences in these levels, experiments utilising the neutral comet assay require single radiation doses of above 20Gy, in contrast to the more clinically relevant doses administered with the alkaline comet assay.

The technique involves embedding cells in a single layer of agarose on a plain glass slide precoated with agarose and dried. The cells are lysed in alkaline buffer with high sodium content, then washed with double distal water and incubated in alkaline solution before electrophoresis. Upon electrophoresis, the DNA extends towards the anode in a structure resembling a comet. The slides are dyed with DNA-binding dye and visualised by fluorescence microscopy. The ‘head’ of comet is made of supercoiled DNA, which is negatively charged as a consequence of the turns made by the double helix around histones of the nucleoplasm. The relaxed supercoiling of damaged DNA are pulled with electrophoresis forming the ‘tail’ of the comet.

The image analysis is conducted using special software to measure the parameters such as tail length, relative fluorescence intensity of the head and tail, and tail moment. The parameter ‘tail moment (TM)’ is commonly used to quantify DNA damage and is calculated as the product of the percentage DNA in the comet tail and the distance between the means of the head and tail distribution (measured in μm), based on the definition by Olive et al [249] (see figure 1.6 and 1.7).

Figure 1.6: Procedure of Comet Assay by Moller [250]

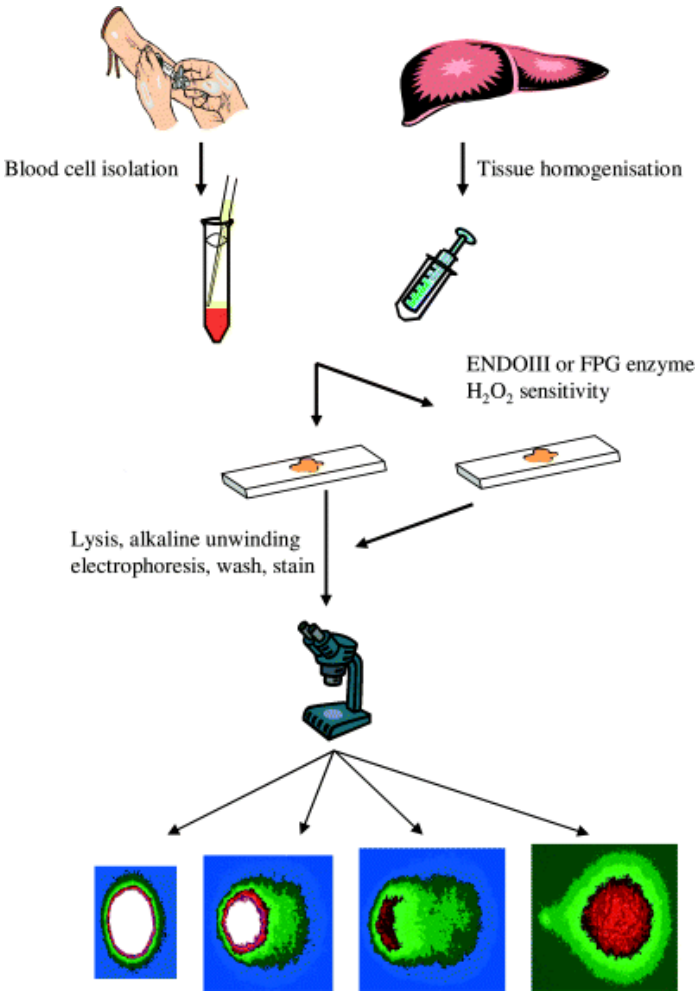

Figure 1.7: Comet Assay – measurement of Tail Moment according to Olive et al. [249]:

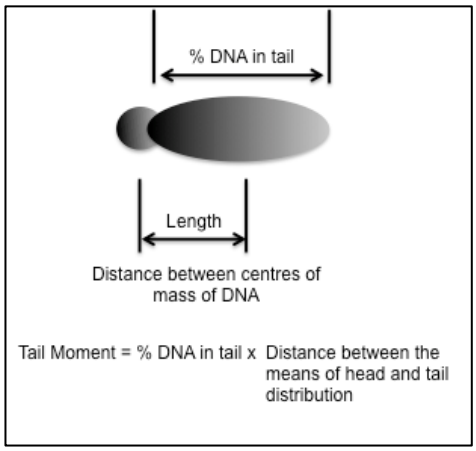

The simple version of the alkaline comet assay detects DNA migration caused by strand breaks, alkaline labile sites and transient repair sites. By incubation with bacterial glycosylase/endonuclease enzymes, broad classes of oxidative DNA damage, alkylation, and ultraviolet light-induced photoproducts are detected as additional DNA migration [250]. Novel application of comet assay include detection of DNA-DNA crosslink, and gene-specific DNA damage detected by the application of fluorescent in situ hybridization methodology in the comet assay [250]

The measurement of DNA repair capacity of a cell using comet assay involves inflicting DNA damage in-vitro and monitoring the speed with which they remove the lesion. The re-joining of DNA strand breaks by most cell types is rapid and this kinetics can be measured by ‘serial or timed’ comet assays.

1.4.1.2.2 Validation

Comet assay has been applied in a broad range of scientific fields, including genetic toxicology, ecotoxicology, DNA repair, and apoptosis. The European Comet Assay Validation Group (ECVAG) trial indicates substantial reliability for the measurement of DNA damage by the comet assay [251]. Sasaki et al [252] validated the use of comet assay as a good screening tool for in vivo genotoxicity by showing DNA damage in eight organs of rodents by exposure to 208 rodent carcinogens. There are a number of clinical studies deploying comet assay to detect DNA damage in leucocytes (see below). Comet assay has been used to establish high levels of DNA damage as risk factor for adenocarcinoma of the oesophagus [253], bladder cancer [254], breast

cancer [255] and thyroid cancers [256]. The results from prospective cohort studies are awaited.

1.4.1.2.3 Clinical Application

Comet assay become established as a convenient tool for measuring radiation-induced DNA damage and attempts have also been made to assess the clinical relevance of such measurements. Clonogenic assays on tumour biopsies, measuring the surviving fraction (SF*X*) of cells exposed to *X*Gy radiation, have been demonstrated to predict clinical response to radiotherapy in patients with cervical cancer and head and neck cancer, respectively [257, 258]. In turn, several studies have investigated whether or not the comet assay can be used to predict clonogenic cell survival. For instance, Price et al [259] used the neutral comet assay in six bladder tumour cell lines to measure initial radiation-induced DNA damage and the time taken to repair this. Both correlated inversely with clonogenic cell survival at 10Gy, but the correlation was less convincing at the more clinically relevant dose of 2Gy. Marples et al [260] performed a similar experiment with seven cervical carcinoma cell lines, in which there was no direct association between either initial or residual DNA damage and SF2 (surviving fraction at 2Gy), but the ratio of these two comet assay measurements did have some predictive value.

More recently, the predictive value of the alkaline comet assay has been investigated in several bladder tumour and colon cancer cell lines exposed to clinically relevant radiation doses [261-263]. In both types of tumour cell, initial DNA damage has been shown to have a close inverse correlation with clonogenic survival, while measures of residual DNA damage and repair were

also predictive to a variable extent. The comet assay has also been utilised as pharmacodynamic endpoint to establish maximum tolerated dose and safety of experimental chemotherapeutics [264, 265].

While many of the clinical studies employing the comet assay have utilised lymphocytes, the technique has also been performed on cells obtained by fine needle aspiration of a variety of accessible primary and metastatic tumours, including colorectal cancer [266-270]. In addition, the comet assay has been successfully performed on normal colonic and rectal mucosal cells obtained from biopsies of patients without cancer [271-273]. Of note, Olive et al [268] took two simultaneous aspirates from each of 33 patients with metastatic tumours: the between-sample correlation was very good, indicating that a single aspirate should generally be representative of the tumour (correlation coefficient r = 0.88). Similarly, McGlynn et al [272] interpreted their measurements of DNA damage within normal colonic mucosa as demonstrating high intra-subject reproducibility, although this was based on a fairly limited statistical analysis.

One final study of relevance to the proposed project performed the neutral comet assay on lymphocytes irradiated at 2Gy, their having been obtained at sequential intervals from patients receiving radiotherapy for a variety of tumour types [274]. There were no apparent differences in either initial DNA damage or repair capacity among the samples collected before radiotherapy, after 5 fractions or after 10 fractions.

1.4.1.2.4 Limitations

The main limitation is the scarcity of publications on the use of the comet assay for non-lymphatic tissues. Comet assay have been classically used to measure DNA damage on easily obtainable cells, e.g leukocytes and tumour cell lines. Analysis of DNA damage in patients with solid tumour by comet assay of their leukocytes may be disadvantageous, as leukocytes are not target tissue for cancer and it is not clear that damage detected in leukocytes reflects the damage in actual target tissue. Comet assay require high viability of cells in a given sample, which may be difficult to achieve from biopsy tissues obtain from solid tumour as these tumour often contain several foci of necrosis that may contaminate the sample. Observer bias may be introduced when measuring TM if the DNA images are not randomly selected, therefore, it is recommended to estimate a range of intra- and inter-subject variation by two observers in a pilot study, which is not always feasible. Studies investigating sample scoring between different laboratories have also reported large variation between observers [251, 275, 276].

1.4.2 Assessment of rectal cancer microenvironment and pathophysiology

Functional imaging techniques are increasingly being used to monitor response to therapies with novel mechanism of action, often predicting the success of therapy before conventional measurements of size are changed [277], activity of residual disease remaining after therapy and to detect

recurrence early at a time when salvage therapy might still be possible [278-280].

In this study, functional MRI and CT were used to investigate temporal and spatial changes in the rectal cancer microenvironment including tumour microvasculature, blood flow, perfusion, tissue oxygenation and cell density. A summary of functional imaging techniques is shown in table 1.9.

Table 1.9: Functional imaging – summary of techniques [281]

Imaging technique	Principles of MR and CT measurement	Biological properties on which imaging is based	Commonly derived quantitative imaging parameters	Pathophysiological correlates
Diffusion-weighted (DW) MRI	Single-shot echo planar DE-MRI acquisition; contrast agent not required	Diffusivity of water	ADC	Tissue architecture: cell density, extracellular space tortuosity, gland formation, cell membrane integrity, necrosis
Intrinsic Susceptibility Weighted (ISW) or Blood Oxygen Level Dependent (BOLD) MRI	T_2* weighted – imaging performed at different echo time to detect susceptibility	Deoxyhaemoglobin slows higher relaxivity than oxyhaemoglobin; measurements reflect blood volume, perfusion and intrinsic composition of tissues	Intrinsic tissue relaxation rates ($R_2^* = 1/T_2^*$)	Ferromagnetic properties of tissues; level of tissue oxygenation
Dynamic Contrast Enhanced (DCE) MRI	T1-weighted MR imaging at high temporal sampling after gadolinium contrast administration; mathematical modelling of acquired data	Contrast medium uptake rate in tissue, which is influenced by transfer rates and extracellular volume; plasma volume fraction	IAUGC; Transfer and rate constant (K^{trans},k_{ep}); leakage space fraction (v_e); fractional plasma volume(v_p)	Vessel density; vascular permeability; perfusion; extravascular space; plasma volume
Dynamic Contrast Enhanced (DCE) CT	First pass imaging at high temporal sampling after iodine contrast administration (image acquisition every 1 second); Second pass images acquired at every 10 seconds for 2 minutes; mathematical modelling of acquired data	Contrast medium uptake rate in tissue, which is influenced by transfer rates and extracellular volume; plasma volume fraction	Flow rate through vasculature (BF); volume of flowing blood through vasculature in a tissue (BV); average time taken to travel from artery to vein (MTT); total flux from plasma to interstitial space (PS)	Vessel density; vascular permeability; perfusion; extravascular space; plasma volume

Table 1.10: Functional Imaging - Summary of validation, clinical applications and limitations

Imaging technique	Validation	Clinical Applications	Limitations
Diffusion-weighted (DW) MRI	ADC values shown to correlate with specific tissue histological properties such as cell density, proliferation index, tumour grade, gland formation, presence of necrosis and tumour cell apoptosis	Successful treatment is reflected by increase in ADC values Rising ADC has been shown with successful treatment in cancers of the breast, liver metastases, bone sarcomas and brain malignancies	The diffusion of water is directional in brain and kidney, therefore MPG needs to be applied in multiple directions. Respiration, cardiac pulsation and peristalsis can adversely affect image quality
Intrinsic Susceptibility Weighted (ISW) or Blood Oxygen Level Dependent (BOLD) MRI	R_2* shows good correlation with tissue hypoxia markers with decrease in baseline R_2* after hyperoxygenation. R_2* values depend of vessel volume (i.e vessel size and maturation)	A fast R_2* relaxation represent hypoxic tumours. Measurement of baseline R_2* and ΔR_2* (after hyperoxygenation) of tumour has been used in treatment planning for cancers of head and neck and predicting radiotherapeutic response in cancers of cervix.	R2* values vary significantly vary between tumour types and site (optimization of magnetic fields). Deoxyhaemoglobin induced resonance of water may not be homogenous
Dynamic Contrast Enhanced (DCE) MRI	DCE-MRI parameters shows good correlation with immunohistochemical markers of angiogenesis, surrogates of tissue perfusion (14C-aminobutyric acid) and correlative imaging modalities (Dynamic susceptibility contrast MRI, (15) O-water PET and microbubble ultrasound)	DCE-MRI parameters were shown to predict treatment response and used to monitor the effects of a variety of oncology treatments. The studies have included cancers of bladder, breast, bone sarcomas, rectal and cervical cancers. DCE-MRI is being used in early clinical development of therapies that target tumour vasculature	There is variation in the mathematical model used to derive the DCE-parameters amongst investigators. Errors in estimation of model based MRI-DCE parameters can results from assumptions used during experimental set-up, for example the choice of AIF and transmembrane water exchange.
Dynamic Contrast Enhanced (DCE) CT	DCE-CT parameters shows good correlation with immunohistochemical markers of angiogenesis and correlative imaging modalities (xenon CT, (15) O-water PET)	DCE-CT parameters has been used in tumour differentiation and grading. DCE-CT is being used in early clinical development of therapies that target tumour vasculature	DCE-CT parameters are sensitive to Image acquisition techniques, post-processing discrepancies and motion artefact. CT involves radiation dosage and contrast load.

1.4.2.1 Diffusion Weighted MRI

DW-MRI provides information on tissue cellularity, extracellular space tortuosity and the integrity of cellular membranes by measuring the random motion of the water molecules in tissue. DW-MRI is the only imaging modality that can display this property. There are convincing data to support DW-MRI usage in the characterization of malignancy, including determination of lesion aggressiveness and for monitoring response to a variety of treatments [282-284].

1.4.2.1.1 Technology, Quantification and Interpretation

The net displacement of molecules across an area of tissue per second is called *apparent diffusion coefficient* (ADC). The ADC is low in regions of restricted diffusion and high in areas of free diffusion (see figure 1.8). DW images can be made sensitive to large or small displacements of water including macroscopic flows, microscopic extracellular space motion or even intracellular water displacements. This is done by applying diffusion-weighting gradients (sometimes called motion probing gradients (MPGs)) to standard T_2-weighted sequences [285] . The weighting of the applied MPGs is indicated by their *b-value*. Application of MPGs results in signal losses on images in proportion to the weighting of the applied gradients. The signal losses observed are used to calculate tissue ADC. Signal losses observed when low b-values (<50–100 s/mm^2) are used results from macroscopic water movements; that is the ADC calculated will be flow dominated [286]. At higher b-values, bulk water motion plays less of a role in the continued signal attenuation and so it is possible to differentiate between the contributions

made by high and low mobility water populations by varying the MPGs used for the calculation of the ADC [287] (see figures 5.3 and 5.4, page 193-194).

Figure 1.8: The movement of water molecules with different tissues

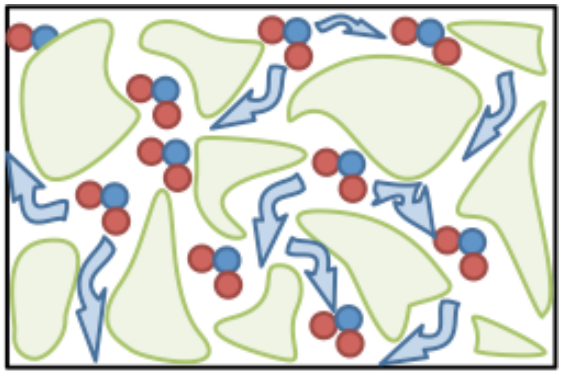

Freely diffusing water:

- Occur in normal tissues
- High ADC
- Lower signal intensity

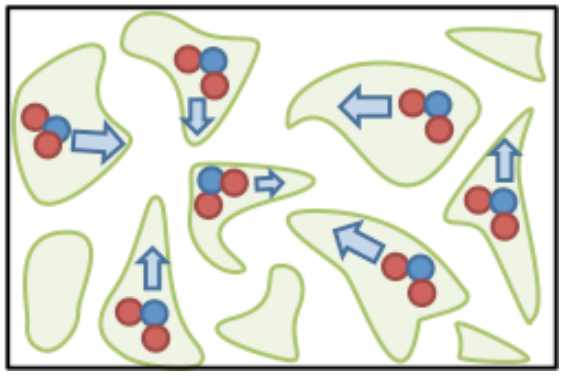

Restricted water:

- Occur in abnormal tissues
- Low ADC
- Higher signal intensity

1.4.2.1.2 Validation

The basic premise for enhanced tumour detection and improved tissue characterisation (for example in the liver [288, 289]) with DW-MRI is the connection between the observation that malignant tissues are generally more cellular than benign tissues; so water diffusion is more restricted in tumours due to a combination of increased cell density, haphazard tissue organisation and increased extracellular space tortuosity. However, when cystic, necrotic and treated metastases are included, then lesion characterisation is less good [290]. In line with these findings, Sumi et al. [291] have shown that lymphoma

nodes had significantly lower ADC than benign nodes in the neck. Sumi et al. [291] also showed that metastatic cervical lymph nodes in patients with squamous head and neck cancers had significantly higher ADC values than benign nodes. These apparently discrepant results are again explained by the common occurrence of necrosis in nodes with metastatic squamous cell carcinomas. These and other studies have repeatedly shown that false positive results occur with infective processes and after thermo-coagulation and false negative results occur with cystic, necrotic lesions and in well-differentiated neoplasms; which emphasises the need to interpret DW-MRI with all other anatomic and clinical data. These observations suggest that ADC values should correlate with specific histological tissue properties such as cell density [292-298], proliferation index [299, 300], tumour grade [297, 301] and gland formation (tissue organisation), presence of necrosis [298, 302] and in the therapy setting with tumour cell apoptosis [302-304].

1.4.2.1.3 Clinical applications

Any pharmacological, physical or radioactive process that causes necrosis or cellular lysis will lead to increases in water diffusion and corresponding increases in ADC values [284, 305]. Since cellular death and vascular changes in response to treatment can both precede changes in lesion size, so changes in DW-MRI may be an effective early biomarker for treatment response for therapies that induce apoptosis [283, 305]. Thus, most studies have shown that successful treatment is reflected by increases in tumour ADC values. Rising ADC values with successful therapy have been noted in several anatomical sites, including breast cancers [306, 307], primary and

metastatic cancers to the liver [308-310], primary bone sarcomas [311, 312] and in brain malignancies [313-315]. Addition of DW-MRI sequences to morphological T2-weighted images has shown to improve the diagnostic accuracy of viable rectal cancers after NCRT [316]. Some studies have shown that increases in ADC values can occur rapidly after the first dose of chemotherapy. For example, Cui et al, showed that increases in metastatic liver lesions from stomach and colorectal cancer occurred as early as 3-7 days after the first cycle of chemotherapy and that ADC increases correlated with therapy response judged by changes in lesion size [310].

As a caveat to the above observations of rising ADC values with successful treatment, it has also been noted that transient decreases in ADC can also be seen; this appears to be related to cellular swelling, reductions in blood flow or due to reductions in extracellular space. For instance, it has been noted that anti-VEGF therapies when given as monotherapy for brain tumours leads to initial reductions of lesion leakage space because of vascular normalization which lowers ADC values [317]. Cellular swelling has also been noted to occur in the early phases of apoptosis in response to anticancer treatment [283] and may be a significant additional reason for reductions in ADC values. Thus it appears that the extent and duration of such ADC reductions depends on the type of treatment administered, tumour type and the timing of imaging with respect to the treatment. These additional observations indicate that ADC changes are dependent on complex interplays of biophysical processes in response to therapy, emphasizing the need to better understand therapy induced tissue changes that are reflected in DW-MRI.

1.4.2.1.4 Limitations

There are a number of mostly technical limitations to DW-MRI. In the brain and kidney the diffusion of water tends to be directional (anisotropic) because of regular tissue organization [318, 319]. The measured ADC will therefore be dependent on the direction of the applied MPGs and multiple directions need to be applied to calculate directionless diffusivity (ADC) and the directionality of diffusion (diffusion tensor imaging) [320]. Fortunately, water diffusion is isotropic in most abdominal organs and in tumours. Therefore, only one MPG direction needs to be applied to obtain DW-MR images for ADC calculation. However, in practice, measurements in three or more gradient directions are often obtained and the signals averaged in order to improve signal-to-noise ratios of images. Physiological water motions and bulk tissue movements such as respiration, cardiac pulsations and peristalsis can also adversely affect image quality. Corrections can be made for bulk motion by incorporating schemes that detect the magnitude and direction of motion. Rapid imaging (i.e. using ultra-fast pulse sequences such as echo-planar imaging and parallel imaging techniques) and performing images in breath-hold can help to minimise the effects of bulk motion artefacts.

1.4.2.2 Intrinsic Susceptibility Weighted MRI

The ISW-MRI is the only non-invasive MRI technique that provides information on the oxygenation status of the blood volume and is also referred as blood oxygenation level dependent (BOLD) MRI. The ISW-MRI is also being used to investigate parameters of tumour angiogenesis such as blood vessel development, remodelling and function.

1.4.2.2.1 Technology, Quantification and Interpretation

ISW-MRI exploits the magnetic susceptibility (degree of magnetization of a material in response to magnetic field) differences between tissues to generate contrast. The magnetic properties of the blood are dependent on its oxygenation levels. Haemoglobin becomes paramagnetic after losing oxygen molecules in the peripheral tissues due to exposure of its iron molecule. The paramagnetic deoxyhaemoglobin creates inhomogeneous magnetic field in its immediate vicinity. This inhomogeneous magnetic field increases T_2* decay and attenuates signal from regions containing deoxyhaemoglobin [321]. In practice, this means there is signal loss proportional to the amount of deoxyhaemoglobin in the red blood cells of the vessels of the tissue. Thus deoxygenated haemoglobin acts as an intrinsic contrast agent (see appendix II, page 373).

1.4.2.2.2 Validation

There is limited evidence on the validation of ISW-MRI technique. The partial pressure of oxygen in blood (P_aO_2) determines oxyhaemoglobin levels and remains in equilibrium with partial pressure of oxygen in tissues (pO_2). Clinical trials have reported good correlation between R_2* measurements and tumour hypoxia markers (needle oxygen measurement and immunohistochemical markers) [322, 323]. Several studies have reported an obvious decrease in baseline R_2* (at room air) after exposure to hyperoxygenation in various model and human tumours [324-330]. However, simultaneous measurement of tumour R_2* and pO_2 (by MR-compatible fibre-optic pO_2 sensor; OxyLite, Oxford Optronix) show R_2* signal response to oxygenation is temporally

correlated with changes in tumour pO_2 without any correlation between absolute R_2* and pO_2 measurements [331]. These finding suggest that carbogen induced reduction in R_2* signal indicates tumour oxygenation but additional techniques are required to obtain absolute tumour pO_2 measurements in vivo. Only 50-60% of human tumours show changes in R_2* after carbogen inhalation and one reason may be vessel quantity and perfusion mismatch in tumour tissue. Thus, ΔR_2* is also determined by vascular volume, which is dependent on tumour vessel size and maturation, that may also explain differential ΔR_2* changes after hyperoxic challenge in different tumours [332] and need for simultaneous measurement of tumour blood volume. Thus, hypoxic tumour with large blood volume will not only have raised R_2* but are more likely to response to carbogen. This will be reflected by large changes in R_2* and it is these hypoxic tumours that show positive radiosensitisation to carbogen. Neeman et al. [333] reported successful mapping of neovascularization and vascular maturation in tumour models validated by fluorescence microscopy. The role of ISW-MRI in monitoring angiogenesis is yet to be established in clinical trials.

Overall, aforementioned trials indicate a promising role of ISW-MR imaging as a biomarker of tumour oxygenation levels.

1.4.2.2.3 Clinical applications

Tumour hypoxia critically decreases efficacy of radiotherapy. ISW-MRI provides the potential to detect hypoxic tumours and predict radiosensitivity. The sensitivity of ISW-MRI parameters in predicting response to intervention has been explored in several pre-clinical studies [334-336] and clinical studies

on prostate tumour [337], brain tumour [327], breast cancer [338] and cervical cancers [339]. In a pre-clinical study, tumours with a fast baseline R_2* (hypoxic) that become well oxygenated after hyperoxygenation treatment (carbogen: 95%O_2, 5%CO_2) were more responsive to radiotherapy [334]. It has been hypothesised that tumours with measurable blood volume and relatively fast pre-treatment R2* may be relatively hypoxic compared to similar tumour exhibiting a slower basal R2* [340], and recent preclinical studies are supportive of this concept [341]. In a small clinical study, selective treatment of patients with head and neck cancer with ARCON regime (accelerated radiotherapy with carbogen and nicotinamide) based on pre-treatment R_2* and carbogen-induced changes in R_2* resulted in low tumour recurrence during long follow-up [327]. In another study on cervical cancers, the baseline R_2* values of tumour was significantly lower than post treatment values and showed negative correlation with final tumour size response but no association with final tumour volume response [339]. The evidence shows measurement of pre-treatment R_2* and ΔR_2* of tumour may contribute to the success of radiotherapeutic response and may ultimately prove prognostic.

1.4.2.2.4 Limitations

There is great variability and hence interpretation of R_2* between different tumour types that may be a confounding factor in ISW-MRI utility as a prognostic index for radiotherapy in practice. The site of the tumour and subsequent ability to optimize magnetic field will also strongly influence the basal R_2* measurements. The deoxyhaemoglobin induced resonance of water and hence R_2*, may not be homogenous as assumed with BOLD MRI.

Another MRI methodology, high spectral and spatial resolution (HiSS) – MRI of tumour has demonstrated that water resonance within each voxel is complex and often contain several resolvable components. In such situation where each of these spectral components can respond differently to, for example, carbogen, the changes in BOLD contrast can be difficult to detect, accurately measured and interpreted. However, it is yet to be shown if measurements of tumour R_2* by HiSS MRI yield superior prognostic value over those obtained by BOLD MRI [342].

1.4.2.3 Dynamic Contrast Enhanced (DCE) – MRI

The DCE-MRI method utilises the pharmacodynamics properties of low-molecular weight contrast agents to provide information about tissue blood volume and perfusion, microvessel permeability and the extracellular space (see appendix III, page 377).

1.4.2.3.1 Technology, Quantification and Interpretation

Clinical dynamic MRI is usually performed using low molecular weight gadolinium-chelate-based contrast agents (Gd; molecular weight <1kDa). When these contrast agents are used, two distinct phenomena can be observed, depending on the experimental set-up. Dynamic relaxivity-based contrast techniques use a rapid series of T1-weighted images to observe the passage of contrast media, usually resulting in tissue ‘brightening’; by default, this technique is referred to as DCE-MRI. This technique is sensitive to the presence of contrast medium both within vessels and in the extravascular-extracellular space - the latter predominates due to the low blood volumes in

tissues and tumours (approximately 5-10%). To enable quantification of signal intensity changes, it is also necessary to incorporate methods that allow the concentration of contrast agent to be obtained at each time point during the measurement period. For DCE-MRI, this is often done by obtaining “T1 maps” prior to contrast medium injection, which effectively allows conversion of the MR signal intensity into contrast agent concentration [343]. DCE-MR images can be analysed by quantitative model dependent or semi-quantitative (non-model dependent) methods. The parameters extracted provide information on blood flow, blood volume, microvessel permeability, extraction fraction, and on plasma and interstitial volumes (see appendix III, page 377).

1.4.2.3.2 Validation

DCE-MRI has been widely validated in the last decade in a number of ways, including direct correlative studies against immunohistochemical microvessel density measurements, and tissue expressions of pro-angiogenic growth factors including vascular endothelial growth factor (broad correlations in some studies and no correlations in others) [344, 345]. Tissue validation studies have also come from correlative studies against widely accepted surrogates of tissue perfusion including 14C-aminoisobutyric acid quantitative autoradiography [346]. More recently, in vivo correlative imaging studies have been performed. Thus, transfer constant as a marker of tumour blood flow has now been validated against blood volume/blood flow derived from Dynamic Susceptibility Contrast-MRI studies [347], (15) O-water PET [348] and microbubble ultrasound [349]. These cross imaging validation studies have shown that the relationship is not upheld in every tumour type (e.g., in

gliomas, because a variably intact blood brain barrier reduces the first pass extraction of the contrast agent [350]). Similarly, the strength of correlations also decreases when therapies that reduced microvessel permeability are used, again because the first pass extraction fraction of small molecular weight contrast agents is reduced. George et al [351] reported significant correlation between K^{trans} and serum VEGF/platelet level at the time of referral for preoperative NCRT or palliative chemotherapy in a series of 31 consecutive patients with T3/4 rectal cancer, although this was no longer the case after the treatment was commenced. This circulating marker of angiogenesis showed no association with any DCE-MRI parameter in another series of 12 rectal cancer patients proceeding directly to surgical resection, but tumour microvessel density was reported to correlate inversely with K^{trans} [191]. Although this is a small study, this apparently counterintuitive finding suggests that any relationship between K^{trans} and the degree of angiogenesis in rectal cancer is unlikely to be straightforward.

1.4.2.3.3 Clinical applications

All response assessment studies show that successful treatment results in decreases in the rate and magnitude of enhancement and that poor response results in persistent abnormal enhancement, however judged (semi-quantitatively or quantitatively). This general observation holds true for most therapeutic approaches except for radiotherapy where there is an initial increase in rate and magnitude of enhancement corresponding the recognized acute hyperaemic response probably mediated via release of cytokines including VEGF. Changes in DCE-MRI kinetic parameters are able

to predict response or monitor the effects of a variety of treatments including chemotherapy in bladder and breast cancers and bone sarcomas [352-355]. In breast cancer, for example, it has been shown repeatedly that progressive decreases in tumour K^{trans} accompanies response to chemotherapy and that an increase or no changes in permeability predict for non-responsiveness [353, 354]. Other treatments that can be monitored include radiotherapy in rectal and cervix cancers [356, 357] androgen deprivation in prostate cancer [358] and vascular embolization of uterine fibroids [359]. An important new application of DCE-MRI is in the early clinical development of therapies that target the tumour vasculature [360].

The effects of antiangiogenic drugs and vascular disruptive agents (VDAs) on DCE-MRI kinetic vascular parameters have been found to be similar with the dominant effect of successful therapy being reductions in blood flow and permeability. Importantly, it is the timing of the onset and duration of vascular changes that enables antiangiogenic drugs and VDA to be distinguished on imaging. Both xenograft and human imaging studies of antiangiogenic drugs show that antivascular effects are not immediate, arising at least 1-2 days post drug administration. In contrast, VDAs cause rapid shutdown of the vasculature within minutes to hours of drug administration and reversibility of effects being visible in the short term (usually seen within 24-48 hours). “Normalisation” of the vasculature induced by antiangiogenic drugs as described originally by Jain [361] can be detected on DCE-MRI by regional increases in non-enhancing pixels (representing vascular pruning) with

reductions in permeability and leakage space. Improved flow in non-pruned vessels can also be detected often in other regions [317, 362].

1.4.2.3.4 Limitations

There are uncertainties in the accuracy of kinetic parameter estimates derived from the application of tracer kinetic models in clinical DCE-MRI experiments. These derive from model-based assumptions and from assumptions made for the determination of tissue Gd-DTPA concentrations. For example, in the original implementation of Tofts' model, population based AIFs were used (although this is not a strict requirement) [363] and it was assumed that tissue blood volume contributes negligible signal compared with that arising from contrast medium in the interstitial space [364]. It was recognised by Buckley that the application of these model-based assumptions leads to systematic overestimation of the transfer constant in tumours [365]. Modern two compartment model implementations leave AIF choice to investigators and allow derivation of plasma volume fraction provided that AIF choice and temporal data sampling rates are appropriate. An important point is that the presence of gadolinium containing contrast medium is detected only indirectly, by its effect on tissue water (that is, the contrast medium itself is not detected). In tissues, contrast medium is confined to the extracellular space, whereas the bulk of water is intracellular. As a result, transmembrane water exchange can affect the accuracy of the tissue contrast agent concentration estimates [366, 367], which additionally needs to be taken into account.

1.4.2.4 Dynamic Contrast Enhanced (DCE) CT

The DCE-CT method utilises the pharmacodynamics properties of iodinated contrast agents to provide information about tissue blood flow, blood volume and microvessel permeability. The DCE sequence can be applied to standard CT scanners making it a widely available and low cost technique. DCE-CT has reached the technical maturity for use in therapeutic trials in oncology. Guidelines on the application of DCE-CT in clinical trials have been published in 2012 [368].

1.4.2.4.1 Technology, Quantification and Interpretation

The fundamental principle of perfusion CT is based on temporal changes in tissue enhancement after administration of intravenous iodinated contrast agent (see appendix II, page 373). The tissue enhancement after administration of intravenous contrast agent can be divided into two phases: during the initial phase, the enhancement is mainly attributable to contrast present within the intravascular compartment (40 to 60 seconds from the time of contrast arrival); during the second phase, the contrast has passed through capillary membrane into the extravascular compartment and the tissue enhancement results from contrast present in both intra- and extravascular compartments. Thus in the initial phase, the enhancement is determined to a great extent by blood flow (BF) and blood volume (BV), whereas in the later phase, it is influenced by vascular permeability to the contrast agent [369]. The tissue enhancement (unit: Hounsfield) is directly proportional to contrast agent concentration, facilitating kinetic modelling. Hence perfusion CT involves a succession of images before and during the passage of contrast

agent within the tissue vasculature of interest. There are a variety of perfusion CT protocols and are typically determined by target organ, clinical objective, CT scan configurations and mathematical modelling. The coverage area for the study depends on the CT scanner available (4, 16, 64, 128 or 320 multi-detector rows scanner are available variable coverage area). The initial localiser sequence involves an unenhanced CT acquisition with wide coverage of the organ of interest. The recommended protocol for contrast agent administration involves a small volume (40–70 mL depending on the contrast medium) at high flow injection rates (usually >4mL/s: 5mL/s for compartment model; 7–10mL/s for deconvolution model; see appendix IV, page 389) followed by 20-40mL of saline flush at a similar flow rate is needed to obtain a narrow bolus for optimal perfusion analysis [370]. The dynamic acquisition is performed sequentially after the intravenous injection of contrast agent and covers both phases of tissue contrast enhancement: the early phase capture requires high temporal sampling (less than 2 seconds: every 3-5 seconds for compartmental model; every 1 second for deconvolution model) and lasts up to 45 seconds followed by low temporal sampling required for the later phase (5-15 seconds per acquisition: every 10 - 20 seconds for compartmental model; every 10 second for 2 minutes for deconvolution model). The total time and sampling interval within the later phase is dependent on the mathematical model used [368, 371, 372]. The tube current also depends on the mathematical model used (higher tube current with lower image frequency to reduce image noise for compartmental analysis and low tube current with higher image frequency for dynamic acquisition) (see figure 1.9).

Figure 1.9: Acquisition sequence for DCE-CT

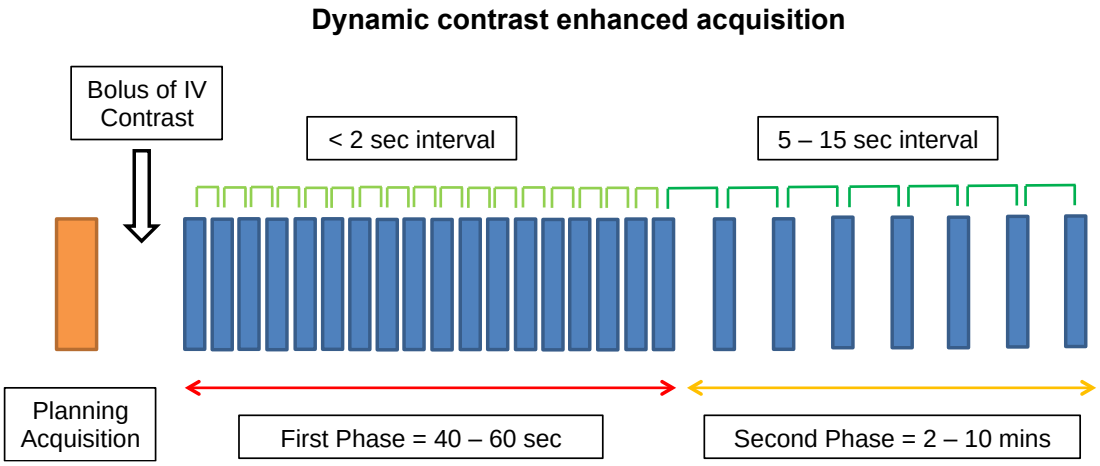

The time-intensity curves obtained can be checked qualitatively to distinguish between normal and diseased tissue. The quantitative parameters obtained through fitting of tissue contrast enhancement curve (time-intensity curve) into any mathematical model include (i) regional BF (which expresses the rate of delivery of oxygen and nutrients), (ii) tumour BV (representing the volume of the vascular network that is functional) and (iii) permeability-surface area product (which describes the rate of constant leakage into the extracellular space [373].

1.4.2.4.2 Validation

The DCE-CT parameters of microcirculation have been validated against various techniques. For example, DCE-CT produced similar assessment of microcirculation compared to Xenon CT for brain ischaemia [374], (15)O-water PET for solid tumours [375] and immunohistochemical MVD for brain tumours, lung cancer, adrenal tumour, prostate cancer and oesophageal cancers (immunohistochemical staining for MVD, VEGF) [376-380]. For colorectal cancer, however, there are conflicting reports on association of

DCE-CT parameters and MVD in published literature: whilst majority of the studies show no association between DCE-CT and histopathological markers of angiogenesis in colorectal cancers [381-383], some have found a significant correlation [384]. Reproducibility studies have shown good correlation between DCE-CT measurements with variability of 13–30% in studies involving normal brain tissue, colorectal cancer, lung cancers and hepatocellular carcinoma [385-388].

1.4.2.4.3 Clinical applications

The DCE-CT has been successfully applied in combination with standard imaging to differentiate between benign and malignant lesions [377], histopathological differentiation [389, 390], tumour grading [391, 392] and tumour staging [393-395]. Qualitative analysis showing early peak enhancement (high BF and BV) can differentiate malignant from benign tumours [390]. High perfusion values are commonly seen in malignancies [390, 396, 397], however, in advance tumours, where growth exceeds blood supply, lower perfusion parameters were also seen [381, 397]. Some tumours with low baseline perfusion also show early nodal involvement [377, 398]. Hence DCE-CT can provide vital insight into tumour behaviour.

The DCE-CT has been applied in response assessment of chemotherapeutics. After standard chemoradiotherapy, a decrease in all DCE-CT parameters has been reported in cancers of aerodigestive tract [399], lung [400], oesophagus [401], liver [402] and rectum [403-405]. However, as with DW-MRI, where a decline in ADC is seen due to cell oedema immediately after radiotherapy, the DCE-CT parameters may also

show a transient increase immediately after radiotherapy attributable to inflammatory reaction and endothelial cell death [406, 407].

A more popular application of DCE-CT has been in the early physiological response assessment to novel anti-angiogenic agents. The DCE-CT has been used to monitor response in rodent studies on cancers of breast [408], colon [409] and clinical studies on cancers of head and neck [410], liver [411, 412], kidneys [413], lung [400] and various solid tumours [414] and in clinical study on metastatic renal cancer [415] . The common response to anti-angiogenic treatment is a decrease in BV and BF values (or equivalent parameters derived from other mathematical models), whilst, changes in other parameters are more variable [400, 414, 416, 417]. Interestingly, some anti-angiogenic agents, such as VEGFR blockade of tumour, may cause transient normalization of tumour vascular structure and function causing an increase in BF and PS vales initially, a circumstance that may hide the real effect of these drugs [418], whereas, vascular disruptive agents, such as A4 phosphate, has shown an abrupt reduction in BV within 4 hours of its administration [419]. Hence, the timing of imaging acquisition after administration of chemotherapeutics will affect the values of DCE-CT parameters and should be taken into account when designing such studies.

1.4.2.4.4 Limitations

The major limitation of DCE-CT includes image acquisition effects, post-processing discrepancies, radiation dosage and contrast load. Motion artefact due to breathing and bowel peristalsis can degrade image quality; such artefacts can be minimised by vocal instruction during image acquisition, use

of spasmolytic agents and motion correction software. Reproducibility and observer variability of has been addressed in earlier studies and proved DCE-CT parameters analysis to be reproducible in body tumours [387] with good intra- and inter-observer variability [386]. The perfusion parameters are sensitive to ROI, arterial input and mathematical models. Care should be taken to avoid sampling error; AIF should be derived from large arteries to avoid averaging from surrounding tissues that will lead to over-estimation of BF[370]; variation in commercial software and different mathematical model has shown a discrepancy of up to 44% between parameter values and difficulties in interplatform or intermodal comparisons [420-422]. There is risk of high radiation exposure, especially for patients requiring serial acquisitions; techniques including reduced tube current, tube potential and alteration in protocols such as scanning every 2-3 seconds instead of every 1 second during high temporal sampling, limiting coverage, first pass analysis only (if BF or MTT are required only) can help reduce irradiation exposure. Lastly, adequate cautions should be taken to prevent contrast-induced nephropathy.

1.4.2.5 Author's conclusion on functional imaging techniques

In conclusion, DW-MRI is the only functional imaging modality thus far with immediate impact on clinical decision making. The use of DW-MRI to investigate liver metastasis and residual rectal cancer after NCRT is gaining momentum at multidisciplinary team meetings. The reason for popularity of DW-MRI include readily available technology, for example, MRI scanners and software in everyday use can be configured to produce DW images and generate ADC. In addition, the calculation and interpretation of ADC is directly related to actual tissue microarchitecture and does not require derivation from complex mathematical models which makes it adoptable and less prone to error and discrepancy.

The lack of consistency in various components of DCE imaging has limited the success of this technology in clinical practice. Investigators in the field have used various image acquisition methods, especially designed experimental software not readily available, different mathematical models to derive DCE parameters and used different DCE parameters to interpret dynamic perfusion. Toft et al [423] have addressed this problem by promoting common nomenclature amongst investigators. Hence, despite the origin of DCE technology more than a decade ago, it still remains in its rudimentary stages with most useful application in rodent experiment for anti-angiogenic drug development.

The use of ISW-MRI techniques to detect tumour hypoxia and direct therapy largely remains experimental. The value of R_2* doesn't purely depend on tissue hypoxia and other factors such as vascular volume, vessel size and

maturation also play a role. Hence, this technology requires further evaluation before we would know the capacity of its application.

2 CHAPTER 2: HYPOTHESIS AND AIMS

2.1 Hypothesis

1. We believe that effects of NCRT are time-limited and aggressive rectal cancers can overcome the effects of NCRT after certain time by repairing their DNA and re-generating functional vascularity
2. We believe that after NCRT, there are functional changes in rectal cancer tissues, such as cellularity, hypoxic foci and functional vascularity, which may be detectable with functional imaging techniques.
3. We believe that baseline and changes after NCRT in DNA repair properties, cellularity, hypoxic foci and functional vascularity may affect clinical outcomes

2.2 Project Aims

2.2.1 Primary aims

We aim to establish the optimal interval between NCRT and surgery based on DNA repair properties and functional vascular changes in rectal cancers

2.2.2 Secondary aims

1. We aim to quantify DNA repair properties of rectal cancers at baseline and changes during the period between NCRT and surgery by comet assay technique
2. We aim to quantify tissue cellularity, hypoxic foci and functional vascularity at baseline and changes during the period between NCRT and surgery by functional imaging techniques
3. For studies on functional imaging, we also aim to quantify observer agreement for functional MRI and CT techniques and effects of volume coverage for functional CT techniques for rectal cancers.
4. We aim to identify patterns in measured parameters that may help recognise patient at risk of treatment failure.

3 CHAPTER 3: STUDY DESIGN

3.1 Introduction

This prospective observational study is designed to investigate the mechanisms of tumour response in rectal cancer during NCRT and the subsequent interval to surgery, focusing on radio-sensitivity and angiogenesis. It was intended to provide information that may help risk-stratify patients for individualised treatments including optimal timing of surgery. It does not involve any alterations to the actual treatment of study patients.

3.2 Patients population

Adult patients with locally advanced, non-metastatic rectal cancer, who were considered suitable for neoadjuvant chemoradiotherapy, were offered to participate in the study. This population included all consecutive patients treated at Mount Vernon Cancer Centre, a tertiary oncology unit covering five District General Hospital in Northwest London Cancer Network. The patients were recruited during the period May 2009 until May 2012.

3.3 Inclusion criteria

1. Histologically proven adenocarcinoma of the rectum within 15cm of the anal verge.
2. Preoperative chemoradiotherapy indicated by virtue of either: (a) a locally advanced (T3/T4) tumour which threatens the anticipated surgical resection margins (i.e. within 2 mm of mesorectal fascia), based on a

combination of clinical and MRI assessment; or (b) MRI evidence of extramural vascular invasion or lymph node involvement.

3. Fulfilment of all other existing inclusion criteria for long-course preoperative NCRT with or without additional biological agents.
4. WHO performance status 0 or 1.
5. Able to comply reliably with protocol by attending for serial assessments.
6. Written informed consent.

3.4 Exclusion criteria

1. Previously treated rectal adenocarcinoma.
2. Previous radiotherapy to pelvis.
3. WHO performance of status of 2 or more.
4. Specific exclusion criteria is mentioned in individual chapters

3.5 Long-term follow-up

Patients were to reviewed as outpatients at 6, 12, 24 and 36 months after completion of NCRT, as isstandard follow-up, for the purposes of recording crude data regarding disease recurrence and survival.

3.6 Experiment design to analyse biological behaviour of rectal cancer cells

Experiments were designed to investigate patient's rectal cancer cell behaviour in response to NCRT. In order to obtain detailed information about the dynamic changes occurring within the cell DNA and surrounding microenvironment, serial tests were undertaken to analyse cell DNA repair pattern, tumour vascular

morphology, blood flow and blood oxygenation levels. The experiments included:

1. Single cell gel electrophoresis (comet) assay of rectal cancer cells to assess DNA repair function (radio-resistance)
2. Perfusion CT to determine tumour blood flow, blood volume and perfusion
3. MRI assessment of tumour pathophysiology. Multi-parametric analysis included following MRI protocols:
    a. Dynamic Contrast Enhanced MRI: to assess microvascular physiology
    b. Diffusion-weighted MRI: to determine tumour cellularity
    c. Intrinsic susceptibility contrast MRI: to determine changes in tumour blood oxygenation levels

3.7 Schedule of serial tests

Serial tests are undertaken at specific time-point during the treatment timeline to assess dynamic changes in rectal cancers (see figure 3.2).

Figure 3.2: Schedule of serial assessments

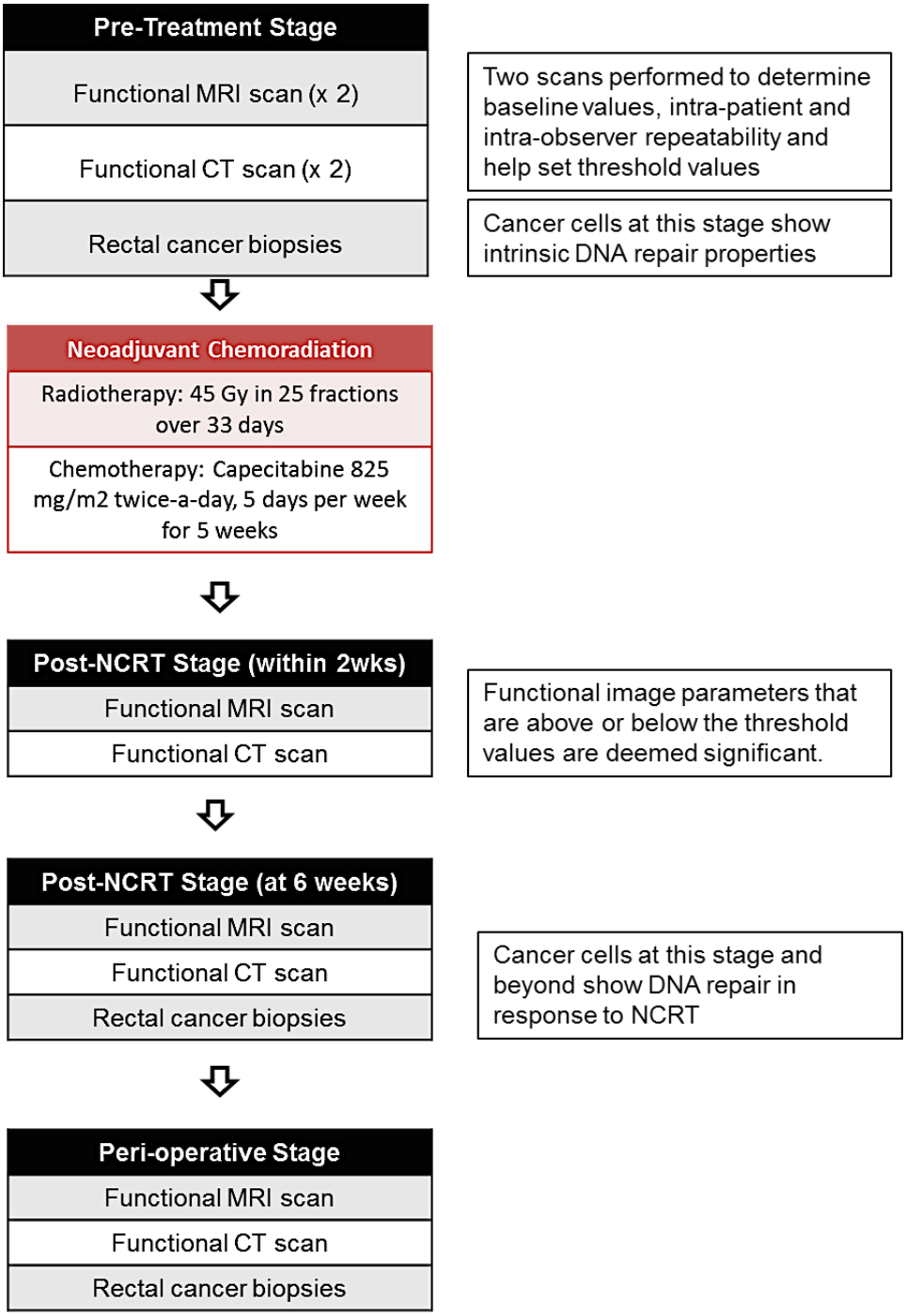

3.8 Regulatory Issues

3.8.1 Ethical considerations

Those recruited into this study were to undergo additional MRI scans and CT scans. Each CT scan will involve exposure to an estimated 7mSv (maximum

8.5mSv), which should be considered in the light of the 45Gy prescribed as standard treatment.

The 2 sets of serial rectal biopsies taken while patients are awake may cause discomfort, but the risks of serious complications (e.g. perforation) are negligible and these procedures are already a routine part of patient care, albeit less frequently than in this study. The main inconvenience to participants is likely to be the additional attendances required to perform the various procedures.

The study was approved by Hertfordshire/Bedfordshire Research Ethics Committee. The study was conducted in accordance with the recommendations for physicians involved in research on human subjects adopted by the 18th World Medical Assembly (Helsinki, 1964) and later revisions.

3.8.2 Informed consent

Verbal and written information on the study, including objectives, procedures and the risks involved, were provided to each patient, who were required to give signed consent after sufficient time for consideration. The right of the patient to refuse to participate at any stage will be respected, with no obligation to provide a reason for doing so. All patients were informed of their right to withdraw from the study at any time without risk of prejudicing their treatment.

3.9 Violation of protocol

All recruited patients did not undergo all components of proposed protocol, for example, one patient was taken out of the study after metastatic disease was found on two baseline scans, one patient did not consent for serial biopsy but proceeded with serial imaging, whilst two patients declined participation after

completing baseline and immediate post-NCRT scans. Therefore, despite recruiting 17 patients, the three experiments have different study population and this has been specified in relevant chapters.

4 CHAPTER 4: DNA REPAIR ANALYSIS

Measurement of radiosensitivity and its impact on clinical outcomes – The DNA repair analysis of locally advanced rectal cancer cells

4.1 Introduction

The standard treatment of locally advance rectal cancers (LARC) involves long course fluoropyrimidine-based neo-adjuvant chemoradiotherapy (NCRT) followed by TME surgery after an interval. The response to NCRT for similar staged locally advanced rectal cancers varies between patients: whilst in some patients the tumour completely disappears, others show stable or progressive disease. A good response to NCRT improves long-term clinical outcomes as evidenced by lower recurrence rates and longer survival [238]. Patients who achieve pathological complete response have improved long-term outcomes in terms of excellent local control rates and this is independent of their initial clinical T and N stages [424, 425]. Mostly European trials report a clinical downstaging in the range of 50-60% including complete pathological response in 13-20% after NCRT. Hence a large cohort of patients is subjected to toxic NCRT without any benefit. To date, little is known about the molecular basis for such heterogeneous response to NCRT. Therefore, recent studies have focused on prognostic stratification based on rectal tumour biology and proposed the need for individualised treatment regimes.

A simple measure, such as, increasing the interval to surgery after NCRT has shown to increase response rates in patients [239]. However, the exact duration

of radiotherapy-induced continued cell death after completion of NCRT remains unknown. Cell death in response to radiotherapy is a complex process that also depends on the integrity of cell DNA repair and apoptosis pathways. It may be hypothesised that radiosensitive tumour load is eliminated during or immediately after radiotherapy leaving behind relatively radioresistant residual tumour cells. The progressive downstaging seen in some rectal cancers with increased interval to surgery may be due to continued apoptosis of residual tumour cells unable to repair DNA damage. In contrast, rectal cancers that remain stable or show progressive disease may overcome irradiation-induced DNA damage by re-populating tumour with cells harbouring upregulated DNA repair mechanisms. Hence, the assessment of intrinsic radiosensitivity by measuring DNA damage and repair profiles of rectal tumour cells may help determine outcomes of therapy and individualise treatment protocols.

The single cell gel electrophoresis (Comet assay) is an established technique to assess DNA damage induced by clinically relevant doses of radiation [248]. While many of the clinical studies employing the comet assay have utilised lymphocytes, the technique has also been performed on cells obtained by fine needle aspiration of a variety of accessible primary and metastatic tumours, including colorectal cancer [262, 266, 268].

To date there have been no reports on the application of the comet assay to predict response of individual rectal cancers to radiotherapy. Hence, the aims of this experiment are as follows: (1) to assess the feasibility of conducting comet assay on fresh rectal cancer samples, (2) to investigate baseline DNA damage and DNA repair profiles of rectal cancer cells subjected to long course

neoadjuvant chemoradiotherapy (NCRT) and determine the duration of impaired DNA repair after irradiation, and (3) to investigate any relation between rectal cancer radiosensitivity and clinicopathological markers and long-term outcomes.

4.2 Methods

4.2.1 Patient population

See chapter 3 for detail of patient population. Additional exclusion criteria were inability to undergo biopsy without sedation/anaesthesia (n=1; post-NRCT grade III perianal pain); metastatic disease (n=1; metastatic liver disease)

4.2.2 Patient Compliance and Exclusions

Thirty-two patients were screened; 17 patients consented to participate in the study. Pre-treatment biopsy was successfully obtained from 16 patients: 1 patient declined to give a biopsy. Post-NCRT biopsy was successfully obtained in 12 patients: one patient was excluded from study due to finding of metastatic disease; one patient declined further participation in the study; two patients declined to give biopsy due to severe rectal pain. Pre-operative biopsy was successfully obtained in only 6 patients: one patient died due to cause unrelated to rectal cancer or treatment; two patients declined biopsy; in three patients the operating surgeon could not obtain pre-operative biopsy due to technical reasons. There were further exclusions at the biopsy processing stage. Patient and data available for analysis is presented in table 4.1.

CHAPTER 4: DNA REPAIR ANALYSIS

Table 4.1: Patient compliance and exclusions

Code		T_0	T_1	T_2	Reason for exclusion
1	RY	✓	✓	✓	First biopsy was lost during transfer
2	DG	✓	✓	✓	
3	DJ	✓	X	X	Excluded from study metastatic disease
4	AH	✓	✓	✓	
5	KB	✓	X	✓	Declined biopsy at T_1
6	ED	✓	✓	X	Declined further participation
7	AF	✓	✓	X	Biopsy sample not viable
8	JN	✓	✓	X	Biopsy sample not viable
9	SD	✓	✓	X	Patient died after NCRT
10	JH	✓	✓	X	Biopsy sample not viable
11	DP	✓	X	X	Declined participation after NCRT
12	GA	X	X	X	Declined participation for biopsy
13	PO	✓	✓	X	Biopsy sample not viable
14	MM	✓	✓	X	Biopsy sample not viable
15	RC1	✓	✓	✓	
16	RC2	✓	X	✓	Declined biopsy at T_1
17	JT	✓	✓	✓	
Biopsy Completed		16	12	7	
Included in Study		**13**	**11**	**6**	

'✓' – completed experiment and included in analysis, '✓' – completed experiment but not included in analysis; 'X' did not complete experiment;

4.2.3 Single Cell Gel Electrophoresis (Comet Assay) of rectal cancer cells

The procedure was performed according to standard operating procedures developed within the laboratory of Professor John Hartley [426]. All procedures were carried on ice and subdued lightening. All chemical used were from Sigma Chemical (Poole, United Kingdom) unless otherwise stated. The steps are as follows:-

4.2.3.1 Rectal cancer biopsy and preparation of single cell suspension

Serial samples of rectal cancer tissue were obtained at three stages

(i) Pre-treatment (T_0)

(ii) Post-NCRT (T_1)

(iii) Pre-operative (T_2)

Rectal cancer tissue biopsy was obtained using a rigid sigmoidoscopy or a proctoscopy and disposable biopsy forceps (Stericom ®, Chesham, UK). Single cell suspension is prepared under sterile conditions within a laboratory hood. Freshly harvested tumour tissue was immediately soaked in a few drops of RPMI 1640 medium and finely chopped using surgical scalpel (blade size 11) to release single rectal cancer cells embedded in connective tissue. Once all solid tissue had been chopped, the sample was transferred into a conical tube and suspended in additional RPMI 1640 medium to reach a total volume of 10mL. The mixture was centrifuged at 200 g for 5 minutes at 4^{o}C. The rectal cancer cells accumulated at the bottom of the tube and were aspirated using a pipette. The rectal cancer cells were then mixed with freezing mixture (fetal calf serum with 10% DMSO, 2ml divided in 2 cryovials) and stored at - 80^{0}C until analysis.

4.2.3.2 Cell count, viability and histopathological assessment

At the time of analysis, the mixture of rectal cancer cells in freezing mixture was thawed on ice. Once thawed, the mixture was assessed for the presence of cancer cells, cell count and cell viability. In the first instance, cell count was performed using standard haemocytometer followed by Trypan Blue® test for cell viability. A portion of sample was saved for histopathological assessment to

ascertain presence of cancer cells, whilst another portion was diluted in tissue culture medium to achieve a concentration of 2.5 x 10^4 cells per mL and divided into seven aliquots as below (see figure 4.1). One sample was taken as 'control' and not irradiated. The other samples were all irradiated *ex-vivo* using 15Gy of radiation (AGO HS X-ray system 320kV, AGO Xray limited, Yeovil, UK) to introduce a fixed level of random DNA single strand breaks, followed by serial comet assays at six time points to assess the DNA repair over 2 hours (see figure 4.1). The control and 1st irradiated aliquot are assayed at '0' time point (T_0) (immediately after irradiation), the remaining samples were incubated at 37ºC for the appropriate post-incubation time.

Figure 4.1: Experiment design of timed comet assays

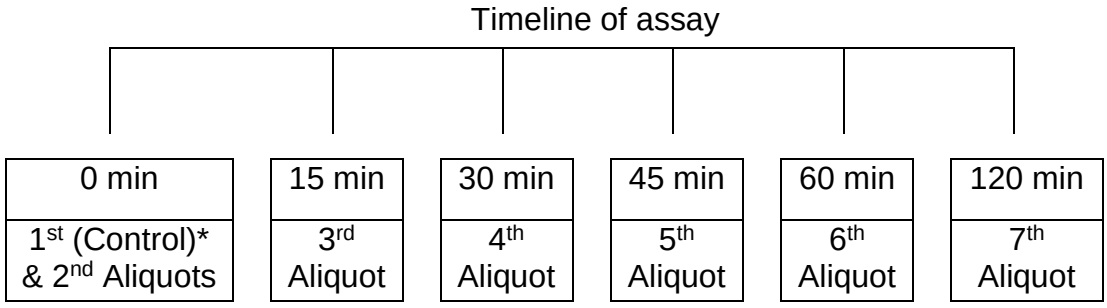

*Control is not irradiated

The histopathological assessment was conducted separately at a later time. During this process, the rectal cancer cells and residual tissue are isolated after centrifuge and smeared onto a slide followed by fixation and standard haematoxylin-eosin staining. A consultant histopathologist examined the fixed specimen and determined presence of rectal cancer cells.

4.2.3.3 Preparation of slides and electrophoresis:

After irradiation, the cells were embedded in 1% low gelling temperature agarose on a pre-coated microscope slide and lysed for 1 hour in ice-cold lysis buffer (100mM disodium EDTA, 2.5M NaCl, 10MM Tris-HCl, pH 10.5) containing 1% Triton X-100 added immediately before use in assay and then washed every 15 minutes in distilled water for 1 hour. Slides were then incubated in alkali buffer (50mM NaOH, 1mM disodium EDTA, pH 12.5) for 45 minutes, followed by electrophoresis in the same buffer for 25 minutes at 18V (0.6 V/cm), 250 mA. The slides were finally rinsed with neutralizing buffer (0.5M Tris-HCl, pH 7.5) then saline and left to dry overnight. After drying, the slides were stained with propidium iodide (2.5 μg/mL) for 30 minutes then rinsed in distilled water and dried.

4.2.3.4 Image analysis and quantification of tail moment

The images were visualised on NIKON inverted microscope with high-pressure mercury light (NIKON UK Limited, Kingston-Upon-Thames, United Kingdom), 510–560nm excitation filter, and 590 nm barrier filter at x20 magnification. Images were captured by using an on-line charge-coupled device (CCD) camera and analysed by using Komet Analysis software (Version 6.0, Andor Technology, Belfast, Northern Ireland). For each duplicate slide 15 cells are examined (total 30 cells). The tail moment for each image was calculated by using the Komet Analysis software as the product of the percentage DNA in the comet tail and the distance between the means of the head and tail distribution (measured in ‘μm’), based on the definition by Olive et al [249] (see figures 4.2 and 4.3).

Figure 4.2: Measurement of tail moment as defined by Olive et al.

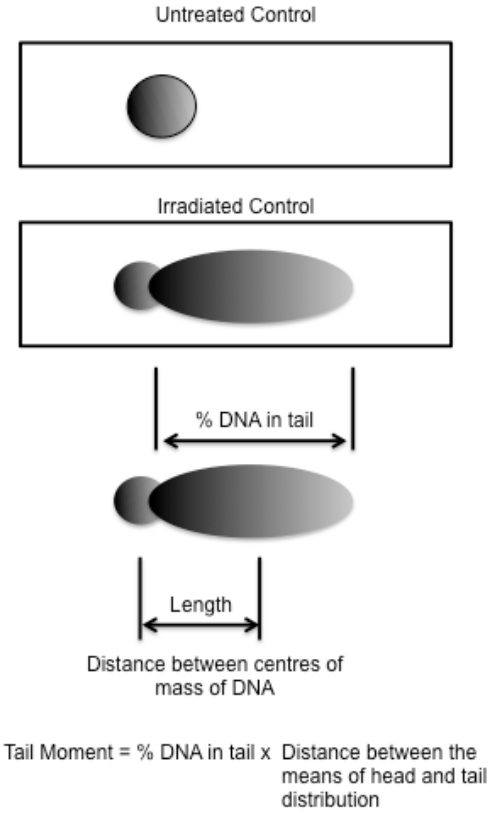

CHAPTER 4: DNA REPAIR ANALYSIS

Figure 4.3: Typical comet images of rectal cancer cells after exposure to 15 Gy *ex vivo* irradiation

	Pre-Treatment	Post-NCRT	Pre-Operative
T_0	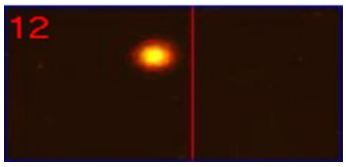	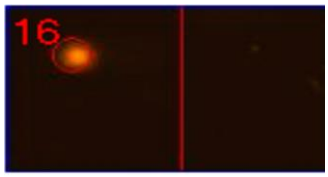	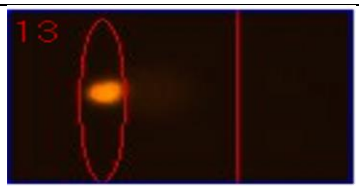
T_{0X}	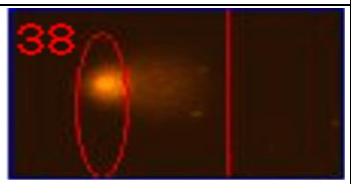	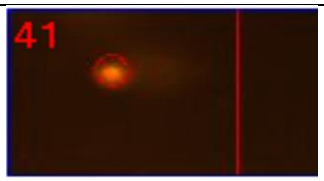	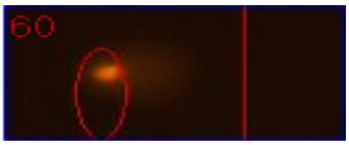
T_{15}	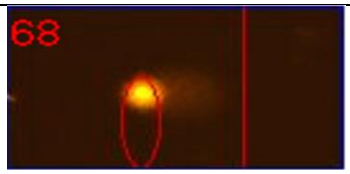	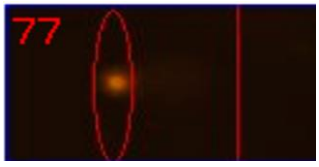	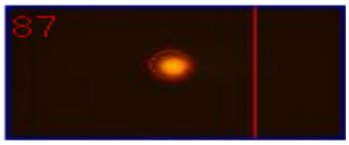
T_{30}	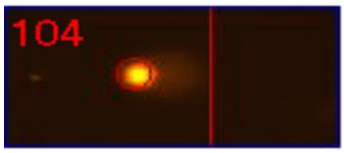	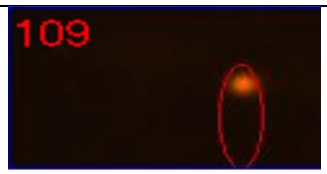	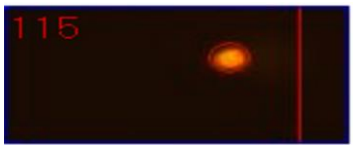
T_{45}	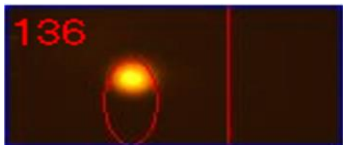	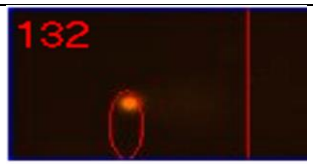	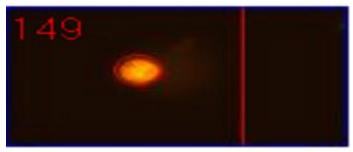
T_{60}	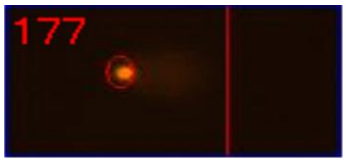	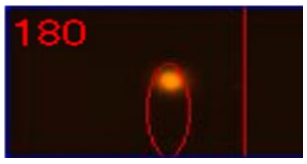	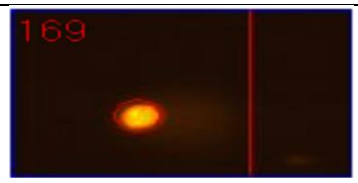
T_{120}	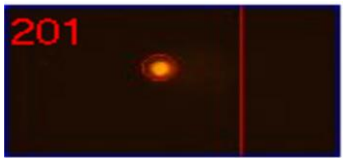	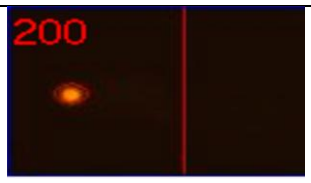	

T (subscript) – timing of biopsy (serial number); T_0 – Control; T_{0X} to T_{120} – samples exposed to 15 Gy ex vivo irradiation

4.2.4 Definition of terms

The 'Control' is the aliquot of tumour cells not exposed to *ex vivo* irradiation. Hence the control for pre-treatment cancer cells represents native tumour tissue. 'Complete response' is defined as TM values at 120 minutes assay to be below or within the 95% confidence interval of baseline TM value. 'No response' is defined as TM measurements at the 120 minutes assay to be above the 95% confidence interval of baseline TM value (see table 4.21).

4.2.5 Statistical Analysis

The distribution of measurement was checked for normality with Shapiro-Wilk test and Q-Q plots. The tail moment is reported with standard deviation and standard error as calculated by Komet software (version 6.0, Andor Technology, Belfast, Northern Ireland). The percentage change is used to elaborate DNA tail moment changes after ex vivo irradiation. The percentage change was calculated as follow:

$$\frac{TM\ at\ serial\ time\ points - TM\ for\ control}{TM\ for\ control} \times 100$$

where, '*TM'* is tail moment, '*TM for control*' is the non-irradiated sample, '*TM at serial time points'* include '0' min', '15 min', '30 min', '45 min', '60 min' and '120 min'. The comparisons between TM measurements at different time-points were compared with Wilcoxon signed rank test. Any significant difference in serial samples was assessed by Friedman tests. The association between DNA repair pattern and clinical outcomes was assessed by Spearman rho correlational (for non-parametric data) and Chi-squared or Fisher exact tests. All statistical

analysis was conducted using IBM® SPSS® statistical software (version 22.0, 2014; USA).

4.3 Results

4.3.1 Patient population

Patient characteristics, tumour staging and long-term outcomes are given in table 4.2. Most patients had locally advance rectal cancer with nodal involvement and only one patient had T4 disease without any nodal disease on pre-treatment MRI staging. All patient tolerated NCRT bar one patient who suffered coronary artery syndrome secondary to capecitabine, but completed the long-course radiotherapy. One patient died during the interval between NCRT and surgery due to factors unrelated to rectal cancer. Two other patients declined surgery after complete response seen on 6 weeks post-NCRT MRI scan. The mean interval between completion of NCRT and surgery was 12.3 weeks.

4.3.2 Clinical Outcomes

The majority of patients (87%) showed tumour downstaging (see table 4.2). There was statistical significant T (p 0.004) and N (p 0.002) downstaging between pre- and post-NCRT upon tumour stage assessment (see table 4.3). Three patients (20%) had complete response: two patients showed complete response on post-NCRT MRI scans and declined surgery, whilst another patient showed pathological complete response on surgical specimen. In only two patients there was neither T- nor N- downstaging after NCRT: both patients

developed distant recurrence within the follow-up period as a result of which one patient died. The median follow-up was 31 months. During this period, one patient developed local recurrence and two patients developed distal metastasis. One patient was successfully treated from rectal cancer but later developed pancreatic cancer and died from pancreatic cancer metastasis. Including the latter case there were a total of three deaths; one patient died as a result of distant recurrence whilst another died of a cause unrelated to rectal cancer. The mean survival time was 47.6 months (95% CI 40.3 to 54.9 months) in this cohort.

Table 4.2: Patient characteristics, tumour staging and long-term outcomes

Code		Gender	Age	cTNM	NCT	NRT	TME	ypTNM	Local Recurrence	Distant Recurrence	Death
1	RY	M	59	T3N1M0	✓	✓	✓	T3N0			
2	DG	M	52	T3N1M0	✓	✓	✓	T3N1		✓: Lung	✓
3	DJ*	M	72	T3N1M2	-	-	-	-	-	✓: Liver	✓
4	AH	M	74	T3N2M0	✓	✓	✓	T2N1			
5	KB	M	78	T3N1M0	✓	✓	✓	T2N0			✓
6	ED	F	72	T3N1M0	✓	✓	✓	T1N0			
7	AF	F	60	T3N1M0	✓	✓	✓	T2N0			
8	JN	M	79	T3N2M0	X	✓	✓	T2N0	✓		
9	SD**	M	71	T3N1M0	✓	✓	-	-			✓
10	JH	M	67	T3N0M0	✓	✓	✓	T3N0		✓: Pancreas	✓
11	DP	M	58	T3N1M0	✓	✓	✓	T2N0			
12	GA***	M	53	T2N2M0	✓	✓	X	-			
13	PO	F	59	T3N2M0	✓	✓	✓	T3N2		✓: Liver	
14	MM***	F	78	T4N0M0	✓	✓	X	-			
15	RC1	M	76	T3N1M0	✓	✓	✓	T2N0			
16	RC2	M	56	T3N1M0	✓	✓	✓	T0N0			
17	JT	F	79	T3N1M0	✓	✓	✓	T3N0			

**Diagnosed with liver metastasis on baseline scans; **Died after NCRT due to cause unrelated to rectal cancer; ***Had complete response on post NCRT MRI scan and declined surgery. Prefix 'c' – clinical; yp – post-NCRT; TNM – Tumour, Node, Metastasis staging; NCT – neoadjuvant chemotherapy; NRT – Neoadjuvant radiotherapy; TME – total mesorectal excision surgery;* ✓-completed; X – not completed.

Table 4.3: T- and N- downstaging after NCRT

		Post-NCRT Staging				
		T0	**T1**	**T2**	**T3**	**Total (%)**
Clinical Staging	**T2**	1*				1 (6.6%)
	T3	1	1	6	5	13 (86.6%)
	T4	1*				1 (6.6%)
	Total (%)	3 (20%)	1 (6.6%)	6 (40%)	5 (33.3%)	**p =0.004****
		N0	**N1**	**N2**	**Total (%)**	
	N0	1			1 (6.6%)	
	N1	8	1		9 (60%)	
	N2	2 + 1*	1	1	5 (33.3%)	
	Total (%)	12 (80%)	2 (13.3%)	1 (6.6%)	**p = 0.002****	

**On 6 weeks post-NCRT MRI scan*

***Wilcoxon signed rank test*

4.3.3 Response Evaluation Criteria In Solid Tumour (RECIST)

According to RECIST criteria: at the immediate post NCRT stage, there were 10 partial responders and 5 with stable disease; at post-operative stage, three partial responders progressed to complete response (see table 4.5).

Table 4.5: RECIST Criteria of Tumour response

Code		cL (mm)	nL (mm)	pL (mm)	nRECIST
1	RY	85	46	20	PR
2	DG	49	26	35	PR
3	DJ*	-	-	-	-
4	AH	34	34	25	SD
5	KB	53	40	32	SD
6	ED	37	20	20	PR
7	AF	77	19	15	PR
8	JN	57	40	36	PR
9	SD	55	42	-	SD
10	JH	61	60	10	SD
11	DP	60	-	60	-
12	GA*	54	38	-	PR
13	PO	30	13	10	PR
14	MM*	37	30	-	SD
15	RC1	62	33	20	PR
16	RC2	75	30	0	PR
17	JT	34	20	25	PR

** Treated as Complete responders on later MRI scans; prefix 'c' – Clinical; prefix 'p' – pathological; prefix 'n' – post-NCRT; PR – Partial response; SD – stable disease; CR – complete response*

4.3.4 Cell count, viability and histopathology

In general, most completed slides showed frequent dead cells with debris. However, there was adequate number of viable cells for comet assay (>50% cell viability in all samples). The histopathology analysis (conducted by a Consultant Pathologist) confirmed the presence of cancer cells in all samples.

4.3.5 Combined results:

4.3.5.1 Effects of long course NCRT on rectal cancer cells

In general, the biopsy specimen taken at the pre-treatment stage showed a slightly damaged baseline DNA in tumour cells (median baseline TM 5.47μ, see table 4.6 and figure 4.4), indicating presence of volatile and damaged cells that frequently compose solid cancers.

After long course NCRT, there was significant increase in the DNA damage as quantified by tail moment (mean TM= 6.94 vs 5.12, p=0.01, see table 4.7 and figure 4.4), indicating lasting effects of chemoradiotherapy with increased in damaged and necrotic cell within surviving fraction of rectal cancer.

The tumour cells obtained at the preoperative stage show return of DNA damage to the pre-treatment levels (pre-treatment cell mean TM=5.98 vs pre-surgery TM=5.76, p=0.71, see table 4.7), indicating either elimination of damaged cells or enhance DNA repair capability of surviving fraction in the interval between NCRT and surgery.

CHAPTER 4: DNA REPAIR ANALYSIS

Table 4.6: DNA Tail Moment values of rectal cancer cells before and after treatment with long course NCRT

Code		Pre-Treatment (T_0)	Post-NCRT (T_1)	Pre-Operative (T_2)	Statistical significance
		TM [µm] (SD; SE)	TM [µm] (SD; SE)	TM [µm] (SD; SE)	
2	DG	4.44 (2.83; 0.51)	6.90 (2.4; 0.43)	11.23 (7.69; 1.4)	
4	AH	5.50 (2.5; 0.45)	5.57 (2.52; 0.46)	4.41 (1.91; 0.34)	
5	KB	13.92 (6.02; 1.1)	-	7.25 (4.12; 0.75)	
6	ED	6.72 (3.09; 0.56)	7.03 (2.84; 0.52)	-	
7	AF	3.81 (2.68; 0.49)	3.90 (2.62; 0.47)	-	
8	JN	6.23 (2.94; 0.53)	7.46 (4.06; 0.74)	-	
9	SD	3.51 (3.47; 0.63)	9.50 (2.56; 0.46)	-	
10	JH	4.50 (2.39; 0.43)	7.38 (1.55; 0.28)	-	
13	PO	6.53 (2.28; 0.41)	7.77 (2.82; 0.51)	-	
14	MM	5.05 (2.39; 0.43)	9.32 (3.56; 0.65)	-	
15	RC1	5.47 (3.28; 0.60)	8.15 (2.47; 0.45)	3.49 (1.84; 0.33)	
16	RC2	5.47 (3.02; 0.55)	-	3.76 (2.45; 0.44)	
17	JT	4.57 (9.36; 1.71)	3.31 (2.77; 0.50)	3.91 (1.73; 0.31)	
Mean		5.82	6.94	5.68	0.779*
Median		5.47	7.38	4.16	
SD		2.52	1.88	2.78	
SE		0.69	0.56	1.13	
Minimum		3.51	3.31	3.49	
Maximum		13.92	9.50	11.23	

TM – Tail moment; SD – Standard Deviation; SE – Standard error; T (subscript) – timing of biopsy (serial number); Statistical Tests: Friedman Test ; p – statistical significance of <0.05*

CHAPTER 4: DNA REPAIR ANALYSIS

Table 4.7: Comparison of DNA Tail Moment values of rectal cancer cells before and after treatment with long course NCRT

Comparison	n	Mean TM [µm] (SD; SE)		Statistical significance*
T_0 vs T_1	11	5.12 (2.52; 0.69)	6.94 (1.88; 0.56)	**0.01**
T_0 vs T_2	6	6.56 (3.31; 1.3)	5.67 (2.78; 1.13)	0.34
T_1 vs T_2	4	5.98 (1.79; 0.89)	5.76 (3.17; 1.58)	0.71

TM – DNA Tail Moment; SD – Standard Deviation; SE – Standard error; T (subscript) – timing of biopsy (serial number); Statistical Tests: Wilcoxon signed ranked test; p – statistical significance of <0.05;* ***Bold*** *– significant difference*

Figure 4.4: Box plot graph showing changes in DNA tail moments of rectal cancers treated with long course NCRT

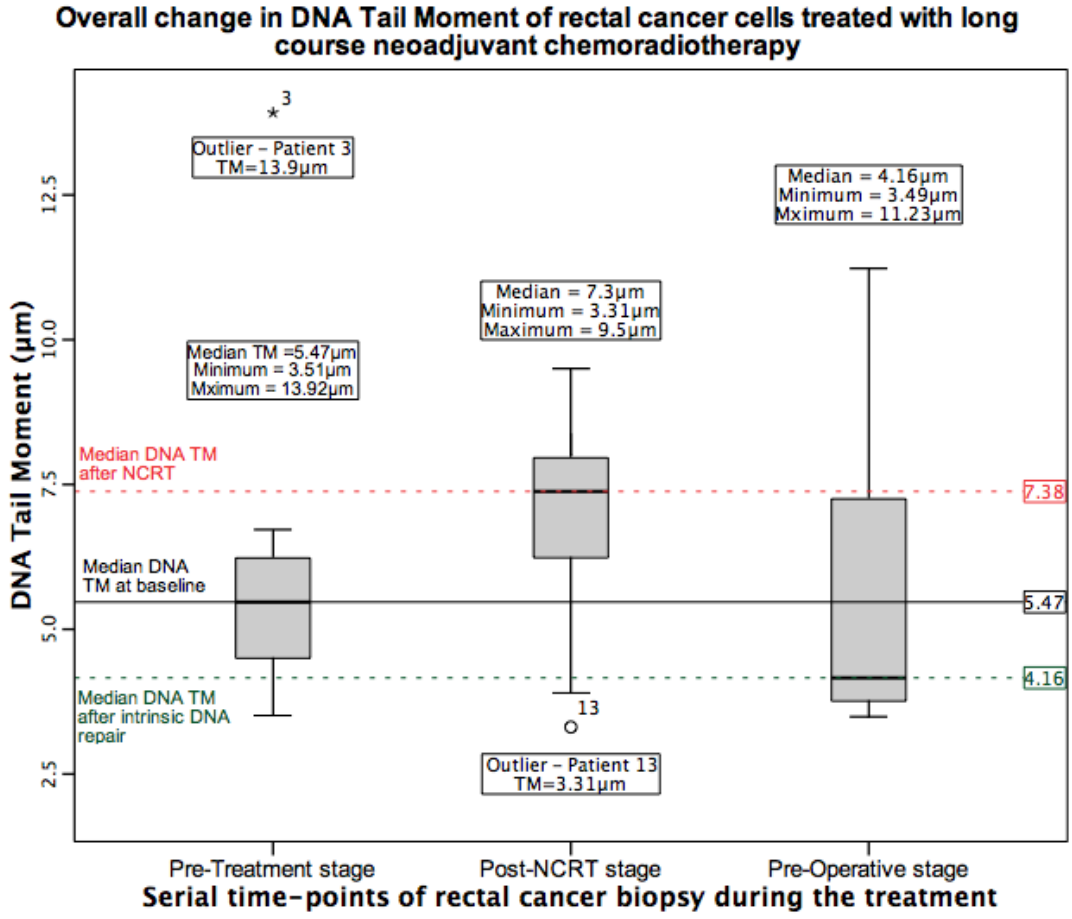

4.3.6 Individual Patient results

The data from individual patient and representative graphs are shown in table 4.8.The data shows DNA damage and repair after exposure to 15Gy ex vivo irradiation measured by comet assay.

The rectal cancer cells harvested at pre-treatment stage (red line on graphs in table 4.8) show significant DNA damage (several fold increase in TM) after exposure to 15Gy ex vivo irradiation. The same cells show active DNA repair with exception in patients 2 (KB) and 4 (AH). In addition, there is relatively less change in TM between 60 and 120 minutes after irradiation. The patient 9 (SD) shows atypical pattern and this is because of presence of frequent non-viable cells in their sample.

The rectal cancer cells harvested at post-NCRT stage (green line on graphs in table 4.8) show less increase in TM after irradiation, except for patients 2 (KB), 7 (AF) and 17 (JT). This may indicate enhanced DNA repair properties in surviving fraction of rectal cancer cells after long course NCRT.

The rectal cancer cells harvested at pre-operative stage (blue line on graphs in table 4.8) show features similar to rectal cancer cells obtain at pre-treatment stage with better DNA repair capability. In addition, the decrease in TM continues between 60 and 120 minutes after irradiation except in patient 15 (RC1). The patient 17 (JT) shows atypical pattern and this is because of presence of frequent non-viable cells in their sample.

CHAPTER 4: DNA REPAIR ANALYSIS

Table 4.8: Percentage change in TM of rectal cancer cells harvested at different time-points for individual patients

Patient Code 2 (DG)

	Pre-Treatment TM [µm]	Post-NCRT TM [µm]	Pre-operative TM [µm]
Control	4.44	6.9	11.23
0	15.8 (256%)	15 (118%)	23.27 (107%)
15	12.21 (175%)	15.03 (118%)	20.74 (85%)
30	12.51 (182%)	14.73 (113%)	19.21 (71%)
45	13.88 (213%)	13.68 (98%)	16.5 (47%)
60	13.16 (196%)	14.22 (106%)	13.22 (178%)
120	12.77 (188%)	14.51 (110%)	11.32 (0.8%)

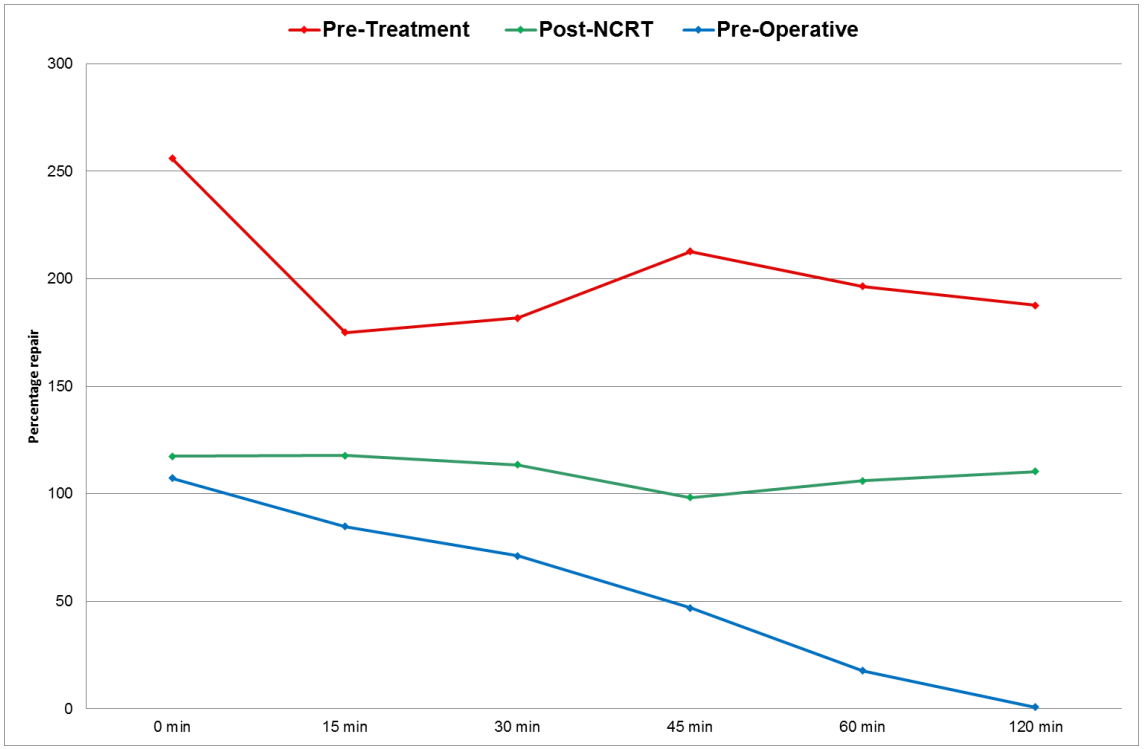

Percentage decrease in TM (DNA repair) over time after exposure to 15 Gy ex vivo irradiation

TM – Tail moment

CHAPTER 4: DNA REPAIR ANALYSIS

Patient Code 4 (AH)

	Pre-Treatment TM [µm]	Post-NCRT TM [µm]	Pre-operative TM [µm]
Control	5.5	5.57	4.41
0	11.18 (103%)	23.12 (315%)	14.65 (232%)
15	7.13 (30%)	15.36 (176%)	10.76 (144%)
30	8.8 (60%)	12.75 (129%)	10.08 (129%)
45	8.7 (58%)	10.92 (96%)	9.15 (107%)
60	9.68 (76%)	8.82 (58%)	8 57 (94%)
120	8.31 (51%)	7.16 (29%)	7.28 (65%)

TM – Tail moment

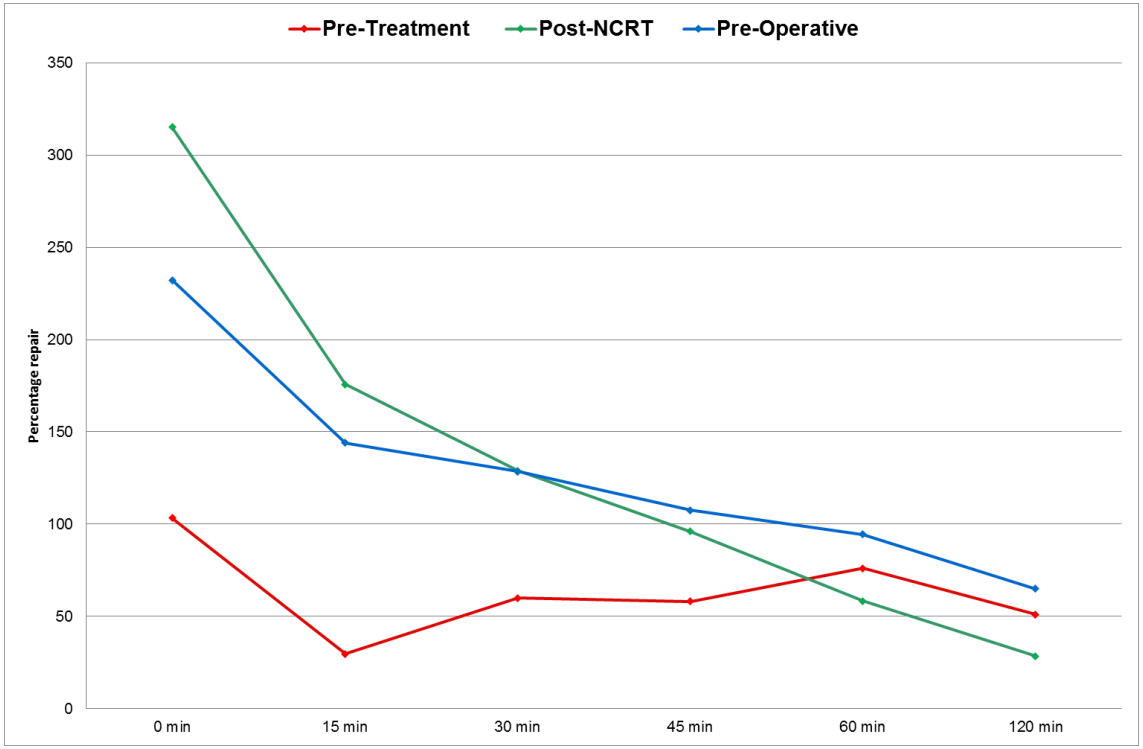

Percentage decrease in TM (DNA repair) over time after exposure to 15 Gy ex vivo irradiation

CHAPTER 4: DNA REPAIR ANALYSIS

Patient Code 5 (KB)

	Pre-Treatment TM [µm]	Post-NCRT TM [µm]	Pre-operative TM [µm]
Control	13.92	-	7.25
0	24.46 (78%)	-	12.23 (69%)
15	20.01 (44%)	-	11.37 (57%)
30	14.67 (5%)	-	10.86 (50%)
45	14.7 (5%)	-	9.67 (33%)
60	13.49 (-3%)	-	9.46 (30%)
120	12.61 (-9%)	-	7.98 (10%)

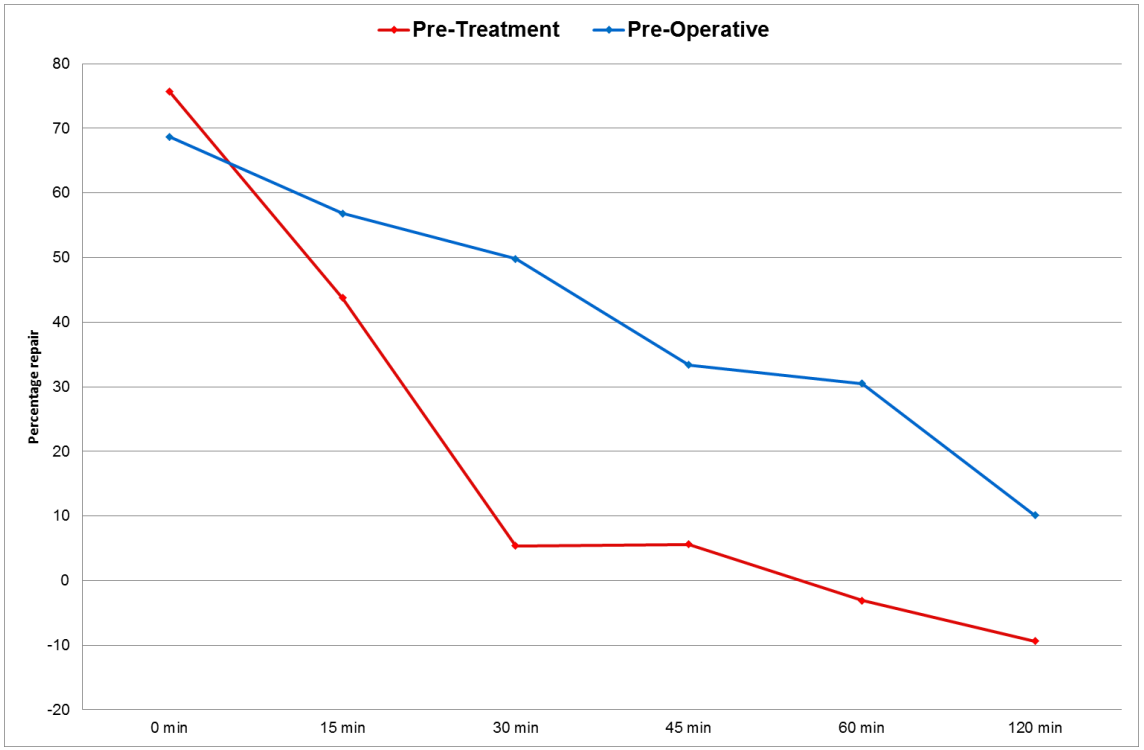

Percentage decrease in TM (DNA repair) over time after exposure to 15 Gy ex vivo irradiation

TM – Tail moment

CHAPTER 4: DNA REPAIR ANALYSIS

Patient Code 6 (ED)

	Pre-Treatment TM [µm]	Post-NCRT TM [µm]	Pre-operative TM [µm]
Control	6.72	7.03	-
0	15.64 (133%)	11.47 (63%)	-
15	12.7 (89%)	11.02 (57%)	-
30	9.14 (36%)	10.78 (53%)	-
45	9.04 (35%)	10.18 (45%)	-
60	7.33 (9%)	9.52 (35%)	-
120	6.22 (-7%)	8.88 (26%)	-

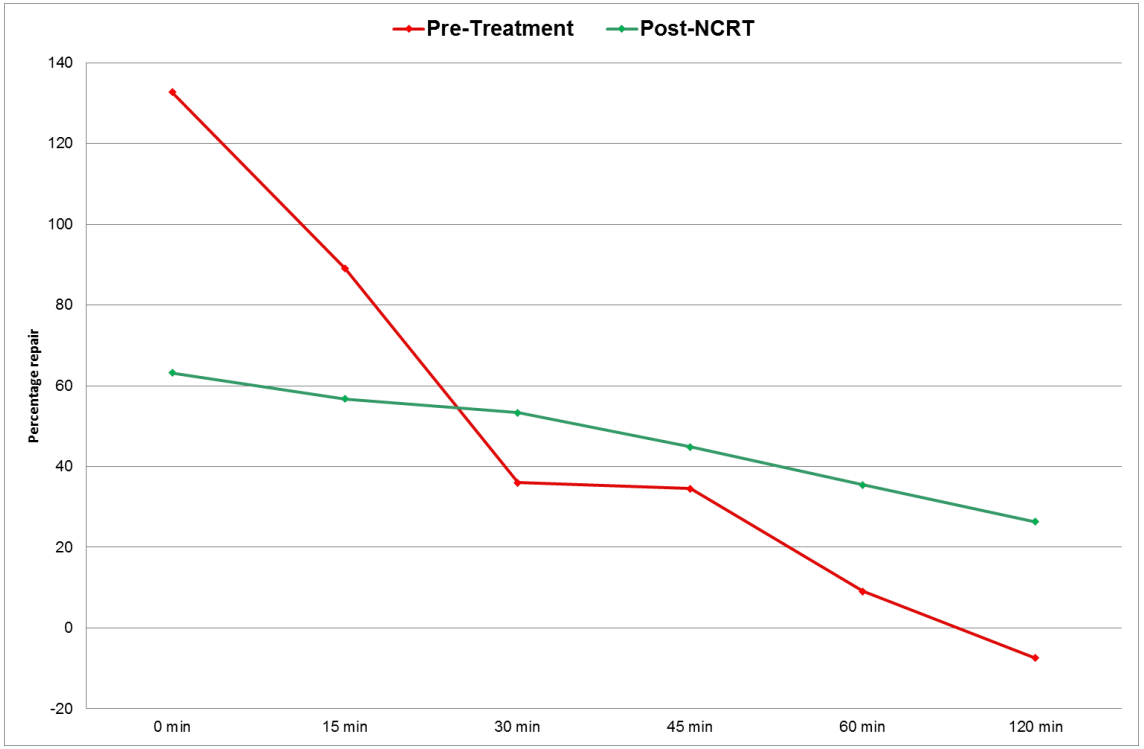

Percentage decrease in TM (DNA repair) over time after exposure to 15 Gy ex vivo irradiation

TM – Tail moment

CHAPTER 4: DNA REPAIR ANALYSIS

Patient Code 7 (AF)

	Pre-Treatment TM [µm]	Post-NCRT TM [µm]	Pre-operative TM [µm]
Control	3.81	3.9	-
0	11.58 (204%)	14.09 (261%)	-
15	8.83 (132%)	11.2 (187%)	-
30	7.12 (87%)	10.68 (174%)	-
45	5.39 (41%)	9.39 (141%)	-
60	4.96 (30%)	8.85 (127%)	-
12	4.07 (7%)	8.84 (127%)	-

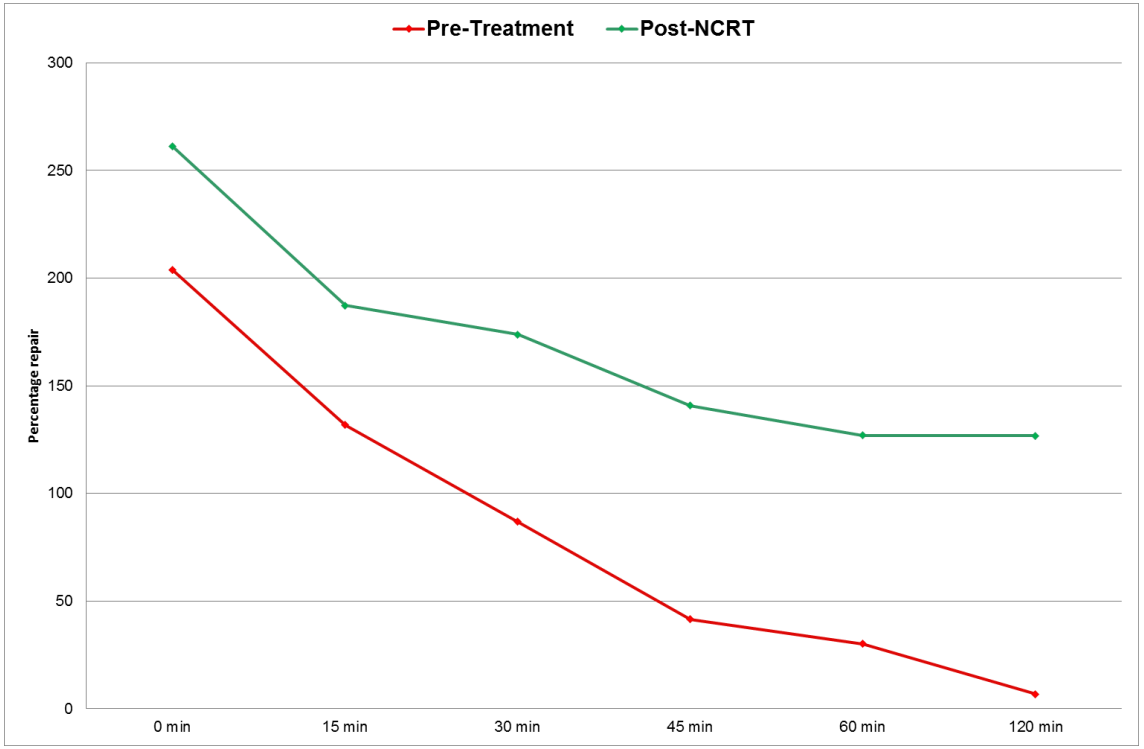

Percentage decrease in TM (DNA repair) over time after exposure to 15 Gy ex vivo irradiation

TM – Tail moment

CHAPTER 4: DNA REPAIR ANALYSIS

Patient Code 8 (JN)

	Pre-Treatment TM [µm]	Post-NCRT TM [µm]	Pre-operative TM [µm]
Control	6.23	7.46	-
0	17.73 (185%)	13.88 (86%)	-
15	14.64 (135%)	11.81 (58%)	-
3	11.66 (87%)	10.7 (43%)	-
45	9.16 (47%)	9.8 (31%)	-
60	8.99 (44%)	9.09 (22%)	-
120	7.8 (25%)	10.02 (34%)	-

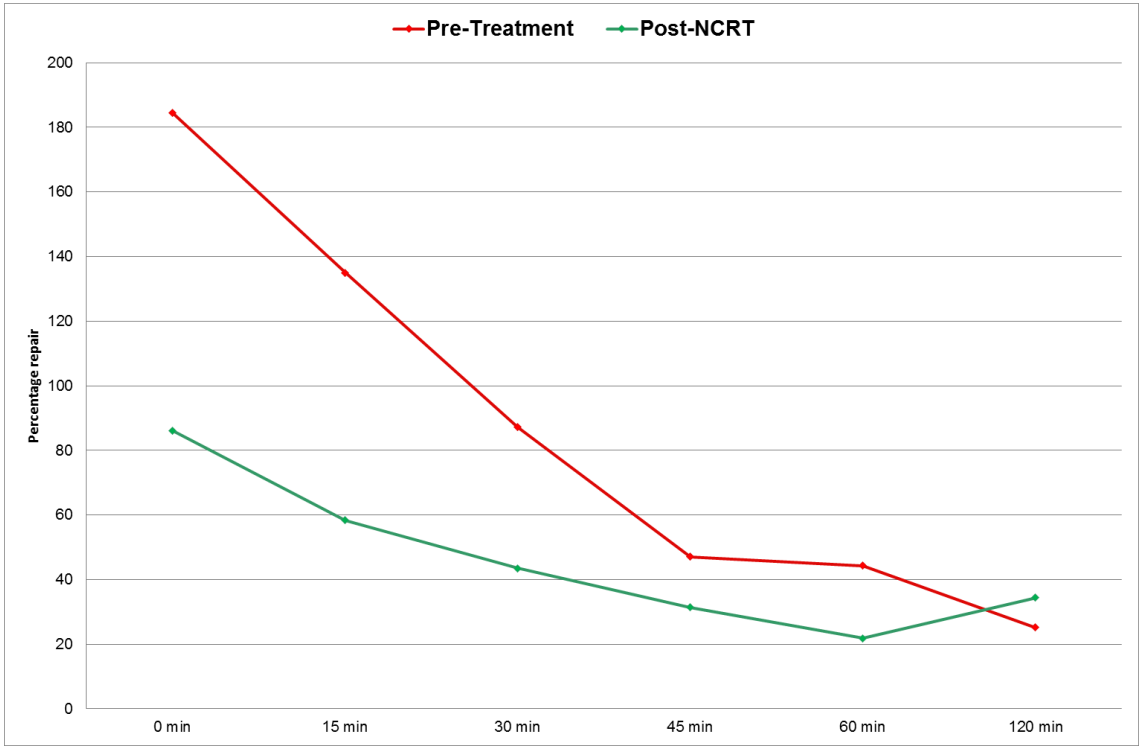

Percentage decrease in TM (DNA repair) over time after exposure to 15 Gy ex vivo irradiation

TM – Tail moment

CHAPTER 4: DNA REPAIR ANALYSIS

Patient Code 9 (SD)

	Pre-Treatment TM [µm]	Post-NCRT TM [µm]	Pre-operative TM [µm]
Control	3.51	9.5	-
0	14.95 (326%)	11.52 (21%)	-
15	9.7 (176%)	11.06 (16%)	-
30	8.28 (136%)	10.08 (6%)	-
45	11.18 (219%)	9.98 (5%)	-
60	9.61 (174%)	9.79 (3%)	-
120	9.62 (174%)	9.85 (4%)	-

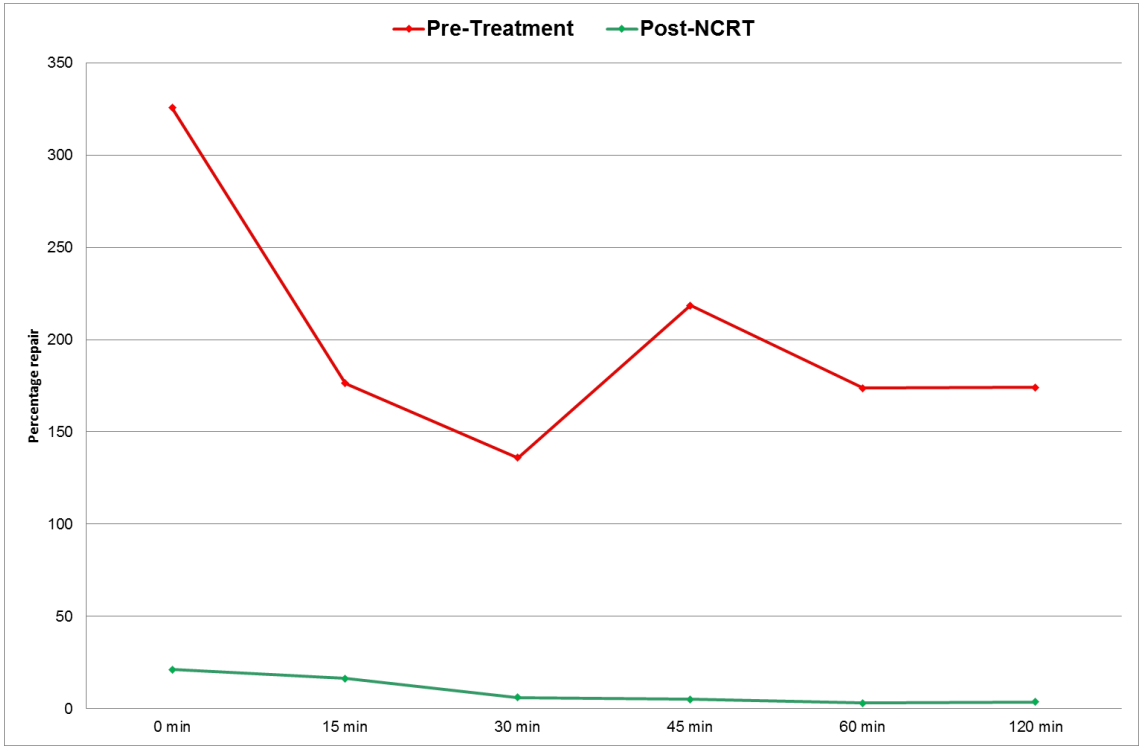

Percentage decrease in TM (DNA repair) over time after exposure to 15 Gy ex vivo irradiation

TM – Tail moment

CHAPTER 4: DNA REPAIR ANALYSIS

Patient Code 10 (JH)

	Pre-Treatment TM [µm]	Post-NCRT TM [µm]	Pre-operative TM [µm]
Control	4.5	7.38	-
0	11.53 (156%)	14.78 (100%)	-
15	8.99 (100%)	12.21 (65%)	-
30	7.47 (66%)	12.46 (69%)	-
45	7.24 (61%)	11.57 (57%)	-
60	7.04 (56%)	11.94 (62%)	-
120	6.95 (54%)	11.89 (61%)	-

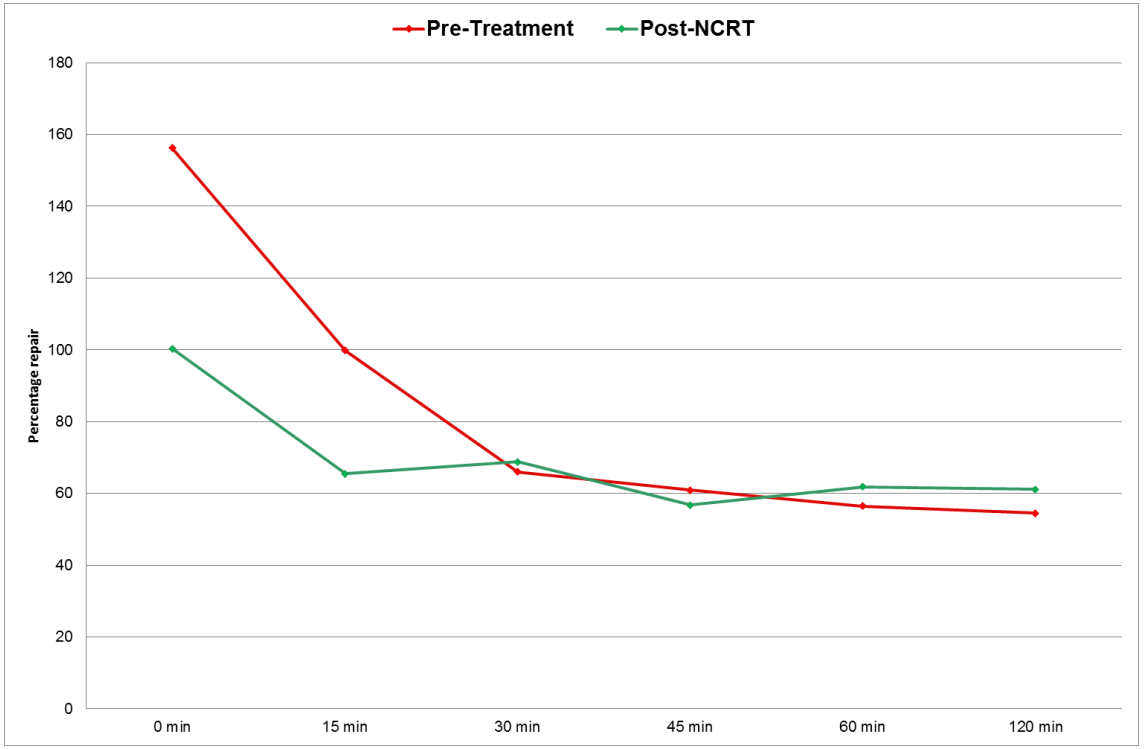

Percentage decrease in TM (DNA repair) over time after exposure to 15 Gy ex vivo irradiation

TM – Tail moment

CHAPTER 4: DNA REPAIR ANALYSIS

Patient Code 13 (PO)

	Pre-Treatment TM [µm]	Post-NCRT TM [µm]	Pre-operative TM [µm]
Control	6.53	7.77	-
0	14.35 (120%)	13.73 (77%)	-
15	13.61 (108%)	12.94 (67%)	-
30	13.18 (102%)	10.92 (40%)	-
45	12.67 (94%)	10.7 (38%)	-
60	11.09 (70%)	10.05 (29%)	-
120	10.71 (64%)	9.88 (27%)	-

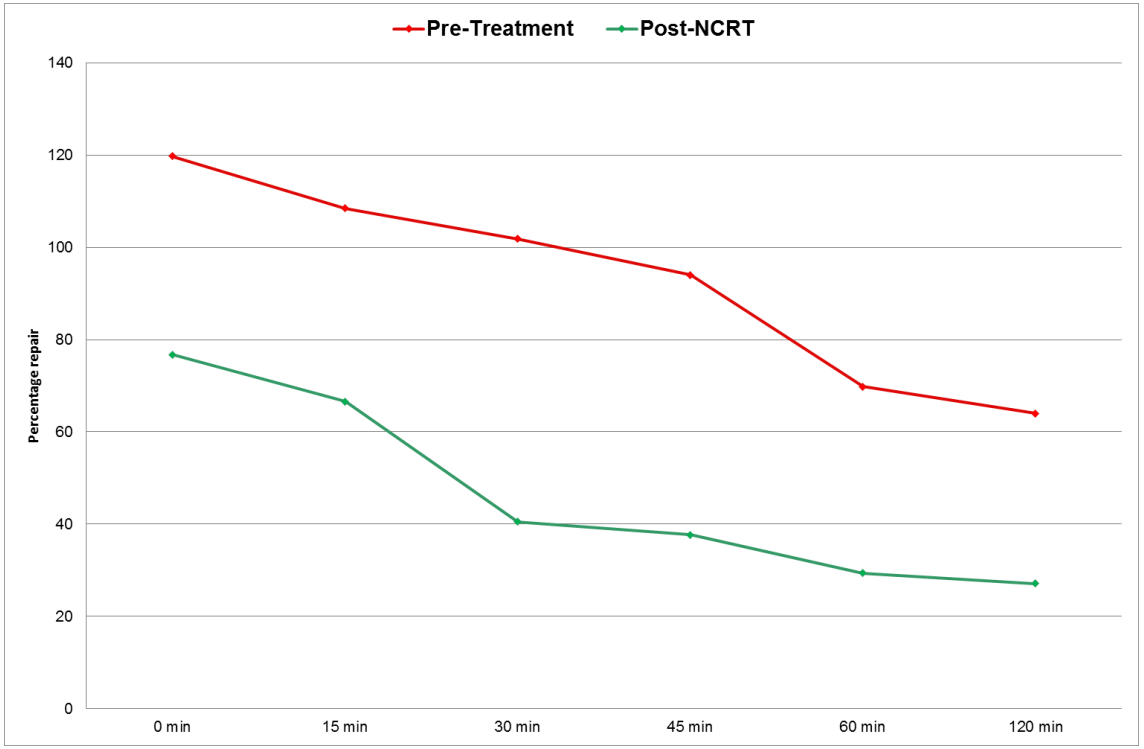

Percentage decrease in TM (DNA repair) over time after exposure to 15 Gy ex vivo irradiation

TM – Tail moment

CHAPTER 4: DNA REPAIR ANALYSIS

Patient Code 14 (MM)

	Pre-Treatment TM [µm]	Post-NCRT TM [µm]	Pre-operative TM [µm]
Control	5.05	9.32	-
0	12.13 (140%)	13.26 (42%)	-
15	10.2 (102%)	12.43 (33%)	-
30	8.31 (65%)	10.69 (15%)	-
45	6.48 (28%)	10.69 (15%)	-
60	6.95 (38%)	12.05 (29%)	-
120	6.09 (21%)	10.1 (8%)	-

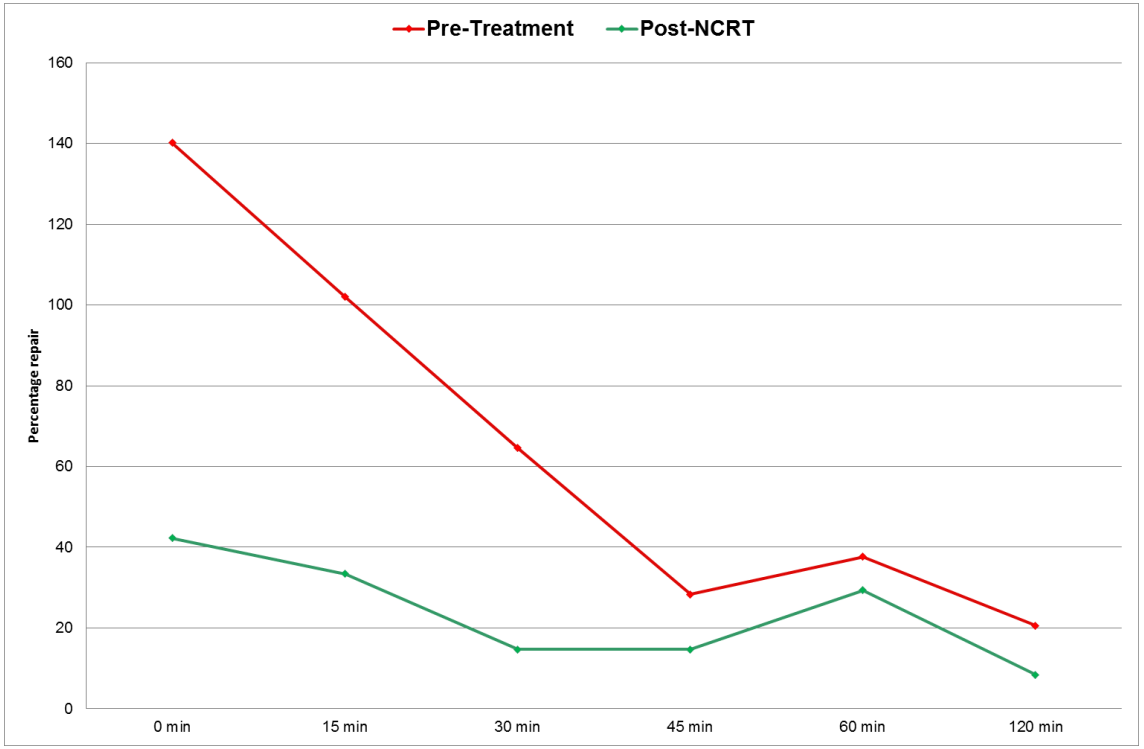

Percentage decrease in TM (DNA repair) over time after exposure to 15 Gy ex vivo irradiation

TM – Tail moment

CHAPTER 4: DNA REPAIR ANALYSIS

Patient Code 15 (RC1)

	Pre-Treatment TM [µm]	Post-NCRT TM [µm]	Pre-operative TM [µm]
Control	5.47	8.15	3.49
0	18.42 (237%)	15.15 (86%)	12.91 (270%)
15	13.23 (142%)	17.19 (111%)	9.93 (185%)
30	11.39 (108%)	11.51 (41%)	8.82 (153%)
45	10.22 (87%)	11.72 (44%)	8.49 (143%)
60	10.77 (97%)	12.58 (54%)	7.91 (127%)
120	11.27 (106%)	5.54 (-32%)	8.07 (131)

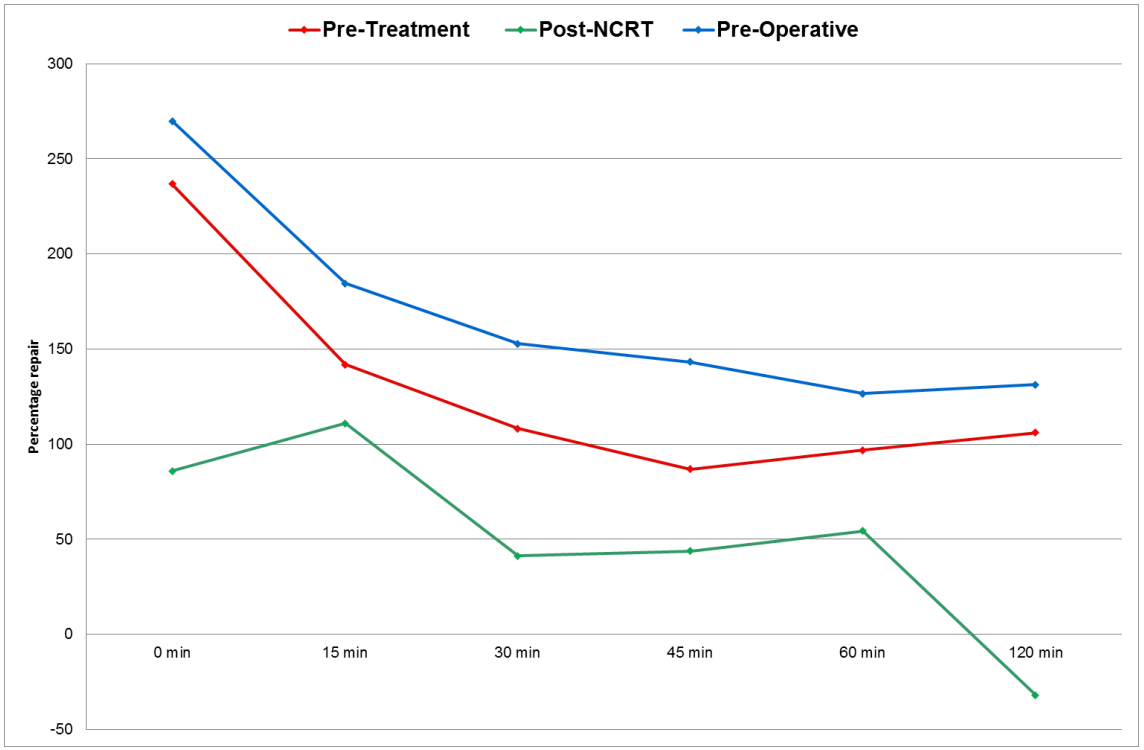

Percentage decrease in TM (DNA repair) over time after exposure to 15 Gy ex vivo irradiation

TM – Tail moment

CHAPTER 4: DNA REPAIR ANALYSIS

Patient Code 16 (RC2)

	Pre-Treatment TM [µm]	Post-NCRT TM [µm]	Pre-operative TM [µm]
Control	5.47	-	3.76
0	12.67 (132%)	-	6.07 (61%)
15	9.93 (82%)	-	4.89 (30%)
30	8.29 (52%)	-	4.64 (23%)
45	8.15 (49%)	-	4.09 (9%)
60	7.3 (33%)	-	5.51 (47%)
120	8.16 (49%)	-	4.99 (33%)

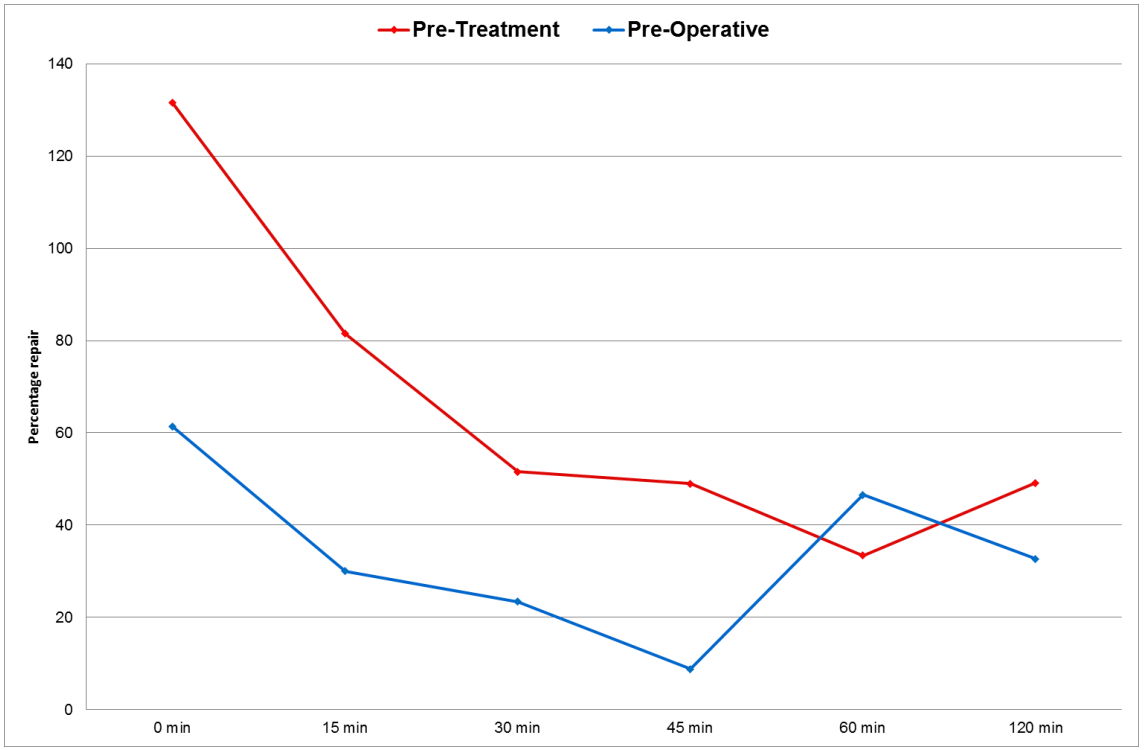

Percentage decrease in TM (DNA repair) over time after exposure to 15 Gy ex vivo irradiation

TM – Tail moment

CHAPTER 4: DNA REPAIR ANALYSIS

Patient Code 17 (JT)

	Pre-Treatment TM [µm]	Post-NCRT TM [µm]	Pre-operative TM [µm]
Control	4.57	3.31	3.91
0	10.7 (134%)	10.85 (228%)	12.42 (218%)
15	8.43 (82%)	7.56 (128%)	12.93 (231%)
30	7.53 (65%)	7.03 (112%)	12.59 (222%)
45	6.79 (49%)	6.44 (95%)	12.02 (207%)
60	5.87 (28%)	6.18 (87%)	9.61 (146%)
120	6.12 (34%)	7.65 (131%)	9.39 (140%)

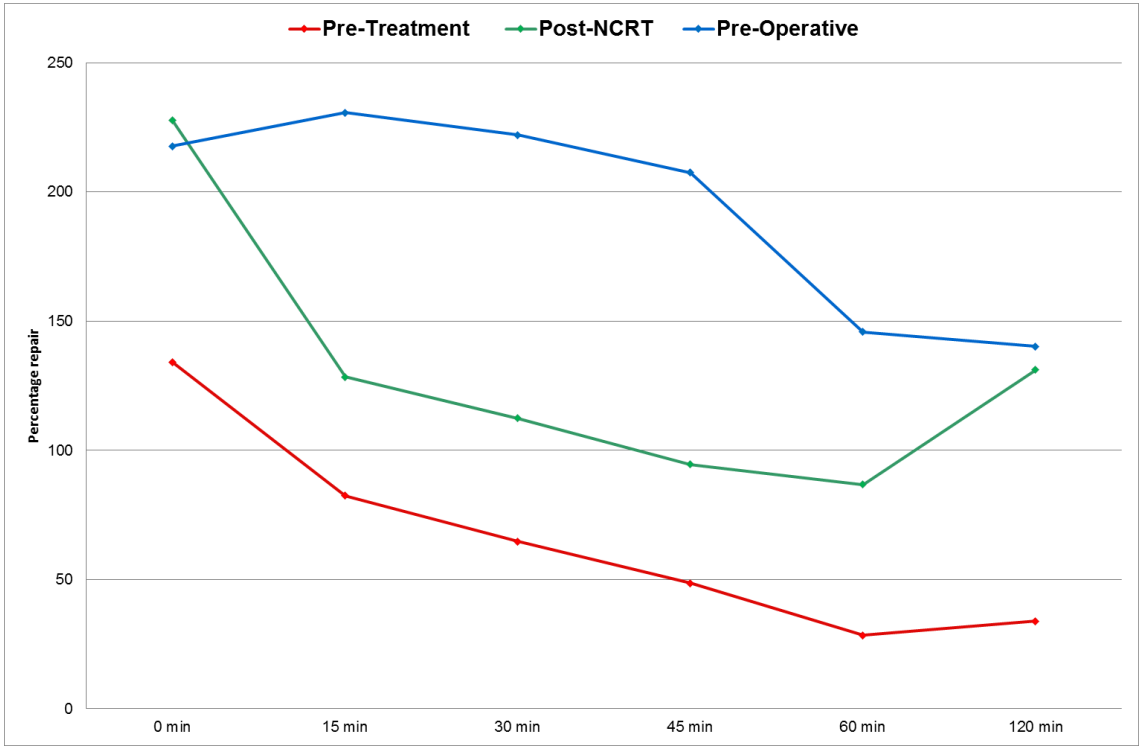

Percentage decreased in TM (DNA repair) over time after exposure to 15 Gy ex vivo irradiation

TM – Tail moment

4.3.7 Effects of 15Gy ex vivo irradiation on rectal cancer cells harvested at serial time-points before and after treatment with long course NCRT

4.3.7.1 Rectal cancer cells harvested at "pre-treatment stage"

The descriptive measurements of tail moments from timed comet assay DNA repair analysis are given in table 4.9 and the cumulative statistical analysis is shown in table 4.10 and figure 4.5. The percentage changes in DNA tail moments after 15Gy ex vivo irradiation is shown in table 4.11 and figure 4.6.

The rectal cancer cells harvested at pre-treatment stage showed severe damage (increased tail moment) after exposure to 15Gy *ex-vivo* irradiation (mean TM = 5.82μm in control versus mean TM=14.7μm immediately after irradiation, p 0.001; see table 4.10 and figure 4.5). There seems to be active repair following irradiation evidenced by a statistically significant decrease in serial tail moments on Friedman test ($p < 0.001$), however, at 120 minutes the DNA damage remained significant as compared to the baseline value (TM = 5.82μm in control versus 8.51μm at 120 minutes, p 0.006; see table 4.10 and figure 4.5).

The percentage change in DNA tail moment further elaborates cell DNA damage after irradiation and DNA repair capabilities. As seen in table 4.11 and figure 4.6, the percentage DNA tail moment sharply increases several folds after ex vivo irradiation (red bar in figure 4.6) in each patient, followed by lowering percentage over 120 minutes. In majority of patients, the percentage DNA tail moment decreases over time towards baseline value, but DNA does not fully recover.

Table 4.9: Changes in individual patient DNA tail moment (DNA repair) of rectal cancer cells at "pre-treatment stage" after exposure to 15Gy *ex vivo* irradiation

Code		Baseline TM	TM at serial time points after exposure to 15 Gy ex vivo irradiation					
		Control	*0 (min)*	*15 (min)*	*30 (min)*	*45 (min)*	*60 (min)*	*120 (min)*
		TM [µm] (SD; SE)	*TM [µm] (SD; SE)*	*TM [µm] (SD; SE)*	*TM [µm] (SD; SE)*	*TM [µm] (SD; SE)*	*TM [µm] (SD; SE)*	*TM [µm] (SD; SE)*
2	DG	4.44 (2.83; 0.51)	15.80 (2.32; 0.42)	12.21 (3.95; 0.72)	12.51 (3.08; 0.56)	13.88 (4.63; 0.84)	13.16 (4.33; 0.79)	12.77 (3.86; 0.70)
4	AH	5.50 (2.5; 0.45)	11.18 (3.22; 0.56)	7.13 (3.65; 0.66)	8.80 (3.31; 0.60)	8.70 (2.71; 0.49)	9.68 (2.74; 0.50)	8.34 (3.35; 0.62)
5	KB	13.92 (6.02; 1.1)	24.46 (6.62; 1.2)	20.01 (6.4; 1.16)	14.67 (7.04; 1.28)	14.70 (6.57; 1.2)	13.49 (5.62; 1.02)	12.61(3.99; 0.73)
6	ED	6.72 (3.09; 0.56)	15.64 (5.08; 0.92)	12.70 (5.19; 0.94)	9.14 (3.43; 0.62)	9.04 (4.55; 0.83)	7.33 (3.24; 0.59)	6.22 (3.2; 0.58)
7	AF	3.81 (2.68; 0.49)	11.58 (4.07; 0.74)	8.83 (3.79; 0.69)	7.12 (3.06; 0.55)	5.39 (2.77; 0.50)	4.96 (2.62; 0.47)	4.07 (2.32; 0.42)
8	JN	6.23 (2.94; 0.53)	17.73 (4.64; 0.84)	14.64 (3.64; 0.66)	11.66 (2.81; 0.51)	9.16 (3.59; 0.65)	8.99 (1.98; 0.36)	7.80 (2.71; 0.49)
9	SD	3.51 (3.47; 0.63)	14.94 (3.28; 0.59)	9.70 (6.97; 1.27)	8.28 (3.23; 0.58)	11.18 (2.17; 0.39)	9.61 (2.97; 0.54)	9.62 (2.86; 0.52)
10	JH	4.50 (2.39; 0.43)	11.53 (2.76; 0.50)	8.99 (2.78; 0.50)	7.47 (1.72; 0.31)	7.24 (1.49; 0.27)	7.04 (2.58; 0.47)	6.95 (1.51; 0.27)
13	PO	6.53 (2.28; 0.41)	14.35 (4.22; 0.77)	13.61 (2.25; 0.41)	13.18 (1.94; 0.35)	12.67 (1.28; 0.23)	11.09 (1.47; 0.27)	10.71 (1.81; 0.33)
14	MM	5.05 (2.39; 0.43)	12.13 (3.13; 0.57)	10.20 (2.72; 0.49)	8.31 (2.89; 0.52)	6.48 (2.34; 0.42)	6.95 ()2.5; 0.45	6.09 (2.21; 0.40)
15	RC1	5.47 (3.28; 0.60)	18.42 (3.2; 0.58)	13.23 (4.14; 0.75)	11.39 (2.91; 0.53)	10.22 (2.41; 0.44)	10.77 (3.11; 0.56)	11.27 (1.99; 0.36)
16	RC2	5.47 (3.02; 0.55)	12.67 (3.64; 0.66)	9.93 (3.2; 0.58)	8.29 (2.79; 0.51)	8.15 (1.91; 0.34)	7.30 (2.27; 0.41)	8.16 (2.04; 0.37)
17	JT	4.57 (9.36; 1.71)	10.70 (3.84; 0.70)	8.34 (2.78; 0.50)	7.53 (2.47; 0.45)	6.79 (2.29; 0.41)	5.87 (2.11; 0.38)	6.12 (1.64; 0.29)

TM – Tail moment; SD – Standard Deviation; SE – Standard error

Table 4.10: Changes in mean DNA tail moments of rectal cancer cell DNA at "pre-treatment stage" after exposure to 15Gy ex-vivo irradiation

Time Points (min)	Mean TM [µm] (SD; SE)	Mean Percentage Change	Statistical difference in mean TM between control and specific time points*
Control	5.82 (2.52; 0.69)		
0	14.70 (3.71; 1.03)	+169%	0.001
15	11.50 (3.30; 0.91)	+107%	0.001
30	9.87 (2.39; 0.88)	+81%	0.001
45	9.50 (2.78; 0.77)	+76%	0.001
60	8.94 (2.56; 0.71)	+65%	0.002
120	8.51(2.60; 0.72)	+58%	0.006
Statistical difference in mean TM from time '0' min to '120' min	<0.001**		

*TM – Tail moment; SD – Standard Deviation; SE – Standard error; Statistical Tests: Shapiro-Wilk test of normality; *Wilcoxon signed ranked test; Friedman Test** ; p – statistical significance of <0.05*

Figure 4.5: Box plot graph showing serial tail moments of rectal cancer DNA at "pre-treatment stage" after exposure to 15Gy ex-vivo irradiation

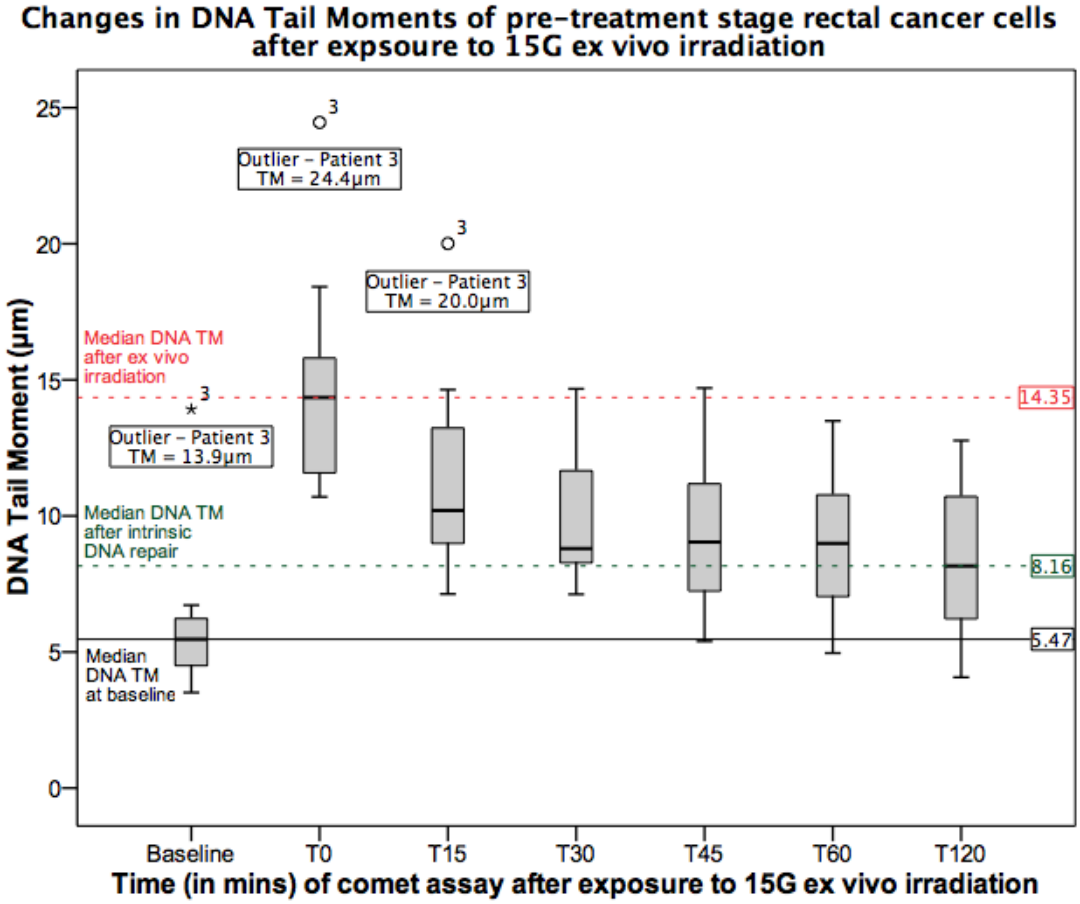

Table 4.11: Percentage change in DNA Tail Moment (DNA repair) of rectal cancer cells at "pre-treatment stage" after exposure to 15Gy *ex vivo* irradiation

Code		Baseline TM [µm]	Percentage change in TM [µm] at serial time-points after exposure to 15 Gy ex vivo irradiation					
		Control	0 (min)	15 (min)	30 (min)	45 (min)	60 (min)	120 (min)
2	DG	4.44	15.80 (+255%)	12.21 (+175%)	12.51 (+182%)	13.88 (+213%)	13.16 (+196%)	12.77 (+187%)
4	AH	5.50	11.18 (+103%)	7.13 (+30%)	8.80 (+60%)	8.70 (+58%)	9.68 (+76%)	8.31 (+51%)
5	KB	13.92	24.46 (+76%)	20.01 (+44%)	14.67 (+5%)	14.70 (+5.6%)	13.49 (-3.09%)	12.61 (-9.41%)
6	ED	6.72	15.64 (+133%)	12.70 (+89%)	9.14 (+36%)	9.04 (+35%)	7.33 (+9%)	6.22 (-7.44%)
7	AF	3.81	11.58 (+204%)	8.83 (+132%)	7.12 (+87%)	5.39 (+41%)	4.96 (+30%)	4.07 (+7%)
8	JN	6.23	17.73 (+185%)	14.64 (+135%)	11.66 (+87%)	9.16 (+47%)	8.99 (+44%)	7.80 (+25%)
9	SD	3.51	14.94 (+326%)	9.70 (+176%)	8.28 (+136%)	11.18 (+219%)	9.61 (+174%)	9.62 (+174%)
10	JH	4.50	11.53 (+156%)	8.99 (+100%)	7.47 (+66%)	7.24 (+61%)	7.04 (+56%)	6.95 (+54%)
13	PO	6.53	14.35 (+120%)	13.61 (+108%)	13.18 (+102%)	12.67 (+94%)	11.09 (+70%)	10.71 (+64%)
14	MM	5.05	12.13 (+140%)	10.20 (+102%)	8.31 (+65%)	6.48 (+28%)	6.95 (+38%)	6.09 (+21%)
15	RC1	5.47	18.42 (+237%)	13.23 (+142%)	11.39 (+108%)	10.22 (+87%)	10.77 (+97%)	11.27 (+106%)
16	RC2	5.47	12.67 (+132%)	9.93 (+82%)	8.29 (+52%)	8.15 (+49%)	7.30 (+33%)	8.16 (+49%)
17	JT	4.57	10.70 (+134%)	8.34 (+82%)	7.53 (+65%)	6.79 (+49%)	5.87 (+28%)	6.12 (+34%)

DNA TM – Tail moment

Figure 4.6: Bar chart showing percentage changes in DNA tail moment of rectal cancer cell at "pre-treatment stage" after exposure to 15Gy ex-vivo irradiation – individual cases

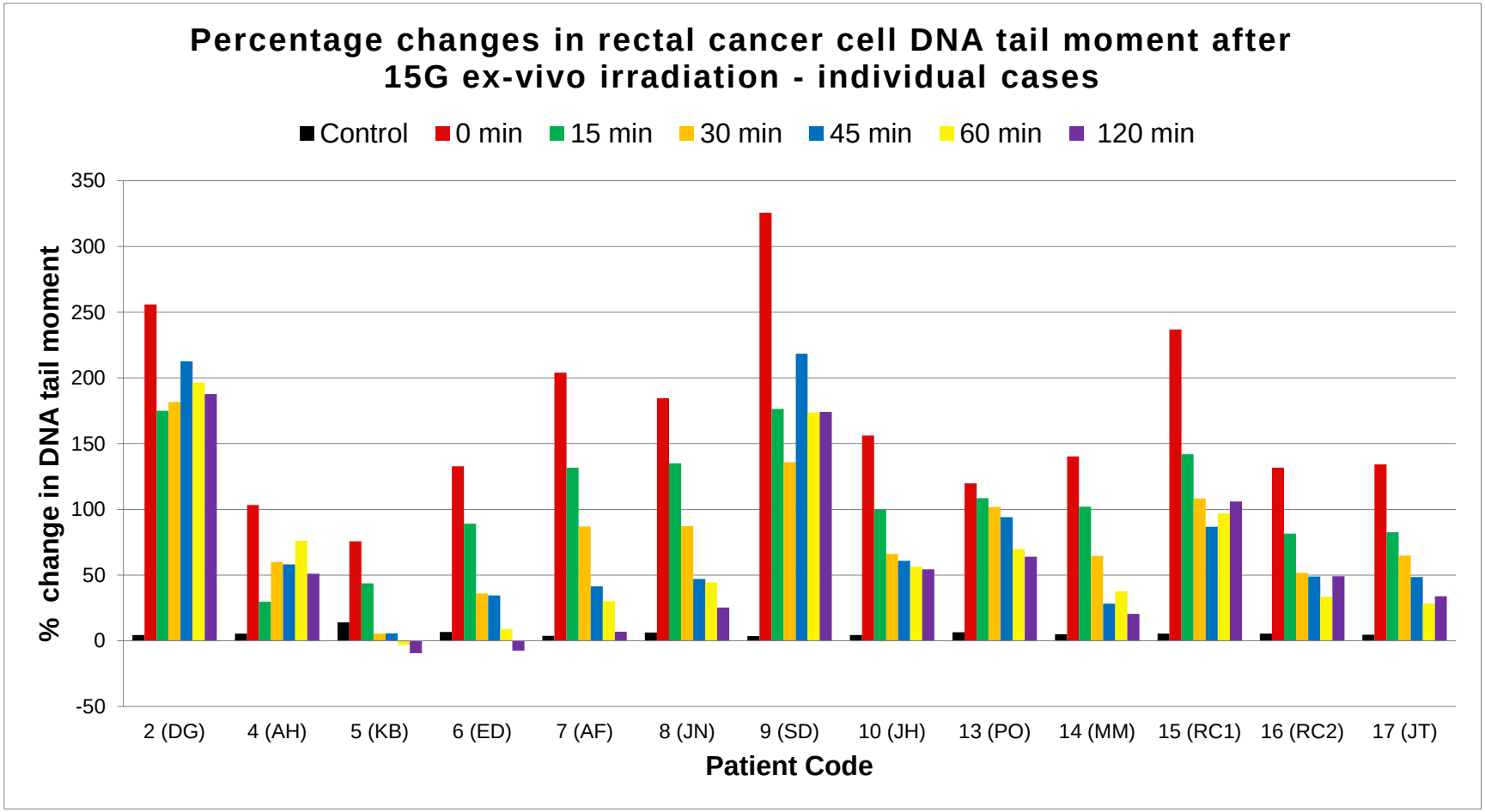

4.3.7.2 Rectal cancer cells harvested at "post-NCRT stage"

The descriptive measurements of tail moments from timed comet assay DNA repair analysis are given in table 4.12 and the cumulative statistical analysis is shown in table 4.13 and figure 4.7. The percentage changes in DNA tail moments after 15Gy ex vivo irradiation is shown in table 4.14 and figure 4.8.

There is augmented damage to DNA after irradiation in rectal cancer cells retrieved after long course NCRT (mean TM=6.93μm for control versus mean TM=14.25μm at '0' mins, a 206% increase, p 0.003; see table 4.13). A sharp decline in DNA tail moments (DNA repair) is seen only until 45 minutes, followed by a limited change (see table 4.13 and figure 4.7). Despite a drop in TM values after irradiation, there is persisted statically significant difference between control and DNA repair by 120 minutes (mean TM= 6.93μm for control versus mean TM=9.48μm at '120mins', p 0.02; see table 4.13 and figure 4.7). The poor DNA repair is obvious in patient 1 and the persistent elevated TM values appear as outlier in box plot graph (see figure 4.7).

The slow decline in percentage change of DNA tail moment after irradiation further shows a low potential of DNA repair in rectal cancer cell at this stage of treatment (see table 4.14 and figure 4.8).

CHAPTER 4: DNA REPAIR ANALYSIS

Table 4.12: Changes in DNA tail moment (DNA repair) of rectal cancer cells at "post-NCRT stage" after exposure to 15Gy *ex vivo* irradiation

Codes		Baseline TM	TM at serial time points after exposure to 15Gy ex vivo irradiation					
		Control	*0 (min)*	*15 (min)*	*30 (min)*	*45 (min)*	*60 (min)*	*120 (min)*
		TM [µm] (SD; SE)	*TM [µm] (SD; SE)*	*TM [µm] (SD; SE)*	*TM [µm] (SD; SE)*	*TM [µm] (SD; SE)*	*TM [µm] (SD; SE)*	*TM [µm] (SD; SE)*
2	DG	6.90 (2.4; 0.43)	15 (2.35; 0.43)	17.26 (3.73; 0.68)	14.73 (3.82; 0.70)	13.68 (1.99; 0.37)	14.22 (2.54; 0.46)	14.51(3.63; 0.66)
4	AH	5.57 (2.52; 0.46)	23.12 (36.12; 6.6)	15.36 (4.92; 0.89)	12.75 (4.97; 0.90)	10.92 (3.99; 0.72)	8.82 (2.42; 0.44)	7.16 (3.59; 0.65)
5	KB	-	-	-	-	-	-	-
6	ED	7.03 (2.84; 0.52)	11.47 (3.54; 0.64)	11.02 (2.0; 0.36)	10.78 (2.32; 0.42)	10.18 (2.63; 0.48)	9.52 (2.06; 0.37)	8.88 (2.31; 0,42)
7	AF	3.90 (2.62; 0.47)	14.09 (4.06; 0.74)	11.20 (2.74; 0.50)	10.68 (3.64; 0.66)	9.39 (3.81; 0.69)	8.85 (2.53; 0.46)	8.84 (2.31; 0.42)
8	JN	7.46 (4.06; 0.74)	13.88 (5.09;x)	11.81 (5.17; 0.94)	10.70 (3.7; 0.67)	9.80 (2.79; 0.50)	9.09 (3.66; 0.67)	10.02 (2.39;0.43)
9	SD	9.50 (2.56; 0.46)	11.52 (2.58; 0.47)	11.06 (1.66; 0.30)	10.08 (3.06; 0.55)	9.98 (2.59; 0.47)	9.79 (2.23; 0.40)	9.85 (2.85; 0.52)
10	JH	7.38 (1.55; 0.28)	14.78 (2.16; 0.39)	12.21 (1.96; 0.35)	12.46 (2.27; 0.41)	11.57 (2.59; 0.47)	11.94 (1.9; 0.34)	11.89 (2.41; 0.44)
13	PO	7.77 (2.82; 0.51)	13.73 (2.74; 0.50)	12.94 (1.94; 0.35)	10.92 (.85; 0.33)	10.70 (1.80; 0.32)	10.05 (2.35; 0.41)	9.88 (2.33; 0.42)
14	MM	9.32 (3.56; 0.65)	13.26 (3.01; 0.54)	12.43 (2.41; 0.44)	10.69 (2.48; 0.45)	10.69 (3.17; 0.57)	12.05 (3.0; 0.54)	10.10 (5.41; 0.98)
15	RC1	8.15 (2.47; 0.45)	15.15 (5.05; 0.92)	17.19 (3.63; 0.59)	11.51 (3.24; 0.59)	11.72 (5.81; 1.06)	12.58 (4.26; 0.77)	5.54 (2.77; 0.50)
16	RC2	-	-	-	-	-	-	-
17	JT	3.31 (2.77; 0.50)	10.85 (2.23; 0.40)	7.56 (2.61; 0.47)	7.03 (2.86; 0.52)	6.44 (2.64; 0.48)	6.18 (2.95; 0.53)	7.65 (2.53; 0.46)

TM – Tail moment; SD – Standard Deviation; SE – Standard error; x – results not available

Table 4.13: Changes in mean DNA tail moments of rectal cancer cell DNA at "post-NCRT stage" after exposure to 15Gy ex-vivo irradiation

Time Points (min)	Mean TM [µm] (SD; SE)	Mean Percentage Change	Statistical difference in TM between control and specific time points*
Control	6.93 (1.88; 0.56)		
0	14.25 (3.14; 0.94)	106%	0.003
15	12.52 (2.48; 0.74)	81%	0.003
30	11.12 (1.81; 0.54)	60%	0.003
45	10.46 (1.69; 0.51)	51%	0.003
60	10.28 (2.13; 0.64)	48%	0.003
120	9.48 (2.10; 0.63)	42%	0.021
Statistical difference in TM from time '0' min to '120' min	<0.001**		

*TM – Tail moment; SD – Standard Deviation; SE – Standard error ; Statistical Tests: Shapiro-Wilk test of normality; Wilcoxon signed ranked test; Friedman Test** ; p – statistical significance of <0.05*

Figure 4.7: Box plot graph showing serial tail moments of rectal cancer DNA at "post-NCRT stage" after exposure to 15Gy ex-vivo irradiation

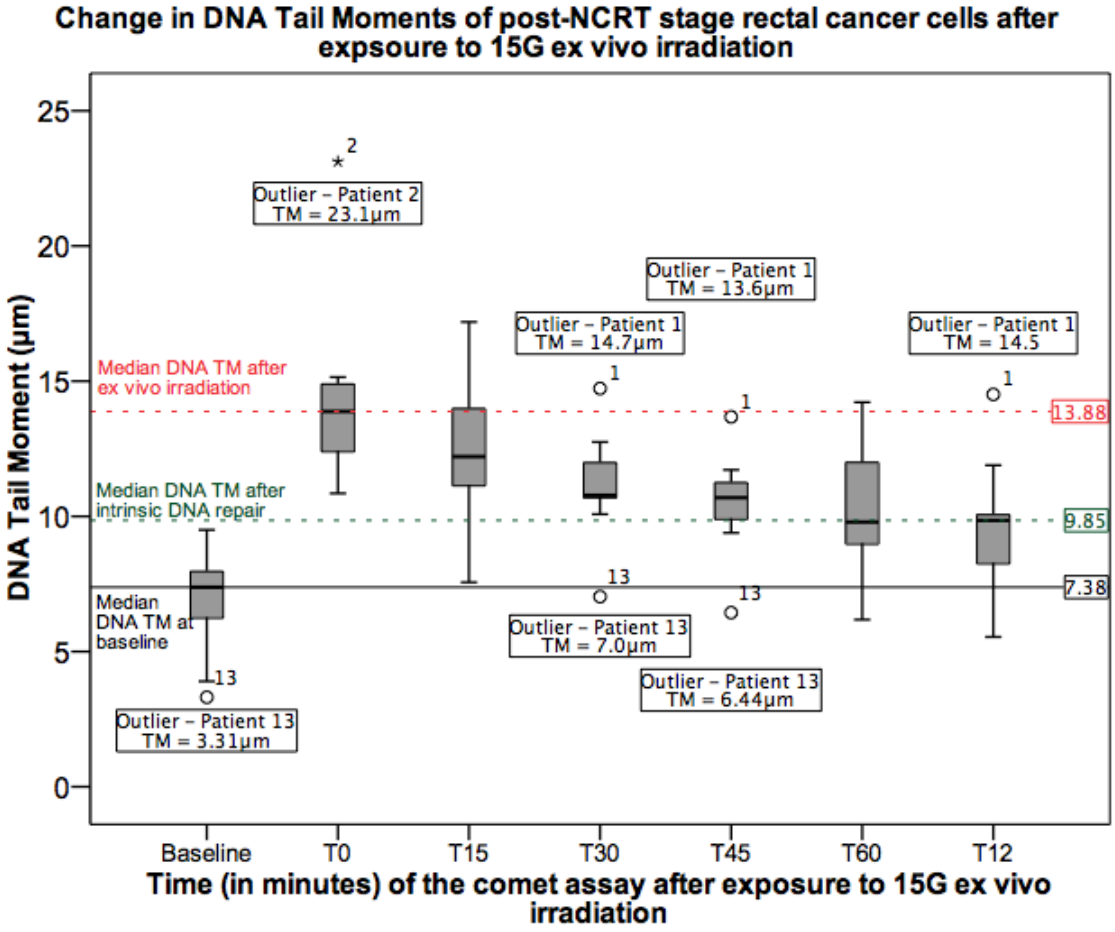

Table 4.14: Percentage change in DNA Tail Moment (DNA repair) of rectal cancer cells at "post-NCRT stage" after exposure to 15Gy *ex vivo* irradiation

Codes		Baseline TM [μm]	Percentage change in TM [μm] at serial time-points after exposure to 15Gy ex vivo irradiation					
		Control	0 (min)	15 (min)	30 (min)	45 (min)	60 (min)	120 (min)
2	DG	6.90	15 (+117%)	17.26 (+116%)	14.73 (+113%)	13.68 (+98%)	14.22 (+106%)	14.51 (+110%)
4	AH	5.57	23.12 (+315%)	15.36 (+176%)	12.75 (+129%)	10.92 (+96%)	8.82 (+58%)	7.16 (+29%)
5	KB	-	-	-	-	-	-	-
6	ED	7.03	11.47 (+63%)	11.02 (+57%)	10.78 (+53%)	10.18 (+45%)	9.52 (+35%)	8.88 (+26%)
7	AF	3.90	14.09 (+261%)	11.20 (+187%)	10.68 (+174%)	9.39 (+141%)	8.85 (+127%)	8.84 (+127%)
8	JN	7.46	13.88 (+86%)	11.81 (+58%)	10.70 (+43%)	9.80 (+31%)	9.09 (+22%)	10.02* (+34%)
9	SD	9.50	11.52 (+21%)	11.06 (+16%)	10.08 (+6%)	9.98 (+5%)	9.79 (+3%)	9.85 (+3.68%)
10	JH	7.38	14.78 (+100%)	12.21 (+65%)	12.46 (+67%)	11.57 (+57%)	11.94 (+62%)	11.89 (+61%)
13	PO	7.77	13.73 (+77%)	12.94 (+66%)	10.92 (+40%)	10.70 (+38%)	10.05 (+29%)	9.88 (+27%)
14	MM	9.32	13.26 (+42%)	12.43 (+33%)	10.69 (+15%)	10.69 (+15%)	12.05 (+29%)	10.10 (+8.37%)
15	RC1	8.15	15.15 (+86%)	17.19 (+111%)	11.51 (+41%)	11.72 (+44%)	12.58 (+54%)	5.54* (-32%)
16	RC2	-	-	-	-	-	-	-
17	JT	3.31	10.85 (+228%)	7.56 (+128%)	7.03 (+112%)	6.44 (+94%)	6.18 (+87%)	7.65 (+131%)

TM – Tail moment

Figure 4.8: Bar chart showing percentage changes in DNA tail moment of rectal cancer cell at "post-NCRT stage" after exposure to 15Gy ex-vivo irradiation – individual cases

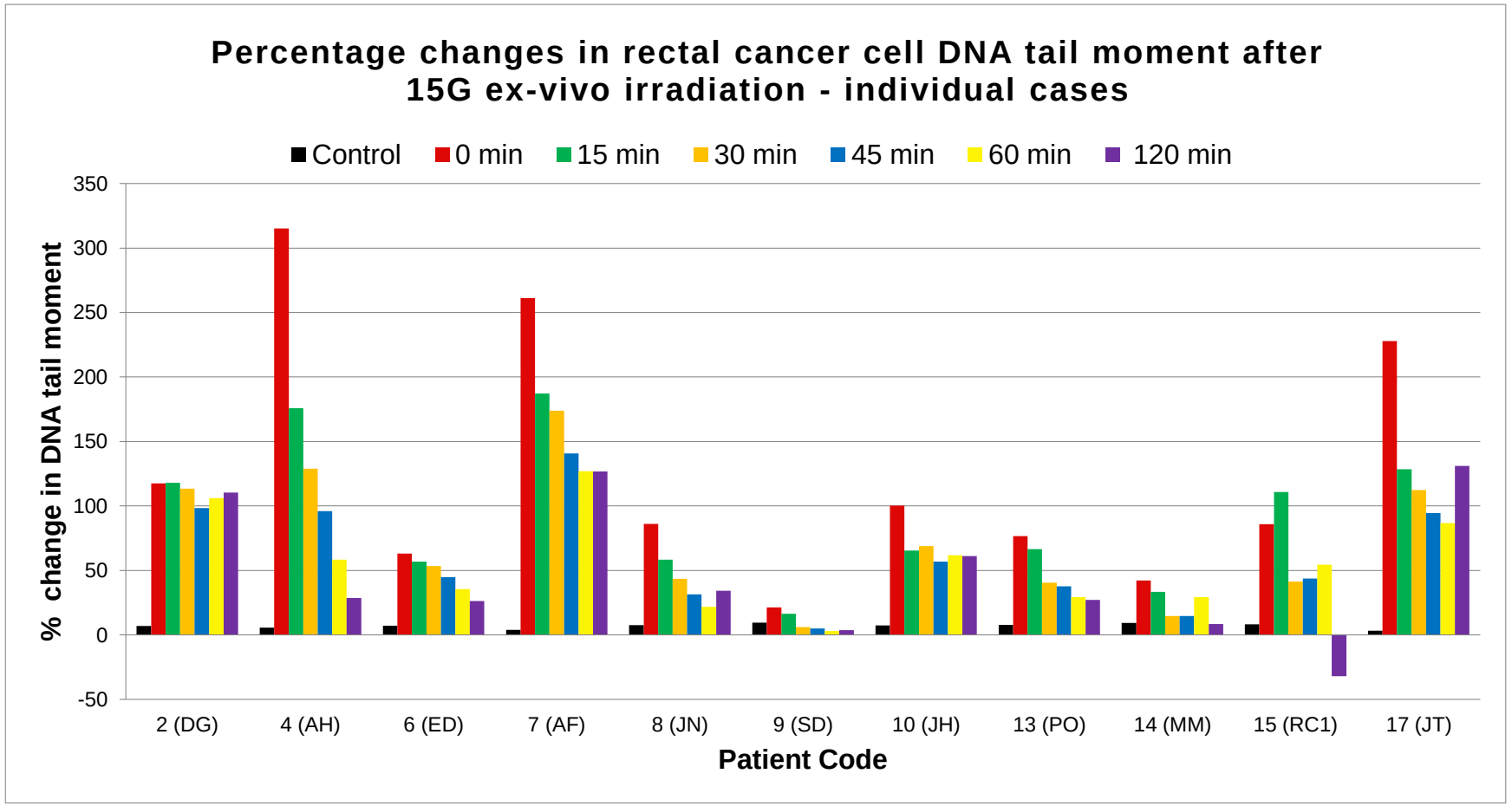

4.3.7.3 Rectal cancer cells harvested at “pre-operative stage”

The descriptive measurements of tail moments from timed comet assay DNA repair analysis are given in table 4.15 and the cumulative statistical analysis is shown in table 4.16 and figure 4.9. The percentage changes in DNA tail moments after 15Gy ex vivo irradiation is shown in table 4.17 and figure 4.10.

The tumour cells harvested before surgery showed severe damage after exposure to ex-vivo irradiation (TM = 5.6μm in control versus 13.59μm immediately after irradiation). There was active repair following irradiation with a decrease in tail moment of statistical significance (p 0.001), however, at 120 minutes the DNA damage remained significant as compared to the baseline value (p 0.028). Patient 1 appears as outlier in figure 4.16, however, there is good DNA repair in this patient albeit relatively higher TM values. This is in contrast to biopsy samples from the same patient at “post-NCRT stage” when there was obvious poor DNA repair (see figure 4.7). Patient 12 has overall poor DNA repair seen as poor decline in TM after 15 minutes (see tables 4.15 and 4.17) which is also demonstrated by lack of percentage decline in figure 4.10.

CHAPTER 4: DNA REPAIR ANALYSIS

Table 4.15: Changes in DNA tail moment (DNA repair) of rectal cancer cells at "pre-operative stage" after exposure to 15Gy *ex vivo* irradiation

Codes		Baseline TM [µm]	TM [µm] at serial time points after exposure to 15 Gy ex vivo irradiation					
		Control	*0 (min)*	*15 (min)*	*30 (min)*	*45 (min)*	*60 (min)*	*120 (min)*
		TM [µm] (SD; SE)	*TM [µm] (SD; SE)*	*TM [µm] (SD; SE)*	*TM [µm] (SD; SE)*	*TM [µm] (SD; SE)*	*TM [µm] (SD; SE)*	*TM [µm] (SD; SE)*
2	DG	11.23 (7.69; 1.4)	23.27 (3.63; 0.66)	20.74 (3.97; 0.70)	19.21 (4.71; 0.85)	16.65 (3.24; 0.59)	13.22 (3.1; 0.56)	11.32 (2.54; 0.46)
4	AH	4.41 (1.91; 0.34)	14.65 (2.98; 0.54)	10.76 (4.12; 0.75)	10.08 (3.79; 0.69)	9.15 (2.6; 0.47)	8.57 (2.45; 0.44)	7.28 (1.83; 0.33)
5	KB	7.25 (4.12; 0.75)	12.23 (2.59; 0.47)	11.37 (2.47; 0.45)	10.86 (1.81; 0.33)	9.67 (1.47; 0.26)	9.46 (2.11; 0.38)	7.98 (2.11; 0.38)
6	ED	-	-	-	-	-	-	-
7	AF	-	-	-	-	-	-	-
8	JN	-	-	-	-	-	-	-
9	SD	-	-	-	-	-	-	-
10	JH	-	-	-	-	-	-	-
13	PO	-	-	-	-	-	-	-
14	MM	-	-	-	-	-	-	-
15	RC1	3.49 (1.84; 0.33)	12.91 (3.55; 0.64)	9.93 (3.16; 0.57)	8.82 (2.02; 0.37)	8.49 (2.39; 0.43)	7.91 (3.21; 0.58)	8.07 (1.76; 0.32)
16	RC2	3.76 (2.45; 0.44)	6.07 (3.16; 0.57)	4.89 (3.38; 0.61)	4.64 (2.63; 0.48)	4.09 (2.97; 0.54)	5.51 (2.67; 0.48)	4.99 (2.85; 0.52)
17	JT	3.91 (1.73; 0.31)	12.42 (2.73; 0.49)	12.93 (2.76; 0.50)	12.59 (5.46; 0.99)	12.02 (4.78; 0.87)	9.61 (4.99; 0.91)	9.39 (3.48; 0.63)

TM – Tail moment; SD – Standard Deviation; SE – Standard error

Table 4.16: Changes in mean DNA tail moments of rectal cancer cell DNA at "pre-operative stage" after exposure to 15Gy ex-vivo irradiation

Time Points (min)	Mean TM [µm] (SD; SE)	Mean Percentage Change	Statistical difference in TM between control and specific time points*
Control	5.67 (2.78;1.13)		
0	13.59 (5.08; 2.07)	+139%	0.028
15	11.77 (4.72; 1.92)	+107%	0.028
30	11.03 (4.39; 1.79)	+94%	0.028
45	9.98 (3.7; 1.53)	+76%	0.028
60	9.04 (2.30; 0.94)	+59%	0.028
120	8.17 (1.93; 078)	+44%	0.028
Statistical difference in TM from time '0' min to '120' min	0.001**		

*TM – Tail moment; SD – Standard Deviation; SE – Standard error; Statistical Tests: Shapiro-Wilk test of normality; Wilcoxon signed ranked test; Friedman Test** ; p – statistical significance of <0.05*

Figure 4.9: Box plot graph showing serial tail moments of rectal cancer DNA at "pre-operative stage" after exposure to 15Gy ex-vivo irradiation

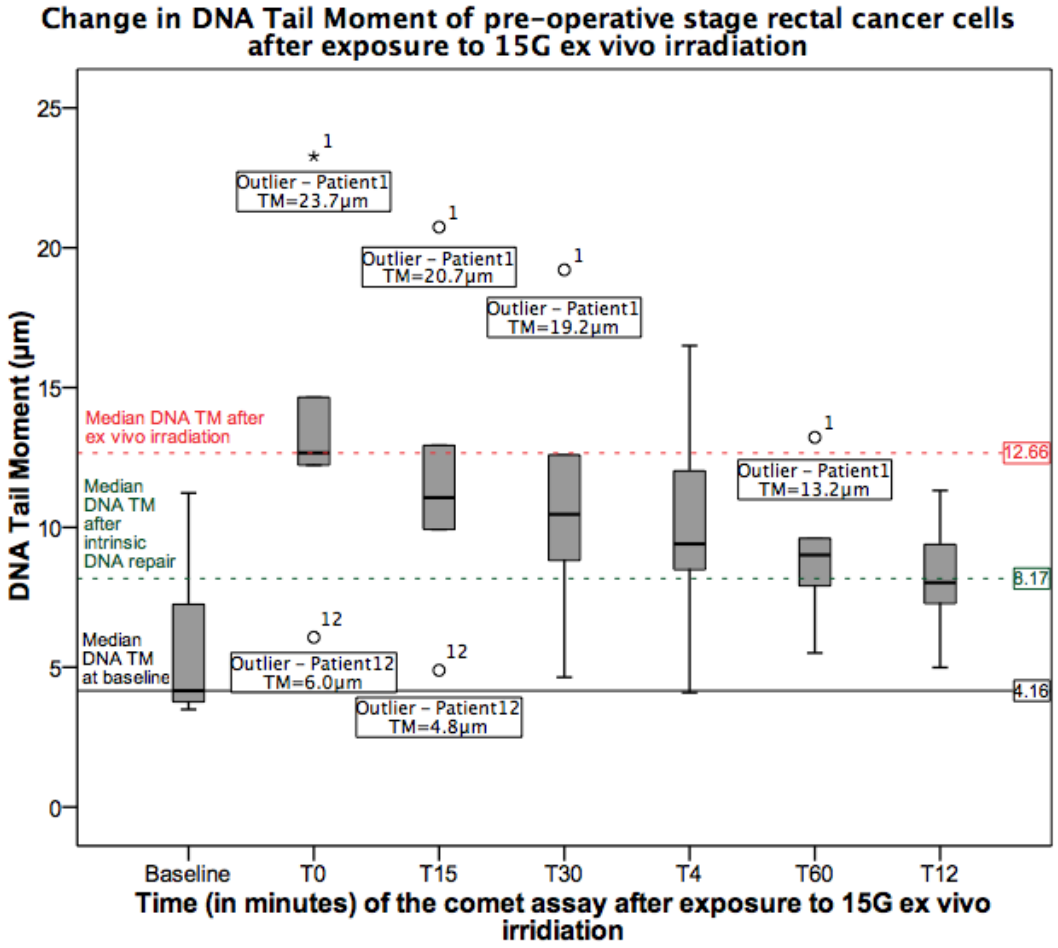

Table 4.17: Percentage change in DNA Tail Moment (DNA repair) of rectal cancer cells at "pre-treatment stage" after exposure to 15Gy *ex vivo* irradiation

Codes		Baseline TM [µm]	Percentage change in TM [µm] at serial time-points after exposure to 15Gy ex vivo irradiation					
		Control	0 (min)	15 (min)	30 (min)	45 (min)	60 (min)	120 (min)
2	DG	11.23	23.27 (+107%)	20.74 (+85%)	19.21 (+71%)	16.50 (+47%)	13.22 (+18%)	11.32 (+0.8%)
4	AH	4.41	14.65 (+232%)	10.76 (+144%)	10.08 (+129%)	9.15 (+107%)	8.57 (+94%)	7.28 (+65%)
5	KB	7.25	12.23 (+69%)	11.37 (+57%)	10.86 (+50%)	9.67 (+33%)	9.46 (+30%)	7.98 (+10%)
6	ED	-	-	-	-	-	-	-
7	AF	-	-	-	-	-	-	-
8	JN	-	-	-	-	-	-	-
9	SD	-	-	-	-	-	-	-
10	JH	-	-	-	-	-	-	-
13	PO	-	-	-	-	-	-	-
14	MM	-	-	-	-	-	-	-
15	RC1	3.49	12.91 (+270%)	9.93 (+184%)	8.82 (+153%)	8.49 (+143%)	7.91 (+127%)	8.07 (+131%)
16	RC2	3.76	6.07 (+61%)	4.89 (+30%)	4.64 (+23%)	4.09 (+9%)	5.51 (+47%)	4.99 (+33%)
17	JT	3.91	12.42 (+218%)	12.93 (+231%)	12.59 (+222%)	12.02 (+207%)	9.61 (+146%)	9.39 (+140%)

Figure 4.10: Bar chart showing percentage changes in DNA tail moment of rectal cancer cell at "pre-operative stage" after exposure to 15Gy ex-vivo irradiation – individual cases

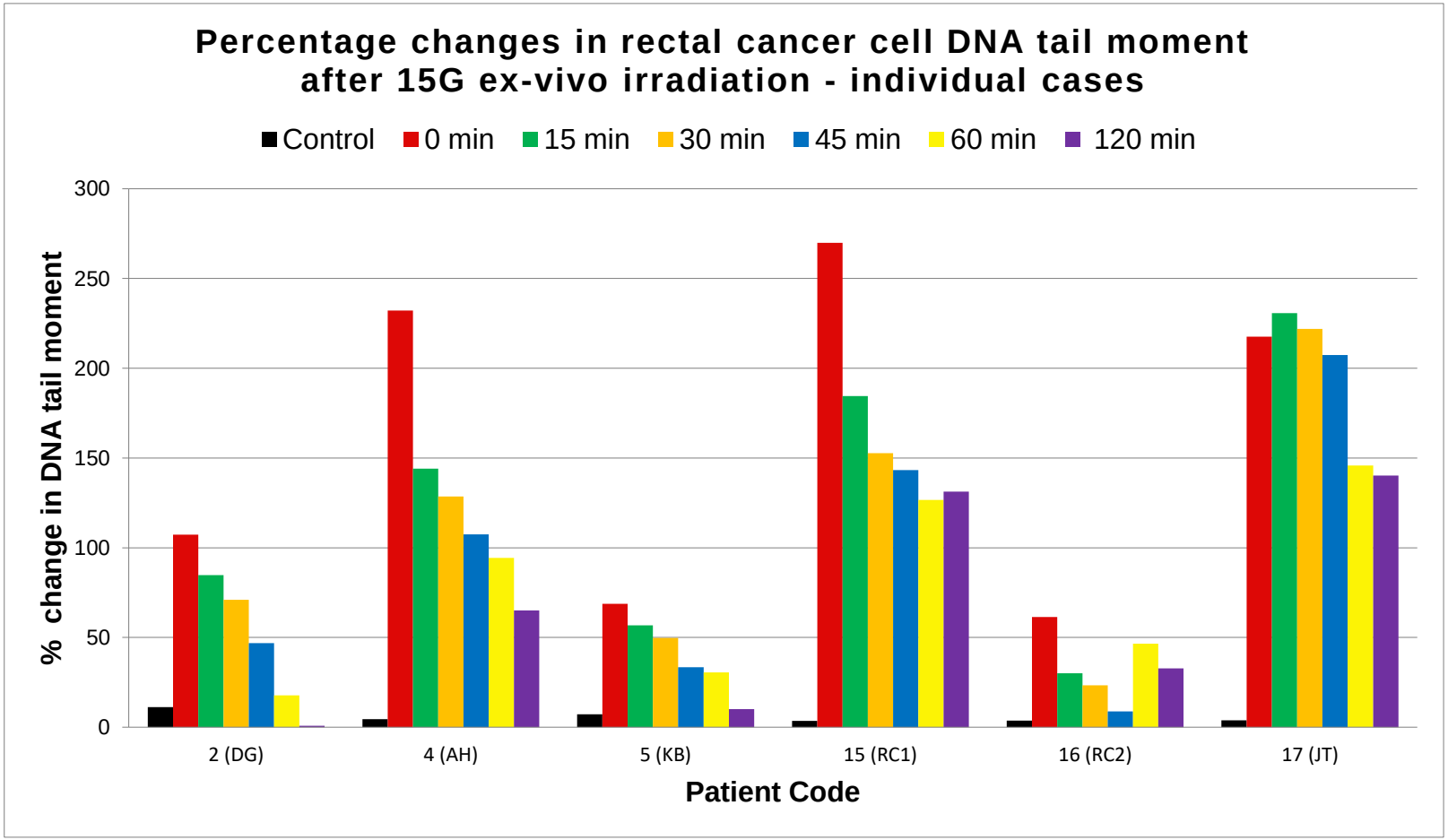

4.3.8 Comparison of DNA repair potential between rectal cancer cells harvested at serial time-points

The DNA repair potential of rectal cancer cells harvested at three serial time-point is given in table 4.18 and figure 4.11; statistical analysis in table 4.19. The percentage changes are given in table 4.20 and figure 4.12.

As expected, the maximum change of mean TM occurs immediately after exposure to *ex-vivo* irradiation. Thereafter, the mean TM decreased in the following 120 minutes, corresponding with cell DNA repair properties. The tumour cells harvested immediately after NCRT (T_1 time-point) show relatively impaired DNA repair as compared to those harvested at other time points: the difference in mean TM between T_0 and T_1 tumour cells is close to and reaches statistical significance for timed assay at 30 and 60 minutes, whilst, there is no statistical significant difference in mean TM between T_0 and T_2 tumour cells for any timed assay (see table 4.19).

Comparative percentage changes shows similar pattern of DNA repair over time for rectal cancer cells harvested at different time points (see table 4.20 and figure 4.12)

CHAPTER 4: DNA REPAIR ANALYSIS

Table 4.18: Changes in mean tail moments following *ex-vivo* irradiation in rectal cancer cells harvested at serial time-points

Timing of assay (min)	Pre-treatment Mean TM [µm] (SD; SE)	Post-NCRT Mean TM [µm] (SD; SE)	Pre-Operative Mean TM [µm] (SD; SE)
Control	5.82 (2.52; 0.69)	6.93 (1.88; 0.56)	5.67 (2.78;1.13)
0	14.70 (3.71; 1.03)	14.25 (3.14; 0.94)	13.59 (5.08; 2.07)
15	11.50 (3.30; 0.91)	12.52 (2.48; 0.74)	11.77 (4.72; 1.92)
30	9.87 (2.39; 0.88)	11.12 (1.81; 0.54)	11.03 (4.39; 1.79)
45	9.50 (2.78; 0.77)	10.46 (1.69; 0.51)	9.98 (3.7; 1.53)
60	8.94 (2.56; 0.71)	10.28 (2.13; 0.64)	9.04 (2.30; 0.94)
120	8.51(2.60; 0.72)	9.48 (2.10; 0.63)	8.17 (1.93; 078)

T (subscript) – timing of biopsy (serial number)

Table 4.19: Comparison of DNA repair profiles (difference in mean tail moments) following *ex-vivo* irradiation in rectal cancer cells harvested at serial time points

Timing of Assay	T_0 vs T_1				T_0 vs T_2			
	n	Mean TM [µm]		p	n	Mean TM [µm]		p
0	11	14.00	14.25	0.59	6	15.53	13.59	0.60
15	11	10.87	12.52	0.11	6	11.80	11.77	0.91
30	11	9.58	11.12	0.06	6	10.53	11.03	0.73
45	11	9.15	10.46	0.11	6	10.40	9.98	0.91
60	11	8.67	10.28	0.03	6	10.04	9.04	0.34
120	11	8.17	9.48	0.13	6	9.87	8.17	0.24

*T (subscript) – timing of biopsy (serial number); n – number of patients included in analysis; Statistical Tests: Shapiro-Wilk test of normality; Wilcoxon signed ranked test; Friedman Test** ; p – statistical significance of <0.05*

Figure 4.11: Comparison of mean TM (timed DNA repair) of rectal cancer cells harvested at different time-points after exposure to 15Gy *ex-vivo* irradiation

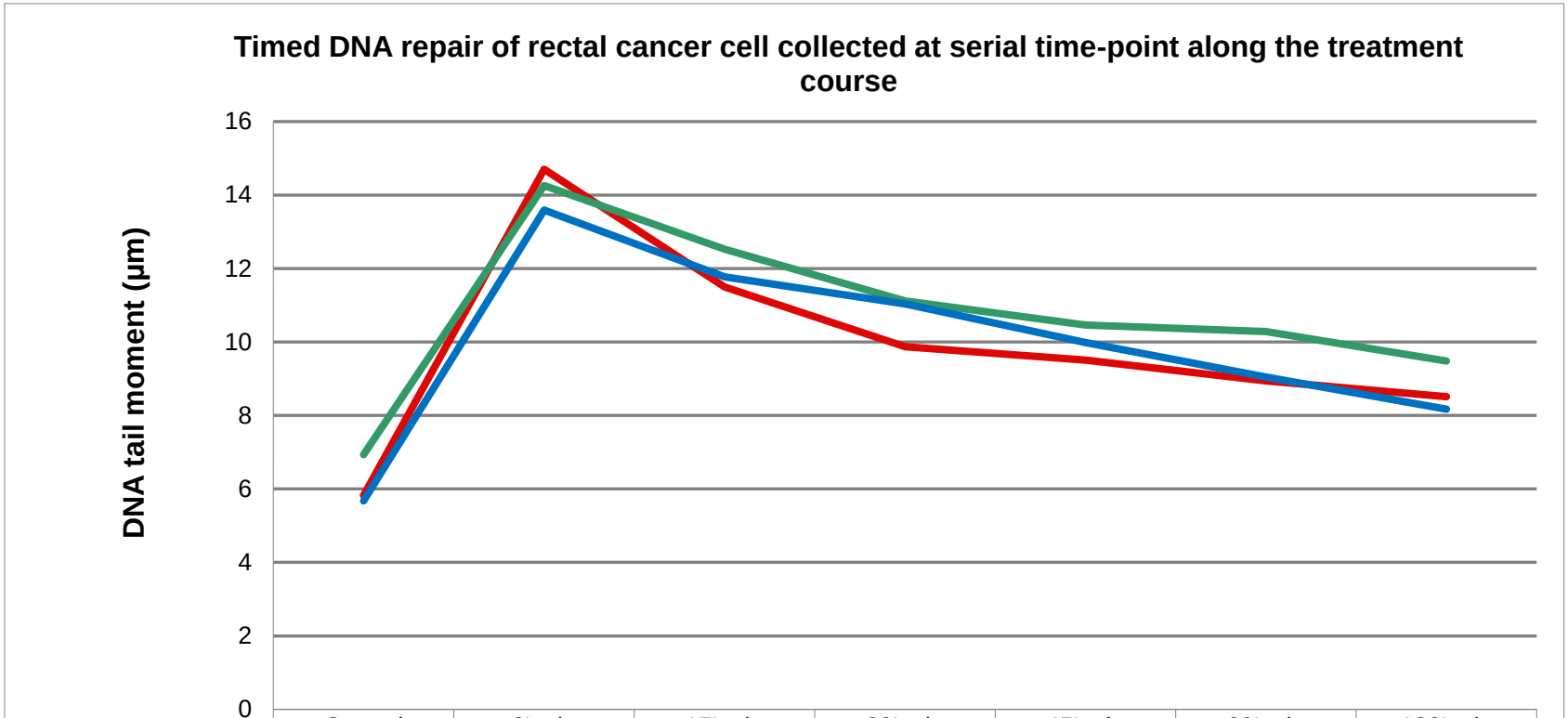

	Control	0' min	15' min	30' min	45' min	60' min	120' min
Pre-Treatment	5.82	14.70	11.50	9.87	9.51	8.94	8.52
Post-NCRT	6.94	14.26	12.53	11.12	10.46	10.28	9.48
Pre-operative	5.68	13.59	11.77	11.03	9.99	9.05	8.17

Table 4.20: Percentage change in mean tail moment

Timing of assay (min)	Pre-treatment Mean TM [µm] (percentage change)	Post-NCRT Mean TM [µm] (percentage change)	Pre-Operative Mean TM [µm] (percentage change)
Control	5.82	6.93	5.67
0	14.70 (+152%)	14.25 (+106%)	13.59 (+139%)
15	11.50 (+97%)	12.52 (+81%)	11.77 (+107%)
30	9.87 (+69%)	11.12 (+60%)	11.03 (+94%)
45	9.50 (+53%)	10.46 (+51%)	9.98 (+76%)
60	8.94 (+54%)	10.28 (+48%)	9.04 (+59%)
120	8.51 (+46%)	9.48 (+37%)	8.17 (+44%)

T (subscript) – timing of biopsy (serial number)

Figure 4.12: Comparison of percentage DNA repair of rectal cancer cells harvested at serial time-points after exposure to 15Gy ex-vivo irradiation

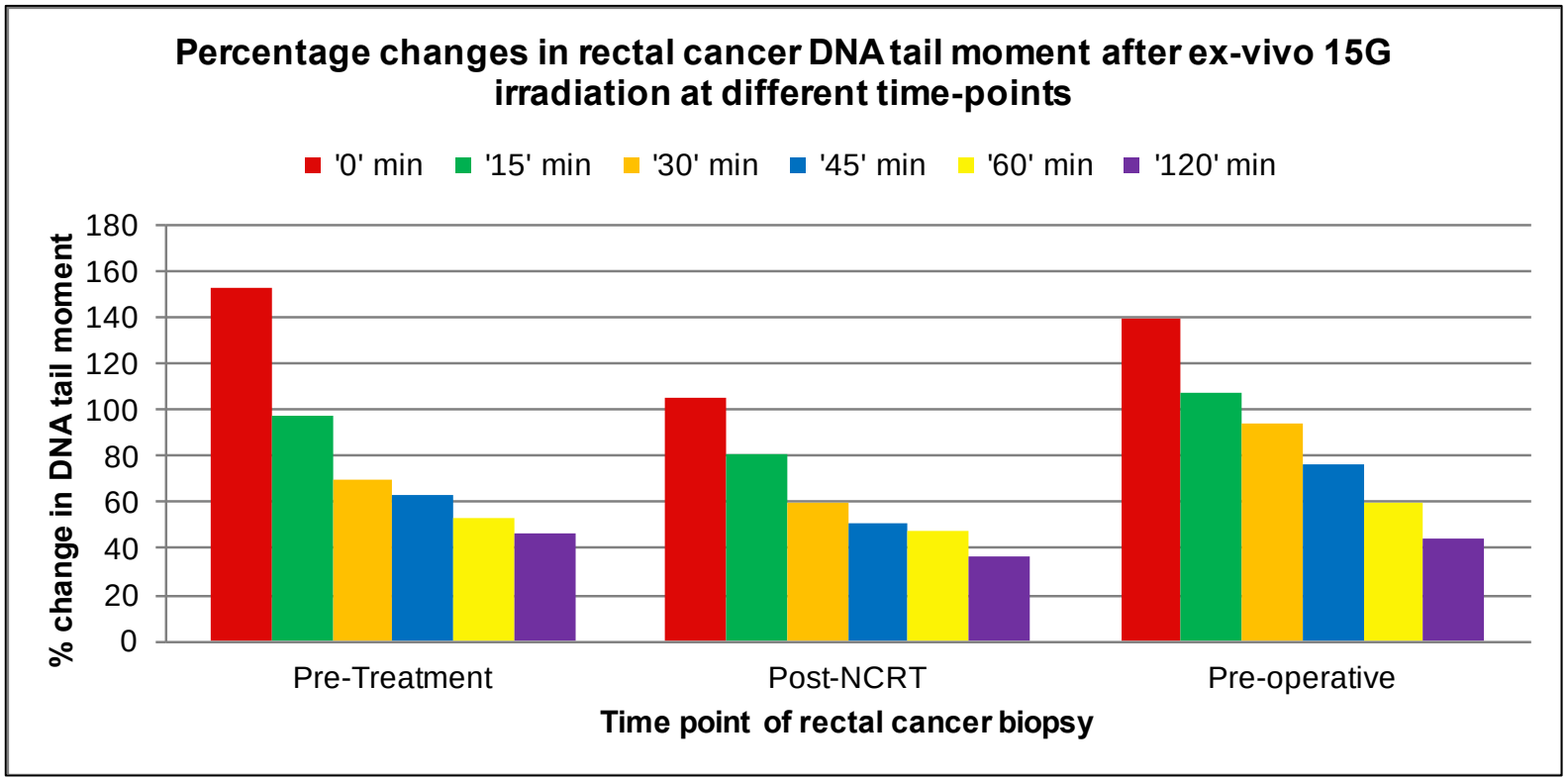

4.3.9 Complete DNA repair in rectal cancer cells within 120 minutes after exposure to *ex-vivo* 15Gy irradiation

Patients who achieved complete DNA repair within 120 minutes after exposure to ex-vivo 15Gy irradiation are shown in table 4.21. For rectal cancer cells harvested at pre-treatment stage, 5/13 (38%) showed completed repair; for rectal cancer cells harvested at post-NCRT stage, 3/11(27%) showed complete repair and for rectal cancer cells harvested at pre-operative stage (median interval 11 weeks after NCRT), 4/6 (66%) showed complete repair.

Table 4.21: Complete DNA repair in rectal cancer cells within 120 minutes after exposure to ex-vivo 15Gy irradiation

Codes		Pre-treatment mean TM [µm]	Post-NCRT mean TM [µm]	Pre-Operative mean TM [µm]
Mean (95% CI)		5.82 (4.4 – 7.25)	6.94 (5.77 – 8.10)	5.68 (3.23 – 8.12)
2	DG	12.77	14.51	11.32
4	AH	8.31	**7.16**	**7.28**
5	KB	12.61	-	**7.98**
6	ED	**6.22**	8.88	-
7	AF	**4.07**	8.84	-
8	JN	7.80	10.02	-
9	SD	9.62	9.85	-
10	JH	**6.95**	11.89	-
13	PO	10.71	9.88	-
14	MM	**6.09**	10.10	-
15	RC1	11.27	**5.54**	**8.07**
16	RC2	8.16	-	**4.99**
17	JT	**6.12**	**7.65**	9.39

*Values compared with baseline values and their 95% confidence interval; **Bold** – complete repair; CI – confidence interval*

4.3.10 Rectal cancer DNA repair profiles and clinical response to NCRT

A descriptive summary of DNA repair profiles for responders and non-responders to NCRT is given in table 4.22. For patients that showed response after NCRT (RECIST criteria; n= 9): 5 (62%) had impaired DNA repair profile at pre-treatment stage whilst 3 (37.5%) patients showed intact DNA repair. Similarly, for patients that showed no response after NCRT (n=5): only 2 (40%) patients showed intact DNA repair profiles. During the interval between NCRT and surgery, for the 8 post-NCRT partial responders (RECIST criteria): one patient (12.5%) achieved complete pathological response, five patients (62.5%) continued to have partial response and two patient (25%) had stable disease at surgery; whereas, for the 5 post-NCRT stable disease patients: one patient (20%) developed complete response, two (40%) patients developed partial response and only one patient (20%) remained in stable disease at the time of surgery. There was impaired DNA repair after NCRT for one patient (50%) with complete response, 5 (71%) patients who remained in partial response and 1 (33%) with stable disease. The DNA repair analysis for the pre-operative specimen (n=5) showed that all three responders and one non-responder (TNM and RECIST criteria) had intact DNA repair pathways.

CHAPTER 4: DNA REPAIR ANALYSIS

Table 4.22: DNA repair profiles and clinical response to NCRT

Code		Staging		RECIST		DNA Repair profiles		
		cTNM	ypTNM	Post-NCRT	Pre-Operative	Pre-Treatment	Post-NCRT	Pre-Operative
2	DG	T3N1	T3N1	PR	SD	X	X	X
4	AH	T3N2	T2N1	SD	SD	X	✓	✓
5	KB	T3N1	T2N0	SD	PR	X	-	✓
6	ED	T3N1	T1N0	PR	PR	✓	X	-
7	AF	T3N1	T2N0	PR	PR	✓	X	-
8	JN	T3N2	T2N0	PR	PR	X	X	-
9	SD	T3N1	-	SD	-	X	X	-
10	JH	T3N0	T3N0	SD	PR	✓	X	-
13	PO	T3N2	T3N2	PR	PR	X	X	-
14	MM	T4N0	-	SD	CR*	✓	X	-
15	RC1	T3N1	T2N0	PR	PR	X	✓	✓
16	RC2	T3N1	T0N0	PR	CR	X	-	✓
17	JT	T3N1	T3N0	PR	SD	✓	✓	-

*'✓ – complete DNA repair; 'X' – impaired DNA repair; * complete response on imaging only; PR – Partial response; SD – stable disease; CR – complete response*

4.3.11 Relations between DNA repair properties and clinicopathological characteristic, response to NCRT and long-term outcomes

The correlation between DNA repair property of rectal cancer cells harvested at different time-points and clinical features is given in tables 4.23–4.26. In general, there were non-significant negative correlations between cancer cell repair and poor clinical markers. Rectal cancer cells harvested at pre-treatment stage with the ability to repair DNA damage secondary to irradiation showed less aggressive nodal spread. Rectal cancer cells harvested at pre-operative stage with the ability to repair DNA damage secondary to irradiation had large craniocaudal tumour length but did not show higher pathological T-stage. There were no correlations between DNA repair properties and response to treatment or long-term outcomes.

CHAPTER 4: DNA REPAIR ANALYSIS

Table 4.23: Correlation analysis between DNA repair pattern and clinic-pathological features, response to NCRT and long-term outcomes

Repair Pattern		Clinicopathological Features							Response to NCRT				Long-term Outcomes		
		cT	cN	pT	pN	cL	nL	pL	T↓	N↓	pCR	nRECIST	LR	DM	Death
T_0	ρ	0.365	**-0.60**	-0.05	-0.48	-0.02	-0.27	-0.37	-0.15	0.18	0.10	-0.02	-0.22	-0.05	-0.18
	p	*0.22*	***0.02***	*0.87*	*0.11*	*0.94*	*0.36*	*0.23*	*0.60*	*0.54*	*0.74*	*0.93*	*0.45*	*0.85*	*0.54*
T_1	ρ / r	-0.19	0.21	0.081	0	-0.19	0.03	0.30	0.03	0.46	-0.19	0.039	-0.19	-0.37	-0.37
	p	*0.56*	*0.52*	*0.82*		*0.56*	*0.92*	*0.38*	*0.91*	*0.15*	*0.56*	*0.91*	*0.56*	*0.25*	*0.25*
T_2	ρ / r	0	0.31	**-0.89**	-0.25	0.52	**0.82**	-0.52	0	0.63	0.31	-0.50	0	-0.63	-0.25
	p		*0.54*	***0.01***	*0.63*	*0.28*	***0.04***	*0.28*		*0.17*	*0.54*	*0.31*		*0.17*	*0.63*

'+' positive correlation; '-' negative correlation; prefix 'c' –Clinical; prefix 'p' – pathological; prefix 'n' – post-NCRT; suffix '↓' – downstage; T – TNM T-stage; N – TNM N-stage; L – craniocaudal tumour length; RECIST – response evaluation criteria in solid tumours; CR – complete response; LR – local recurrence; DM – Distant metastasis; Statistical test – Shapiro-Wilk test for normality; Spearman rho correlation analysis (ρ) non-parametric data, p – significant value at 0.05

Table 4.24: Difference in mean multiparametric values according to clinical features

Repair Pattern		cT				cN				pT					pN		
		cT2	**cT3**	***cT4***	***p***	**cN0**	**cN1**	**cN2**	***p***	**pT0**	**pT1**	**pT2**	**pT3**	***p***	**pN0**	**pN1**	***p***
T_0	No	0	8	0	*0.38**	**0**	**5**	**3**	***0.03***	1	0	4	2	*0.75*	4	3	*0.13*
	Yes	0	4	1		**2**	**3**	**0**		1	1	1	2		5	0	
T_1	No	0	7	1	*0.72**	2	4	2	*0.488*	1	1	2	3	*0.53*	5	2	*0.58*
	Yes	0	3	0		0	2	1		0	0	2	1		2	1	
T_2	No	0	2	0	*	0	2	0	*0.66**	0	0	0	2	*0.11*	1	1	*0.60*
	Yes	0	4	0		0	3	1		1	0	3	0		3	1	

*prefix 'c' –Clinical; prefix 'p' – pathological; prefix 'n' – post-NCRT; suffix '↓' – downstage; T – TNM T-stage; N – TNM N-stage; L – craniocaudal tumour length; RECIST – response evaluation criteria in solid tumours; CR – complete response; LR – local recurrence; DM – Distant metastasis; Statistical test – Chi Square/ Fisher exact test**

Table 4.25: Difference in mean multiparametric values according to response to NCRT

Repair Pattern		T- downstaging			N-downstaging			Post-NCRT RECIST			Post-Operative NCRT			
		$T_{\downarrow}$	$T_{\oslash}$	*p*	$N_{\downarrow}$	$N_{\oslash}$	*p*	PR	SD	*p*	CR	PR	SD	*p*
T_0	No	6	2	*0.51**	5	3	*0.49**	3	5	*0.68**	1	4	2	*0.92*
	Yes	3	2		4	1		2	3		1	3	1	
T_1	No	5	3	*0.72**	4	4	*0.21**	5	3	*0.72**	1	5	1	*0.22*
	Yes	2	1		3	0		2	1		0	1	2	
T_2	No	0	2	*0.067**	1	1	*0.33*	2	0	*0.40*	0	0	2	*0.15*
	Yes	4	0		4	0		2	2		1	2	1	

*prefix 'c' –Clinical; prefix 'p' – pathological; prefix 'n' – post-NCRT; suffix '↓' – downstage; T – TNM T-stage; N – TNM N-stage; L – craniocaudal tumour length; RECIST – response evaluation criteria in solid tumours; CR – complete response; LR – local recurrence; DM – Distant metastasis; Statistical test – Chi Square/ Fisher exact test**

Table 4.26: Difference in mean multiparametric values according to long-term outcomes

Repair Pattern		Local Recurrence			Distant Metastasis			Survival		
		Yes	**No**	***p***	**Yes**	**No**	***p***	**Yes**	**No**	***p***
T_0	No	1	7	*0.61**	2	6	*0.68**	5	3	*0.49*
	Yes	0	5		1	4		4	1	
T_1	No	1	7	*0.72*	3	5	*0.33*	5	3	*0.33*
	Yes	0	3		0	3		3	0	
T_2	No	0	2	.*	1	1	*0.33*	1	1	*0.60*
	Yes	0	4		0	4		3	1	

*prefix 'c' –Clinical; prefix 'p' – pathological; prefix 'n' – post-NCRT; suffix '↓' – downstage; T – TNM T-stage; N – TNM N-stage; L – craniocaudal tumour length; RECIST – response evaluation criteria in solid tumours; CR – complete response; LR – local recurrence; DM – Distant metastasis; Statistical test – Chi Square/ Fisher exact test**

4.4 Discussion

This series of experiments represents the first study on the application of the comet assay on tumour cells harvested from fresh rectal cancer tissue measuring DNA damage and repair profiles against clinicopathological markers and long-term outcomes. The findings show a degree of baseline DNA damage in untreated rectal cancer (mean TM=5.82) that shows good repair in response to ex-vivo irradiation. Until at least six weeks after long course NCRT, DNA showed persistent damage (long tail moment) and the additional DNA damage induced by *ex-vivo* irradiation was more enhanced with impaired DNA repair properties; thereafter, at the time of operation, the DNA damage to *ex-vivo* irradiation and its repair were comparable to pre-treatment tumour cells.

The cytoreductive effects of radiotherapy results by the production of a variety of ionizing radiation-induced lesions in DNA, including DNA single strand breaks, double strand breaks, DNA base alterations, and DNA terminal growth arrest senescence [427]. The DNA lesion instigates a cascade of pro- and anti-apoptotic pathways that leads to programmed cell death [428]. There is also emerging evidence, suggesting generation of anti-tumour immune response after expression of tumoural antigens in response to radiotherapy that augments cytoreduction [429]. The efficacy of radiotherapy is mainly dependent on tissue oxygenation levels and radiosensitivity of tumour cells. Radiotherapy works by generating oxygen radicals capable of causing damage to DNA and at low partial pressures of oxygen (<10 mmHg), tumour cells are 3 times more radioresistant than in well oxygenated state (radiobiologic hypoxia) [430]. The radiosensitivity of cells depends on several factors. Certain genetic

characteristics or mutations in the DNA and/or DNA repair pathways within tumour cells dictate their radiosensitivity, for example, rectal cancers with mutant p53 genotype were shown to resist tumour down-staging after radiotherapy [431]. The radiosensitivity of cells also varies throughout the cell cycle; for example, S-phase cells are relatively radioresistant than G1 and G2/M cells. There is a predominance of DNA repair pathways during specific cell-cycle phases with preference for repairing specific DNA lesions, for example, there is over-expression of proteins involved in repair pathways for double strand breaks (homologous recombination repair pathway), single strand breaks repair pathway and mismatch repair pathway during the S and G2/M phase, whilst, the same proteins are expressed at low levels in G0-G1 cells; alternatively, non-homologous end joining pathway (NHEJ) is operational in all phases of cell cycle [427]. Tumour hypoxia has been shown to influence expression of DNA repair pathway proteins, for example, chronic hypoxia can lead to decreased expression of homologous recombination (HR) repair pathway genes, which may decrease the radioresistance [427]. In addition acquired radioresistance may also develop with fractionated radiotherapy and involves re-population of tumour between radiotherapy fractions [432]. There are several mechanisms that are thought to contribute to the acquired radioresistance including mutated p53, amplification of DNA repair genes, overexpression of the cell-cycle regulator protein, cyclin D1, and activation of pro-survival oncogenes such as EGFR [433]. Hence, within a given tumour tissue, the radiosensitivity of each cell depends on several internal (e.g. cell cycle phase) and external (e.g. tissue blood supply and oxygenation) factors

and there are heterogeneous populations of cells with varying sensitivities to radiotherapy and the abilities to repair DNA damage [434].

In the current study, all the tumour cells collected at serial time-points (before and after NCRT) from the same tumour tissue showed progressive DNA repair, albeit at different rates. The accumulation of DNA damage may contribute to carcinogenesis and baseline DNA damage has been reported in studies investigating peripheral blood lymphocytes from patients with solid tumours [435, 436]. The baseline DNA damage in the pre-treatment rectal cancer cells may be due to several reasons: rectal cancer cells may have damaged DNA as a result of several oncogenic mutations; the biopsies were typically obtained from endoluminal segment of the tumour which mostly consist of peripheral tumour tissue with cells under hypoxic conditions resulting in damaged DNA; the mechanical process of separating tumour cells from connective tissue for single cell suspension may have also resulted in baseline damage. The technique of obtaining biopsy and post-processing of single cells was consistent for all samples; hence tumour cells from all time-points were comparable.

After long course NCRT, there was tumour downstaging in 87% patients (according to TNM staging; table 4.2) and a decrease in tumour size for 66% (10/15) patients (according to RECIST criteria; table 4.3) corresponding to elimination of radiosensitive tumour load. The majority of rectal tumours that downstaged showed impaired DNA repair properties at the pre-treatment stage (60%); interestingly, 40% tumours with intact DNA repair also showed T-downstaging. Similarly, only 33% patients without tumour downstaging showed intact DNA repair properties. Such findings suggest that in the current cohort,

biopsy samples were possibly not representative of the entire tumour cell radio-sensitivities and support the existence of heterogeneous radiosensitivity within rectal cancers. Such heterogeneity in tumour cell population may also explain the absence of any correlation between biopsy harvested cell DNA repair analysis and clinic-pathological markers. After NCRT, one would expect the cells within the residual tumour tissue to represent the radioresistant fraction with intact DNA repair pathways; however, the tumour cells harvested after NCRT showed greater baseline DNA damage (mean TM = 6.93μm) with relatively poor repair profiles (mean TM = 9.48μm at 120 minutes after exposure to *ex-vivo* irradiation). The baseline DNA damage at six weeks after NCRT was statistically significantly increased as compared to pre-treatment samples with poor DNA repair profiles (section 4.3.7.2; page 149) and may reflect persistent effect of irradiation. Therefore, in the case of residual tumour cells obtained at six week after NCRT, ionizing radiation induced DNA damage that did not culminate in immediate cell death. Such cells may either of the two pathways: (i) the cells may be eliminated later during the interval to surgery, or (ii) the cells may survive and become resistant to treatment by improving DNA repair mechanism and upregulating anti-apoptotic pathways (see figure 4.13). In the clinical setting, a study comparing the outcomes of patients with rectal cancer patients operated at 4-6 weeks and at 6-8 weeks after NCRT did not find any significant difference between two groups in terms of T-downstaging, volume reduction rate, complete response rate and long-term outcomes [437]. In contrast, two systematic reviews of published trial has shown higher rate of pathological complete response in patients undergoing surgical resection at longer interval after NCRT but without any impact on surgical complication rates

and long-term outcomes [239, 438]. Similarly, in the current study, the majority of partial response and stable disease patients (RECIST criteria) at six weeks after NCRT showed a progressive response until the time of surgery (11 weeks after NCRT) and their tumours comprised of cells with persistent impaired DNA repair profiles. A relatively small percentage of patients developed stable disease till the time of surgery and their tumours comprised of cells with intact DNA repair after NCRT (see section 4.3.6, page 129). Interestingly, the majority of tumour cells (80%) harvested at the time of operation also showed intact DNA repair properties. Hence, the current analysis confirms the presence of truly radioresistant tumour cells within residual tumour tissue at 11 weeks after NCRT. Such radioresistance within residual tumour may be intrinsic or acquired in response to NCRT. It may be inferred from these results that effects of radiotherapy possibly subside between six to eleven weeks after NCRT and the optimal time of surgery may lie during this period.

Figure 4.13: Residual tumour cell survival after radiotherapy

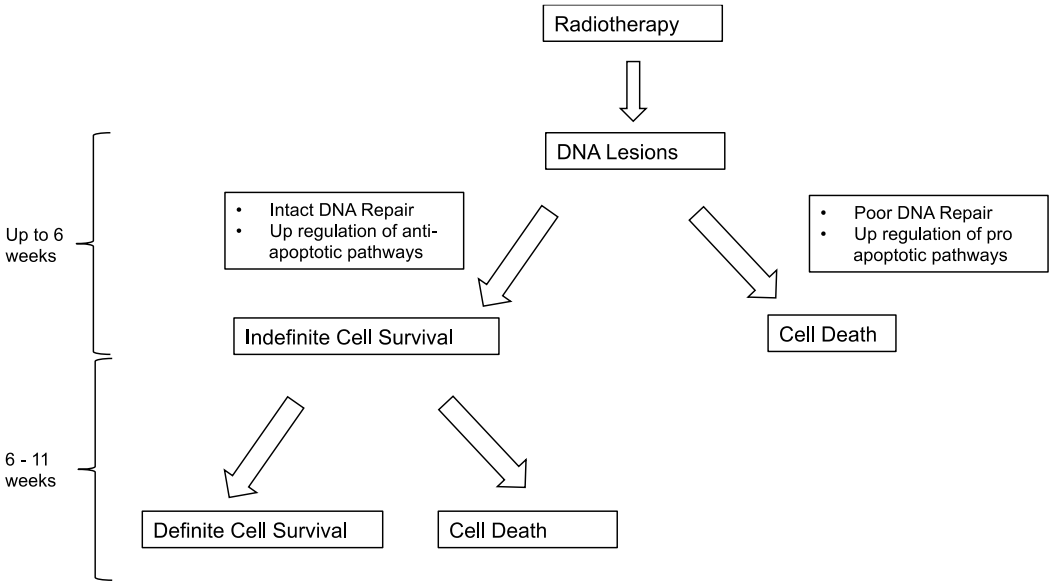

CHAPTER 4: DNA REPAIR ANALYSIS

The study adds to current literature by showing single cancer cells can be harvested from rectal cancer for the assessment of DNA repair by means of Comet assays. The study shows rectal cancer DNA damage and repair profiles at different stages during treatment timeline and provides critical insight into the time period of inhibited DNA repair after NCRT. This pilot study presents the first evidence on rectal cancer alterations after NCRT at a molecular level and similar studies with larger cohorts may help determine the optimal time of interval TME surgery.

There are some weaknesses in the current study: the results should be inferred with care due to small sample size, which decreased further with serial biopsy collection. Several suitable patients declined participation in the current study to avoid repeated rectal tumour biopsy. The endoluminal harvesting of tumour sample is an invasive and uncomfortable procedure especially after radiation-induced proctalgia and highlights a major pitfall in such study designs that leads to low participant recruitment and compliance. Some pre-operative samples were deemed non-viable, mainly those collected from the resected specimen immediately after surgery: one reason would be a ligation of rectal blood vessels at early stages of the surgical procedure with resultant ischaemia and tissue death by the time specimen was retrieved. Challenges faced during tumour cell preparation for comet assays were twofold: firstly the presence of frequent dead cells with debris in collected samples was managed by cell viability test (Trypan® blue test) and a lower count of 15 cells per slide was undertaken; secondly, biopsy samples contained a mixture of tumour and normal epithelial cells which was analysed by consultant histopathologist and high presence of tumour cell was confirmed, hence any bias in results caused

by normal epithelial cell DNA was minimised. Lastly, no intra- and inter-subject variations in TM measurements were established due to the availability of only one observer.

In conclusion, rectal cancer cell populations show heterogeneous radiosensitivity and actively repair DNA damage in response to *ex-vivo* irradiation. The cytoreductive effects of the standard fluoropyrimidine based long-course NCRT inhibits DNA repair at least until six week after treatment. Thereafter, by the 11th week after NCRT, the residual rectal cancer cells mostly harbour intact DNA repair abilities. The results from the current study need to be confirmed in a larger sample size.

5 CHAPTER 5: MAGNETIC RESONANCE IMAGING Multi-parametric analysis of rectal cancer pathophysiology

5.1 Introduction

The modern MRI scanner provides a range of versatile imaging techniques and the simultaneous advances in post processing software has enabled assessment of multiple tissue physiological parameters. Each MRI method provides specific information on different aspects of tumour pathophysiology; for example, ‘diffusion weighted MRI (DW-MRI)’ provides information on tissue cellularity, extracellular space tortuosity and the integrity of cellular membranes by measuring the random motion of the water molecules in tissue; the ‘dynamic contrast enhanced MRI (DCE-MRI)’ method utilises the pharmacodynamics properties of low-molecular weight contrast agents to provide information about tissue blood volume and perfusion, microvessel permeability and the extracellular space; and, the intrinsic susceptibility MRI (ISW-MRI) utilises the paramagnetic property of deoxygenated haemoglobin to establish tissue oxygenation levels and tumour angiogenesis. DWI-MRI and DCE-MRI have been validated in several studies, whereas, ISW-MRI is a developing technology (see table 1.9 and 1.10, page 75 – 76).

The unpredictable outcomes in patients with locally advanced rectal cancer despite evidence-based standard management (NCRT down staging followed by interval TME surgery) may be due to lack of pathophysiological parameters taken into account during tumour staging. We know that pathophysiological

alterations occur prior to any morphological changes in response to neoadjuvant therapy, especially after biological agents. Early detection of such changes may help predict individual tumour behaviour and allow tailored treatment regimes.

MRI assessment of pathophysiological parameters and any changes in response to treatment may help serve this purpose. Previous studies have shown that alteration in water diffusion secondary to cell necrosis (measured as apparent diffusion coefficient (ADC), and vascular changes (measured as the rate and magnitude of enhancement in response to anticancer treatment precede changes in tumour size. An increase in ADC and decrease in vascular transfer constant (K^{trans}) corresponds with a good response, whereas, a persistent low ADC and abnormal enhancement reflects poor response. The aim of this experiment is two-fold: firstly, to evaluate multiple MRI parameters of tumour pathophysiology and their alterations in response to neoadjuvant therapy in patients with locally advanced rectal cancer; and secondly, to correlate baseline and altered values post-NCRT with tumour characteristics, staging and clinical outcomes.

5.2 Methods

5.2.1 Patient population

See chapter 3 for details of patient population. Additional exclusion criteria to MRI applied as well as impaired renal function (eGFR <50mL/min) and previous gadolinium contrast agent hypersensitivity reaction.

5.2.2 Patient Compliance and Exclusions

The study group comprised of 17 patients (12 males, 5 females, median age 71 years (range 52 - 79). Two patients (codes: 13 PO, 16 RC2) completed only one baseline examination and one more patient (code: 3 DJ) was diagnosed with liver metastasis on baseline reproducibility scans and excluded from study thereafter. During the interval between NCRT and TME surgery, immediately after NCRT (T_1) scan, one patient (code: 9 SD) died after developing acute peritonitis not related to rectal cancer or NCRT, whilst another patient (code 11 DP) declined further research related examinations. One patient (code: 6 ED) was unable to complete the last examination. During post-processing stage, one patient was excluded from all analysis due to mucinous histopathology resulting in inconsistent parametric values compared to study cohort; one patient was excluded from both DW- and ISW-MRI due to susceptibility artefact; one patient was excluded from ISW-MRI due to susceptibility artefact. The patient compliance, exclusion and the number included in final analysis are given in table 5.1.

CHAPTER 5: MRI – MULTIPARAMETRIC ANALYSIS

Table 5.1: Patient Compliance and Exclusions

Code		DW-MRI					ISW-MRI					DCE-MRI					Reason
		$T_0^{(1)}$	$T_0^{(2)}$	T_1	T_2	T_3	$T_0^{(1)}$	$T_0^{(2)}$	T_1	T_2	T_3	$T_0^{(1)}$	$T_0^{(2)}$	T_1	T_2	T_3	
1	RY	✓	✓	✓	✓	✓	✓	✓	✓	✓	✓	✓	X	✓	✓	✓	Technical failure
2	DG	✓	✓	✓	✓	✓	✓	✓	✓	✓	✓	✓	✓	✓	✓	✓	
3	DJ	✓	✓	X	X	X	✓	✓	X	X	X	✓	✓	X	X	X	Metastasis - excluded
4	AH	✓	✓	✓	✓	✓	✓	✓	✓	✓	✓	✓	✓	✓	✓	✓	
5	KB	✓	✓	✓	✓	✓	✓	✓	✓	✓	✓	✓	✓	✓	✓	✓	
6	ED	✓	✓	✓	✓	X	✓	✓	✓	✓	X	✓	✓	✓	✓	X	Did not attend last scan
7	AF	✓	✓	✓	✓	✓	✓	✓	✓	✓	✓	✓	✓	✓	✓	✓	
8	JN	✓	✓	✓	✓	✓	✓	✓	✓	✓	✓	✓	✓	✓	✓	✓	
9	SD	✓	✓	✓	X	X	✓	✓	✓	X	X	✓	✓	✓	X	X	Died after NCRT
10	JH	✓	✓	✓	✓	✓	✓	✓	✓	✓	✓	✓	✓	✓	✓	✓	
11	DP	✓	✓	✓	X	X	✓	✓	✓	X	X	✓	✓	✓	X	X	Declined participation
12	GA	✓	✓	✓	✓	✓	✓	✓	✓	✓	✓	✓	✓	✓	✓	✓	
13	PO	✓	X	✓	✓	✓	✓	X	✓	✓	✓	✓	X	✓	✓	✓	Mucinous tumour
14	MM	✓	✓	✓	✓	✓	✓	✓	✓	✓	✓	✓	✓	✓	✓	✓	R_2* susceptibility artefact
15	RC1	✓	✓	✓	✓	✓	✓	✓	✓	✓	✓	✓	✓	✓	✓	✓	
16	RC2	✓	X	✓	✓	✓	✓	X	✓	✓	✓	✓	X	✓	✓	✓	R_2* susceptibility artefact
17	JT	✓	✓	✓	✓	✓	✓	✓	✓	✓	✓	✓	✓	✓	✓	✓	
Imaging Completed		17	15	16	14	14	17	15	16	14	13	17	14	16	14	12	
Included in Study		**15**	**14**	**13**	**11**	**11**	**14**	**14**	**12**	**11**	**10**	**16**	**14**	**15**	**13**	**11**	

✓ *Completed scan and included in analysis* ✓ *Completed scan but not included in analysis* X *Did not complete scan; DNA- did not attend*

5.2.3 MRI analysis of rectal tumour

All patients underwent multi-parametric MRI within a single examination on 5 occasions: Two baseline scans within 14 days ($T_0^{(1)}$ + $T_0^{(2)}$) for reproducibility analysis, thereafter, one scan each within two-weeks post-NCRT (T_1), six-weeks post-NCRT (T_2) and 11-weeks post-NCRT or pre-operatively (T_3). The MRI examination schedule is shown in figure 5.1.

Figure 5.1: MRI examination schedule and completion rates

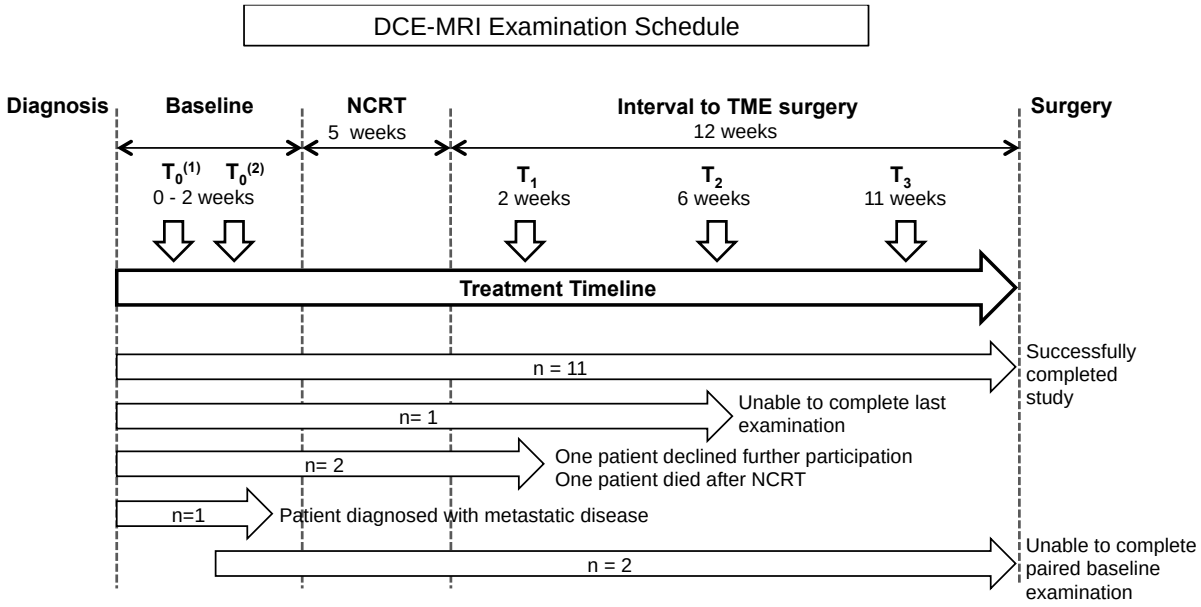

where, T (subscript) represent timing of the examination along the treatment line: $T_0^{(1)}$ and $T_0^{(2)}$ were paired baseline examination on day 1 and day 2, respectively; T_1, T_2 and T_3 were post-NCRT examination at second week, sixth week and eleventh week, respectively. The 'n' denotes number of patients completing examination.

5.2.4 Image acquisition

MRI was performed using a 1.5T system (Avanto or Symphony or TIM Symphony; Siemens Medical Systems, Erlangen, Germany), with a pelvic phased array coil and the protocols specified in table 5.2. The images were obtained in the following order:

1. Standard morphological images
2. Diffusion-weighted
3. Intrinsic susceptibility
4. Dynamic contrast enhanced (after injection of contrast agent)

Table 5.2: MRI scanner protocols:

	Symphony TIM	Symphony	Avanto
DCE-MRI			
Sequence	T1-weighted volume interpolated breath-hold excitation gradient-echo (VIBE)		
TR (ms)	6.6	6.6	6.6
TE (ms)	1.8	1.38 /1.44	1.22
NEX	1	1	1
FOV (mm)	260^2	260^2	260^2
Flip Angles (degree)	3° (PDW) 21° (T1W)	3° (PDW) 21° (T1W)	3° (PDW) 21°(T1W)
Acquisition matrix*	256x174	192 x 131	256x174
Receiver bandwidth (kHz)	700	700	698
Slice thickness (mm)	5	5	5
Number of slices	12	12	12
DW- MRI			
Sequence	Echo planar imaging (EPI)		
TR (ms)	5900	4500	4500
TE (ms)	92	75	75
FOV (mm)	380^2	380^2	380^2
Acquisition matrix	190x139	190x140	190x139
Receiver Bandwidth (kHz)	1195	1185	1654
b-value (s/mm^2)	0, 100, 500, 800	0, 100, 500, 800	0, 100, 500, 800
Fat suppression	Spectral FS	Spectral FS	Spectral FS
Diffusion mode	3-scan trace	3-scan trace	3-scan trace
Slice thickness (mm)	5	5	5
Number of slices	20	20	20
ISW-MRI			
Sequence	Gradient recall echo (GRE)		
TR (ms)	100	100	100
TE (ms)	4.76,14.3,23.8,33.4 ,61.9	5,10.15, 30, 45, 60	4.76,14.3,23.8,33.4 ,61.9
NEX	5	5	5
FOV (mm)	260^2	260^2	260^2
Flip angle (degree)	25°	25°	25°
Acquisition matrix	256^2	128^2	256^2
Slice thickness (mm)	5	5	5
Number of slices	6	6	6

TE – time to echo; TR – repetition time; NEX – number of excitation; FOV – field of view; PDW – proton density weighted; T1W – T1-weighted

**Reconstructed to 256^2*

5.2.4.1 Morphological Imaging:

Breath-hold gradient echo T1-weighted and turbo–spin echo T2-weighted sequences were acquired to stage the tumour and to identify the tumour slice location. The central 4 tumour slices served as reference points for future serial scans on the same patient (figure 5.2.). Care was taken when repositioning the patient exactly in the same position on subsequent visits in order to obtain the same anatomical slice location.

Figure 5.2: Image slice placement and selection

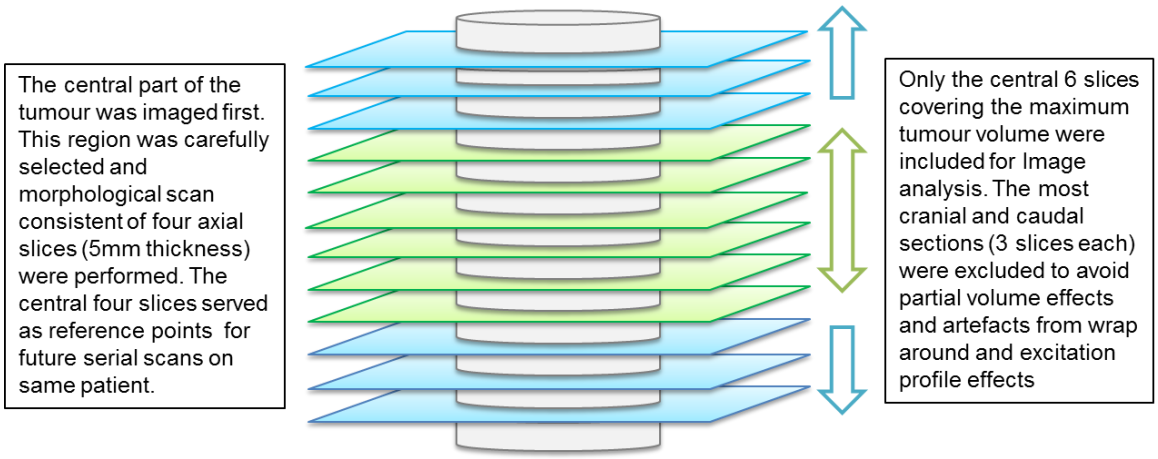

5.2.4.2 Diffusion Weighted Images:

DW-MRI measurements were acquired with a free- breathing, multiple-averaging technique, using single- shot echo-planar MR imaging. Four motion probing gradients with b-values of 0, 100, 500, 800 s/mm^2 were applied in the three orthogonal directions of the magnet (frequency, phase and slice-select). The orthogonal directional images were used to generate trace images for each b-values. Fat suppression was achieved with spectral FS sequences.

5.2.4.3 Intrinsic susceptibility weighted images:

Multiple spoiled gradient-recalled-echo sequences with increasing echo times were acquired, from which R_2* maps were calculated (see table 5.2).

5.2.4.4 Dynamic contrast enhanced images

Initially proton density-weighted 3-dimensional (3-D) gradient recalled echo volume interpolated breath hold examination (VIBE) sequences were acquired (flip angle 3°; see table 5.2) at the same slice positions to enable the calculation of tissue contrast concentration. Thereafter, a dynamic series of T1-weighted 3-D VIBE sequence images were acquired sequentially (flip angle 21°; see table 5.2) with a time resolution of 10 seconds (40 time points over 6 minutes), with four images prior to a bolus of contrast agent. During the acquisition of fifth image (i.e, beginning after 48 seconds) a bolus of 0.1mmol/kg body weight of gadopentetate dimeglumine (Gd-DTPA, Magnevist; Bayer) contrast agent was administered at 4ml/s using a power injector, followed by a 20 ml bolus of normal saline at the same rate. No muscle relaxants were administered during any scanning sequence.

5.2.5 Image Analysis

Image analysis was performed in consensus by an experienced consultant radiologist and a MRI physicist with specialist interest in MR based tumour physiology imaging (more than 15 years' experience). Any motion artefact was minimised using propriety motion correction software (Tissue 4D^{TM}, Siemens). The images were analysed using a specialist MRI software package developed at the Institute of Cancer Research, London, UK [439]. The DCE-MR images

were analysed using Magnetic Resonance Imaging Workbench (MRIW© ICR, v 4.4), whilst DW-MR and ISW-MR images were analysed using Diffusion View (DV© ICR, v 2.1.3).

5.2.5.1 Region of interest (ROI):

The central 6 slices with maximal tumour volume were used. For each axial image section, using the information from morphological T1 or T2 weighted images and post contrast T1 weighted images, ROIs were carefully drawn free hand around the tumour by the radiologist excluding pulsatile artefacts from blood vessels and susceptibility artefacts from adjacent bowel lumen. The process was repeated for all axial image sections that contained the tumour.

5.2.5.2 Diffusion Weighted MRI

ADC was calculated using all b-values. ROIs were drawn on the trace/index b-value = 800 s/mm^2 images (see figure 5.3). The ROI was then copied on to the corresponding ADC map to enable each voxel value within the ROI on ADC map to be recorded. The process was repeated for all axial section that included the target lesion. Median ADC at each time point was calculated by analysing all the voxel within the tumour (see figure 5.4).

Figure 5.3: DW-MRI Images at different b value

Images obtained at different b values. For the purpose of current experiment ROI were drawn on the trace/index b-value = 800 s/mm^2 images.

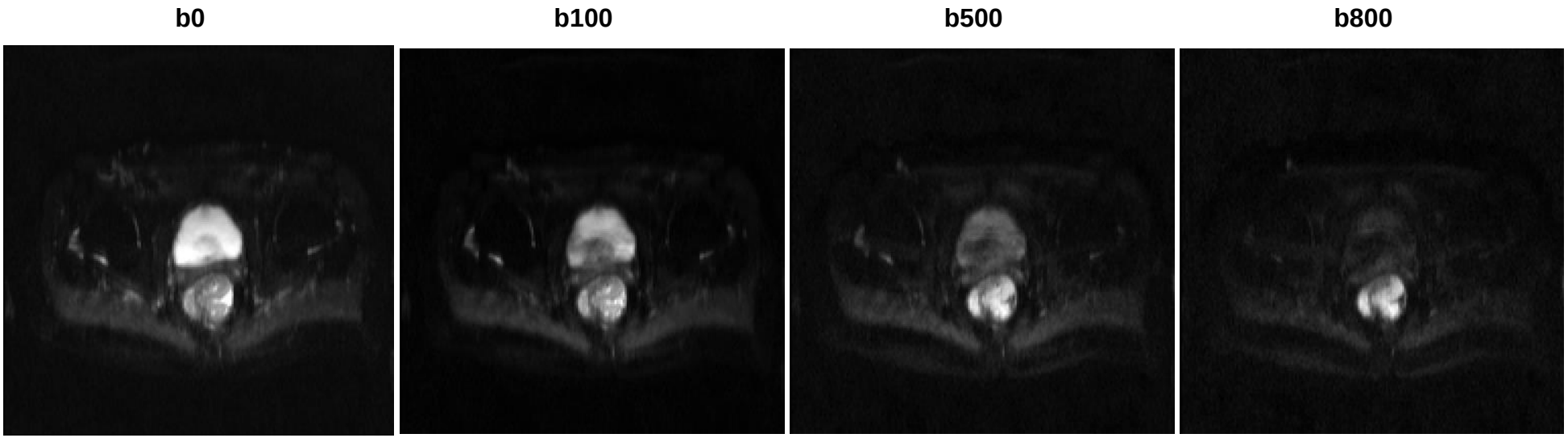

Figure 5.4: DWI versus standard T2 weight image acquisition

The actual images of patient number 1 are presented below: columns show ADC maps (calculated from b0 and b800 s/mm^2 images), diffusion weighted b800 and T2-weighted images. Progressive decrease in tumor size is seen with increases in ADC values consistent with tumor cell death.

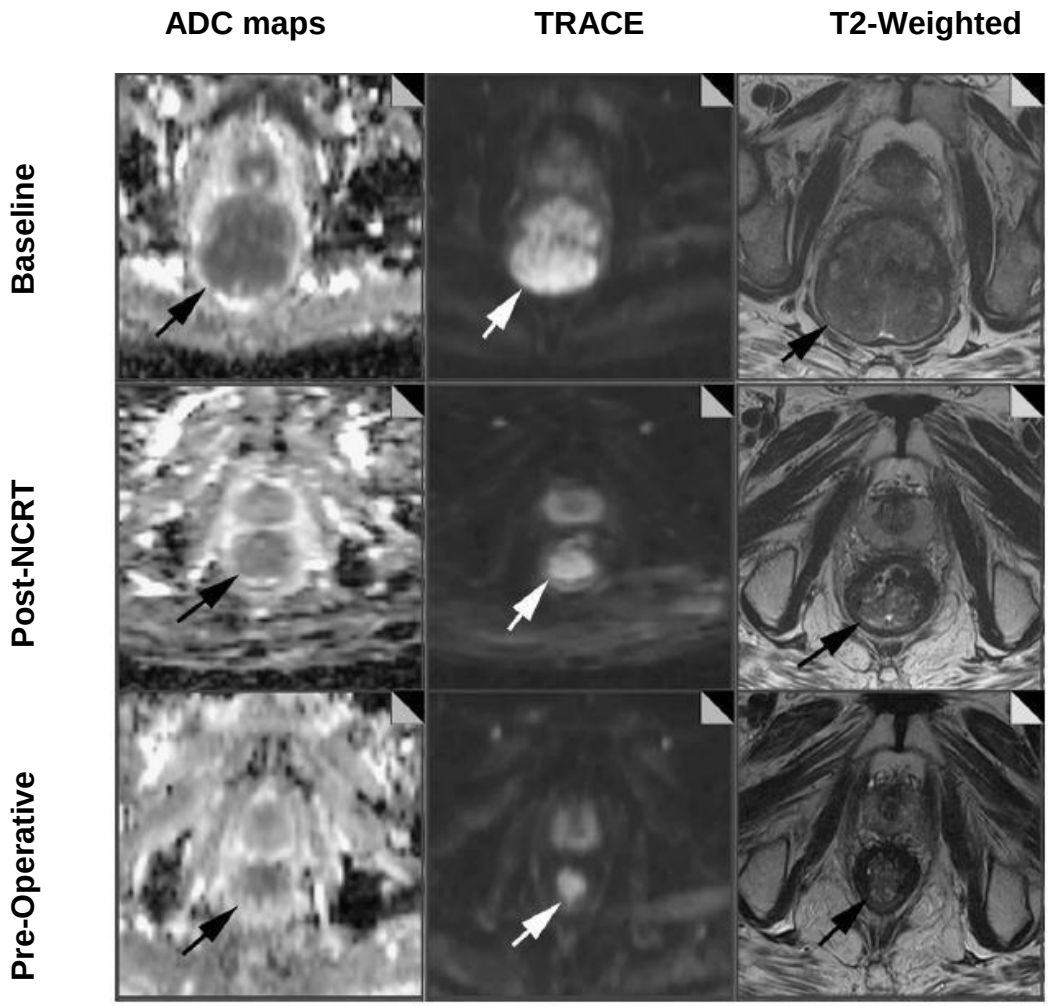

5.2.5.3 Intrinsic Susceptibility Weighted MRI

The signal changes on the ISW-MR images were used to calculate intrinsic T_2* relaxivity. The R_2* maps were calculated on a voxel-by-voxel basis from a straight line fitted to a plot of natural logarithm of 'ln' of signal intensity (T_2*) against echo times (TE) using a least squares approach, of which the gradient is $-R_2$*(unit: seconds^{-1}). Voxels with either negative or zero value were excluded from analysis.

5.2.5.4 Dynamic Contrast Enhanced MRI:

The dynamic image data were analysed using both quantitative and semi-quantitative approaches. Semi quantitative analysis was performed directly from T1-weighted images but quantitative analysis required conversion of MR signal intensities to Gd-DTPA concentrations. MRIW© software was used to convert MRI signal intensities of the T1-weighted DCE-MRI dataset into T1 relaxation rates (R1) and then into Gd-DTPA concentrations for individual voxels, using methods described by Parker et al [343]. The changing tissue Gd-DTPA curve was fitted to a standard compartmental model [364] (see appendix IV, page 389). A pooled arterial input function, based on cosine plasma bolus method defined by Parker et al [440], was used for modelling procedure. The following T1-weighted parameters were calculated in the MRIW© software: the initial area under the GD-DTPA concentration-time curve for the first 60 seconds ($IAUGC_{60}$; mM.second), transfer constant (K^{trans}; minute^{-1}), rate constant (k_{ep}; minute^{-1}) and leakage space (v_e; %). Voxels that did not enhance and those enhancing voxels that failed the modelling process or had values >5.0 minute^{-1} were excluded from statistical analysis of K^{trans}, v_e and k_{ep} parameters, However

$IAUGC_{60}$ estimates include voxels that failed the modelling process as these will include $K^{trans} > 5$ $minute^{-1}$.

5.2.6 Statistical Analysis

The parameters values from baseline MRIs were analysed to assess baseline reproducibility using Bland-Altman agreement analysis [441, 442] as described previously [443]. We included data from all patients (no outliers excluded).

The distribution of the differences in paired baseline MR parameters was tested for normality by Shapiro-Wilk's test. The mean (SD) was determined for each parameter and for each study. Any relation between the difference and mean values of paired baseline MR parameters was tested with Kendal's tau test of correlation. In case of either skewed distribution or significant correlation, the data was log transformed. Analysis of variance (ANOVA) was used to determine the difference between paired measurements and derive the statistical measures described below in tables 5.3–5.5. Bonferroni correction was applied to the statistical power of 0.05 for multiple comparisons. The confidence intervals for statistical estimates were calculated using t- and Chi-squared distribution scores due to small sample size.

Day-to-day reproducibility was assessed using Bland-Altman statistics. The mean difference and 95% limits of agreement (i.e., mean difference - 2 standard deviations and mean difference + 2 standard deviations) were determined. Within this framework, the 95% repeatability coefficient was determined as 2.77 of the standard deviation of the differences.

The coefficient of variation between-patients was estimated as follows: The partial differences between the readings were calculated, and then their standard deviation was divided by their mean and expressed as a percentage. The coefficient of variation between readings was assessed according to the root mean squared approach, whereby (SD/M) 2, where SD is standard deviation and M is mean, was calculated across the patient's two readings. These values were then averaged across patients, and the square root was taken and then reported as a percentage.

Variance-components analysis was undertaken using a linear model with random effects on intercept, given patient as a grouping factor. The intra-class correlation coefficient and its 95% confidence interval were also estimated.

Any changes in MR parameter values on serial examinations after NCRT were converted to percentage change from baseline (see formula below) and tested for significance.

$$\frac{Parametric\ value\ at\ serial\ time\ points - Parametric\ value\ at\ baseline}{Parametric\ value\ at\ baseline} \times 100$$

where, 'baseline is the mean parametric values at $T_0^{(1)}$ and $T_0^{(2)}$' and serial time points is the parametric values at T_1 (pre-treatment stage), T_2 (post-NCRT stage) and T_3 (pre-operative stage). Any changes beyond '95%CI of mean difference' for group and '95% repeatability coefficient (r)' for individual patients were considered significant.

Clinical data was tested for normality by Shapiro-Wilk test. The correlation between DCEI parameters and clinicopathological markers was assessed by

CHAPTER 5: MRI – MULTIPARAMETRIC ANALYSIS

Person and Spearman rank correlation analysis for parametric and non-parametric data respectively. Similarly, the difference in mean parametric values amongst clinicopathological markers was analysed by analysis of variance for normally distributed data and Kuskal-Wallis of Mann-Whitney-U test for non-normally distributed data. The MR multi-parametric measurements at different time-points and their alterations post-NCRT were evaluated against clinical data by means of one-way analysis of variance and chi-square or Fisher exact test plus Spearman rank correlation analysis, respectively.

Subgroup analysis comparing difference in mean parametric values before and after treatment and clinicopathological markers was performed by Wilcoxon-signed rank test. Statistical significance was taken at $p < 0.05$.

Table 5.3: Statistical measures of spontaneous changes within-subject between paired measurements

Statistical Measure	Abbreviation	Definition and Derivation
Mean squared difference	dSD	Estimation of spontaneous change in a parameter between two measurement $dSD = \sqrt{\frac{d^2}{n}}$
95% Confidence Interval of dSD	$CI\,cohort$	Measures magnitude of spontaneous change in a parameter expected in a group. Any change in a group of 'n' greater than this value would be significant at the 5% level. $CI = \pm\left(1.96 \times \frac{dSD}{\sqrt{n}}\right)$ or, for natural log transformed data $\%\ CI = \frac{(100 \times antilog\ (log_{10})\ mean \pm CI}{mean}$
Variance ratio	F	The ratio of between-patient variance to within-patient variance. It is a sensitive measure of reproducibility. Parameters with large F have small within-patient variance and large between-patient variance.

Table 5.4: Statistical measures of repeatability

Statistical Measure	Abbreviation	Definition and Derivation
Within-subject standard deviation	wSD	It is the standard deviation of repeated measurements. The wSD measures the size of the measurement error [444]. $wSD = \sqrt{within\ subject\ variance}$
Repeatability Coefficient	r	The difference between two measurements for the same subject is expected to be less than 2.77 (wSD) for 95% of pairs of observations. The *r* is expressed at percentage. $r = \sqrt{2} \times 1.96(wSD) = 2.77\ (wSD)$ or, for transformed data %r = [100x antilog ($\log_{10}$ mean ± r)]/ mean
Bland-Altman Limits of agreement	LoA	Gives an estimate of the range within which we expect 95% of future measurements between two observers / observers/ methods to lie. $95\%\ LoA = mean\ difference \pm 1.96 \times SD\ (differnece)$ Note: the 1.96 was replaced with t-distribution score according to degree of freedom for current analysis (dependent on sample size)

Table 5.5: Statistical measures of reproducibility

Statistical Measure	Abbreviation	Definition and Derivation
Inter-class correlation coefficient	ICC	A measure of precision of parameters estimates. The proportion of total variance within the data that is explained by variance between observers; ICC = 1 means perfect agreement between observer; ICC = 0 means no agreement between observers. $ICC = \frac{bVAR}{bVAR + wVAR}$
Variance components (within-subject and between-subject)	$wVAR\ and\ bVAR$	Measure variability of the results within patients (for example, within patients over two measurements: 1-2 days, 1-2 observer) and between patients (for example, the same observer on day 1 or the same day different observer).
Coefficient of variation (within-subject and between-subject)	$wCV\ and\ bCV$	Estimates the spread of measurements around the mean. The wCV estimates the degree of variation of measurements in an individual in relation to mean of the group. The bCV compares the degree of variation of measurements between groups. The value of > 0.5 is unreliable [445]. Expressed as percentage. $CV = \frac{SD}{Mean}$ The wCV is estimated with the root mean squared approach. $wCV = \sqrt{mean\left[\left(\frac{SD}{mean}\right)^2\ for\ each\ paired\ measurement\right]}$ or, for natural log transformed data $wCV = antilog\ (wSD) - 1$ The bCV is estimated by the values of differences between repeated measurements $bCV = \frac{SD\ of\ mean\ difference}{mean\ of\ difference}$

CHAPTER 5: MRI – MULTIPARAMETRIC ANALYSIS

5.3 Results

5.3.1 Patient population, characteristics and clinical outcomes

Please refer to chapter 4, sections 4.3.1, 4.3.2 and 4.3.3 (pages 121-125).

5.3.2 Baseline measurement reproducibility and observer agreement of MR parameters in rectal cancers

Multi-parametric MR data of 14 patients was suitable for reproducibility analysis as shown in the table 5.6. Overall, all the measured parameters had satisfactory reproducibility.

Table 5.6: Baseline measurement reproducibility of MR parameters

Parameter	*Mean*	Spontaneous Change			Repeatability		Reproducibility		
		dSD	CI cohort (as %)	F	r (as %)	wSD	wCV	ICC	LoA
ADC (x10^{-3} mm^2/sec)	*1.35*	0.07	±0.039 (±2.91%)	35.1	±0.14 (±10.9%)	0.05	0.03	0.94	±0.15
❖R_2* (min^{-1})	*22.9 (ln 3.12)*	0.09	±0.04 (-4.67 to 4.9 %)	6.7	0.17 (-16.38 to +19.6 %)	0.06	0.06	0.74	-0.16 to 0.19
K^{trans} (min^{-1})	*0.17*	0.04	±0.02 (±13.7%)	4.3	±0.09 (±51.4%)	0.03	0.18	0.60	-0.06 to 0.10
v_e (%)	*0.24*	0.06	±0.03 (±14.1%)	2.4	±0.12 (± 52.9%)	0.04	0.19	0.38	-011 to 0.14
k_{ep} (min^{-1})	*0.73*	0.15	± 0.08 (±11.1%)	4.9	±0.3 (±41.5%)	0.1	0.15	0.64	-0.23 to 0.35
❖$IAUGC_{60}$ (min^{-1})	*3.03*	0.21	±0.113 (-10.7% to 12.0 %)	35.3	0.42 -34.6% to +52.9%	0.15	0.16	0.94	-0.33 to 0.48

dSD – mean squared differences, CI cohort – 95% confidence interval for the cohort, F – variance ratio, r – individual patient repeatability, wSD - within-patient standard deviation, wCV - within-patient coefficient of variation, , ICC – interclass correlation coefficient, LoA – Limits of agreement (Bland-Altman); ❖ log transformed

For DW-MRI, ADC values showed minimal spontaneous change (CI cohort ±2.91%, F 35.1) with excellent repeatability (r ±10.9%) and minimal observer introduced variability (wCV 3%, ICC 94%, LoA ±0.15) on paired measurements.

Bar plots of paired mean ADC and corresponding Bland-Altman limits of agreement plots are shown in figure 5.5 and 5.6 respectively.

Figure 5.5: Baseline ADC reproducibility for individual patient data changes values to x10^{-3}

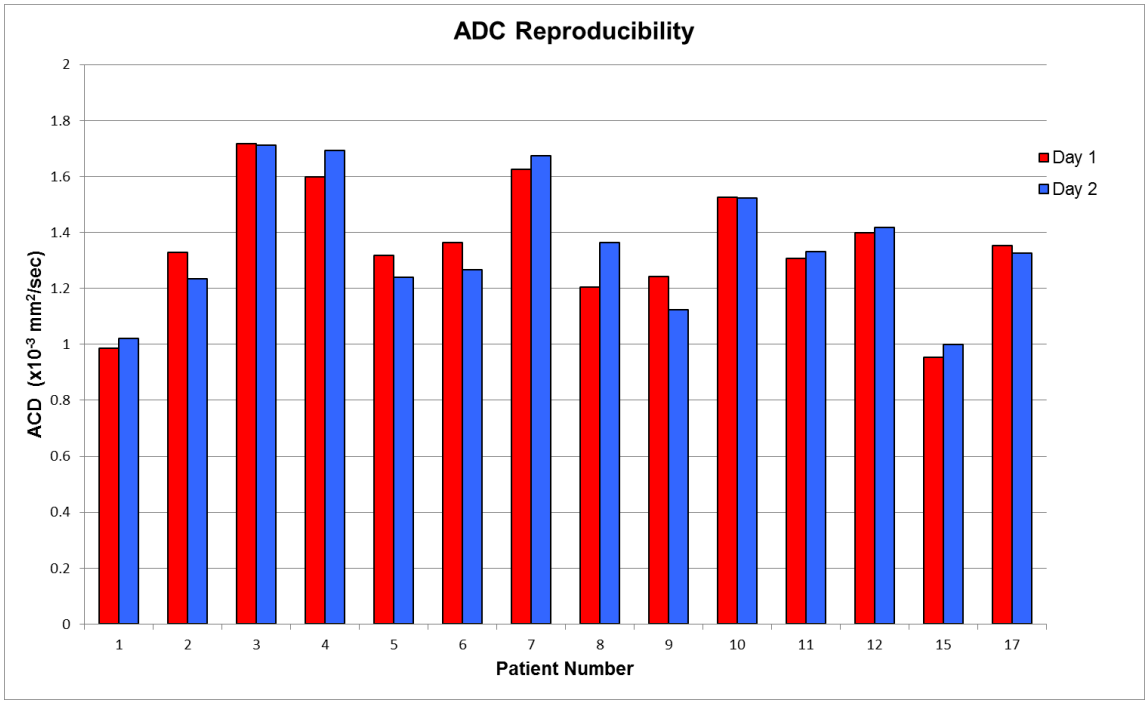

Figure 5.6: Bland-Altman plot for ADC measurement agreement changes values to x10^{-3}

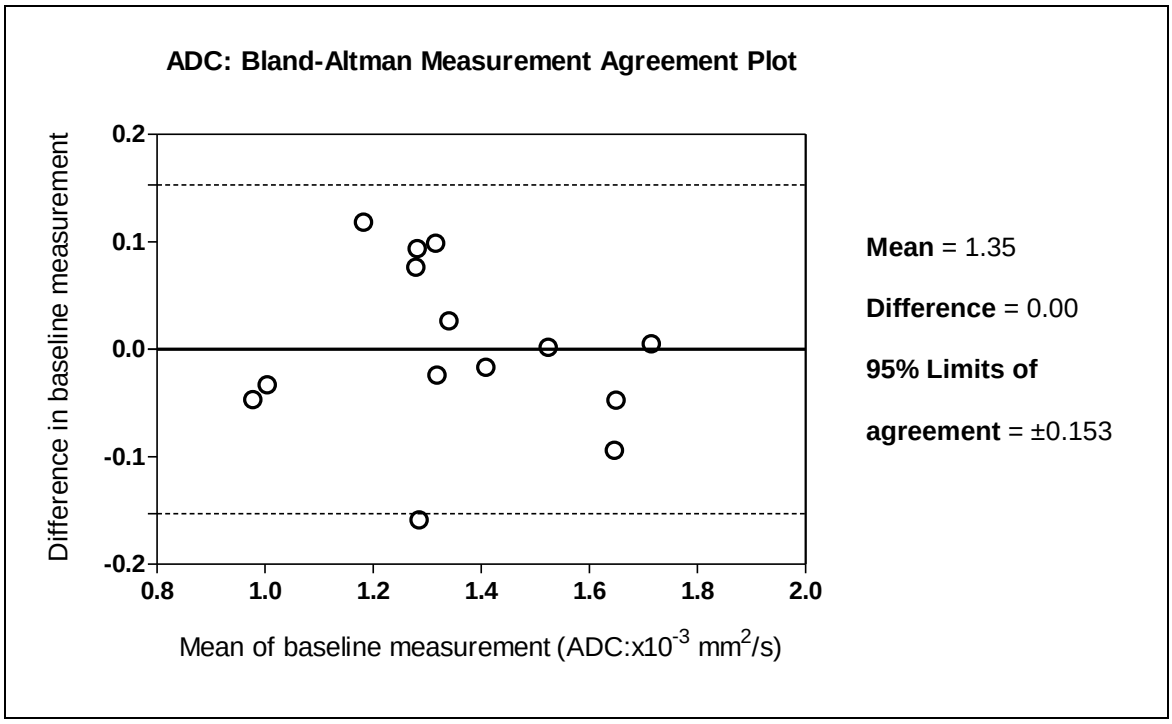

For ISW-MRI, the difference between the mean R_2* values from paired measurements was not normally distributed and, therefore, the data was natural log transformed for analysis. The R_2* measurement showed minimal spontaneous changes (CI cohort -4.67 to +4.9%, F 6.7), better repeatability than dynamic parameters (r -16.3 to +19.6%) and minimal observer influence (ICC 74%, LoA -0.16 to +0.19) between readings.

Bar plots of paired mean R_2* value and corresponding Bland-Altman plots are shown in figure 5.7 and 5.8, respectively.

Figure 5.7: Baseline R_2* reproducibility for individual patient data

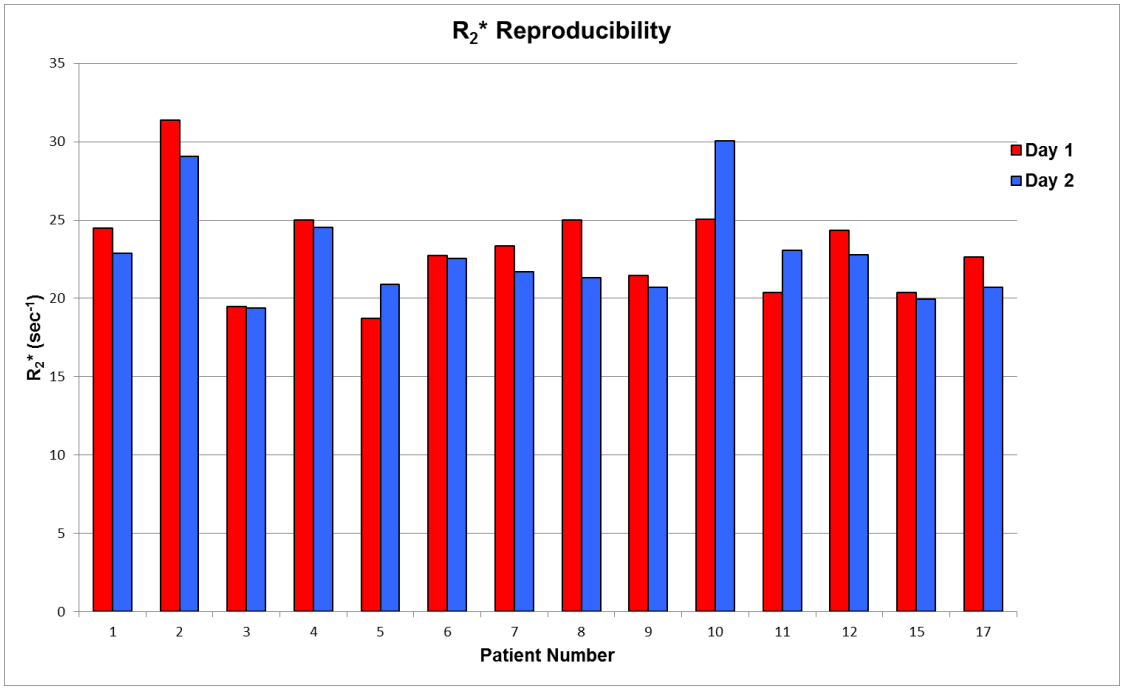

Figure 5.8: Bland-Altman plot for R_2* measurement agreement

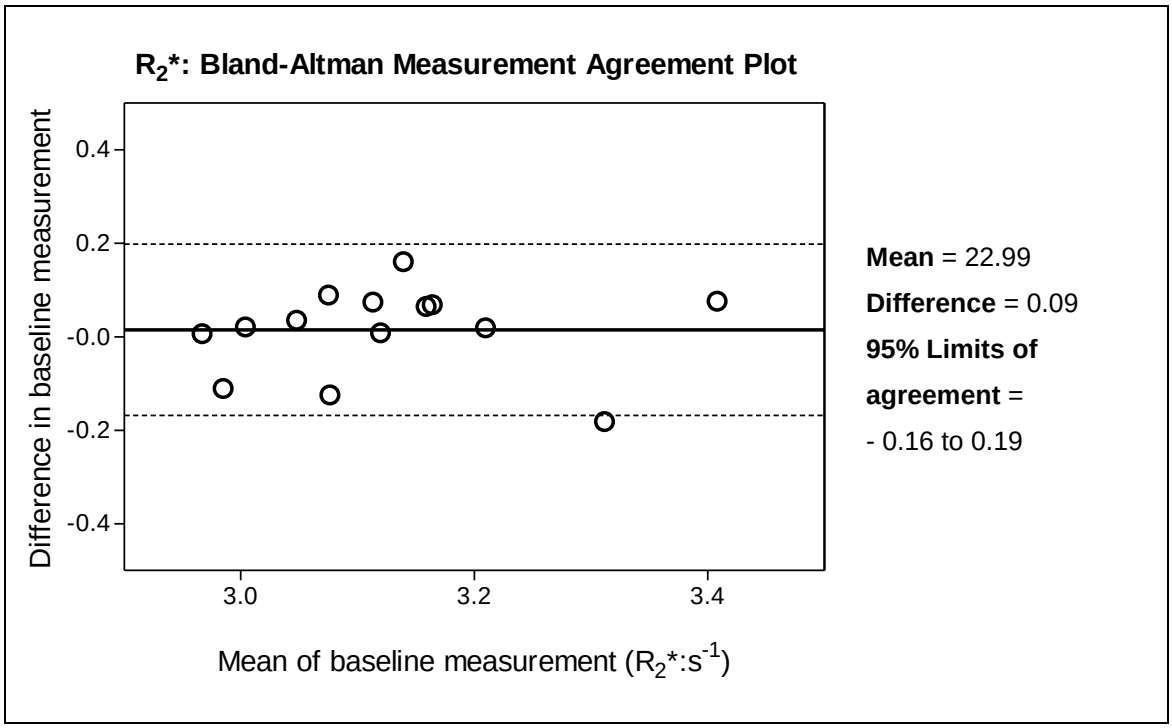

For DCE-MRI parameters, the reproducibility of cohort was better than an individual patient and non-model based measurements ($IAUGC_{60}$) had best reproducibility. In summary, for paired measurements of model driven parameters: K^{trans} and k_{ep} showed less spontaneous changes (CI cohort ±13.7%, ±11.1% and F 4.3, 4.9, respectively) than v_e (CI cohort ±14.1%, F 2.4); k_{ep} showed best repeatability (r ±41.5); the observer interference on readings was poor for v_e (ICC 38%) and moderate for K^{trans} and k_{ep} (ICC 60% and 64%, respectively). For non-model driven parameters, i.e. $IAUGC_{60,}$ the difference between the mean values from paired measurements was not normally distributed and, therefore, log transformed for analysis. For paired $IAUGC_{60}$ readings, there was minimal spontaneous change (CI cohort -10.75 to +12%, F 35.3), better repeatability than model driven parameters (r -34.6% to +52.9%) and minimal observer influence (ICC 94%).

Bar plots of paired mean K^{trans} values and corresponding Bland-Altman plots are shown in figure 5.9 and 5.10, respectively.

Bar plots of paired mean v_e values and corresponding Bland-Altman plots are shown in figure 5.11 and 5.12, respectively.

Bar plots of paired mean k_{ep} values and corresponding Bland-Altman plots are shown in figure 5.13 and 5.14, respectively.

Bar plots of paired mean $IAUGC_{60}$ values and corresponding Bland-Altman plots are shown in figure 5.15 and 5.16, respectively.

Figure 5.9: Baseline K^{trans} reproducibility for individual patient data

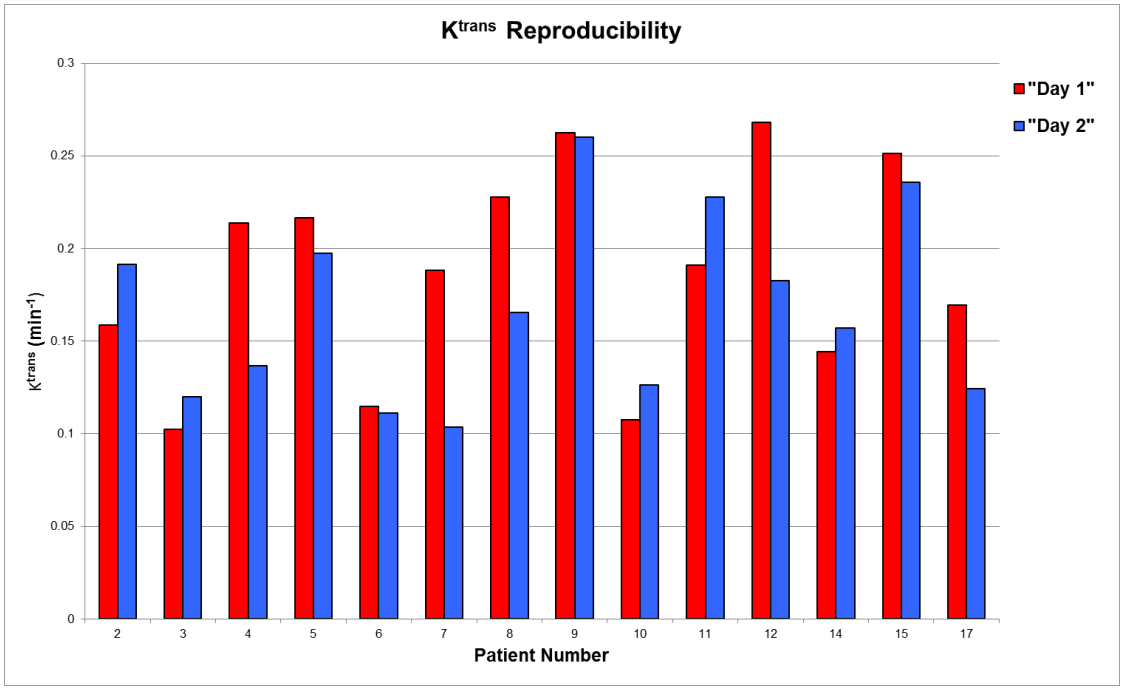

Figure 5.10: Bland-Altman plot for K^{trans} measurement agreement

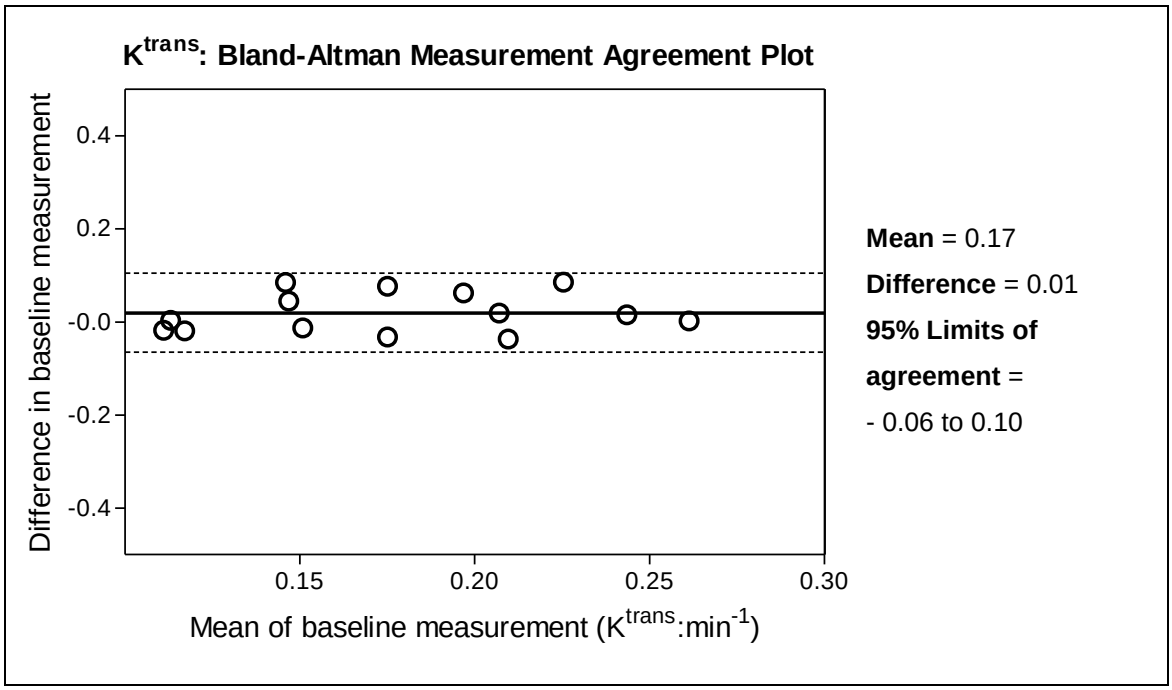

Figure 5.11: Baseline v_e reproducibility for individual patient data

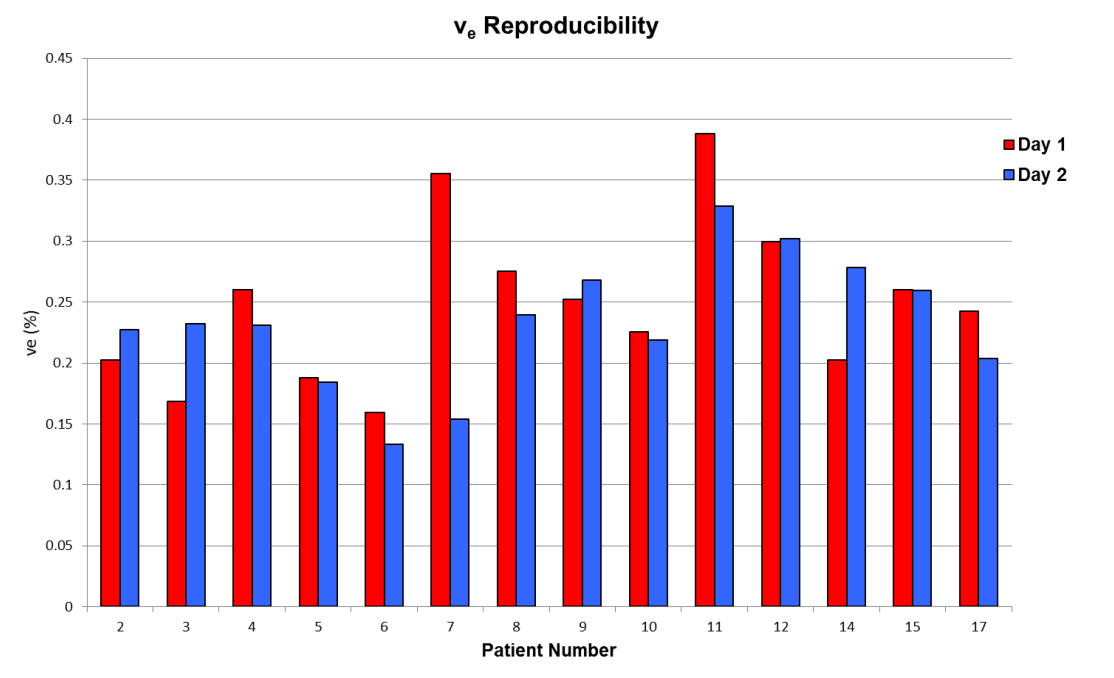

Figure 5.12: Bland-Altman plot for v_e measurement agreement

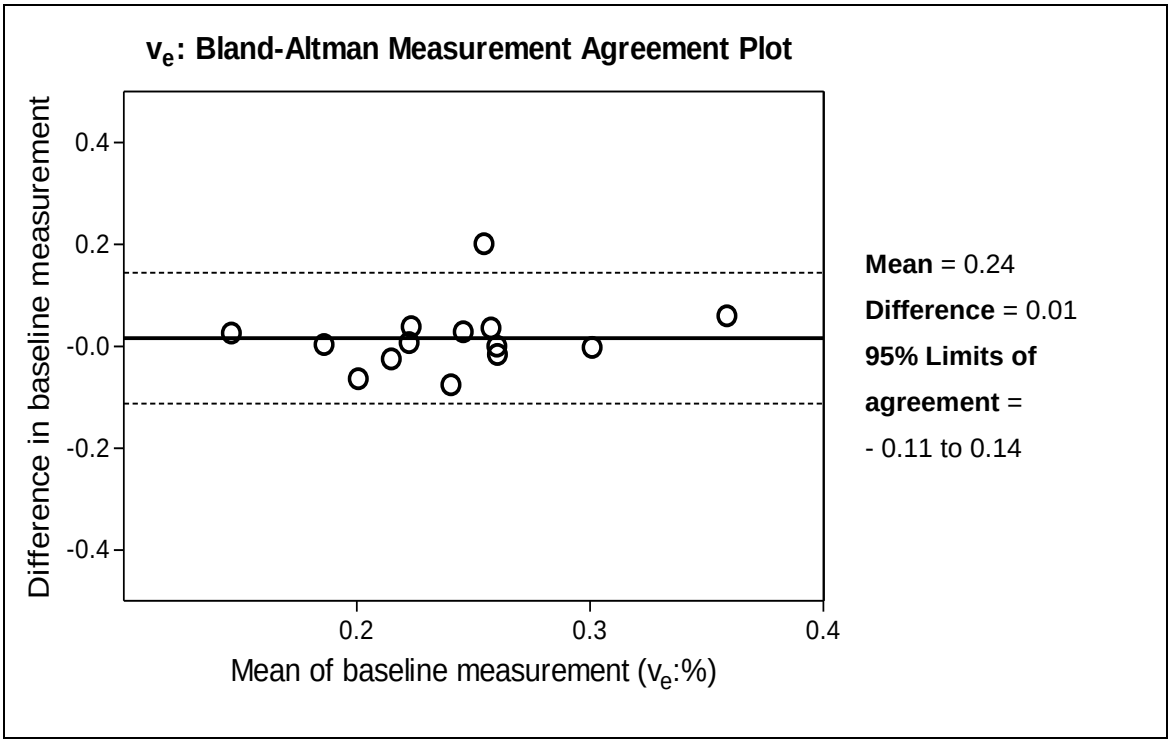

Figure 5.13: Baseline k_{ep} reproducibility for individual patient data

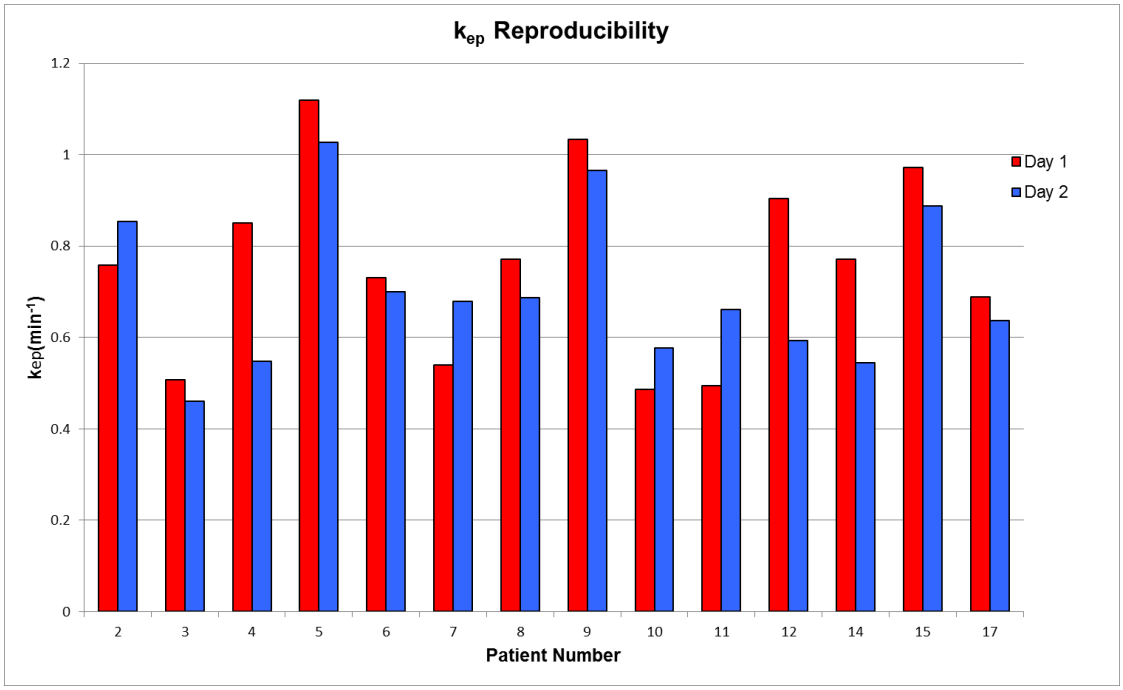

Figure 5.14: Bland-Altman plot for k_{ep} measurement agreement

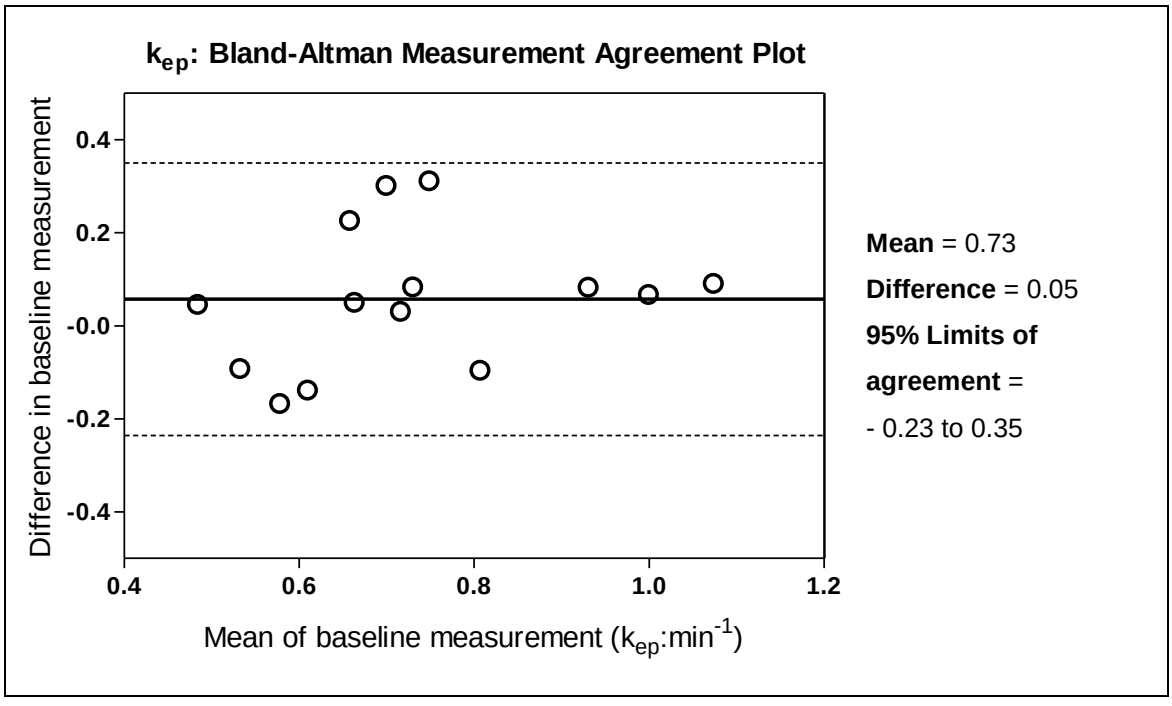

Figure 5.15: Baseline $IAUGC_{60}$ reproducibility for individual patient data

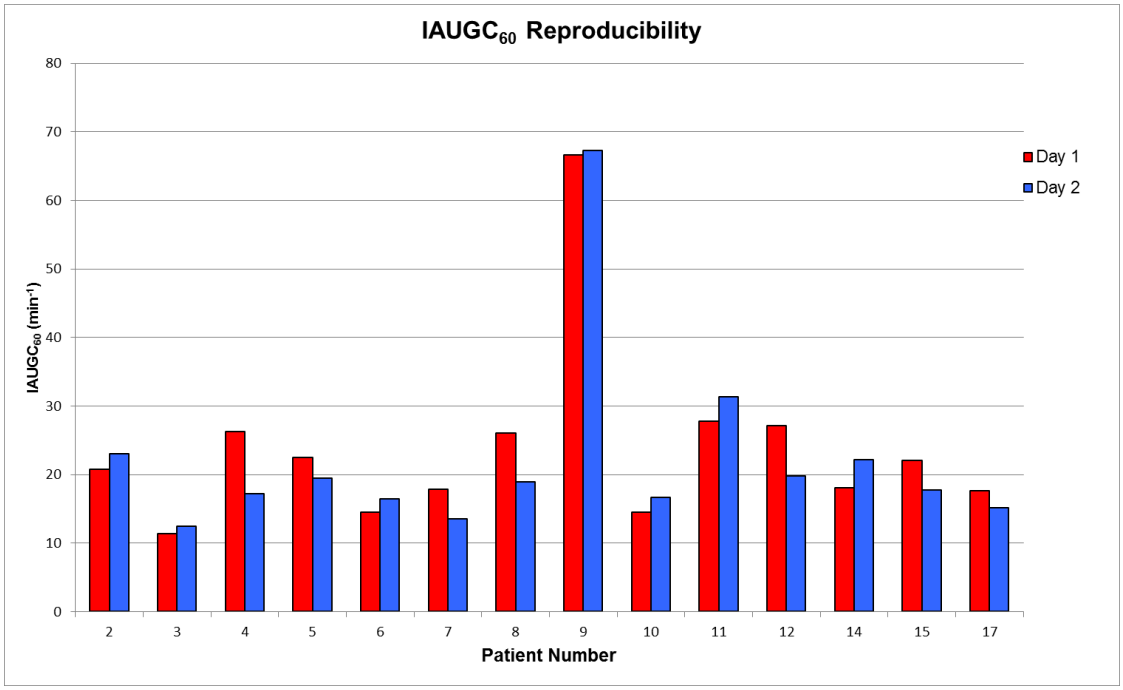

Figure 5.16: Bland-Altman plot for $IAUGC_{60}$ measurement agreement

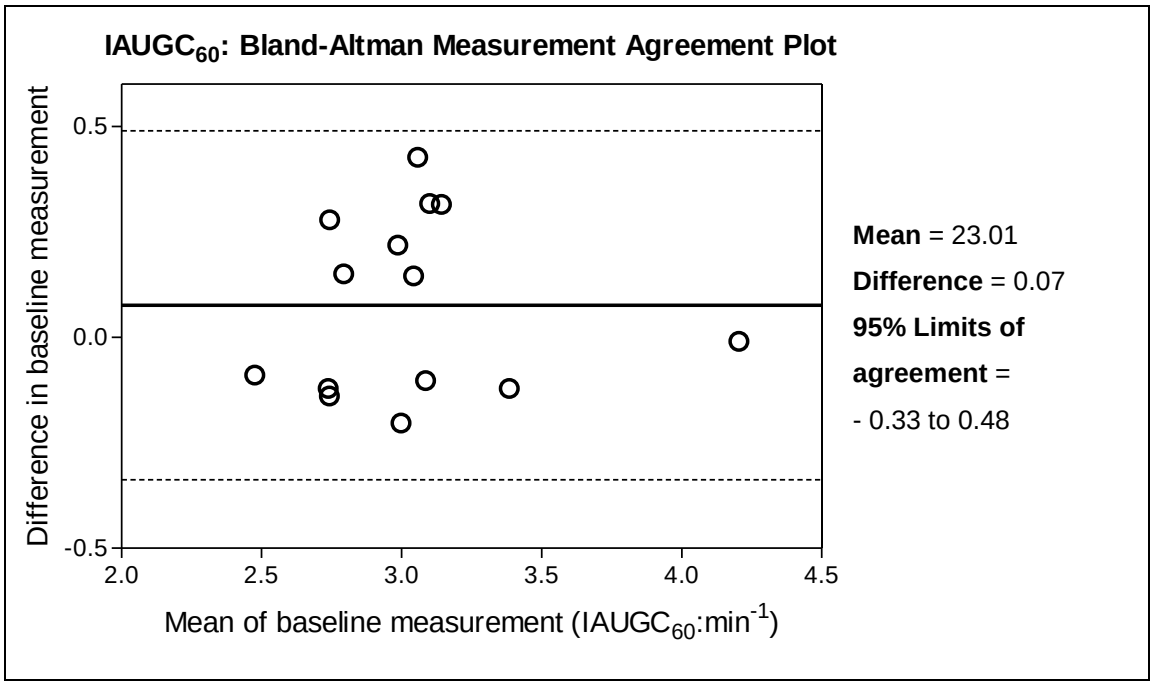

5.3.3 Alterations in MR parameters in response to NCRT

5.3.3.1 Estimation of significant changes in parametric measurements for cohort of patients

The significance of therapy-induced changes on a cohort basis was gauged by the 95% confidence interval of cohort (CI cohort) of the baseline measurement reproducibility. Thus, significant changes during the interval between NCRT and TME surgery (T_1-T_3) were deemed to be present in study cohort if the percentage change of MR parameters increased or decreased beyond the upper or lower limits of 'cohort 95% CI', respectively. The alterations in absolute and percentage values of MR parameters are shown in tables 5.7-5.8 and figure 5.17, respectively.

5.3.3.1.1 DW-MRI - ADC measurement alteration by cohort analysis

For ADC measurement alterations by cohort, there was significant increase in ADC measurement between the interval after NCRT and TME surgery. The pattern of ADC increase was as follows: a relative percentage increase by +23.83% at T_1 followed by lower percentage increase by +21.53% at T_2 and then a maximum percentage increase by +27.06% at T_3 from baseline.

5.3.3.1.2 ISW-MRI – R_2* measurement alteration by cohort analysis

For R_2* measurement alterations by cohort, there was an increase in R_2* by +4.76% at T_1 followed by a significant increase by + 9.91% at T_2 reducing to +3.6% at T_3 from baseline.

5.3.3.1.3 DCE-MRI – K^{trans} measurement alteration by cohort analysis

For K^{trans} measurement alterations by cohort, there was consistent significant percentage decrease from baseline during the interval between completion of NCRT and TME surgery. The K^{trans} levels fell by -19% at T_1 followed by further decline by -32.1% at T_2 and finally falling down by -46.5% at T_3 from baseline.

5.3.3.1.4 DCE-MRI – v_e measurement alteration by cohort analysis

For v_e measurement alterations by cohort basis, there was significant increase in v_e by +13.3% at T_1, followed by a relatively lower but significant increase by 8.57% at T_2 and finally a non-significant increase by 1.69% at T_3 from baseline.

5.3.3.1.5 DCE-MRI – k_{ep} measurement alteration by cohort analysis

For k_{ep} measurements by cohort analysis, there was a persistent significant decrease from T_1 – T_3. The k_{ep} decreased to -29.32% at T_1, followed by further decline by -49.37% at T_2 and then down by -50.09% at T_3 from baseline.

5.3.3.1.6 DCE-MRI – $IAUGC_{60}$ measurement alteration by cohort analysis

For $IAUGC_{60}$ measurements by cohort analysis, there was a persistent significant decrease from T_1 – T_3. The $IAUGC_{60}$ decreased by a non-significant -5.28% at T_1, followed by further decline by -22.31% at T_2 and by -28.12% at T_3 from baseline.

Table 5.7: MRI multi-parametric alterations after NCRT by absolute mean values

Parameter	n	T_0	T_1	p	n	T_0	T_2	p	n	T_0	T_3	P
		(mean)				(mean)				(mean)		
ADC ($x10^{-3}$ mm^2/s)	14	1.31	1.6	**0.000**	12	1.36	1.57	**0.01**	11	1.33	1.65	**0.003**
R_2* (s^{-1})	13	23.27	24.1	0.60	11	23.6	25.8	0.11	10	23.7	24.23	0.69
K^{trans} (min^{-1})	15	0.180	0.141	**0.03**	13	0.171	0.114	**0.01**	11	0.178	0.089	**0.001**
v_e (%)	15	0.247	0.269	0.375	13	0.237	0.244	0.82	11	0.237	0.205	0.344
k_{ep} (min^{-1})	15	0.748	0.496	**0.002**	13	0.741	0.415	**<0.001**	11	0.748	0.311	**<0.001**
$IAUGC_{60}$ (mmol.s)	15	16.27	15.04	0.36	13	15.47	11.75	**0.03**	11	15.88	11.25	**0.003**

Bold *– significant changes; Statistical test – paired sample T-test*

Table 5.8: MRI multi-parametric alterations after NCRT by percentage change

Parameter	% Change at T_1 [Cohort CI for 'n']	% Change at T_2 [Cohort CI for 'n']	% Change at T_3 [Cohort CI for 'n']
ADC (mm^2/s)	**23.83%** [±3 (n=13)]	**21.53%** [±3.2 (n=11)]	**27.06%** [±3.2 (n=11)]
R_2* (s^{-1})	4.76% [-5.2 to +5.5% (n=11)]	**9.91%** [-5.5 to +5.8% (n=10)]	3.60% [-6.1 to +6.5 (n=8)]
K^{trans} (min^{-1})	**-19.01**% [±5.9% (n=15)]	**-32.1%** [±6.3% (n=13)]	**-46.52%** [±6.9% (n=11)]
v_e (%)	**13.43%** [±6.9% (n=15)]	**8.57%** [±7.4% (n=13)]	1.69% [±8% (n=11)]
k_{ep} (min^{-1})	**-29.32%** [±5.4% (n=15)]	**-41.37%** [±5.8% (n=13)]	**-50.09%** [6.4% (n=11)]
$IAUGC_{60}$ (mmol.s)	-5.28% [-6.9 to +7.4% (n=15)]	**-22.31%** [-7.4 to +7.9% (n=13)]	**-28.12%** [-8 to +8.7% (n=11)]

Bold *– significant changes; Statistical test – cohort analysis*

Figure 5.17: MRI multi-parametric alterations after NCRT by percentage change (cohort)

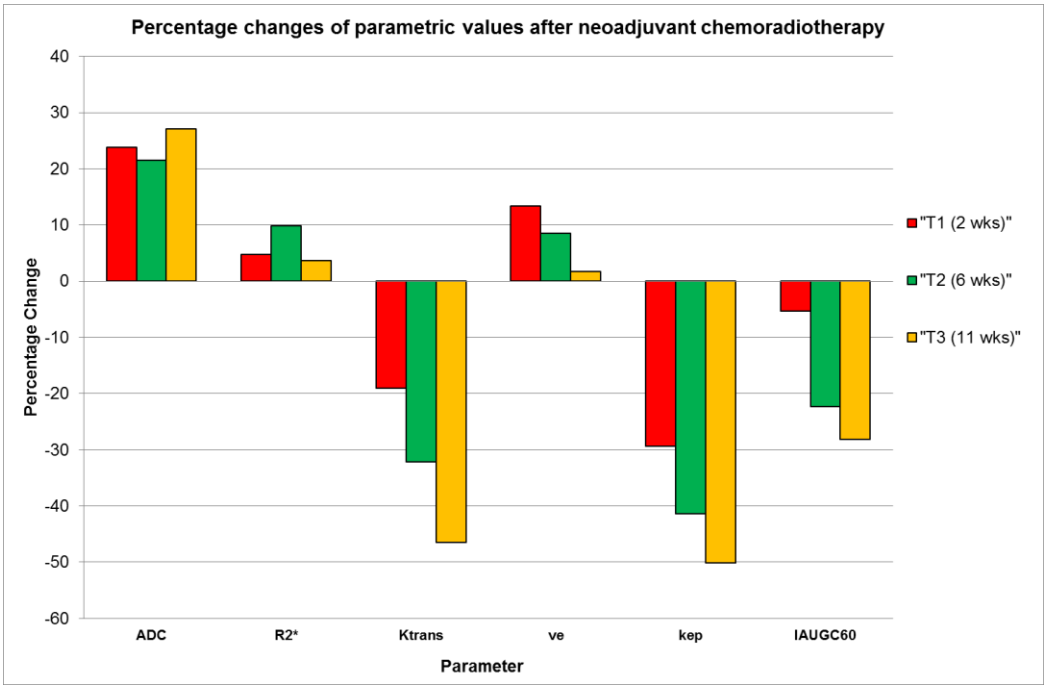

5.3.3.2 Estimation of significant changes in parametric measurements for an individual patient

The significance of therapy-induced changes on an individual basis was gauged by the percentage coefficient of repeatability (% r) derived from Bland-Altman analysis of baseline measurement. Thus, significant changes during the interval between NCRT and TME surgery (T_1-T_3) were deemed to be present in an individual if the percentage change of MR parameters increased or decreased beyond the upper or lower limits of '% r'.

5.3.3.2.1 DW-MRI - ADC measurement alteration for individual patients

Post-NCRT ADC measurement were available from the following time-points: T_1 to T_3 from 11/14 patients; T_1 to T_2 from 1/14 patient; T_1 only from 2/14 patient.

For ADC measurement alterations by individual basis, 12/14 (85%) patients showed significant percentage increase from baseline to final measurements (see figure 5.19 and 5.20). The remaining two patients showed a decrease in ADC values with time, one patient (code: 7 AF) had an isolated significant percentage decrease in ADC measurement at T_2 measurements (-22.3%), whilst the other patient (code: 17 JT) had a non-significant percentage decrease from baseline from T_1-T_3.

The following patterns of ADC changes were observed in patients who had T_1 to T_3 measurements available and showed significant increase in ADC values: 4/10 rectal tumours the ADC values showed relatively high positive percentage change at T_1 followed by lower positive percentage change at T_2 and then another high positive percentage change at T_3 from baseline; 2/10 rectal tumours showed a relatively modest positive percentage change in ADC at T_1 followed by maximum positive percentage change at T_2 then a low positive percentage change at T_3 from baseline; 2/10 showed a gradual linear percentage increase in ADC values from T_1 to T_3.

The actual DW-MRI images are presented in figure 5.18. The alterations in ADC values and pattern of changes are shown in table 5.9 and figure 5.19 and 5.20 respectively.

Figure 5.18: Serial DW-MRI images with ROIs

The actual DW-MRI images of patient number 5 (KB) are presented below:

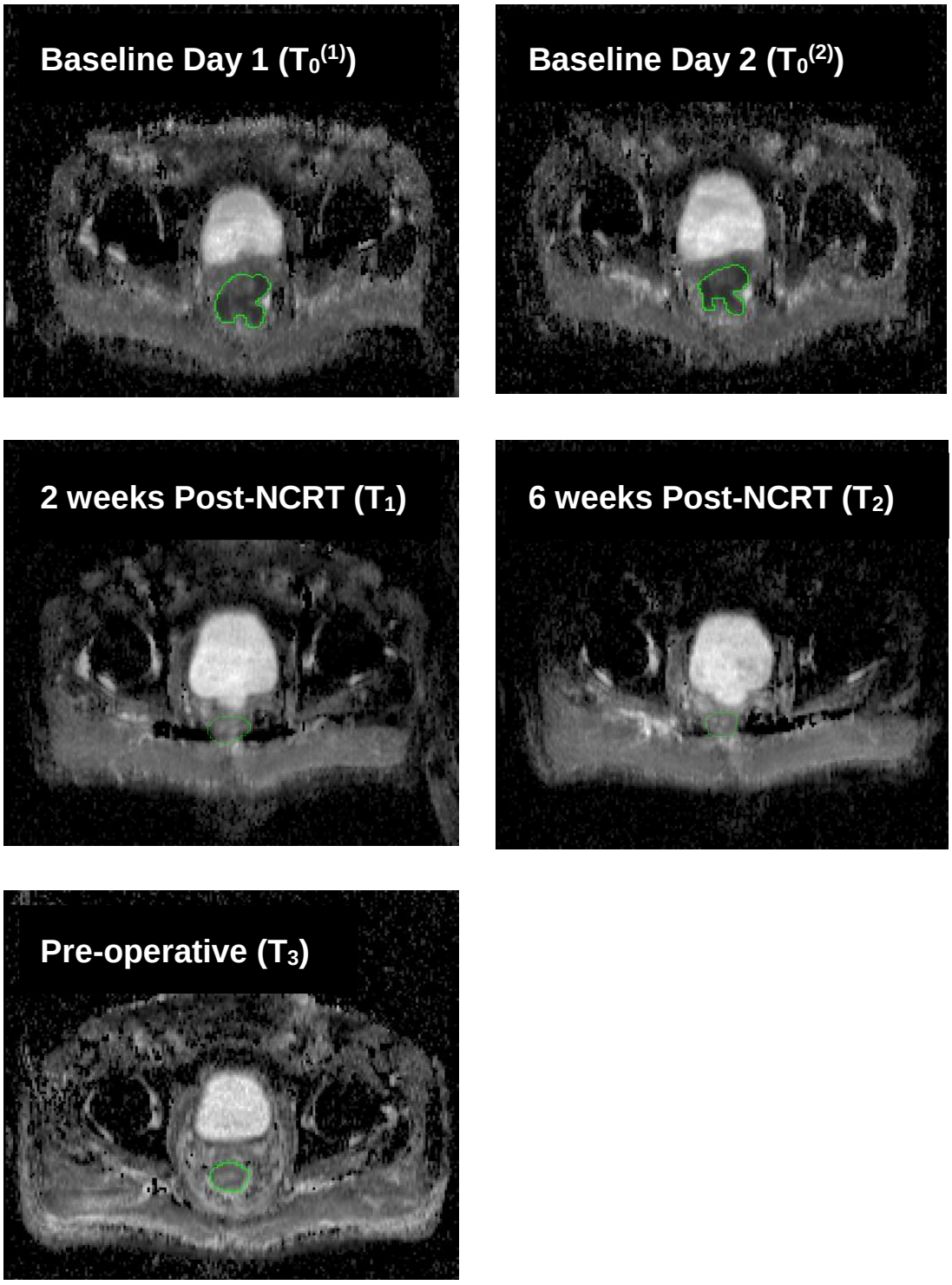

Table 5.9: ADC values and percentage changes after NCRT by individual basis (%r ±10.86%)

Code		Baseline	Post-NCRT		
		$T_{0\ (mean)}$	T_1 (% change)	T_2 (% change)	T_3 (% change)
1	**RY**	1.00 x 10^{-3}	**1.81 x 10^{-3} (81%)**	**1.74 x 10^{-3} (73.4%)**	**1.85 x 10^{-3} (84.3%)**
2	**DG**	1.28 x 10^{-3}	**1.55 x 10^{-3} (21%)**	**1.59 x 10^{-3} (24.6%)**	**1.50 x 10^{-3} (17%)**
4	**AH**	1.64 x 10^{-3}	**1.94 x 10^{-3} (18.7%)**	**1.83 x 10^{-3} (11.6%)**	**1.90 x 10^{-3} (16%)**
5	**KB**	1.27 x 10^{-3}	**1.62 x 10^{-3} (26.9%)**	**1.57 x 10^{-3} (23.1%)**	**1.75 x 10^{-3} (37.3%)**
6	**ED**	1.31 x 10^{-3}	**1.51 x 10^{-3} (15.1%)**	**1.59 x 10^{-3} (21 %)**	-
7	**AF**	1.64 x 10^{-3}	1.61 x 10^{-3} (-2.1%)	**1.28 x 10^{-3} (-22.3%)**	1.56 x 10^{-3} (-4.9%)
8	**JN**	1.28 x 10^{-3}	1.38 x 10^{-3} (7.6%)	**1.56 x 10^{-3} (21.8%)**	**1.46 x 10^{-3} (13.8%)**
9	**SD**	1.18 x 10^{-3}	**1.42 x 10^{-3} (20.2%)**	-	-
10	**JH**	1.52 x 10^{-3}	**1.71 x 10^{-3} (12.3%)**	**1.76 x 10^{-3} (15.4%)**	**1.88 x 10^{-3} (23.5%)**
11	**DP**	1.31 x 10^{-3}	**1.76 x 10^{-3} (33.6%)**	-	-
12	**GA**	1.40 x 10^{-3}	**1.75 x 10^{-3} (24.7%)**	**1.60 x 10^{-3} (14.1%)**	**1.88 x 10^{-3} (33.9%)**
15	**RC1**	0.97 x 10^{-3}	**1.60 x 10^{-3} (64.2%)**	**1.63 x 10^{-3} (67%)**	**1.58 x 10^{-3} (62.5%)**
16	**RC2**	1.24 x 10^{-3}	1.29 x 10^{-3} (4.3%)	1.31 x 10^{-3} (5.8%)	**1.46 x 10^{-3} (17.8%)**
17	**JT**	1.34 x 10^{-3}	1.42 x 10^{-3} (6.2%)	1.37 x 10^{-3} (2.9%)	1.29 x 10^{-3} (-3.4%)

Bold *– significant changes; Statistical test – individual patient analysis*

Figure 5.19: Absolute ADC values changes after NCRT (individual patients)

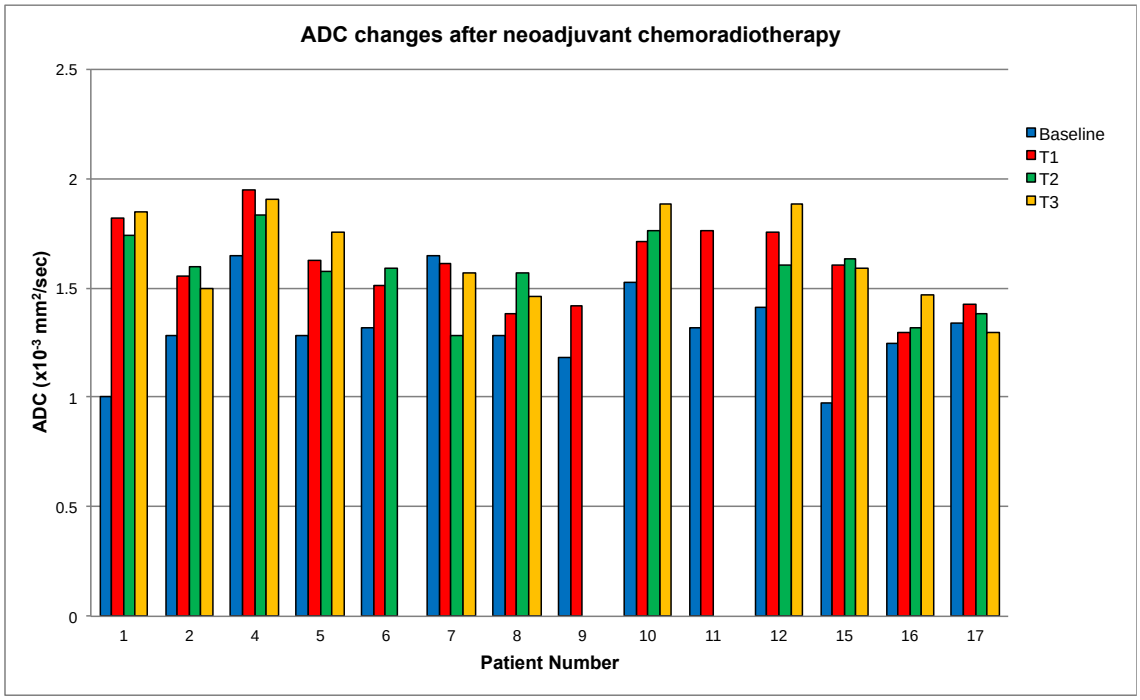

Figure 5.20: Percentage ADC changes after NCRT (individual patients)

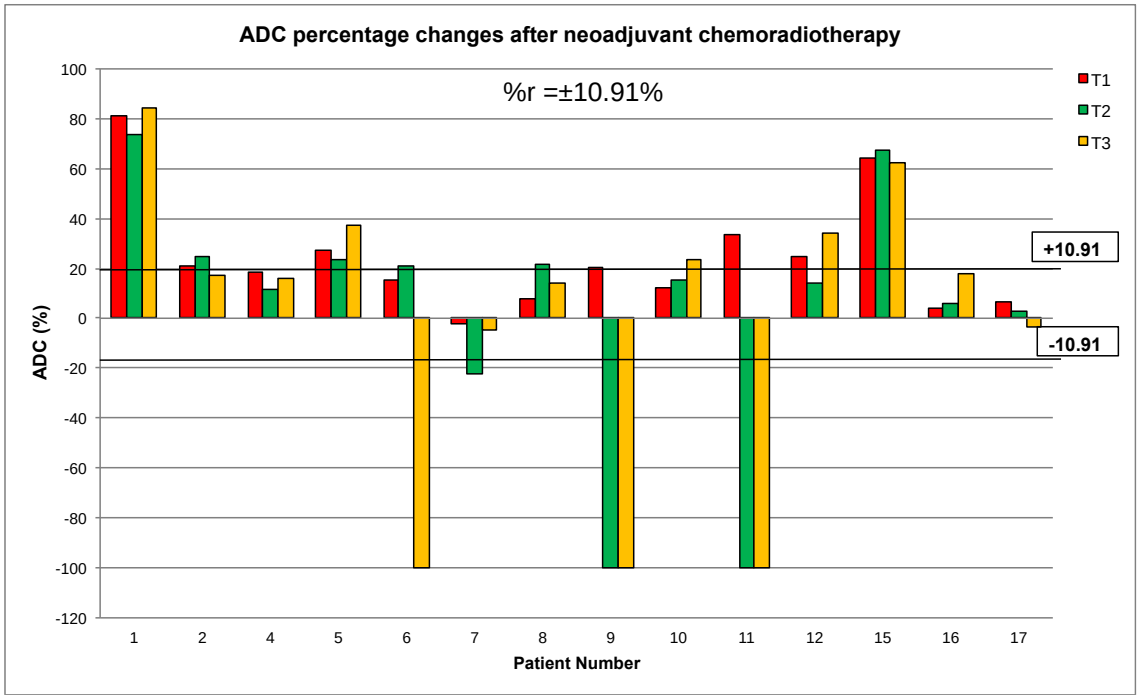

5.3.3.2.2 ISW-MRI – R_2* measurement alteration by individual patients

Post-NCRT R_2* measurement were available from the following time-points: T_1 to T_3 from 10/13 patients; T_1 to T_2 from 1/13 patient; T_1 only from 2/13 patient.

There was heterogeneous pattern of alteration in R_2* measurement by individual basis. There were only non-significant alterations in R_2* measurements in 6/13 (46.1%) patients: 4 patients showed percentage increases from baseline, whereas, 2 patients showed negative percentages change from baseline. In another 2 patients, there was significant percentage increase in R_2* and in 2 patients there was significant negative percentage change in R_2* from baseline on final measurements. One patient showed significant positive percentage change at T_1 stage followed by non-significant positive percentage change at T_2 stage from baseline and one patient had an isolated significant positive percentage change at T_2 followed by non-significant positive percentage change from baseline at T_3 stage. One patient had significant negative percentage change at T_1 stage followed by non-significant negative percentage change from baseline at T_2 and T_3 stages.

The actual ISW-MRI images are presented in figure 5.21. The alterations in R_2* values and pattern of changes are shown in table 5.10 and figure 5.22 and 5.23 respectively.

Figure 5.21: Serial ISW-MRI images with ROIs

The actual ISW-MRI images of patient number 3 are presented below: the ROI showing R_2* (scale 0-100s^{-1})

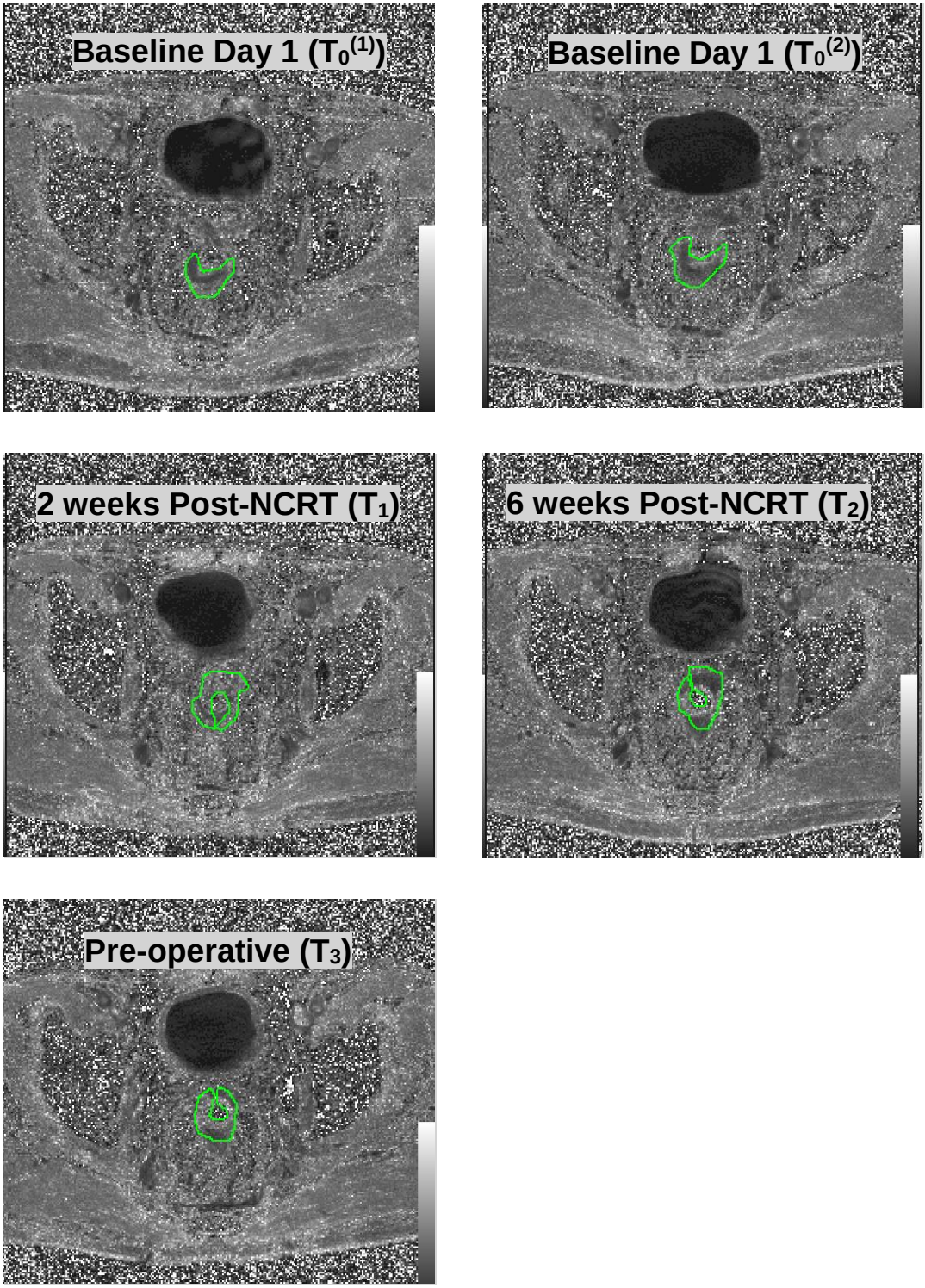

Table 5.10: R_2* values and percentage changes after NCRT (%r -16.38 – 19.6%)

Code		Baseline	Post-NCRT		
		T_0	T_1 (% change)	T_2 (% change)	T_3 (% change)
1	**RY**	23.68	24.72 (4.3%)	24.12 (1.8%)	27.44 (15.89%)
2	**DG**	30.23	29.53 (-2.3%)	35.93 (18.8%)	**24.99 (-17.35 %)**
4	**AH**	24.77	**19.27 (-22.2%)**	22.52 (-9 %)	23.92 (-3.47 %)
5	**KB**	19.81	19.22 (-3 %)	19.77 (-0.19%)	19.78 (-0.15%)
6	**ED**	22.64	**38.46 (69.9%)**	23.19 (2.4%)	-
7	**AF**	22.51	21.73 (-3.4%)	**31.63 (40.5%)**	**28.64 (27.25%)**
8	**JN**	23.16	21.70 (-6.3%)	21.80 (-5.8%)	22.83 (-1.41%)
9	**SD**	21.07	21.31 (1.1%)	-	-
10	**JH**	27.54	**19.82 (-28 %)**	24.95 (-9.4%)	**20.99 (-23.79%)**
11	**DP**	21.72	22.38 (3%)	-	-
12	**GA**	23.55	23.62 (0.28%)	**30.70 (30.3%)**	24.83 (5.42%)
15	**RC1**	20.17	**26.89 (33.3%)**	**28.16 (39.6%)**	23.41 (16.1%)
17	**JT**	21.67	24.97 (15.21%)	21.67 (-0.04%)	25.49 (17.59%)

Bold *– significant changes; Statistical test – individual patient analysis*

Figure 5.22: Absolute R_2* values changes after NCRT (individual patients)

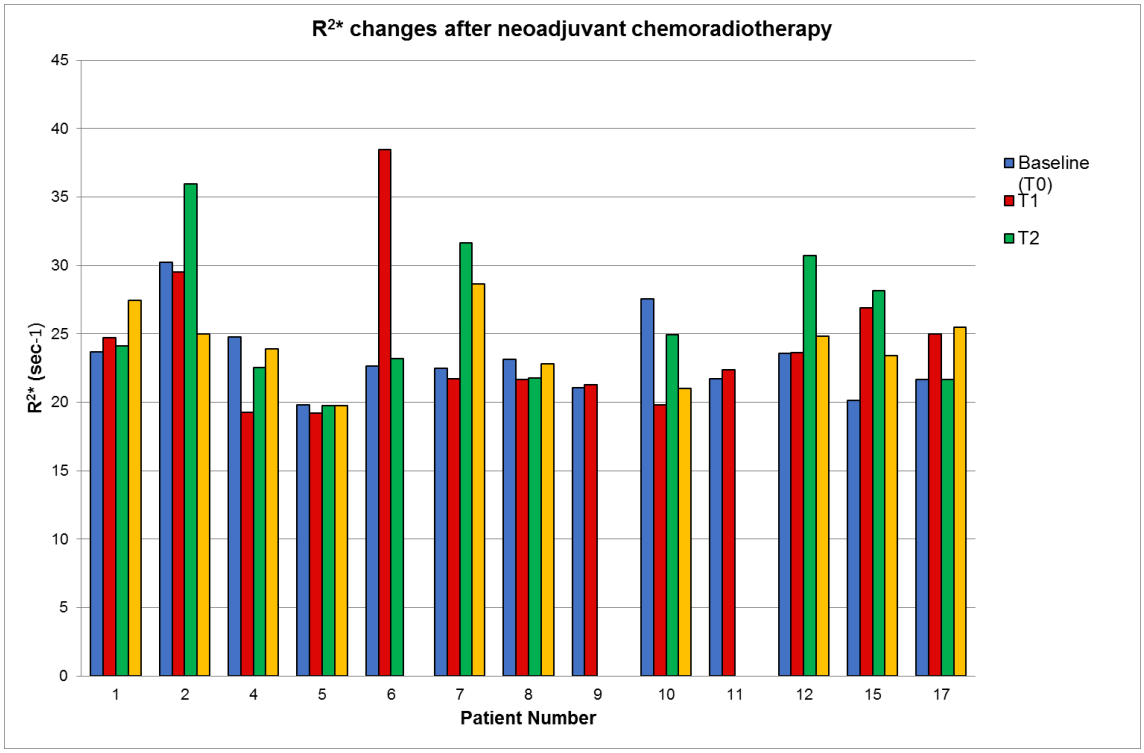

Figure 5.23: Percentage R_2* changes after NCRT (individual patients)

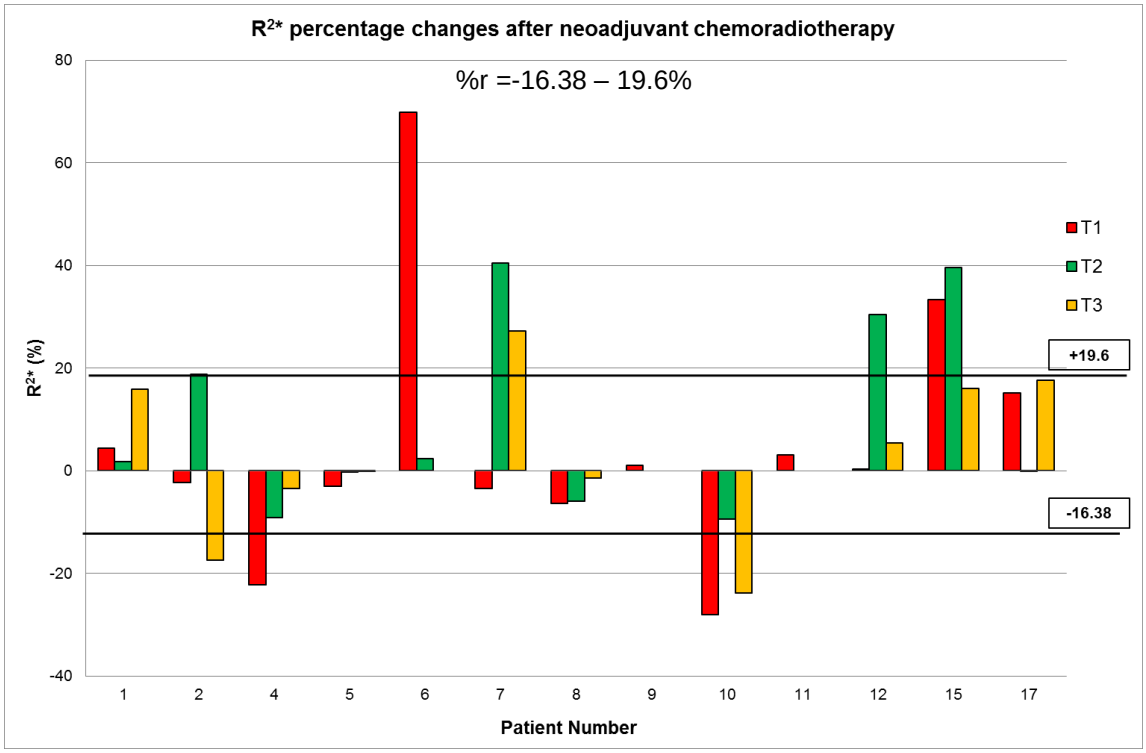

5.3.3.2.3 DCE-MRI – K^{trans} measurement alteration by individual patients

Post-NCRT K^{trans} measurements were available from the following time-points: T_1 to T_3 from 11/15 patients; T_1 to T_2 from 2/15 patients and T_1 only from 2/15 patient.

For K^{trans} measurement alterations by individual basis, all patients showed a percentage decrease from baseline in K^{trans} values after NCRT. There was significant percentage decrease on final measurements in 11/15 (73.3%) patients. The pattern of K^{trans} alterations was as follows: 6 patients had crescendo negative percentage changes from T_1 to T_3 from baseline; maximum percentage decrease from baseline was seen at T_2 in 2 patients and at T_1 in 1 patient. Another patient showed a significant positive percentage change at T_2 before a significant negative percentage change at T_3 from baseline. Two patients had non-significant percentage decrease.

The actual DCE-MRI images are presented in figures 5.24 and 5.25. The alterations in K^{trans} values and pattern of changes are shown in table 5.11 and figures 5.26 and 5.27, respectively.

Figure 5.24: Alteration in MR parameters after NCRT

The actual images of patient number 1 are presented below: columns show changes in transfer constant (color scale 0–1 min^{-1}), leakage space (color scale 0–100%) and normalized $IAUGC_{60}$ (color scale 0–0.4 unit less). Note increases in transfer constant and leakage space consistent with tumor hyperemia at the end of radiation.

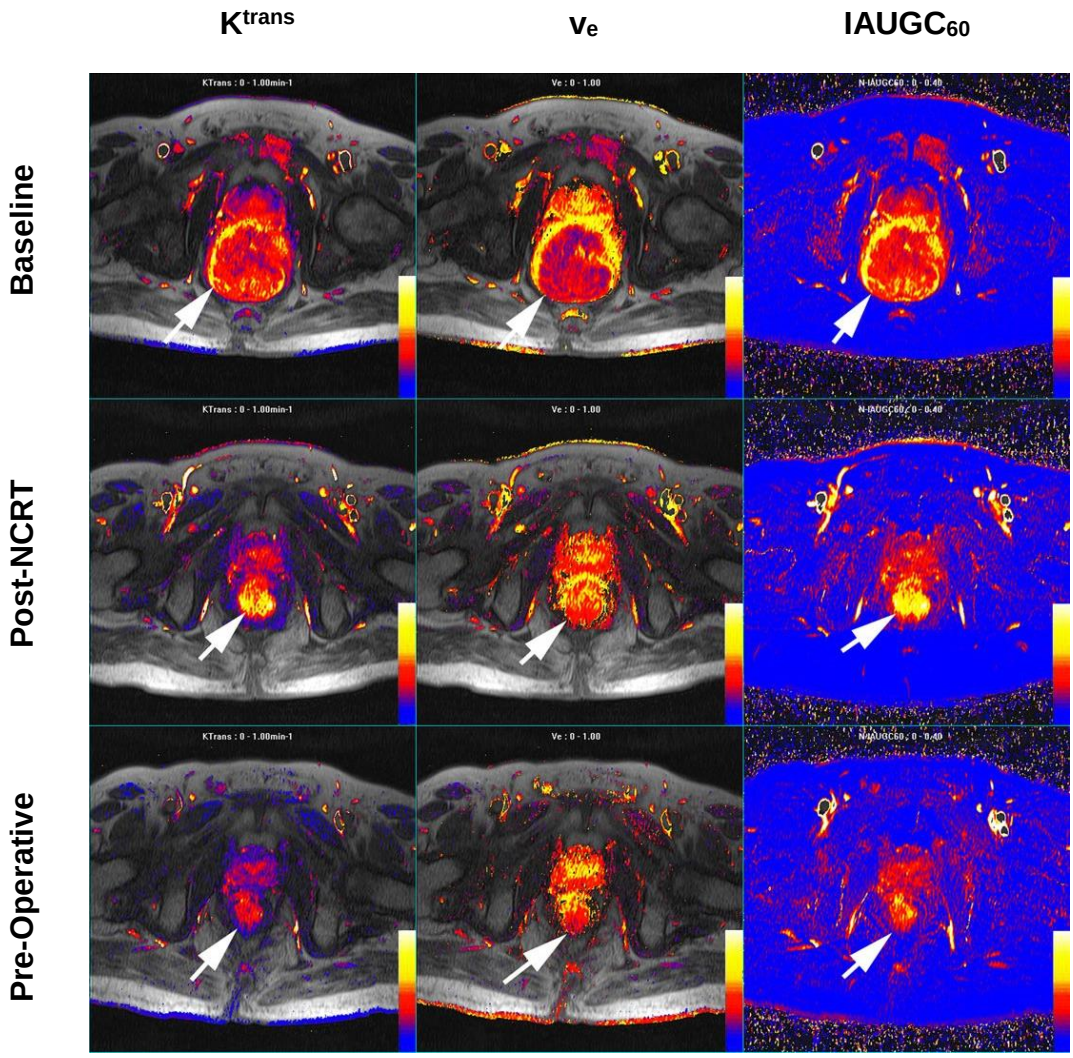

Figure 5.25: Alteration in MR parameters after NCRT

Baseline day 1 ($T_0^{(1)}$) **Baseline day 2 ($T_0^{(2)}$)** **2 wks post-NCRT (T1)** **6 wks post-NCRT (T2)** **Pre-Operative (T3)**

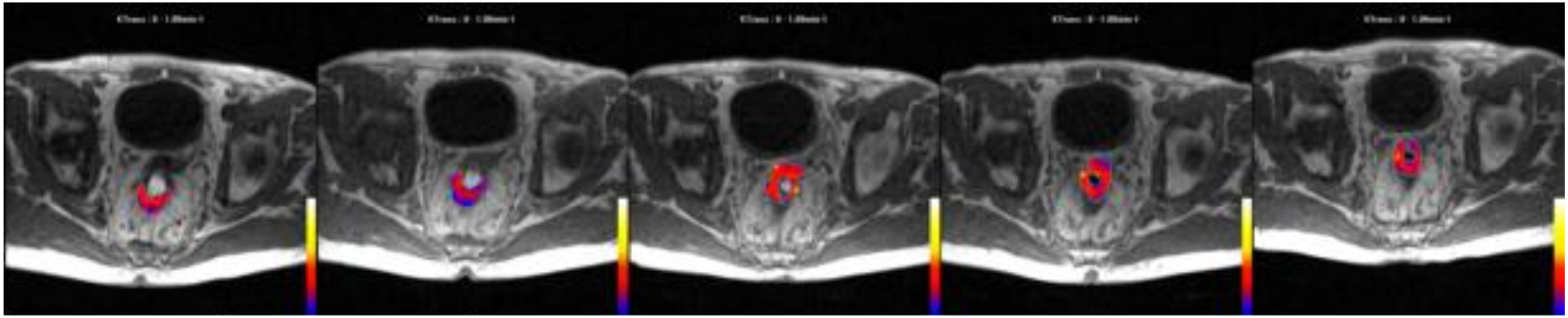

ROI showing K^{trans} (scale 0-1 min^{-1})

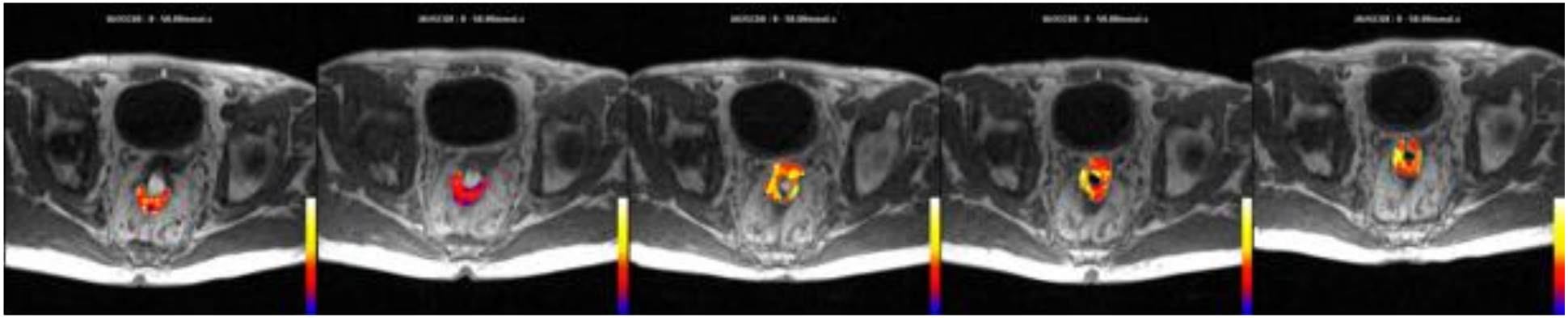

ROI showing $IAUGC_{60}$ (scale 0-50 mmol.s)

Table 5.11: K^{trans} values and percentage changes after NCRT (%r = ±22.95%)

Code		Baseline	Post-NCRT		
		T_0	T_1 (% change)	T_2 (% change)	T_3 (% change)
1	**RY**	0.1933	**0.09 (-52.4%)**	**0.062 (-67.6%)**	**0.05 (-69%)**
2	**DG**	0.17505	0.13 (-21.3%)	**0.09 (-43.3%)**	**0.12 (-31%)**
4	**AH**	0.1751	0.18 (8 %)	**0.12 (-26.3%)**	**0.09 (-48.4%)**
5	**KB**	0.207	0.18 (-8.7%)	**0.26 (25.8%)**	**0.09 (-54.9%)**
6	**ED**	0.1131	0.13 (14.9%)	0.12 (12.1%)	-
7	**AF**	0.1459	0.15 (3.1%)	**0 (-100%)**	**0.08 (-45%)**
8	**JN**	0.19675	0.23 (19.6%)	0.22 (14.2%)	0.19 (-1.8%)
9	**SD**	0.26125	0.25 (-2.9%)	-	-
10	**JH**	0.1171	0.10 (-11.4%)	**0.08 (-28.6%)**	0.09 (-22.8%)
11	**DP**	0.20955	**0.11 (-45.3%)**	-	-
12	**GA**	0.225375	**0.10 (-52.5%)**	**0.07 (-65%)**	**0.07 (-65.2%)**
14	**MM**	0.15085	**0 (-100%)**	**0.09 (-34.3%)**	-
15	**RC1**	0.24345	**0.10 (-55.2%)**	**0.1 (-55%)**	**0 (-100%)**
16	**RC2**	0.1425	**0.18 (28.4%)**	0.15 (5.7%)	**0.09 (-36%)**
17	**JT**	0.1468	0.13 (-9.3%)	**0.06 (-54.7%)**	**0.09 (-37.1%)**

Bold *– significant changes; Statistical test – individual patient analysis*

Figure 5.26: Absolute K^{trans} values changes after NCRT (individual patients)

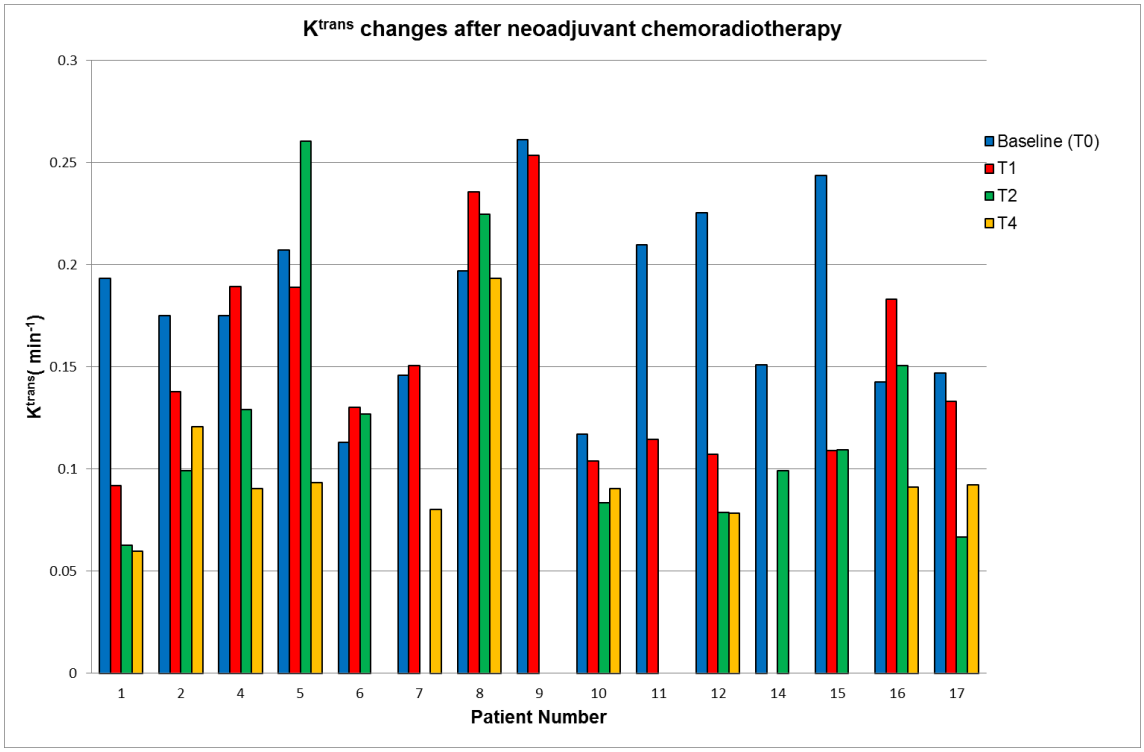

Figure 5.27: Percentage K^{trans} changes after NCRT (individual patients)

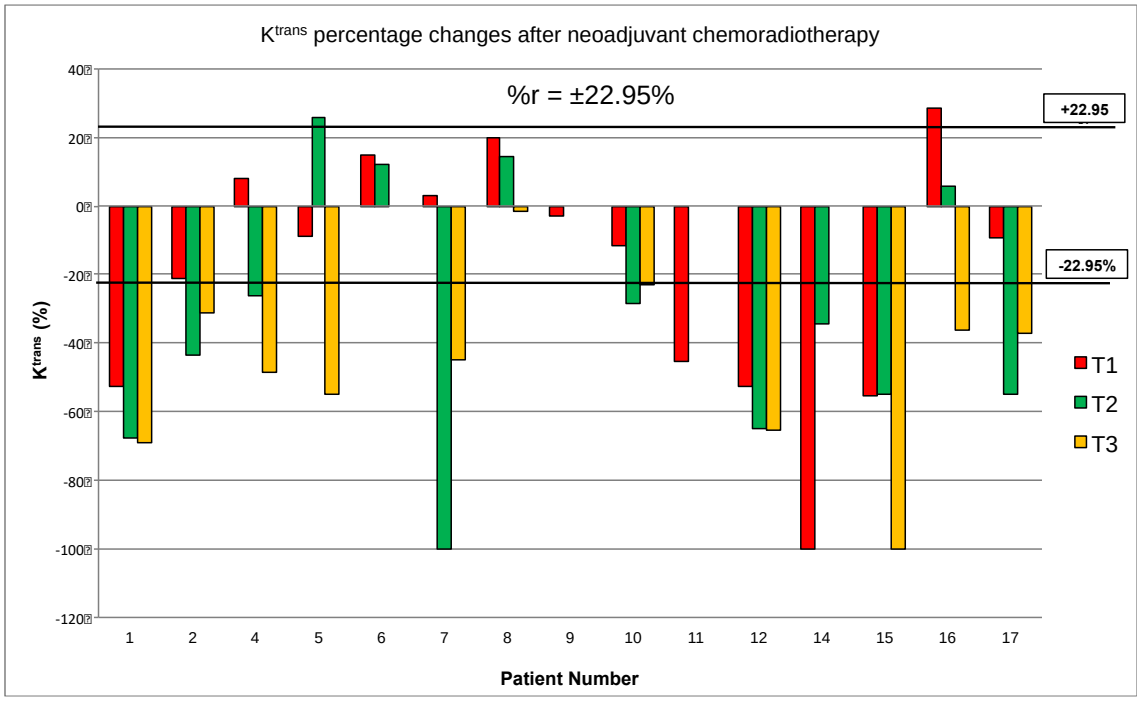

5.3.3.2.4 DCE-MRI – v_e measurement alteration by individual patients

Post-NCRT v_e measurements were available from the following time-points: T_1 to T_3 from 11/15 patients; T_1 to T_2 from 2/15 patients and T_1 only from 2/15 patient.

For v_e measurement alterations by individual basis, the percentages changes were heterogeneous between patients. Three patients had a significant positive percentage and one patient had negative percentage change from baseline on last examination. The pattern of percentage v_e changes from T_1-T_3 (where available) were as follows: In 11/15 patients, there was initially a high positive percentage change at T_1, thereafter, in 5 patients this was followed by relative percentage decrease at T_2 (3 patient had negative percentage and 2 had lower positive percentage change) and finally a relative percentage increase at T_3 from baseline (2 remained altered by lower negative percentage change); in 3 patients there was further higher positive percentage at T_2 before decline at T_4 from baseline (in one patient v_e altered by negative percentage change); in 2 patients there was persistent relative percentage decrease at T_2 followed by T_3 from baseline (one patient altered by negative percentage change). In remaining 4/15 patients, there was initial negative percentage change at T_1, thereafter, in 2 patients this was followed by percentage increase in v_e (one still remained altered by negative percentage change) and in 1 patient there was crescendo negative percentage change in v_e at T_2 and T_3 from base line.

The actual DCE-MRI images are presented in figures 5.24 and 5.25. The alterations in v_e values and pattern of changes are shown in table 5.12 and figure 5.28 and 5.29 respectively.

Table 5.12: v_e values and percentage changes after NCRT (% r = ±26.77%)

Code		Baseline	Post-NCRT		
		T_0	T_1 (% change)	T_2 (% change)	T_3 (% change)
1	RY	0.17385	0.2095 (20.5%)	0.2139 (23%)	0.1604 (-7.7%)
2	DG	0.21475	0.2393 (11.4%)	0.1964 (-8.5%)	0.2391 (11.3%)
4	AH	0.2456	**0.3352 (36.5 %)**	0.2614 (6.4%)	**0.3038 (23.7 %)**
5	KB	0.18585	**0.3244 (74.5%)**	**0.3297 (77.4%)**	**0.2775 (49.3 %)**
6	ED	0.1462	**0.27 (84.7%)**	**0.2779 (90.1 %)**	-
7	AF	0.25445	0.259 (1.8%)	**0 (-100 %)**	0.2468 (-3 %)
8	JN	0.25745	0.3193 (24 %)	0.3162 (22.8%)	0.3162 (22.8 %)
9	SD	0.26025	0.321 (23.3%)	-	-
10	JH	0.22235	0.2141 (-3.7%)	0.21815 (-1.9%)	0.2222 (-0.1%)
11	DP	0.3586	0.2998 (-16.4%)	-	-
12	GA	0.3008	0.3123 (3.8 %)	0.2737 (-9 %)	0.29385 (-2.3%)
14	MM	0.2403	**0 (-100%)**	**0.3144 (30.8%)**	
15	RC1	0.25995	0.2988 (14.9%)	0.2584 (-0.6 %)	**0 (-100 %)**
16	RC2	0.3682	0.3269 (-11.2 %)	0.288 (-21.8 %)	0.2887 (-21.6 %)
17	JT	0.2232	**0.3062 (37.2 %)**	0.229 (2.6%)	**0.32625 (46.2 %)**

Bold *– significant changes; Statistical test – individual patient analysis*

Figure 5.28: Absolute v_e values changes after NCRT (individual patients)

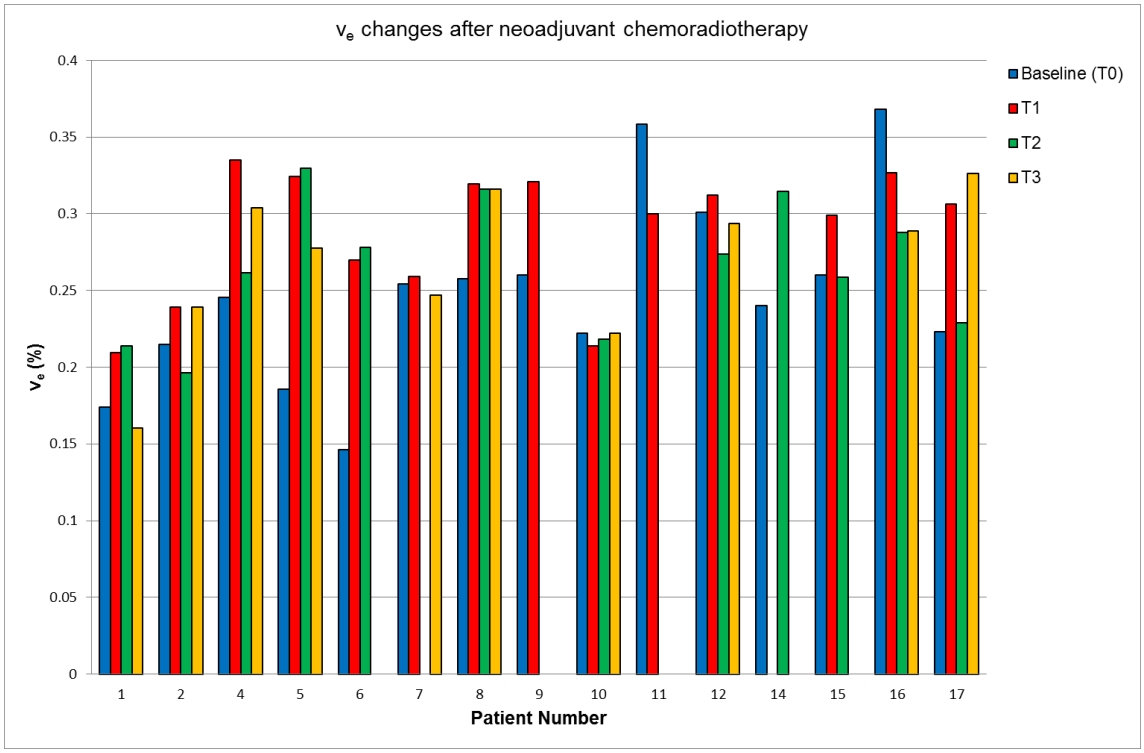

Figure 5.29: Percentage v_e changes after NCRT (individual patients)

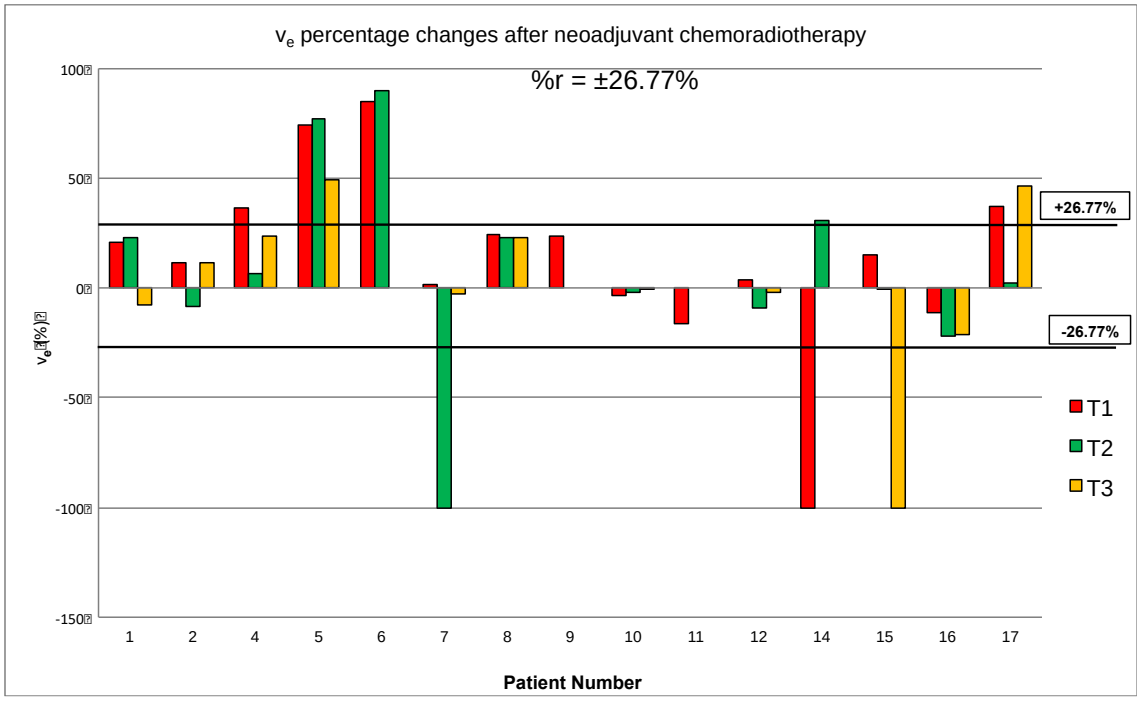

5.3.3.2.5 DCE-MRI – k_{ep} measurement alteration by individual patients

Post-NCRT k_{ep} measurements were available from the following time-points: T_1 to T_3 from 11/15 patients; T_1 to T_2 from 2/15 patients and T_1 only from 2/15 patient.

For k_{ep} measurement alterations by individual basis, all patients showed a decline in k_{ep} values between T_1 and T_3:10/15 patients had a significant decrease on the final examination. The pattern of changes were as follows: 13/15 patients had negative percentage changes (10 significant high negative) at T_1 from baseline, thereafter, 6 patients showed a further decline in k_{ep} at T_2 before a relative lower negative percentage change at T_3 from baseline; 2 patients had a decreasing k_{ep} percentage change from baseline. Two patients had positive percentage changes (1 significant high positive) at T_1, thereafter; both patients had percentage decline in k_{ep} from baseline on subsequent measurements.

The actual DCE-MRI images are presented in figures 5.24 and 5.25. The alterations in k_{ep} values and pattern of changes are shown in table 5.13 and figure 5.30 and 5.31 respectively.

Table 5.13: k_{ep} values and percentage changes after NCRT (%r = ±21.21%)

Code		Baseline	Post-NCRT		
		T_0	T_1 (% change)	T_2 (% change)	T_3 (% change)
1	RY	1.07	**0.45 (-57.6%)**	**0.26(-75.5%)**	**0.31(-71.2%)**
2	DG	0.81	**0.57(-29.2 %)**	**0.46(-42.9 %)**	**0.50(-38.0%)**
4	AH	0.70	0.58(-16.5%)	**0.51(-27.3%)**	**0.30(-57.0%)**
5	KB	1.07	**0.61(-42.8%)**	0.86(-20.2 %)	**0.35(-67.5%)**
6	ED	0.72	**0.49(-31.0%)**	**0.47(-34.5%)**	-
7	AF	0.61	0.59(-3.4%)	**0.00(-100.0 %)**	**0.34(-44.8%)**
8	JN	0.73	0.75(+2.9%)	0.61(-17.1 %)	0.61(-17.1%)
9	SD	1.00	**0.74(-25.7%)**	-	-
10	JH	0.53	0.51(-3.3%)	**0.38(-28.9%)**	0.43(-18.6%)
11	DP	0.58	**0.37(-36.3%)**	-	-
12	GA	0.75	**0.36(-52.5%)**	**0.30(-60.1%)**	**0.29(-61.4%)**
14	MM	0.66	**0.00(-100.0%)**	**0.32(-50.9%)**	-
15	RC1	0.93	**0.34(-63.6%)**	**0.42(-55.2%)**	**0.00(-100.0%)**
16	RC2	0.40	**0.56(41.3%)**	**0.52(31.4%)**	0.32(-19.6%)
17	JT	0.66	**0.52(-22.2%)**	**0.29(-56.7 %)**	**0.29(-55.8 %)**

Bold *– significant changes; Statistical test – individual patient analysis*

Figure 5.30: Absolute k_{ep} values changes after NCRT (individual patients)

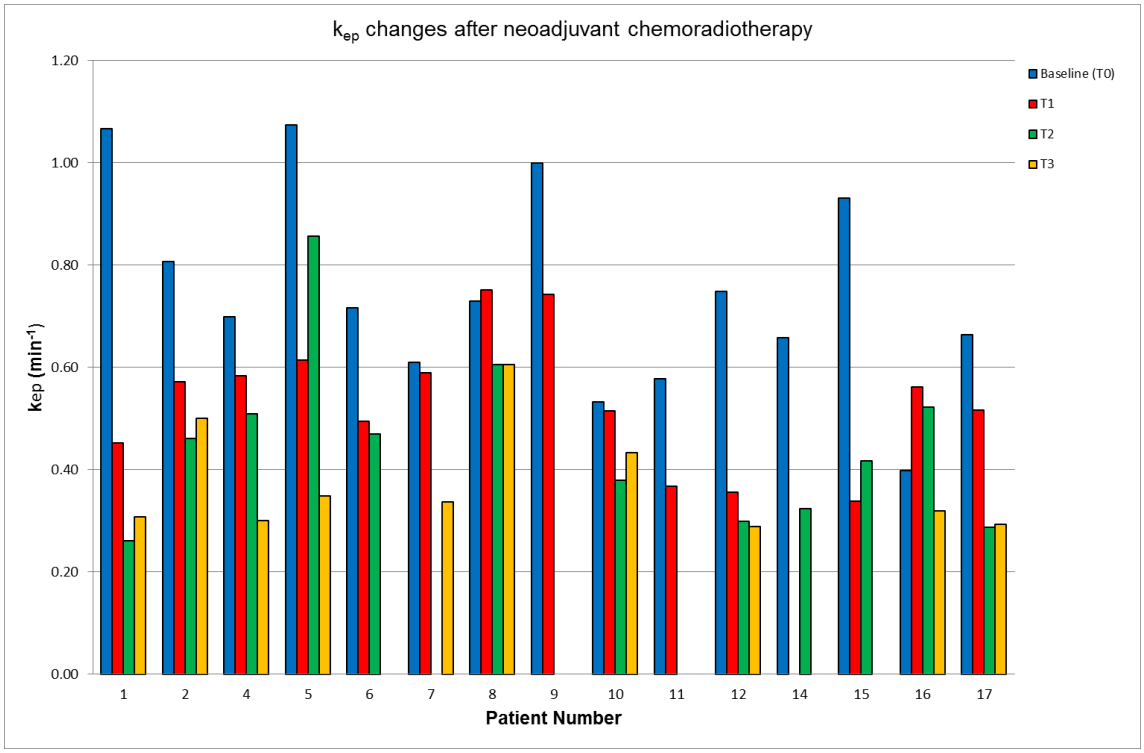

Figure 5.31: Percentage k_{ep} changes after NCRT (individual patients)

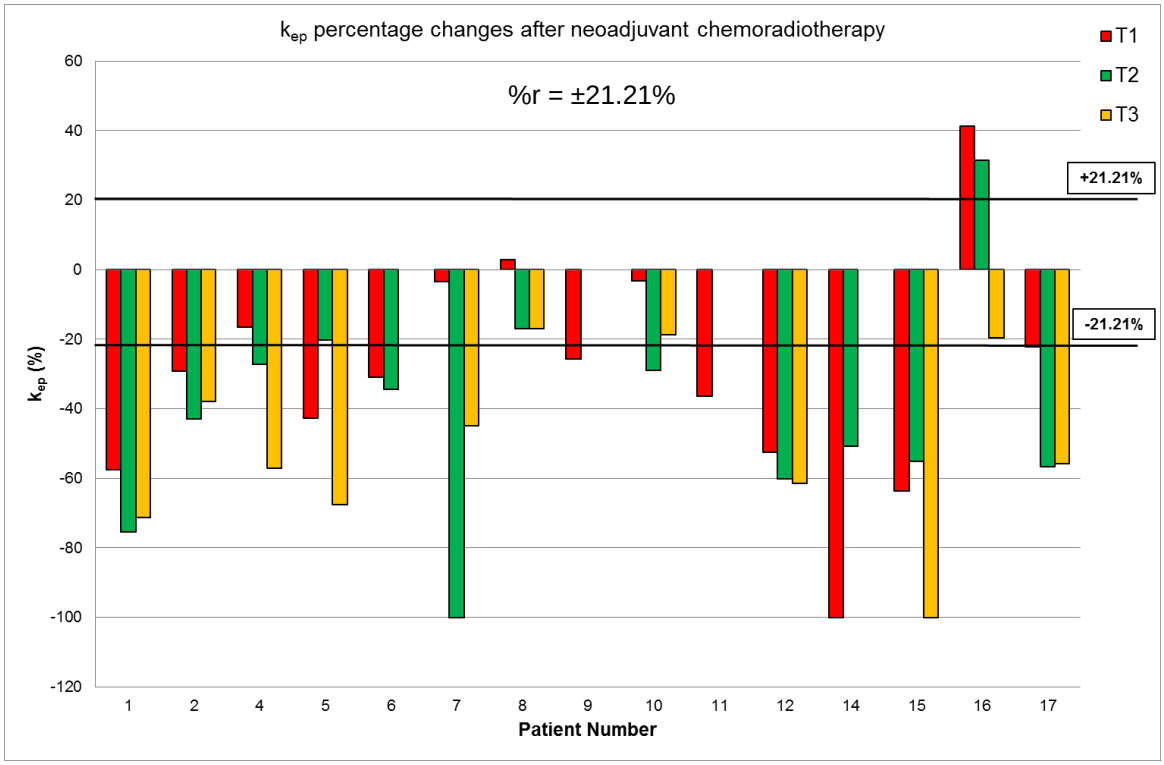

5.3.3.2.6 DCE-MRI – $IAUGC_{60}$ measurement alteration by individual patients

Post-NCRT $IAUGC_{60}$ measurements were available from the following time-points: T_1 to T_3 from 11/15 patients; T_1 to T_2 from 2/15 patients and T_1 only from 2/15 patient.

For $IAUGC_{60}$ measurement alterations by individual basis, there was generally a decrease in $IAUGC_{60}$ after NCRT. In 10/15 patients, there was negative percentage change (9 patients with significant changes) on the last examination. The pattern of changes from T_1-T_3 (where available) were as follows: in 9/15 patients there was initial percentage decrease in $IAUGC_{60}$ at T_1, thereafter, in 5 patients there was further high negative percentage change at T_2 before a relative lower negative percentage change at T_3 in 4 patients and lower positive percentage change in $IAUGC_{60}$ 1 patient at T_3 from baseline; in one patient, there was an increase at T_2 before decline to high negative percentage at T_3; in one patients there was crescendo negative percentage changes from T_1-T_3. In 6/15 patients, there was an initial percentage increase in $IAUGC_{60}$ at T1 from baseline, thereafter, 2 patients had a high negative percentage change at T_2 before a relatively lower negative percentage in one patient and a further higher negative percentage change in the other patients at T3 from baseline; in 2 patients, there was lower positive percentage change at T_2 with one of these patients continued to have lower positive percentage change and the other developed a significantly high negative percentage change of $IAUGC_{60}$ at T_3 from baseline.

The actual DCE-MRI images are presented in figures 5.24 and 5.25.The alterations in $IAUGC_{60}$ values and pattern of changes are shown in table 5.14 and figure 5.32 and 5.33 respectively.

Table 5.14: $IAUGC_{60}$ values and percentage changes after NCRT (%r = -24.2 to 31.9%)

Code		Baseline	Post NCRT		
		T_0	T_1 (% change)	T_2 (% change)	T_3 (% change)
1	RY	16.84	**10.29 (-38.9%)**	**7.09 (-57.9%)**	**7.49 (-55.5%)**
2	DG	16.57	14.90 (-10.1%)	**11.48 (-30.7%)**	13.27 (-19.9%)
4	AH	17.11	**21.39 (25.0%)**	**12.55 (-26.7%)**	**8.46 (-50.6%)**
5	KB	16.71	15.57 (-6.8%)	20.84 (24.7%)	**10.29 (-38.4%)**
6	ED	11.24	**16.58 (47.5%)**	13.97 (24.4%)	-
7	AF	13.81	14.80 (7.2%)	**1.81 (-86.9%)**	**8.48 (-38.6%)**
8	JN	15.75	**22.04 (40%)**	20.56 (30.6%)	19.74 (25.4%)
9	SD	22.10	24.27 (9.8%)	-	-
10	JH	11.00	10.78 (-2 %)	9.36 (-14.9%)	11.36 (3.3%)
11	DP	20.84	12.92 (-38%)	-	-
12	GA	17.11	13.19 (-22.9%)	**9.43 (-44.9 %)**	**8.79 (-48.6%)**
14	MM	15.16	**5.56 (-63.3%)**	**10.28 (-32.2%)**	-
15	RC1	19.94	**12.57 (-36.9%)**	**11.13 (-44.2%)**	15.92 (-20.1%)
16	RC2	13.56	17.24 (27.1%)	16.15 (19%)	**8.99 (-33.7%)**
17	JT	16.38	13.62 (-16.8%)	**8.12 (-50.4%)**	**11 (-32.5%)**

Bold *– significant changes; Statistical test – individual patient analysis*

Figure 5.32: Absolute $IAUGC_{60}$ values changes after NCRT (individual patients)

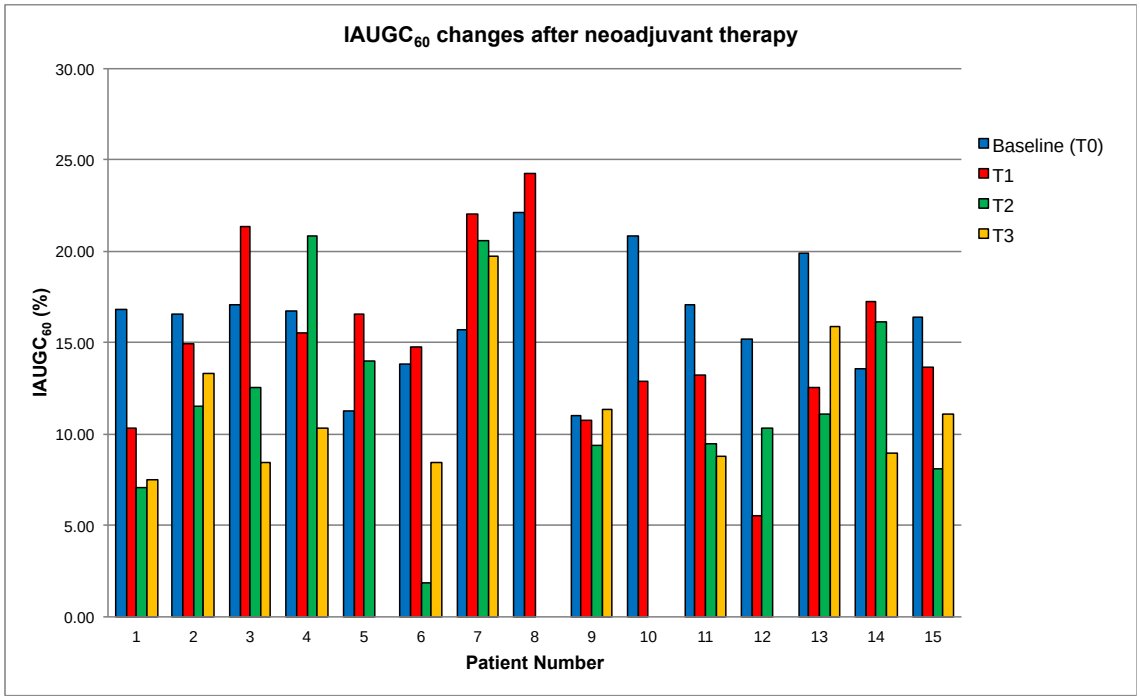

Figure 5.33: Percentage $IAUGC_{60}$ changes after NCRT (individual patients)

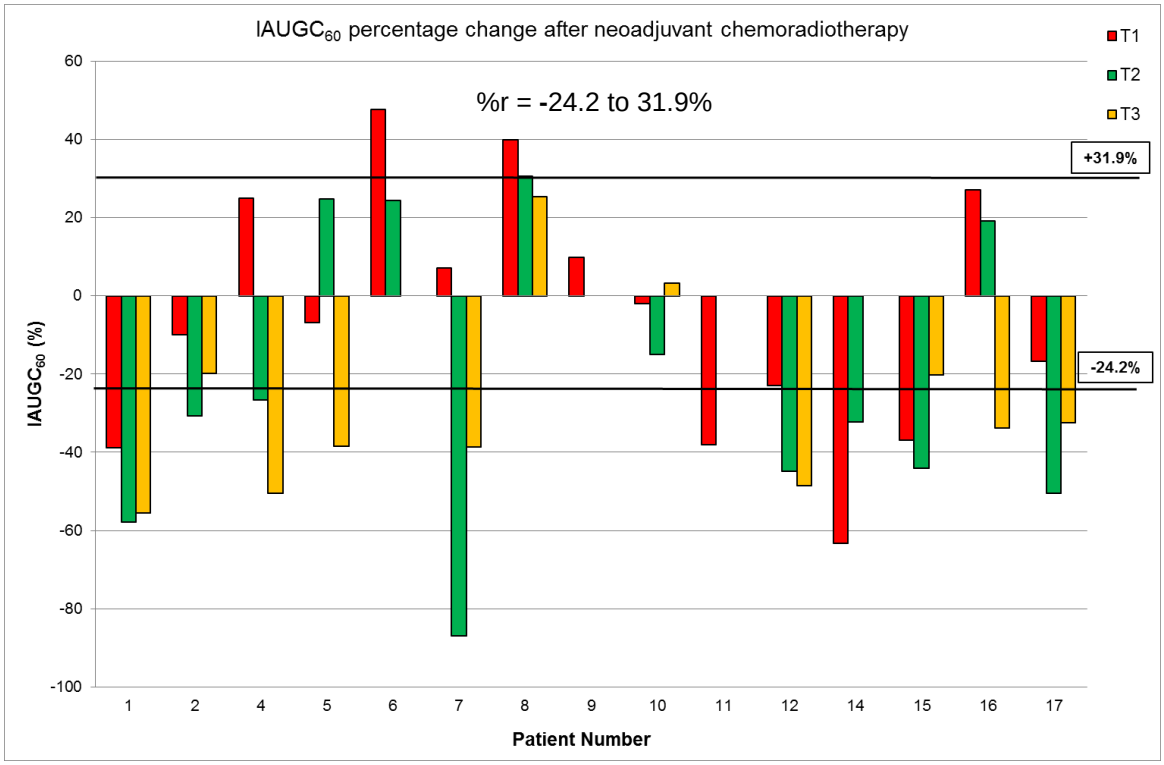

5.3.4 Relationship between MR multi-parametric measurements and clinical markers

5.3.4.1 Multiparametric analysis of tumour clinicopathological characteristics, response to therapy and long-term outcomes

The summary of association between MR multiparametric measurements at different time-points and clinical markers is presented in tables 5.15 and 5.16. The correlation between MR parameters and clinical markers is presented in tables 5.17 to 5.22. The association between mean values of MR parameters and clinical markers is presented in tables 5.23 to 5.25.

At pre-treatment stage, hypoxic tumours showed nodal involvement, resisted tumour downstaging and recurred distally; large tumours had higher perfusion and tumour with higher interstitial space showed T-downstaging resulting in lower pathological T-stage.

Immediately after NCRT, hypoxic tumours decreased in size; higher staged tumours maintained better perfusion, whilst tumours with decline in perfusion and interstitial space showed nodal downstaging.

Six weeks after NCRT, tumours with T-downstaging had decreased cellularity with increasing interstitial space.

Pre-operatively, tumours that remained or developed hypoxia (after NCRT) decreased in size, but showed nodal involvement, poor nodal downstaging with distant metastasis and shortened survival; large size tumours had decreased cell density, increased interstitial space and relatively less hypoxia; tumours

remaining perfused or re-developing perfusion (after NCRT) showed better nodal downstaging but higher recurrence and poor survival, whilst tumours developing increased transit of contrast within interstitium showed nodal involvement and poor nodal downstaging and higher distant metastasis rates.

Table 5.15: Summary of correlation between MR multi-parametric measurements and clinical markers during treatment timeline

	Clinicopathological Features							Response to NCRT				Long-term Outcomes		
	cT	**cN**	**pT**	**pN**	**cL**	**nL**	**pL**	**T↓**	**N↓**	**pCR**	**nRECIST**	**LR**	**DM**	**OS**
T_0	-	-	-	+ R_2*	-	-	+IAUGC$_{60}$	+ v_e	-	-	-	-	+R_2*	-
T_1	-	+v_e, +IAUGC$_{60}$	-	-	-	-	-	-	-	-	+R_2*	-	-	-
T_2	-		-v_e	-	-	+ADC	-	+v_e	-	-	-	-	-	-
T_3	-	+v_e	-	+ΔR_2* -Δk_{ep},	-	+ADC	-		-ΔR_2* +Δk_{ep}, +ΔIAUGC$_{60}$	-	+R_2*	-	+ΔR_2*, -Δk_{ep}, -ΔIAUGC$_{60}$	+ΔR_2*, -ΔIAUGC$_{60}$

'+' positive correlation; '-' negative correlation; prefix 'c' –Clinical; prefix 'p' – pathological; suffix '↓' – downstage; CR – pathological complete response; LR – local recurrence; DM – Distant metastasis; OS – overall survival

Table 5.16: Summary of association between mean multiparametric measurements and clinical markers during treatment timeline

	Clinicopathological Features							Response to NCRT				Long-term Outcomes		
	cT	**cN**	**pT**	**pN**	**cL**	**nL**	**pL**	**T↓**	**N↓**	**pCR**	**nRECIST**	**LR**	**DM**	**OS**
T_0	-	-	v_e	R_2*	-	-	-	R_2*	R_2*	-	-	-	-	-
T_1	K^{trans}, v_e, k_{ep}	v_e, $IAUGC_{60}$	R_2*	-	-	-	-	-	-	-	R_2*	-	-	-
T_2	-	-	-	-	-	-	-	-	-	-	-	-	-	-
T_3	-	-	-	-	-	-	-	-	-	-	ADC, R_2*	K^{trans}, $IAUGC_{60}$	-	-

'+' positive correlation; '-' negative correlation; prefix 'c' –Clinical; prefix 'p' – pathological; suffix '↓' – downstage; CR – pathological complete response; LR – local recurrence; DM – Distant metastasis; OS – overall survival

Table 5.17: Correlation between ADC measurement and clinical markers

ADC		Clinicopathological Features							Response to NCRT				Long-term Outcomes		
		cT	cN	pT	pN	cL	nL	pL	T↓	N↓	pCR	nRECIST	LR	DM	Death
T_0	ρ / r	-0.24	0.16	0	0.17	-0.30*	-0.13*	-0.10*	0	0.06	0	-0.16	-0.03	0.15	-0.15
	p	0.40	0.56		0.57	0.29	0.66	0.72		0.82		0.57	0.90	0.60	0.59
T_1	ρ / r	-0.24	0.08	0.17	0.22	-0.004*	0.32*	0.12*	-0.11	0.15	-0.15	-0.38	-0.37	0.05	-0.07
	p	0.40	0.77	0.55	0.45	0.98	0.27	0.67	0.68	0.60	0.60	0.17	0.18	0.86	0.79
T_2	ρ / r	-0.13	0.03	0.27	0.38	-0.21*	**0.63***	0.20*	-0.25	-0.32	-0.19	-0.47	-0.21	0.32	0.19
	p	0.68	0.90	0.38	0.21	0.49	**0.02**	0.52	0.42	0.30	0.54	0.12	0.49	0.30	0.54
T_3	ρ / r	-0.40	0.13	-0.12	0.22	0.10*	**0.68***	-0.27*	0.12	-0.07	0.07	-0.58	-0.40	0.07	0.12
	p	.022	0.68	0.72	0.50	0.75	**0.02**	0.41	0.72	0.82	0.82	0.06	0.22	0.82	0.70

*'+' positive correlation; '-' negative correlation; prefix 'c' –Clinical; prefix 'p' – pathological; prefix 'n' – post-NCRT; suffix '↓' – downstage; T – TNM T-stage; N – TNM N-stage; L – craniocaudal tumour length; RECIST – response evaluation criteria in solid tumours; CR – complete response; LR – local recurrence; DM – Distant metastasis; Statistical test – Shapiro-Wilk test and Q-Q plots for normality, Spearman rho correlation analysis (ρ) for non-parametric data, *Pearson Correlation (r) for parametric data*

Table 5.18: Correlation between R_2* measurements and clinical markers

R_2*		Clinicopathological Features							Response to NCRT				Long-term Outcomes		
		cT	cN	pT	pN	cL	nL	pL	T↓	N↓	pCR	nRECIST	LR	DM	Death
T_0	ρ / r	-0.15	0.11	0.30	**0.58**	-0.04	0.18	-0.18	-0.49	-0.34	0.15	0.12	0.07	**0.627**	0.04
	p	0.61	0.70	0.33	**0.04**	0.87	0.57	0.57	0.08	0.25	0.61	0.68	0.80	**0.02**	0.88
T_1	ρ / r	-0.07	-0.10	0.02	0	-0.04	-0.55	-0.08	-0.26	-0.09	0.077	**0.76**	-0.15	0.05	-0.35
	p	0.80	0.72	0.93		0.88	0.06	0.80	0.37	0.75	0.802	**0.003**	0.61	0.85	0.23
T_2	ρ / r	-0.30	-0.14	0	0.22	0.27*	-0.25*	-0.25*	-0.12	-0.44	0.3	0.38	-0.30	0.44	0.06
	p	0.37	0.66		0.50	0.41	0.45	0.44	0.72	0.16	0.37	0.23	0.37	0.16	0.85
T_3	ρ / r	-0.05	0.01	0.22	0.08	0.37*	-0.56*	-0.22*	-0.28	0.17	0.058	**0.64**	-0.29	-0.17	-0.49
	p	0.87	0.97	0.53	0.81	0.28	0.09	0.53	0.42	0.63	0.87	**0.04**	0.41	0.63	0.14

*'+' positive correlation; '-' negative correlation; prefix 'c' –Clinical; prefix 'p' – pathological; prefix 'n' – post-NCRT; suffix '↓' – downstage; T – TNM T-stage; N – TNM N-stage; L – craniocaudal tumour length; RECIST – response evaluation criteria in solid tumours; CR – complete response; LR – local recurrence; DM – Distant metastasis; Statistical test – Shapiro-Wilk test for normality; Spearman rho correlation analysis (ρ) (non-parametric data)***,** **Pearson Correlation (r) (for parametric data)*

Table 5.19: Correlation between K^{trans} measurement and clinical markers

K^{trans}		Clinicopathological Features							Response to NCRT				Long-term Outcomes		
		cT	cN	pT	pN	cL	nL	pL	T↓	N↓	pCR	nRECIST	LR	DM	Death
T_0	ρ / r	-0.29	0.40	-0.04	0	0.16*	0.26*	0.32*	0.31	0.30	-0.07	-0.18	0.12	-0.31	0.10
	p	0.28	0.13	0.88		0.56	0.36	0.25	0.25	0.29	0.78	0.50	0.66	0.24	0.71
T_1	ρ / r	-0.12	0.50	-0.01	0.35	0.07*	0.06*	0.35*	0.34	0.15	-0.3	-0.06	0.37	-0.18	0.24
	p	0.65	0.05	0.96	0.21	0.79	0.82	0.21	0.20	0.60	0.26	0.82	0.17	0.51	0.38
T_2	ρ / r	0.10	0.26	-0.32	0.17	-0.19*	0.23*	0.41*	0.49	0.11	0	-0.26	0.38	-0.11	0.19
	p	0.73	0.37	0.28	0.57	0.51	0.44	0.16	0.08	0.71		0.37	0.19	0.71	0.52
T_3	ρ / r	0.30	0.05	0.15	0.22	-0.23*	0.03*	0.41*	-0.12	-0.29	-0.14	-0.12	0.50	0.29	0.45
	p	0.37	0.87	0.64	0.50	0.48	0.91	0.20	0.72	0.37	0.66	0.07	0.11	0.37	0.16

*'+' positive correlation; '-' negative correlation; prefix 'c' –Clinical; prefix 'p' – pathological; prefix 'n' – post-NCRT; suffix '↓' – downstage; T – TNM T-stage; N – TNM N-stage; L – craniocaudal tumour length; RECIST – response evaluation criteria in solid tumours; CR – complete response; LR – local recurrence; DM – Distant metastasis; Statistical test – Shapiro-Wilk test for normality; Spearman rho correlation analysis (ρ) (non-parametric data)***,*** **Pearson Correlation (r) (for parametric data)*

CHAPTER 5: MRI – MULTIPARAMETRIC ANALYSIS

Table 5.20: Correlation between v_e measurement and clinical markers

V_e**		Clinicopathological Features							Response to NCRT				Long-term Outcomes		
		cT	cN	pT	pN	cL	nL	pL	T↓	N↓	pCR	nRECIST	LR	DM	Death
T_0	ρ / r	-0.25	0.29	-0.46	-0.15	0.29	0.02	-0.14	**.523**	.304	0.42	-0.03	0.12	-0.31	-0.27
	p	0.36	0.28	0.09	0.60	0.28	0.94	0.62	**.045**	.291	0.11	0.91	0.66	0.24	0.31
T_1	ρ / r	-.038	**0.64**	-0.29	0.15	-0.20	0.08	0.24	.489	.405	0.03	-0.12	0.18	-0.40	0
	p	0.16	**0.01**	0.30	0.60	0.46	0.78	0.39	.065	.151	0.89	0.65	0.50	0.13	
T_2	ρ / r	0.15	0.17	**-0.62**	-0.28	-0.28	0.23	0.02	**.624**	.456	0.39	-0.31	0.38	-0.45	-0.09
	p	0.60	0.56	**0.021**	0.34	0.34	0.43	0.92	**.023**	.117	0.18	0.30	0.19	0.11	0.75
T_3	ρ / r	-0.42	**.642**	0.08	0.17	-0.23	0.03	0.33	0	.172	0	0.09	0.38	-0.17	-0.09
	p	0.15	**.018**	0.77	0.57	0.43	0.90	0.26		.574		0.77	0.19	0.57	0.75

*'+' positive correlation; '-' negative correlation; prefix 'c' –Clinical; prefix 'p' – pathological; prefix 'n' – post-NCRT; suffix '↓' – downstage; T – TNM T-stage; N – TNM N-stage; L – craniocaudal tumour length; RECIST – response evaluation criteria in solid tumours; CR – complete response; LR – local recurrence; DM – Distant metastasis; Statistical test – Shapiro-Wilk test for normality; Spearman rho correlation analysis (ρ) (non-parametric data)***, *Pearson Correlation (r) (for parametric data); ** v_e not normal distribution*

Table 5.21: Correlation between k_{ep} measurement and clinical markers

k_{ep}		Clinicopathological Features							Response to NCRT				Long-term Outcomes		
		cT	cN	pT	pN	cL	nL	pL	T↓	N↓	pCR	nRECIST	LR	DM	Death
T_0	ρ / r	-0.19	0.27	0.19	0.15	0.06*	0.23	0.21	-.035	0.10	-0.29	0.09	.006	-0.13	.297
	p	0.49	0.32	0.51	0.60	0.82	0.42	0.45	0.90	0.73	0.29	0.73	0.82	0.62	.282
T_1	ρ / r	-0.08	0.34	0.26	0.30	0.17*	0.11*	0.34*	0.07	-0.10	-0.42	-0.06	0.43	0.04	.419
	p	0.76	0.20	0.35	0.29	0.53	0.70	0.22	0.80	0.73	0.11	0.82	0.10	0.87	.120
T_2	ρ / r	0.05	0.26	-0.23	0.22	-0.27*	0.26*	0.43*	0.40	0	-0.04	-0.26	0.38	0	.293
	p	0.86	0.37	0.43	0.45	0.37	0.38	0.13	0.17		0.87	0.37	0.19		.332
T_3	ρ / r	0.26	-0.08	0.34	0.19	0.15*	0.34*	0.29*	-0.23	-0.52	-0.16	-0.25	0.48	0.52	**.587**
	p	0.40	0.78	0.27	0.54	0.63	0.27	0.35	0.47	0.08	0.61	0.43	0.11	0.08	**.045**

*'+' positive correlation; '-' negative correlation; prefix 'c' –Clinical; prefix 'p' – pathological; prefix 'n' – post-NCRT; suffix '↓' – downstage; T – TNM T-stage; N – TNM N-stage; L – craniocaudal tumour length; RECIST – response evaluation criteria in solid tumours; CR – complete response; LR – local recurrence; DM – Distant metastasis; Statistical test – Shapiro-Wilk test for normality; Spearman rho correlation analysis (ρ) (non-parametric data)***,** **Pearson Correlation (r) (for parametric data)*

Table 5.22: Correlation between $IAUGC_{60}$ measurement and clinical markers

$IAUGC_{60}$		Clinicopathological Features							Response to NCRT				Long-term Outcomes		
		cT	cN	pT	pN	cL	nL	pL	T↓	N↓	pCR	nRECIST	LR	DM	Death
T_0	ρ / r	-0.27	0.39	0.07	0.22	0.01*	0.07*	**0.53***	0.21	0.30	-0.17	-0.23	-0.12	-0.31	0.03
	p	*0.32*	*0.14*	*0.80*	*0.43*	*0.95*	*0.78*	***0.05***	*0.45*	*0.29*	*0.53*	*0.39*	*0.66*	*0.24*	*0.90*
T_1	ρ / r	-0.21	**0.55**	-0.17	0.35	-0.09*	-0.03*	0.31*	0.38	0.15	-0.19	0.03	0.37	-0.18	0.17
	p	*0.45*	***0.00***	*0.54*	*0.21*	*0.73*	*0.92*	*0.26*	*0.15*	*0.60*	*0.49*	*0.91*	*0.17*	*0.51*	*0.53*
T_2	ρ / r	0.05	0.30	-0.36	0.17	-0.22*	0.19*	0.36*	0.49	0.11	0.04	-0.17	0.38	-0.11	0.19
	p	*0.86*	*0.31*	*0.21*	*0.57*	*0.46*	*0.53*	*0.22*	*0.08*	*0.71*	*0.87*	*0.56*	*0.19*	*0.71*	*0.52*
T_3	ρ / r	0.20	-0.13	0.14	-0.07	-0.21	0.005	0.42	-0.06	-0.37	-0.22	0.12	0.50	0.37	0.32
	p	*0.55*	*0.68*	*0.66*	*0.82*	*0.52*	*0.98*	*0.19*	*0.86*	*0.25*	*0.5*	*0.70*	*0.11*	*0.25*	*0.33*

*'+' positive correlation; '-' negative correlation; prefix 'c' –Clinical; prefix 'p' – pathological; prefix 'n' – post-NCRT; suffix '↓' – downstage; T – TNM T-stage; N – TNM N-stage; L – craniocaudal tumour length; RECIST – response evaluation criteria in solid tumours; CR – complete response; LR – local recurrence; DM – Distant metastasis; Statistical test – Shapiro-Wilk test for normality; Spearman rho correlation analysis (ρ) (non-parametric data)***,*** **Pearson Correlation (r) (for parametric data)*

Table 5.23: Difference in mean multiparametric values according to clinical features

Parameter		cT				cN				pT					pN		
		cT2	**cT3**	***cT4***	***p***	**cN0**	**cN1**	**cN2**	***p***	**pT0**	**pT1**	**pT2**	**pT3**	***p***	**pN0**	**pN1**	***p***
ADC	T_0	1.40	1.31	-	*0.65*	1.52	1.25	1.44	*0.20*	1.32	1.31	1.35	1.28	*0.97*	1.30	1.46	*0.32*
	T_1	1.75	1.59	-	*0.40*	1.71	1.56	1.69	*0.49*	1.52	1.51	1.65	1.62	*0.83*	1.59	1.74	*0.28*
	T_2	1.60	1.57	-	*0.84*	1.76	1.51	1.66	*0.23*	1.46	1.59	1.57	1.61	*0.81*	1.54	1.71	*0.21*
	T_3	1.88	1.62	-	*0.26*	1.88	1.57	1.75	*0.27*	1.67	-	1.65	1.63	*0.97*	1.63	1.70	*0.72*
R_2*	T_0	23.5	23.24	-	*0.92*	27.5	22.6	23.8	*0.27*	23.5	22.6	22.0	*25.7*	*0.28*	**22.6**	**27.5**	***0.02***
	T_1	23.6	23.1	-	*0.92*	19.8	25.4	21.5	*0.40*	**23.6**	**38.4**	**21.8**	***24.7***	***0.01***	24.3	24.4	*0.99*
	T_2	30.7	25.3	-	*0.34*	24.9	26.3	25.0	*0.92*	30.7	23.1	24.7	*26.6*	*0.74*	25.1	29.2	*0.32*
	T_3	24.8	24.1	-	*0.83*	20.9	24.9	23.8	*0.42*	24.8	-	23.7	*24.7*	*0.86*	24.1	24.4	*0.90*
K^{trans}	T_0	0.22	0.17	0.15	*0.51*	0.13	0.18	0.19	*0.26*	0.17	0.11	0.19	0.15	*0.18*	0.17	0.17	*0.98*
	T_1	**0.10**	**0.15**	**0.00**	***0.03***	0.05	0.14	0.17	*0.06*	0.09	0.13	0.16	0.11	*0.35*	0.12	0.16	*0.44*
	T_2	0.07	0.11	0.09	*0.85*	0.09	0.10	0.14	*0.69*	0.10	0.12	0.14	0.07	*0.59*	0.11	0.11	*0.99*
	T_3	0.07	0.09	-	*0.80*	0.09	0.07	0.12	*0.42*	0.08	-	0.09	0.09	*0.98*	0.08	0.10	*0.62*
v_e*	T_0	0.30	0.24	0.24	*0.50**	0.23	0.24	0.26	*0.53**	**0.30**	**0.14**	**0.26**	**0.20**	***0.05****	0.24	0.23	*0.58**
	T_1	0.31	0.28	0.00	*0.25**	0.10	0.28	0.32	*0.50**	0.21	0.27	0.20	0.24	*0.30**	0.26	0.28	*0.58**
	T_2	0.27	0.23	0.31	*0.53**	0.26	0.22	0.28	*0.54**	0.29	0.27	0.23	0.21	*0.16**	0.24	0.19	*0.32**
	T_3	0.29	0.21	0.00	*0.31**	0.11	0.19	0.30	*0.08**	0.19	0.00	0.22	0.23	*0.57**	0.19	0.27	*0.55**
k_{ep}	T_0	0.75	0.75	0.66	*0.91*	0.59	0.78	0.72	*0.48*	0.60	0.72	0.77	0.76	*0.68*	0.72	0.75	*0.85*
	T_1	**0.36**	**0.54**	**0.00**	***0.003***	0.25	0.52	0.56	*0.12*	0.30	0.49	0.54	0.51	*0.31*	0.46	0.57	*0.41*
	T_2	0.30	0.43	0.29	*0.76*	0.35	0.41	0.47	*0.82*	0.38	0.47	0.48	0.34	*0.82*	0.40	0.48	*0.62*
	T_3	0.29	0.31	-	*0.90*	0.43	0.26	0.40	*0.44*	0.30	0.00	0.32	0.38	*0.30*	0.29	0.40	*0.46*
$IAUGC_{60}$	T_0	17.1	16.2	15.1	*0.91*	13.0	16.7	16.6	*0.32*	15.2	11.2	17.3	15.1	*0.18*	15.6	16.8	*0.61*
	T_1	13.1	15.9	5.5	*0.10*	**8.17**	**15.2**	**18.8**	***0.03***	11.9	16.5	16.5	12.3	*0.33*	13.7	18.1	*0.19*
	T_2	9.4	12.0	10.2	*0.87*	9.82	11.3	14.1	*0.65*	11.9	13.9	13.3	9.01	*0.68*	11.7	12.0	*0.94*
	T_3	8.7	11.5	0	*0.51*	11.3	10.7	12.3	*0.86*	8.89	-	12.5	10.7	*0.52*	11.3	10.8	*0.87*

*'+' positive correlation; '-' negative correlation; prefix 'c' –Clinical; prefix 'p' – pathological; prefix 'n' – post-NCRT; T –TNM T-stage; N – TNM N-stage; L – craniocaudal tumour length; RECIST – response evaluation criteria in solid tumours; CR – complete response; LR – local recurrence; DM – Distant metastasis; Statistical test – Shapiro-Wilk test and Q-Q plots for normality; Spearman rho correlation analysis (ρ) (non-parametric data)***,** **Pearson Correlation (r) (for parametric data); Means compared with ANOVA (for normally distributed data) and Kruskal-Wallis test or Mann-Whitney-U test for non-normal distribution; * v_e not normally distributed.*

Table 5.24: Difference in mean multiparametric values according to response to NCRT

Parameter		T- downstaging			N-downstaging			Post NCRT RECIST			Post-Operative NCRT			
		T↓	T⊘	*p*	N↓	N⊘	*p*	PR	SD	*p*	CR	PR	SD	*p*
ADC	T_0	1.33	1.28	*0.79*	1.31	1.32	*0.91*	1.27	1.39	*0.33*	1.32	1.29	1.42	*0.70*
	T_1	1.59	1.62	*0.77*	1.61	1.56	*0.68*	1.55	1.69	*0.17*	1.52	1.61	1.64	*0.82*
	T_2	1.55	1.61	*0.53*	1.55	1.67	*0.36*	1.52	1.72	*0.08*	1.46	1.59	1.60	*0.64*
	T_3	1.66	1.63	*0.83*	1.64	1.69	*0.78*	**1.57**	**1.84**	***0.05***	1.67	1.68	1.56	*0.76*
R_2*	T_0	**22.1**	**25.7**	***0.03***	**22.3**	**26.2**	***0.03***	23.4	22.9	*0.79*	23.5	22.7	25.5	*0.46*
	T_1	23.8	24.7	*0.78*	24.2	23.5	*0.84*	**26.4**	**20.4**	***0.03***	23.6	24.6	24.5	*0.98*
	T_2	25.3	26.6	*0.71*	24.8	30.4	*0.16*	27.1	22.4	*0.17*	30.7	24.8	26.7	*0.57*
	T_3	23.9	24.7	*0.66*	24.5	22.9	*0.49*	**25.3**	**21.5**	***0.02***	24.8	23.8	24.8	*0.88*
K^{trans}	T_0	0.18	0.15	*0.26*	0.17	0.18	*0.86*	0.17	0.18	*0.65*	0.17	0.17	0.16	*0.96*
	T_1	0.15	0.11	*0.36*	**0.13**	0.16	*0.49*	0.14	0.14	*0.99*	0.09	0.14	0.15	*0.45*
	T_2	0.13	0.07	*0.30*	0.11	0.09	*0.62*	0.10	0.14	*0.34*	0.10	0.12	0.09	*0.87*
	T_3	0.08	0.09	*0.96*	0.08	0.10	*0.61*	0.08	0.09	*0.95*	0.08	0.08	0.10	*0.90*
v_e*	T_0	**0.26**	**0.20**	***0.05***	0.25	0.23	*0.73*	0.24	0.25	*0.95*	0.30	0.21	0.26	*0.20*
	T_1	0.27	0.24	*0.06*	0.27	0.25	*0.53*	0.28	0.24	*0.68*	0.21	0.27	0.29	*0.68*
	T_2	**0.25**	**0.21**	***0.03***	0.25	0.20	*0.15*	0.22	0.28	*0.33*	0.22	0.23	0.22	*0.28*
	T_3	0.19	0.23	*1.0*	0.20	0.23	*0.64*	0.20	0.20	*0.82*	0.19	0.17	0.28	*0.27*
k_{ep}	T_0	0.74	0.76	*0.82*	0.74	0.78	*0.76*	0.74	0.75	*0.89*	0.60	0.80	0.68	*0.27*
	T_1	0.49	0.51	*0.43*	0.46	0.60	*0.25*	0.51	0.46	*0.65*	0.30	0.53	0.51	*0.16*
	T_2	0.44	0.34	*0.44*	0.41	0.42	*0.97*	0.37	0.51	*0.24*	0.38	0.42	0.42	*0.95*
	T_3	0.38	0.27	*0.34*	0.28	0.26	*0.18*	0.29	0.36	*0.60*	0.30	0.29	0.36	*0.86*
$IAUGC_{60}$	T_0	16.6	15.1	*0.44*	16.2	16.5	*0.86*	15.6	17.1	*0.39*	15.2	15.0	17.7	*0.30*
	T_1	16.0	12.3	*0.21*	14.6	16.6	*0.52*	15.0	15.0	*0.98*	11.9	14.6	15.7	*0.54*
	T_2	12.9	9.01	*0.22*	11.9	10.4	*0.71*	11.0	13.2	*0.51*	11.9	12.1	10.7	*0.93*
	T_3	11.5	10.7	*0.77*	11.0	12.3	*0.68*	11.7	10.0	*0.53*	8.89	12.2	10.9	*0.59*

*'+' positive correlation; '-' negative correlation; prefix 'c' – Clinical; prefix 'p' – pathological; prefix 'n' – post-NCRT; suffix '↓' – downstage; T – TNM T-stage; N – TNM N-stage; L – craniocaudal tumour length; RECIST – response evaluation criteria in solid tumours; CR – complete response; LR – local recurrence; DM – Distant metastasis; Statistical test – Shapiro-Wilk test and Q-Q plots for normality; Spearman rho correlation analysis (ρ) (non-parametric data), *Pearson Correlation (r) (for parametric data); Means compared with ANOVA (for normally distributed data) and Kruskal-Wallis test or Mann-Whitney-U test for non-normal distribution; * v_e not normally distributed*

Table 5.25: Difference in mean multiparametric values according to long-term outcomes

Parameter		Local Recurrence			Distant Metastasis			Survival		
		Yes	No	*p*	Yes	No	*p*	Yes	No	*p*
ADC	T_0	1.28	1.32	*0.87*	1.40	1.30	*0.53*	1.31	1.31	*0.98*
	T_1	1.38	1.61	*0.23*	1.63	1.59	*0.82*	1.61	1.57	*0.76*
	T_2	1.56	1.57	*0.96*	1.67	1.55	*0.36*	1.54	1.64	*0.43*
	T_3	1.46	1.66	*0.38*	1.69	1.64	*0.78*	1.62	1.71	*0.58*
R_2*	T_0	23.1	23.2	*0.97*	**28.8**	**22.2**	***<0.001***	22.6	24.6	*0.26*
	T_1	21.7	24.3	*0.65*	24.6	24.0	*0.88*	24.6	22.4	*0.47*
	T_2	21.8	26.2	*0.43*	30.4	24.8	*0.16*	25.4	26.8	*0.70*
	T_3	22.8	24.3	*0.61*	22.9	24.5	*0.49*	25.2	21.9	*0.07*
K^{trans}	T_0	0.19	0.17	*0.71*	0.14	0.18	*0.25*	0.17	0.19	*0.62*
	T_1	0.23	0.13	*0.12*	0.12	0.14	*0.62*	0.13	0.17	*0.29*
	T_2	0.22	0.10	*0.09*	0.09	0.11	*0.62*	0.10	0.14	*0.36*
	T_3	**0.19**	**0.07**	***0.008***	0.10	0.08	*0.61*	0.08	0.10	*0.63*
v_e*	T_0	0.25	0.24	*0.64*	0.21	0.25	*0.23*	0.25	0.22	*0.29*
	T_1	0.31	0.26	*0.48*	0.22	0.27	*0.12*	0.26	0.27	*1*
	T_2	0.31	0.23	*0.18*	0.20	0.25	*0.11*	0.24	0.24	*0.73*
	T_3	0.31	0.19	*0.17*	0.23	0.20	*0.55*	0.19	0.24	*0.73*
k_{ep}	T_0	0.73	0.74	*0.92*	0.67	0.76	*0.56*	0.71	0.85	*0.22*
	T_1	0.75	0.47	*0.15*	0.54	0.48	*0.72*	0.45	0.60	*0.16*
	T_2	0.61	0.39	*0.34*	0.42	0.41	*0.97*	0.37	0.56	*0.14*
	T_3	0.61	0.28	*0.07*	0.46	0.28	*0.18*	0.27	0.42	*0.20*
$IAUGC_{60}$	T_0	15.7	16.3	*0.87*	13.7	16.6	*0.24*	16.1	16.5	*0.82*
	T_1	22.0	14.5	*0.14*	12.8	15.3	*0.50*	14.5	16.3	*0.54*
	T_2	20.5	11.0	*0.08*	10.4	11.9	*0.71*	11.1	13.8	*0.44*
	T_3	**19.7**	**10.4**	***0.008***	12.3	11.0	*0.68*	11.1	11.6	*0.84*

*'+' positive correlation; '-' negative correlation; prefix 'c' – Clinical; prefix 'p' – pathological; prefix 'n' – post-NCRT; T – TNM T-stage; N – TNM N-stage; L – craniocaudal tumour length; RECIST – response evaluation criteria in solid tumours; CR – complete response; LR – local recurrence; DM – Distant metastasis; Statistical test – Shapiro-Wilk test and Q-Q plots for normality; Spearman rho correlation analysis (ρ) (non-parametric data), *Pearson Correlation (r) (for parametric data); Means compared with ANOVA (for normally distributed data) and Kruskal-Wallis test or Mann-Whitney-U test for non-normal distribution; * ve not normally distributed*

5.3.4.2 Association between MRI multiparametric alteration after NCRT and clinicopathological characteristics, response to therapy and long-term outcomes

The binary alteration pattern in parametric measurements (increase or decrease) were analysed against clinicopathological characteristics, response to therapy and long-term outcomes. The relation between alterations in MR multi-parametric measurements and clinical data was investigated by Chi-Square or Fisher exact tests and Spearman rho correlation analysis. The results are presented in table 5.26 to 5.28.

During the interval between completion of NCRT and surgery (see table 5.27), tumours that remained large in size had low cell density (low ADC) with large interstitial space (high v_e); tumours that remained (or became) hypoxic (high R_2*) showed localised nodal metastasis, poor nodal downstaging with distant metastasis and shortened survival; tumours remaining perfused or re-developing perfusion showed increased nodal downstaging, decreased distant metastasis and survival, whilst tumours developing increased transit of contrast within interstitium (high k_{ep}) showed poor nodal involvement, good nodal downstaging and low distant metastasis.

None of the MR parameters changes showed any association with clinical markers based on chi-square or Fisher exact tests.

CHAPTER 5: MRI – MULTIPARAMETRIC ANALYSIS

Table 5.26: MR multi-parametric alterations after NCRT and clinical outcomes.

Code		Sex	Age	cTNM	Δ ADC	Δ R_2*	Δ K^{trans}	Δ v_e	Δ k_{ep}	Δ $IUAGC_{60}$	Post NCRT TNM (yp or r)	Local Recurrence	Distant Recurrence	Death
1	RY	M	59	T3N1M0	↑*	↑	↓*	↓	↓*	↓*	T3N0			
2	DG*	M	52	T3N1M0	↑*	↓*	↓*	↑	↓*	↓	T3N1		✓: Lung	✓
3	DJ	M	72	T3N1M2	-	-	-	-	-	-	-	-	✓: Liver	✓
4	AH	M	74	T3N2M0	↑*	↓	↓*	↑	↓*	↓*	T2N1			
5	KB	M	78	T3N1M0	↑*	↓	↓*	↑*	↓*	↓*	T2N0			✓
6	ED	F	72	T3N1M0	↑*	↑	↑*	↑*	↓*	↑	T1N0			
7	AF	F	60	T3N1M0	↓	↑*	↓*	↓	↓*	↓*	T2N0			
8	JN	M	79	T3N2M0	↑*	↓	↓	↑	↓	↑	T2N0	✓		
9	SD**	M	71	T3N1M0	↑*	↑	↓	↓	↓*	↑	T2N0			✓
10	JH	M	67	T3N0M0	↑*	↓*	↓	↓	↓	↑	T3N0		✓: Pancreas	✓
11	DP	M	58	T3N1M0	↑*	↑	↓*	↓	↓*	↓*	T2N0			
12	GA***	M	53	T2N2M0	↑*	↑	↓*	↓	↓*	↓*	RCR			
13	PO	F	59	T3N2M0	-	-	-	-	-	-	T3N2		✓: Liver	
14	MM***	F	78	T4N0M0	-	-	↓*	↑*	↓*	↓*	RCR			
15	RC1	M	76	T3N1M0	↑*	↑*	↓*	↓*	↓*	↓*	T2N0			
16	RC2	M	56	T3N1M0	↑*	-	↓*	↓	↓	↓	PCR			
17	JT	F	79	T3N1M0	↓	↑	↓*	↑*	↓*	↓*	T3N0			

** Statistically significant; PCR – pathological complete response; RCR – radiological complete response*

Table 5.27: Correlation between MR multi-parametric alteration trends after NCRT and clinical markers

Parameter		Clinicopathological Features							Response to NCRT				Long-term outcomes		
		cT	cN	pT	pN	cL	nL	pL	T↓	N↓	CR	nRECIST	LR	DM	Death
Δ ADC	ρ	0.11	-0.12	0.24	-0.18	-0.02	**- 0.60**	-0.08	-0.19	0.18	-0.16	0.30	-0.11	-0.16	-0.25
	p	0.7	0.6	0.4	0.5	0.93	**0.03**	0.78	0.5	0.5	0.56	0.29	0.7	0.5	0.3
Δ R_2*	ρ	0.2	0.11	0.33	**0.53**	-0.33	0.33	0.40	-0.18	**-0.53**	-0.30	-0.21	0.37	**0.54**	**0.51**
	p	0.4	0.6	0.2	**0.05**	0.24	0.25	0.17	0.5	**0.05**	0.29	0.43	0.1	**0.04**	**0.05**
Δ K^{trans}	ρ	0	0.03	0.25	0.11	0.27	0.34	0.03	-0.16	-0.11	0.13	-0.21	0.07	0.1	0.16
	p		0.8	0.3	0.7	0.31	0.22	0.90	0.5	0.7	0.63	0.43	0.8	0.7	0.5
Δ v_e	ρ	-0.36	-0.13	-0.03	-0.4	**0.80**	0.32	-0.41	0.04	0	0.13	0.05	-0.28	-0.02	-0.04
	p	0.1	0.6	0.8	0.1	**<0.001**	0.26	0.14	0.8		0.63	0.84	0.3	0.9	0.88
Δ k_{ep}	ρ	0	0.03	-0.36	**-0.67**	0.18	0.24	-0.31	0.44	**0.67**	0.13	-0.21	0.07	**-0.68**	-0.44
	p		0.8	0.2	**0.008**	0.50	0.40	0.27	0.09	**0.008**	0.63	0.43	0.8	**0.005**	0.09
Δ $IAUGC_{60}$	ρ	0	0.07	-0.27	-0.19	0.115	-0.20	-0.23	0.21	**0.64**	0.35	0	-0.37	**-0.55**	**-0.53**
	p		0.7	0.3	0.5	0.68	0.48	0.41	0.4	**0.01**	0.19		0.1	**0.03**	**0.04**

'+' positive correlation; '-' negative correlation; prefix 'c' –Clinical; prefix 'p' – pathological; suffix '↓' – downstage; CR – pathological complete response; LR – local recurrence; DM – Distant metastasis; Statistical test – Spearman rho correlation analysis. (ρ - rho, p-significance value)

Table 5.28: Association between MR multi-parametric changes after NCRT and clinical markers

Parameters	Clinicopathological Features				Response to NCRT				Long-term Outcomes		
	cT	cN	pT	pN	T↓	N↓	CR	nRECIST	LR	DM	Death
Δ ADC	0.87*	0.47	0.73	0.7*	0.5*	0.7*	0.72*	0.39*	0.8*	0.7*	0.4*
Δ R_2*	0.64*	0.11	0.32	0.12*	0.45*	0.12*	0.39*	0.20*	0.35*	0.11*	0.09*
Δ K^{trans}	0.86	0.65	0.06	0.85*	0.73*	0.85*	0.8*	0.60*	0.93*	0.86*	0.73*
Δ v_e	0.24	0.71	0.63	0.23*	0.66*	0.76*	0.55*	0.62*	0.46*	0.73*	0.66*
Δ k_{ep}	0.86	0.65	0.43	0.14*	0.26*	0.14*	0.8*	0.60*	0.93*	0.13*	0.26
Δ $IAUGC_{60}$	0.41	0.86	0.12	0.5*	0.4*	0.06*	0.26*	0.71*	0.33*	0.09*	0.07*

*Prefix 'c' –Clinical; prefix 'p' – pathological; suffix '↓' – downstage; CR – pathological complete response; LR – local recurrence; DM – Distant metastasis; Statistical tests - Chi-Square; *Fisher exact test*

5.3.5 Role of MRI Multiparametric analysis in predicting response to NCRT and long-term prognosis

The difference in parameters values and statistical significance between baseline and each time point for response and long-terms outcomes is given in tables 5.29–5.31.

In summary, increase in ADC from baseline was statistically significant in responders and patients without recurrence. However, ADC significantly increased in both survived and diseased groups, hence ADC was of value in predicting response and recurrence but not survival. On the other hand, patients with hypoxic tumour at pre-operative stage (significantly increased R_2* at T_3) showed N-downstaging and were alive at the end of study. Amongst DCE parameters: patient with T-downstaging showed a significant decrease in k_{ep} at all time-points, preoperative K^{trans} and $IAUGC_{60}$ at T_3; patients with N-downstaging showed significant decrease in K^{trans} and k_{ep} at all time-points and $IAUGC_{60}$ at T_3; patients without recurrence and who remained alive at the end of the study showed decline in K^{trans} (T_1-T_3), kep (T_2-T_3) and $IAUGC_{60}$ (T_2-T_3).

Table 5.29: Difference in mean parametric values after NCRT between patient with and without TNM downstaging

Parameter		T_0 vs. T_1 (mean)		*p*	T_0 vs. T_2 (mean)		*p*	T_0 vs. T_3 (mean)		*p*
T↓	**ADC**	**1.33**	**1.59**	***0.002***	1.35	1.55	*0.08*	**1.35**	**1.66**	***0.01***
	R_2*	22.4	23.4	*0.43*	22.3	25.3	*0.31**	22.3	23.9	*0.20*
	K^{trans}	0.18	0.15	*0.11*	0.17	0.13	*0.11*	**0.19**	**0.08**	***0.01***
	v_e	0.26	0.27	*0.24**	0.25	0.25	*0.67**	0.25	0.19	*0.21*
	k_{ep}	**0.74**	**0.49**	***0.01****	**0.73**	**0.44**	***0.005***	**0.73**	**0.27**	***0.004***
	$IAUGC_{60}$	16.6	16.0	*0.71*	15.5	12.9	*0.24*	**16.2**	**11.5**	***0.02****
T⊘	**ADC**	1.28	1.62	*0.12*	1.28	1.61	*0.10*	1.28	1.63	*0.16*
	R_2*	25.7	24.7	*0.69*	25.7	26.6	*0.59**	25.7	24.7	*0.73*
	K^{trans}	0.15	0.11	*0.14*	**0.15**	**0.07**	***0.02***	0.15	0.09	*0.06*
	v_e	0.20	0.24	*0.14**	0.20	0.21	*0.71**	0.20	0.23	*0.35*
	k_{ep}	0.76	0.51	*0.06**	**0.76**	**0.34**	***0.05***	0.76	0.38	*0.06*
	$IAUGC_{60}$	15.1	12.3	*0.13*	**15.1**	**9.0**	***0.04***	15.1	10.7	*0.14**
N↓	**ADC**	**1.31**	**1.61**	***0.003***	**1.31**	**1.54**	***0.03***	**1.31**	**1.64**	***0.01***
	R_2*	22.3	24.2	*0.32*	22.4	24.8	*0.26**	**22.4**	**24.5**	***0.04***
	K^{trans}	**0.17**	**0.13**	***0.06***	**0.17**	**0.11**	***0.03***	**0.18**	**0.08**	***0.003***
	v_e	0.25	0.27	*0.20**	0.24	0.25	*0.42**	0.24	0.20	*0.31*
	k_{ep}	**0.74**	**0.46**	***0.01****	**0.75**	**0.41**	***0.001***	**0.76**	**0.28**	***<0.001***
	$IAUGC_{60}$	16.2	14.6	*0.35*	15.7	11.9	*0.70*	**16.3**	**11.0**	***0.01****
N⊘	**ADC**	**1.32**	**1.56**	***0.01***	1.40	1.67	*0.09*	1.40	1.69	*0.15*
	R_2*	26.2	23.5	*0.39*	28.8	30.4	*0.65**	28.8	22.9	*0.07*
	K^{trans}	0.18	0.16	*0.16*	0.14	0.09	*0.23*	0.14	0.10	*0.20*
	v_e	0.23	0.25	*0.28**	0.21	0.20	*0.18**	0.21	0.23	*0.50*
	k_{ep}	0.78	0.60	*0.10**	0.67	0.42	*0.24*	0.67	0.46	*0.30*
	$IAUGC_{60}$	16.5	16.6	*0.94*	13.7	10.4	*0.30*	13.7	12.3	*0.65**

*Statistical Test: Paired sample T-test; *Wilcoxon Signed ranked test*

Note: Complete response not assessed as few small sample size

'↓' denotes downstaging; '⊘' denotes no change

Table 5.30: Difference in mean parametric values after NCRT between patient with and without RECIST downstaging

Parameter		T_0 vs. T_1 (mean)		*p*	T_0 vs. T_2 (mean)		*p*	T_0 vs. T_3 (mean)		*p*
nRECIST↓	**ADC**	**1.27**	**1.55**	***0.02***	**1.27**	**1.52**	***0.05***	**1.27**	**1.57**	***0.03***
	R_2*	23.4	26.4	*0.18*	**23.4**	**27.1**	***0.04***	23.5	25.3	*0.24*
	K^{trans}	0.17	0.14	*0.17*	**0.17**	**0.10**	***0.01***	**0.18**	**0.08**	***0.01***
	***v_e**	**0.24**	**0.28**	***0.05***	0.24	0.22	*0.85*	0.24	0.20	*0.44*
	k_{ep}	**0.74**	**0.51**	***0.03***	**0.74**	**0.37**	***0.003***	**0.74**	**0.29**	***0.002***
	$IAUGC_{60}$	15.6	15.0	*0.70*	**15.6**	**11.0**	***0.05***	**16.2**	**11.7**	***0.01***
nRECIST⊘	**ADC**	**1.39**	**1.69**	***0.002***	**1.48**	**1.72**	***0.01***	**1.48**	**1.84**	***0.02***
	R_2*	22.9	20.4	*0.20*	24.0	22.4	*0.17*	24.0	21.5	*0.35*
	K^{trans}	0.18	0.14	*0.14*	0.16	0.14	*0.48*	0.16	0.09	*0.09*
	***v_e**	0.25	0.24	*0.75*	0.22	0.28	*0.14*	0.22	0.20	*1*
	k_{ep}	**0.75**	**0.46**	***0.03***	**0.74**	**0.51**	***0.01***	0.76	0.36	*0.15*
	$IAUGC_{60}$	17.1	15.0	*0.40*	14.9	13.2	*0.46*	14.9	10.0	*0.21*

*prefix 'n' – post NCRT; Prefix 'p' – pathological; Suffix '↓' denotes downstaging; Suffix '⊘' denotes no change: Statistical Test: Paired sample T-test ; *Wilcoxon Signed ranked test*

Note: Complete response not assessed as few small sample size

Table 5.31: Changes after NCRT and long-term outcomes

		T_0 vs. T_1 (mean)		*p*	T_0 vs. T_2 (mean)		*p*	T_0 vs. T_3 (mean)		*p*
No Recurrence (local or distant)	**ADC**	**1.30**	**1.61**	***0.002***	1.31	1.55	*0.06*	**1.31**	**1.66**	***0.01***
	R_2*	22.3	24.2	*0.27*	22.3	25.2	*0.12**	**22.6**	**24.7**	***0.03***
	K^{trans}	**0.18**	**0.13**	***0.03***	**0.17**	**0.10**	***0.03***	**0.18**	**0.07**	***0.002***
	v_e	0.25	0.27	*0.2**	0.23	0.24	*0.57**	0.23	0.18	*0.25*
	k_{ep}	0.76	0.46	*0.006**	**0.75**	**0.39**	***0.002***	**0.76**	**0.24**	***<0.001***
	$IAUGC_{60}$	16.7	14.8	*0.23*	**15.7**	**11.1**	***0.03***	**16.4**	**9.9**	***0.01****
Recurrence (local or distant)	**ADC**	1.36	1.54	*0.10*	1.36	1.64	*0.10*	1.36	1.61	*0.10*
	R_2*	26.9	23.6	*0.10*	26.9	27.5	*-**	26.9	22.9	*0.10*
	K^{trans}	0.16	0.15	*0.87*	0.16	0.13	*0.46*	0.16	0.13	*0.19*
	v_e	0.23	0.25	*0.28**	0.23	0.24	*-**	0.23	0.25	*0.24*
	k_{ep}	0.69	0.61	*0.41**	0.69	0.48	*0.10*	0.69	0.51	*0.11*
	$IAUGC_{60}$	14.4	15.9	*0.61*	14.4	13.8	*0.84*	14.4	14.7	*0.59**
Alive	**ADC**	**1.31**	**1.61**	***0.008***	1.31	1.54	*0.06*	**1.31**	**1.62**	***0.03***
	R_2*	22.6	24.8	*0.30*	22.7	25.4	*0.23**	**22.7**	**25.2**	***0.04***
	K^{trans}	**0.17**	**0.13**	***0.07***	**0.17**	**0.10**	***0.01***	**0.18**	**0.08**	***0.008***
	v_e	0.25	0.26	*0.32**	0.24	0.24	*0.64**	0.24	0.19	*0.21*
	k_{ep}	**0.71**	**0.45**	***0.01****	**0.72**	**0.37**	***0.002***	**0.73**	**0.27**	***0.002***
	$IAUGC_{60}$	16.1	14.5	*0.39*	**15.6**	**11.1**	***0.03***	**16.3**	**11.1**	***0.01****
Diseased	**ADC**	**1.31**	**1.57**	***0.06***	**1.36**	**1.64**	***0.007***	**1.36**	**1.71**	***0.04***
	R_2*	24.6	22.4	*0.32*	25.8	26.8	*-**	25.8	21.9	*0.18*
	K^{trans}	**0.19**	**0.17**	***0.05***	0.16	0.14	*0.67*	0.16	0.10	*0.12*
	v_e	0.22	0.27	*0.14**	0.20	0.24	*-**	0.20	0.24	*0.29*
	k_{ep}	0.85	0.60	*0.06**	**0.80**	**0.56**	***0.05***	0.80	0.42	*0.17*
	$IAUGC_{60}$	16.5	16.3	*0.81*	14.7	13.8	*0.77*	14.7	11.6	*0.28**

*Statistical Test: Paired sample T-test; *Wilcoxon Signed ranked test*

5.4 Discussion

The role of standard MRI in clinical staging of locally advanced rectal cancers is well established and this imaging modality is part of standard work up in many countries. However, post-NCRT staging of rectal cancer is limited by that fact that T2-weighted MRI is unable to exclude active disease within areas of fibrosis. A pre-requisite for the current trends towards individualised therapy for patients with rectal cancers demands perceptive markers of rectal cancer biology. MR multi-parametric analysis can provide in depth analysis of rectal cancer pathophysiology. As demonstrated in the current study, MR multi-parametric analysis enabled valuable insight into locally advance rectal tumour pathophysiology during the interval between NCRT and surgery. In general, the results of analysis were consistent with theoretical expectations; for example, rise in ADC values and increase in extracellular volume (v_e) during the interval represents a reduction in tumour cell density with necrosis, whilst, decreasing K^{trans}, k_{ep}, $IAUGC_{60}$ and higher R_2* corresponds to progressive tumour devascularisation an hypoxia. Statistically significant clinical correlation were seen with all parameters.

The unique quality of DW-MRI to produce enhanced signals from regions of restricted proton diffusion, such as disorganised cellular architecture in tumours, that accentuates any neoplastic disease process especially residual tumour after neoadjuvant treatments has generated interest in the application of DW-MRI sequence with T2-weighted images in staging/re-staging post-NCRT and management of patients with locally advance rectal cancer [446]. In the current experiment, mean ADC values from pre-treatment paired samples were similar

to that reported earlier and showed best reproducibility and inter-observer agreement amongst all parameters measured [447, 448]. The pre-operative ADC significantly increased from baseline in 85.7% of patients. The relative higher increase at immediately after NCRT may represent tissue oedema due to radiotherapy. Further increase in ADC values later during the interval represents loss of membrane integrity and cell necrosis with increased water diffusion. The negative correlation between ADC and DCE parameters (K^{trans} and k_{ep} at baseline and $IAUGC_{60}$ immediately after NCRT) shows that LARC have several foci of cellular necrosis and poor microvascular circulation that increases after NCRT. In recent years, DWI-MRI has shown the potential to enhance diagnostic/staging accuracy when added to standard T2-weighted images. For example, DW-MRI enhances the characterising of rectal cancers [449-451] and the nodal status [452-454]; delineates involvement of mesorectal resection margin [449, 455]; improves response assessment [456, 457] and prediction of response to NCRT [458]. Most studies have reported a distinct link between ADC values at either baseline [457, 458] and/or post-NCRT [459] and/or percentage changes after NCRT [460, 461] with tumour downstaging after NCRT. In the current study, a rise in ADC was apparent before changes in craniocaudal tumour length demonstrating intra-tumoural changes (cell destruction) earlier than conventional methods based on RECIST criteria. Whilst some studies reported that tumours with lower mean ADC values at pre-treatment have consistent ‘T’ downstaging and pCR [460, 462]; other investigators reported lower pre-treatment ADC values to be related with poor response and predicted early local recurrence [463]. In addition, studies comparing ADC with tumour histopathology have reported low ADC in rectal

cancers that are poorly differentiated, spread to lymph nodes and invade CRM [449, 451]. In the current study, patients with lower baseline mean ADC values also showed poor T-downstaging (see table 5.31, page 260). In other studies, patients with higher ADC value post-NCRT showed complete response [459, 464, 465] and also increased diagnostic accuracy of active tumour when DW sequence was added to post-NCRT conventional MRI [466]. A number of studies have also reported that tumours with significant percentage increase in ADC during NCRT tended to downstage [460, 467] and show pCR [461, 462]. Similarly, in the current cohort, there was a significant rise in ADC values after NCRT in patients who had T- and N-downstaging and survived without recurrence during the follow-up period (see table 5.31, page 260). However, on comparison of mean ADC values with clinical parameters, there was neither correlation nor significant variation in the mean ADC at different time-points and clinical markers (tables 5.17, page 243 and tables 5.23–5.25, page 249-252). Similar non-association of ADC with clinical parameters have been reported in previous studies [468-471]. For example, DeVries et al [468] reported no difference in the mean ADC values between responders and non-responders, however when they investigated the distribution of any single voxel ADC value in a tumour region in a histogram-like fashion, ADC histogram showed a higher relative fraction of high ADC in the therapy non-responder group compared with the therapy responder group. The ADC values and/or changes after NCRT were not useful in distinguishing between worse outcomes with regards to recurrence and survival. Such discrepancies in the results amongst aforementioned studies including current experiment are not only due to variation in techniques (MRI protocol and software for data analysis) but also small sample size, variability in

patient selection criteria, variations in timing of image acquisition during treatment timeline, ADC measurement errors (subtle variations in regions of interest positioning between observers may result in substantial variation in ADC [472]), inter-observer variability especially after NCRT and the inconsistent definition of 'response to NCRT' between studies (some authors use tumour size, whilst others use histopathological T stage and/or pCR).

Tissue hypoxia is a common feature of most advanced solid tumours. ISW-MR assessment of tumour hypoxia has been applied in cancers of prostate [337, 473], brain [327], breast [338, 474] and cervix [339]. In rectal cancers, tissue hypoxia may have a heterogeneous distribution within the same tumour and even within neighbouring micro-areas of the tissue [475]. Hypoxic rectal cancers are not only resistant to radiotherapy, but also release active proteins that promote tumour growth and spread, for example release of hypoxia-induced factor (HIF-1 Alpha) that triggers angiogenesis by activation of VEGF gene. In vivo assessment of rectal tumour hypoxia has been performed successfully by means of PET with hypoxia-detecting agents [476, 477]. In our study the mean baseline R_2* was 22.9 (±2.9) sec^{-1} between paired analysis which is in the range of R_2* values reported for pelvic malignancies (20.8 ±1.6 sec^{-1}) [347], cervical cancers (21.1±6.7 sec^{-1}) [339] and pelvic muscles (25.01 sec^{-1}) [473]. The reproducibility of R_2* was extremely good and better than mentioned studies. These findings suggest that rectal cancer are less hypoxic than other pelvic malignancies, however, given the rich blood supply of rectum, these tumours may still be relatively hypoxic compared to surrounding bowel tissue. After NCRT, the R_2* measurements gradually increased to a maximum value at sixth weeks (see table 5.8, page 214), which may represent the maximum vascular

and cellular disruption caused by NCRT. Another notable observation is the negative correlation between R_2* and v_e that gradually increases after NCRT until significant levels at sixth week (-0.67, p 0.02). As R_2* represents hypoxia immediately in the vicinity of vessels and v_e represents extracellular space, it may be hypothesised that: after NCRT, the surviving tumour cells may locate and concentrate near blood vessels resulting in low v_e and high R2*; a further loss of the tumour cell load (probably most hypoxic cells) after sixth weeks reduces the burden of cells sharing nutrients, and therefore results in further decline in v_e, but also a paradoxical decline in R_2* suggesting a relatively improved oxygenation for the remaining tumour cells. Such cells can survive and may develop aggressive traits (see below). The R_2* measurements were associated with several clinical markers. Tumours with high baseline R_2* measurements were associated with nodal involvement (mean 27.5 sec^{-1}), inhibited T (mean 25.7 sec^{-1}) or N (mean 28.8 sec^{-1}) down-staging and distant metastasis (mean 28.8 sec^{-1}). Hence, these finding supports the theory that intra-tumoural hypoxia is marker of aggressive biological behaviour. Pathological advanced tumours showed significant hypoxia (high R_2*) immediately after NCRT. The pattern of R_2* alteration (Δ R_2*) during the interval between NCRT and surgery showed significant positive correlation with pathological nodal disease, distant metastasis and numbers alive at the end of the study, whilst significant negative correlation with nodal downstaging. These findings not only provide vital insight that hypoxic tumour metastasize early with impact on future outcomes but are also in keeping with previous studies. For example, retrospective studies investigating immunohistochemical markers of hypoxia in rectal cancer specimen have shown poor response to NCRT and

adverse prognosis in patients with hypoxic tumours [181, 478, 479]. PET assessment of rectal tumour with hypoxia-detecting agents has also shown poor downstaging after NCRT and worst survival in patients with hypoxic cancers [476, 477]. The association between R_2* and nodal disease also highlights the potential role of R_2* in predicting nodal involvement in patients with high suspicion but node-negative disease (especially after NCRT) on standard T2-weighted MRI images. In subgroup analysis, there was no role of R_2* measurements or changes after NCRT in differentiating long-term outcomes. There are some limitations associated with R_2*calculation in rectum, these include susceptibility artefact at air-tissue boundaries, motion artefact due to bowel peristalsis and bladder filling, changes in tumour position between sequences and changes in tumour size with treatment.

Amongst DCE parameters, the baseline values and 95% CI for cohort were consistent with previously published reports but the magnitudes of spontaneous changes in an individual patient were very high [347]. Such findings are acceptable given tissue perfusion is a dynamic process with wide variation depending on several factors including cell activity, inflammatory response, stress and cardiac output. With regards to reproducibility, semi-quantitative parameter $IAUGC_{60}$ was most reproducible with minimal spontaneous changes (CI cohort -10.75% to +12%, F 35.5), better repeatability than model driven parameters (r -34.6% to +52.9%) and minimal observer influence (ICC 94%). These findings are in keeping with published studies [414]. In model-based parameters, K^{trans} and k_{ep} showed less spontaneous changes (CI cohort ±13.7%, ±11.1% and F 4.3, 4.9, respectively) than v_e (CI cohort ±14.1%, F 2.4); k_{ep} showed best repeatability (r ±41.5); the observer interference on readings

was poor for v_e (ICC 38%) and moderate for K^{trans} and k_{ep} (ICC 60% and 64%, respectively). In advanced tumours, vascular networks and circulation are poor partly due to abnormal development and partly due to greater rates of cellular necrosis; hence one would expect lower values of perfusion parameters. In the current study, a low value for all DCE parameters was seen in clinically advanced tumour but the differences were not statistically significant. Low levels of baseline and six weeks post-NCRT v_e were associated with pathologically advanced tumours and alteration pattern in Δk_{ep} correlated negatively with pathological nodal disease. As v_e is also related to endothelial cell integrity and membrane permeability, these finding may suggest that intact vascular endothelial lining in tumours may be a biological aggressive trait. In contrast, in another study, a higher level of v_e equivalent (amplitude A: %; Brix model), was seen in patients with pathological lymph node metastases [480]. Previously, a low K^{trans} equivalent (Plasma flow (PF): ml/100ml/min) and k_{ep} has been reported in clinically and pathologically advanced staged rectal tumours, respectively [471, 481], whereas no correlation between any DCE parameters and tumour stage was seen in another study [190]. Microvascular disruption as a result of NCRT also plays a role in tumour downstaging and reflected by changes in DCE parameters. After NCRT, there was a progressive significant percentage decrease in K^{trans}, k_{ep} and $IAUGC_{60}$, whilst v_e values had maximum increase immediately after NCRT followed by lower percentage increases from baseline. The increase in v_e immediately after NCRT may reflect tissue oedema following radiotherapy (as also seen by transient decrease in ADC). These finding suggest a continuing involution of the tumour vascular network during the interval between NCRT and surgery. Hence DCE parameters displayed

detailed insight into tumour pathophysiological processes after NCRT despite modest change in tumour size. Similar patterns of DCE parameters alterations after NCRT have been reported previous studies [482]. Earlier investigators have shown a link between high pre-treatment K^{trans} and $IAUGC_{60}$ (or their equivalent from other models) and poor downstaging [468, 480, 483]. In the current cohort, however, pre-treatment K^{trans} and $IAUGC_{60}$ of responders were higher at each time-points but this was not statistically significant (see tables 5.29–5.30). These findings are still consistent with earlier results [351, 482, 484]. Gollub et al [485] reported high K^{trans} post-chemotherapy in patients not achieving pCR, however, in their study patients received non-standard neoadjuvant chemotherapy only (no irradiation). In the current cohort, a high baseline and post-NCRT v_e and a low post-NCRT k_{ep} were associated with downstaging and complete response, respectively. The patients with T downstaging had a statistically significant drop in pre-operative K^{trans} and $IAUGC_{60}$ but not before that, whilst a significant drop in k_{ep} at all time-points. The patients with N- downstaging had statically significant drop in K^{trans} and k_{ep} at all time-points and pre-operative $IAUGC_{60}$. Similarly Kim et al [486] showed a significant decrease in absolute and percentage values of K^{trans} after NCRT in patients with tumour downstaging. In another study by Dinter et al [487], a decrease in $IAUGC_{60}$ equivalent measure (slope of contrast media enhancement curve) was significantly higher in patients with tumour downstaging after NCRT. Also, the alteration in Δk_{ep} and $\Delta IAUGC_{60}$ correlated positively with N downstaging. These findings simply suggest that patients with continuous tumour vascular decline and cell destruction after NCRT are likely to downstage in size with nodal sterilization. Such response to NCRT will surely

benefit long-term outcomes and in fact, patients who showed significant decrease in K^{trans}, $IAUGC_{60}$ and k_{ep} were alive without any recurrence until the end of the follow-up period for this study. In contrast to a previous reports, where pre-treatment K^{trans} equivalent ($k_{21:}$ min^{-1}; Brix Model) was higher in patients with distant metastasis [480], in the current sample, the pre-treatment K^{trans} was higher in patients without any recurrence. However, a preoperative high K^{trans} and $IAUGC_{60}$ value was associated with local recurrence. These findings indicate the return of angiogenesis and tumour revival with potential enhanced aggressive behaviour prior to surgery that possibly impedes local control. On the other hand, alteration in Δk_{ep} and $\Delta IAUGC_{60}$ negatively correlated with distant metastasis, whilst, $\Delta IAUGC_{60}$ also negatively correlated with survival. These findings together with ΔR_2* association with long-term outcomes mentioned earlier, shows that after NCRT rectal cancers cells remaining viable in an environment with poor circulation and hypoxia represent a subset of tumour cell population that not only resists effects of irradiation but also develop aggressive traits prone to impedes distant disease control with impact on survival. Such findings also provide vital clues about time span of NCRT effects and optimal timing of surgery. In addition to similar limitation as for ADC and R_2*, investigators of DCE-MRI have used different semi-quantitative parameters, pharmacokinetic models to derive quantitative measures and contrast agents. Such inhomogeneity in study designs and methodology makes comparison between results challenging.

There are several limitations to this experiment. In addition to limitation in sample size, multiple visits for scans and simultaneous rectal biopsy deterred patients and also lead to loss of compliance after NCRT. This was further

reduced by technical or operator failures. Since MR multi-parametric analysis is still a developing technique, sample size reductions due to technical errors is not uncommon in published literature [471, 481]. The mean of all parameters values was used for analysis, which can result loss of specific data, for example tumour vascular heterogeneity, but such analysis are time efficient and reproducible at other units.

In summary, MR multi-parametric analyses were reproducible and provided vital information about rectal cancer pathophysiology before and after NCRT, clinical staging and long-term outcomes. With regards to tumour pathophysiology: at baseline, LARC showed high cellularity (low ADC), adequate oxygenation (low R_2*), minimal extracellular space (low v_e) and near normal perfusion (K^{trans}, kep, $IAUGC_{60}$). After NCRT, there were a mixture of changes: in the first 6 weeks, there was gradual decline in tumour cellularity (increasing ADC and high v_e) and functional vascularity (decreasing K^{trans}, k_{ep} and $IAUGC_{60}$), with maximal increase in intra-tumoural hypoxic foci (increase in R_2*); after 6 weeks, the R_2* and v_e measurements were closer to baseline, which indicates decrease in extracellular-extravascular space and improvement in tumour hypoxia. It may be deduced from these findings that declining tumour cell burden had improved relative oxygenation at pre-operative stage and these cells may attain aggressive traits (tumours with low preoperative k_{ep}, $IAUGC_{60}$ and high R_2* has poor prognosis). With regards to clinical staging and outcomes, R_2* and DCE parameters provided vitals clues about tumour behaviours and aggressiveness: a pre-operative return of angiogenesis indicates higher potential for local recurrence, whereas pre-operative tumour cell hypoxia indicates higher potential for distant metastasis and survival. However, the clinical correlation

showed be interpreted with caution due to the small sample size of current study.

The current study has clearly demonstrated a potential role of MR-multiparametric analysis of rectal cancer in tumour staging, prediction of response to NCRT and long-term outcomes. Therefore further studies addressing the shortcomings of current and previous studies and designed as prospective multicentre study, standardization of parameters acquisition and modelling techniques on a larger sample size, would enable validation of our results.

6 CHAPTER 6: DYNAMIC CONTRAST ENHANCED COMPUTED TOMOGRAPHY

Assessment of rectal cancer microcirculation

6.1 Introduction

Dynamic contrast enhanced CT is a validated technique to assess tumour angiogenesis non-invasively and has been utilised effectively in phase I/II trials for the development of anti-angiogenic drugs [488, 489] and monitoring disease control after locoregional therapy [490, 491]. Alterations in DCE-CT parameters may occur before any morphological changes in response to therapy, making perfusion CT a potential surrogate marker of response. In oncology, limited studies have shown its value in characterising lesions including biological behaviour, enhancing tumour staging, and as biomarkers of therapy response and long term prognosis. In terms of clinical integration, DCE-CT offers practical advantages over other imaging modalities including widespread availability of CT, protocols that are readily integrated into clinical coverage, short coverage periods and patient compliance.

Some authors have investigated the correlation between DCE-CT parameters and histopathological markers of angiogenesis in colorectal cancer: such reports are mostly conflicting [381, 382, 384]. One reason for such variable results may be the presence of temporal and spatial functional vascular heterogeneity that is known to exist in most solid tumours [492]. In the last few years, migration of CT coverage from a limited ‘central core’ to a whole tumour

volume using either wide detector MDCT, shuttle or helical perfusion CT techniques has been seen as an advantage [493, 494], particularly for large solid tumours that may contain central areas of necrosis, demonstrating spatial variation in vascularization. Studies on lung [493] and renal cancers [495] using volumetric helical coverage techniques have reported improved reproducibility with whole tumour coverage. The evidence outside of this scenario has been less convincing. It is uncertain, for example, whether this applies readily to primary gastrointestinal cancers. An earlier study of colorectal cancer, for example, has suggested no difference in measurements, though this preliminary study only compared a 5mm and 20mm tumour volume, which is restricted compared with that achievable currently [496].

The correlations between DCE-CT parameters and clinicopathological markers, response to NCRT and long-term outcomes of locally advanced rectal cancers have not been reported in literature to date. Few studies have also shown a difference in baseline DCE-CT parameters between responder and non-responder to NCRT [47, 152, 265], hence indicating a potential role of perfusion CT in tailored treatment regimes.

The current chapter presents a study of the application of DCE-CT using a volumetric coverage technique in patients with locally advanced rectal cancers. The aim of this experiment was to investigate: (1) The effects of volume coverage (2-D versus 3-D whole tumour volume coverage) on baseline day-to-day reproducibility of DCE-CT parameters and observer agreement at baseline; (2) alteration in DCE-CT parameters in response to NCRT, and (3) role of DCE-CT parameters in characterising rectal cancer angiogenesis and their

correlation with clinicopathological markers, response to treatment and long term prognosis.

6.2 Methods

6.2.1 Patient population

See chapter 3 for detail of the patient population. Additional exclusion criteria included standard contraindications to CT iodinated contrast agent i.e. previous hypersensitivity reaction (n=0), impaired renal function (n=0); and the presence of metastatic disease at staging (n=1: metastatic liver disease).

6.2.2 Patient Compliance and Exclusions

Thirty-two patients were screened; 17 patients consented to participate in the study. Thirteen patients completed two scans and four patients completed one scan prior to NCRT. Fourteen patients completed immediate post-NCRT scan and 12 patients completed scans for 6 and 11 weeks post NCRT. One patient was excluded after paired baseline scans due to finding of metastatic disease. After NCRT, one patient died due to a cause unrelated to rectal cancer or treatment, one more patient declined further participation in the study. At the post processing stage, one more patient was excluded due to mucinous histopathology and inconsistent parametric measurements. Patient and data available for analysis is presented in table 6.1 and figure 6.1 below:

CHAPTER 6: DCE-CT: MICROCIRCULATION ANALYSIS

Table 6.1: Patient compliance and exclusions during scan coverage and post processing stage

Code		T_0 (1)	T_0 (2)	T_1	T_2	T_3	Reason for exclusion
1	RY	✓	✓	✓	✓	✓	
2	DG	✓	✓	✓	✓	✓	
3	DJ	✓	✓	X	X	X	Metastasis
4	AH	✓	✓	✓	✓	✓	
5	KB	✓	✓	✓	✓	✓	
6	ED	✓	✓	✓	X	✓	DNA T_2
7	AF	✓	X	✓	✓	✓	
8	JN	✓	✓	✓	✓	✓	
9	SD	✓	✓	X	X	X	T_1: technical failure Died after NCRT
10	JH	✓	✓	✓	✓	✓	
11	DP	✓	✓	✓	X	X	Declined participation
12	GA	✓	✓	✓	✓	X	
13	PO	✓	X	✓	✓	✓	DNA T_0 day 2
14	MM	✓	X	✓	✓	✓	DNA T_0 day 2
15	RC1	✓	✓	✓	✓	✓	
16	RC2	✓	X	✓	✓	✓	DNA T_0 day 2
17	JT	✓	✓	✓	✓	✓	
Scans Completed		**17**	**13**	**15**	**13**	**13**	
Included in Study		**16**	**13**	**14**	**12**	**12**	PO excluded

'✓' Completed scan and included in analysis; '✓' Completed scan but not included in analysis;' X' Did not complete scan; DNA- did not attend

6.2.3 Volumetric helical perfusion CT

At baseline, two examinations were performed within 14 days to allow reproducibility analysis. The examination schedule is shown in figure 6.1.

Figure 6.1: Schedule of DCE-CT

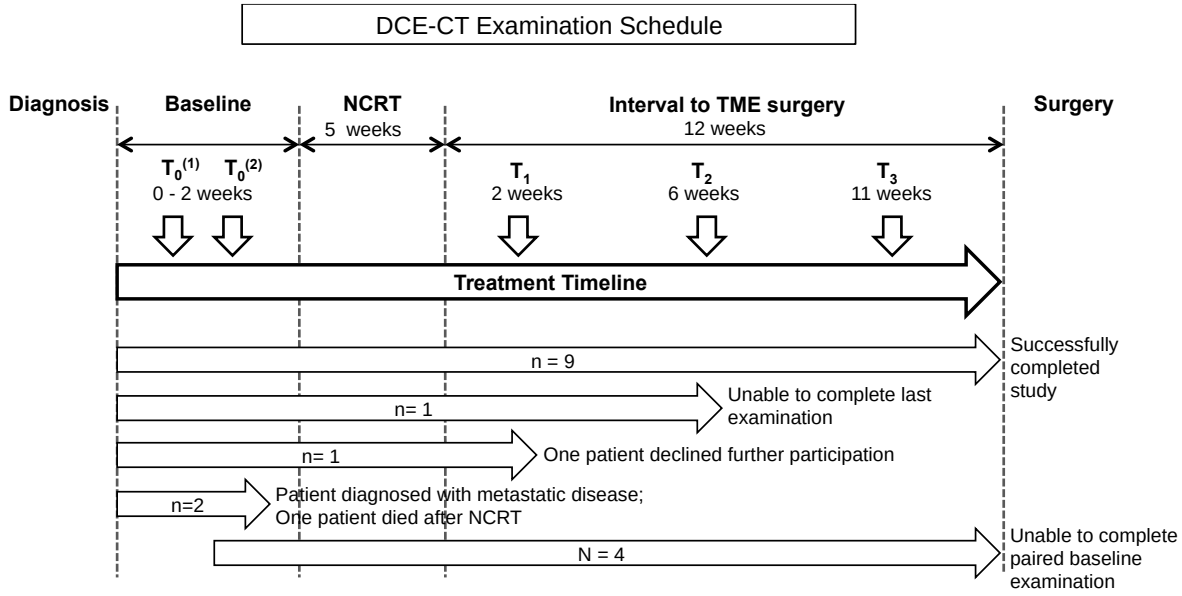

where, T (subscript) represent timing of the examination along the treatment line: T_0 (1) and T_0 (2) were paired baseline examination on day-1 and day-2, respectively; T_1, T_2 and T_3 were post-NCRT examination at second week, sixth week and eleventh week, respectively. The 'n' denotes number of patients completing examination.

6.2.4 Image coverage

All subjects underwent volumetric helical perfusion CT using a '4D-adaptive spiral mode' (Dual Source CT, Somatom Definition, Siemens Healthcare, Forchheim, Germany). The patient examination consisted of a 'topogram', a targeted low-dose unenhanced helical coverage to locate the known tumour

(100kV, effective mAs 70, rotation time 0.5s, detectors 24x1.2mm, pitch 1.2, slice collimation 5mm, SFOV 300-450mm, matrix 512mm), and a volumetric helical dynamic contrast-enhanced coverage following intravenous administration of 50mL of iodinated contrast agent (Ioversol 350 mg/mL iodine; Optiray, Covidien, Mansfield, MA, USA) at 6mL/s using a dual headed pump injector, followed by a 50ml saline chaser at the same rate.

After a delay of 10 s from the start of injection, a volumetric perfusion CT coverage consisting of successive craniocaudal and caudocranial coverages was obtained (100 kV, 110mAs, 4D adaptive spiral with a variable pitch - consisting of a pitch of 1 at the central point of table travel and <1 in the accelerating and decelerating portions, thereby guaranteeing a full rotation was always available for reconstruction), cycle time of 1.5s for the first 30s, decreased to a cycle time of 3.0s between helical coverages after 30s for the remaining 20s; z-axis coverage 11.4 cm; reconstructed slice thickness 5 mm, increment 3 mm; CTDI vol 116.04mGy; figure 6.2). Patients returned within 2 weeks of the initial examination for a second CT examination, with identical parameters, to assess measurement reproducibility.

Figure 6.2: DCE-CT Image Coverage

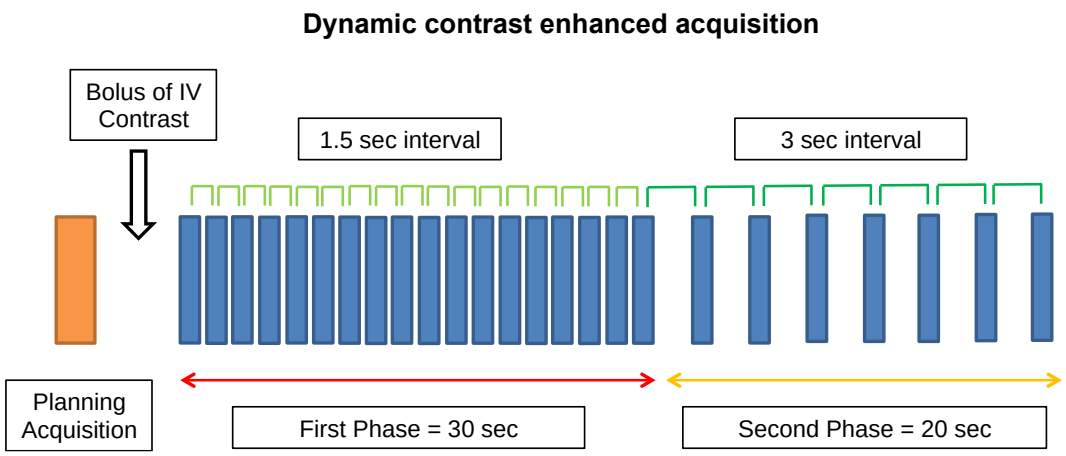

6.2.5 Image Analysis

Image analysis was performed using validated commercially available software (Deconvolution algorithm, vPCT; Siemens Healthcare, Forchheim, Germany). Initial post-processing steps within the software platform included motion correction and application of a noise reduction filter. Motion correction was based on a non-rigid deformable registration technique. The arterial time-attenuation curve was defined by placing a region of interest (ROI) within the common femoral or external iliac artery visible on the images. Parametric maps of regional blood flow (BF; units: mL/min/100 mL), blood volume (BV; units: mL/100 mL), and permeability surface product (PS; units: mL/min/100mL), were then generated in axial, coronal and sagittal planes.

The DCE-CT images (see figure 6.3) were reviewed by two observers using two different image coverage techniques (2D and 3D), hence each individual study produced 4 measurements for an individual patient. The ROIs were drawn freehand using an electronic cursor and mouse outlining the margin of the entire tumour in axial plane. This was placed for two different z-axis coverage: a) a central tumour core of 30mm (consisting of 6 contiguous 5 mm thick axial slices; mean area/slice=15.3 cm^2 for Observer 1 and 15.1 cm^2 for Observer 2; and, b) the entire tumour volume (mean volume= 62.3cm^3 for Observer 1 and 73.0cm^3 for Observer 2). Analysis was performed for all CTs and also repeated by each observer with >4 weeks between readings.

Figure 6.3: CT and DCE-CT images

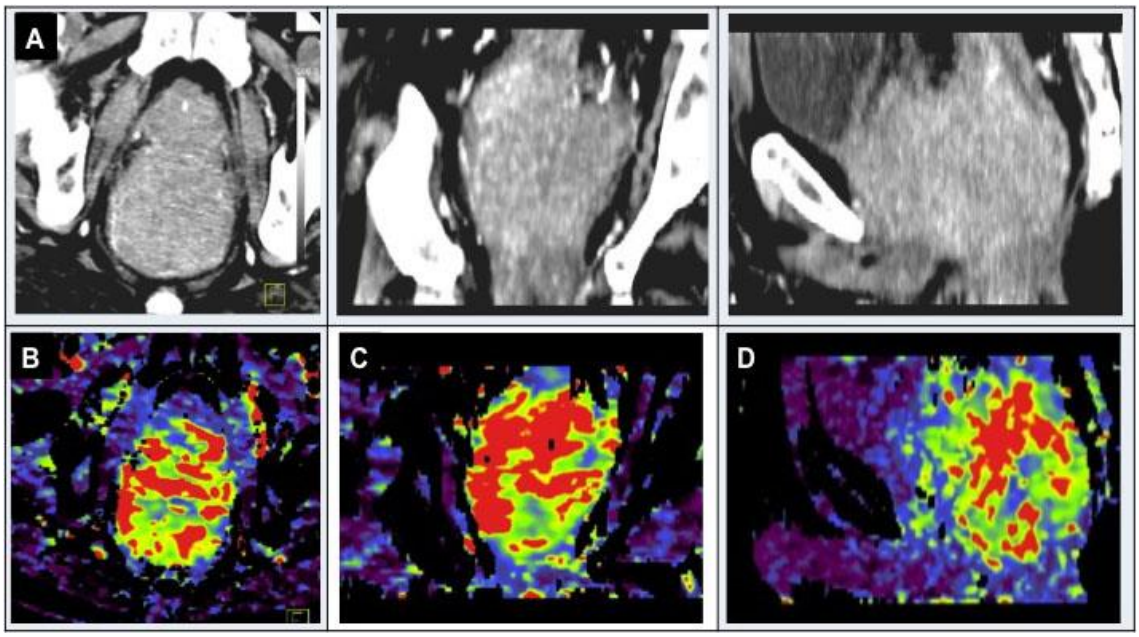

CT MIP (A) images showing a T3N1 rectal cancer and corresponding blood flow parametric maps in the axial (B), coronal (C) and sagittal (D) planes.

6.2.6 Statistical Analysis

A detailed account on statistical methods used are as given in Chapter 5 (see section 5.2.6, page 196). The only difference was as follows: the Wilcoxon signed-rank test was applied to ascertain if there were any differences between paired observations for the different tumour volumes, with statistical significance at 0.0056, after correcting for multiple comparisons.

6.3 Results

The results are presented in the following order

1. Patients characteristics and their outcomes (section 6.3.1)
2. Baseline Day-1:Day-2 reproducibility (section 6.3.2 for 2-D and section 6.3.3 for 3-D image coverage)
3. Inter-observer agreement for Day 1 measurements (section 6.3.2 for 2-D and section 6.3.3 for 3-D image coverage)
4. Alterations in DCE-CT parameters (3-D image coverage) after chemoradiotherapy (section 6.3.7)
5. Association between ‘measured DCE-CT parameters (3-D image coverage)’ and ‘clinicopathological markers’ (section 6.3.8)
6. Association between ‘alteration of DCE-CT parameters before and after chemoradiotherapy (3-D image coverage)’ and ‘clinical outcomes’ (section 6.3.9)

6.3.1 Patient population, characteristics and clinical outcomes

Please refer to chapter 4, sections 4.3.1, 4.3.2 and 4.3.3 (pages 121-125).

6.3.2 Baseline Day-1:Day-2 reproducibility and inter-observer agreement of DCE-CT parametric measurements obtained from 2-D image coverage of rectal cancers

The DCE-CT parameter actual measurements obtained by 2-D coverage are shown in table 6.2 and figure 6.4. The baseline Day1:Day2 reproducibility analysis is shown in table 6.3 and figure 6.5. The inter-observer agreement for day 1 measurements is shown in table 6.4 and figure 6.6.

6.3.2.1 Summary of results

All statistical analysis of BV measurements for observer 1 were affected by outlier data (observer 1 measurement of BV for patient 8 on $T_0^{(2)}$ = 32.35mL/100mL)

For the day-1:day-2 reproducibility analysis (see table 6.3):

- The mean differences between day-1:day-2 measurement was greatest for BF measurements and least for BV measurements for both observers.
- The sensitivity to spontaneous changes was seen in BF and PS measurements as evidenced by narrow range of 95% group CI and high variance ratio. The sensitivity to spontaneous changes was poor for BV measurements: data obtained from observer 1 may have been affected by outliers values (see table 6.2) and data obtained from observer 2 does show a narrow 95% group CI of BV= ±1.25 (12.5%) mL/100mL, however, there was low variance ratio for both observers (F=1.26 and 2.9 for observer 1 and observer 2, respectively)

- For repeatability analysis, the mean difference lie well within the range predicted by repeatability coefficient for all parameters. In general, the Bland-Altman LoA for BF and BV were better than PF. More specifically, Bland-Altman LoA for BF and BV were better for observer 1.
- There was probably acceptable day-1:day-2 reproducibility of all parametric measurements for each observers. The BF and PS analysis for both observers and the BV analysis for observer 2 only showed low wCV, high ICC and greater between/within-subject variance components. The poor results of BV for observer are attributable to outlier value.

For the inter-observer analysis (see table 6.4 and figure 6.6):

- The measurements between observers for all parameters were similar with small mean differences at each time point (T_0 $^{(1)}$ and T_0 $^{(2)}$).
- The mean difference between parametric measurements is well below the values defined by repeatability co-efficient. There was narrow Bland-Altman LoA for BV and BF, but slightly wider for PS measurements.
- There was excellent inter-observer reproducibility for BF and PS measurements (low wCV≤ 0.10, ICC >90% and high between/within-subject variance components) and good for BV measurement.

Table 6.2: The actual Day-1:Day-2 DCE-CT parametric measurements obtained from 2-D image coverage

Code		Blood Flow (mL/min/100mL)				Blood Volume (mL/100mL)				Permeability Surface (mL/min/100mL)			
		Observer 1		Observer 2		Observer 1		Observer 2		Observer 1		Observer 2	
		$T_0^{(1)}$	$T_0^{(2)}$	$T_0^{(1)}$	$T_0^{(2)}$	$T_0^{(1)}$	$T_0^{(2)}$	$T_0^{(1)}$	$T_0^{(2)}$	$T_0^{(1)}$	$T_0^{(2)}$	$T_0^{(1)}$	$T_0^{(2)}$
1	RY	94.61	157.22	137.22	137.63	12.35	12.59	14.02	11.53	18.60	19.59	17.10	18.59
2	DG	66.83	72.03	68.63	71.08	11.38	11.22	10.89	11.20	17.92	30.42	17.44	24.63
3	DJ	50.33	67.67	50.09	70.45	8.65	9.14	8.80	8.99	11.86	13.07	12.25	13.33
4	AH	58.77	66.85	53.86	61.51	9.82	12.01	9.76	11.41	21.40	18.87	20.02	17.04
5	KB	43.74	54.20	52.57	60.53	9.27	9.08	11.13	10.21	15.75	16.86	18.43	18.21
6	ED	45.30	65.50	46.28	64.20	7.77	8.52	8.11	8.18	12.73	12.28	13.21	12.35
8	JN	56.33	74.54	49.52	58.83	9.09	***32.35***	8.10	10.25	15.47	24.84	13.71	24.89
9	SD	59.82	65.10	63.04	65.43	10.0	11.34	10.60	11.48	36.13	41.86	38.52	42.17
10	JH	22.15	33.27	24.49	35.81	5.12	8.49	5.35	9.01	9.77	11.50	10.21	13.86
11	DP	74.01	65.92	71.41	58.26	11.54	10.41	11.22	10.04	21.51	21.51	20.80	20.26
12	GA	81.44	87.33	71.51	79.46	10.68	***16.16***	9.94	14.93	23.84	32.67	20.41	27.00
15	RC1	74.22	85.13	88.72	91.50	11.16	6.22	7.71	6.80	22.04	15.58	18.70	15.71
17	JT	77.26	77.10	87.59	77.81	9.00	9.46	10.15	9.69	15.65	15.66	17.45	16.81

Bold and italic – outlier value; $T_0^{(1)}$- Day 1 scan; $T_0^{(2)}$- Day 2 scan

Figure 6.4: Baseline DCE-CT parameter measurement reproducibility obtained from 2-D image coverage

A - Observer 1

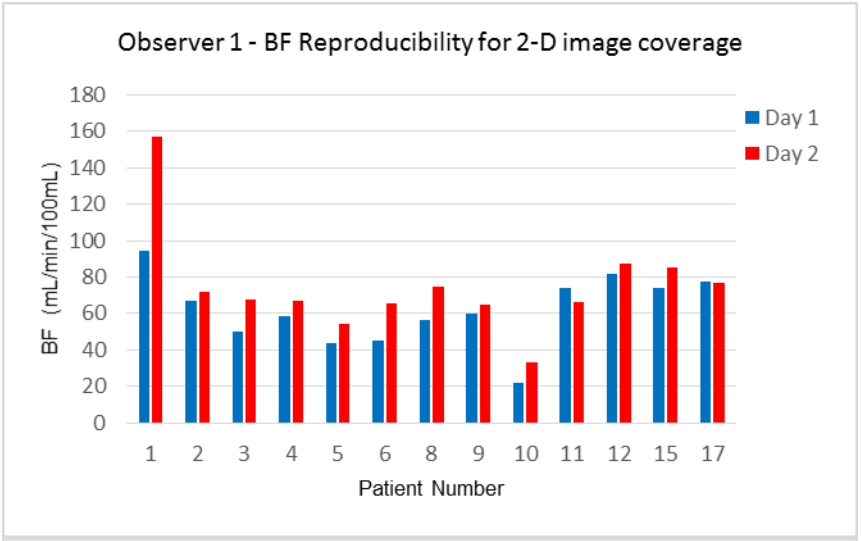

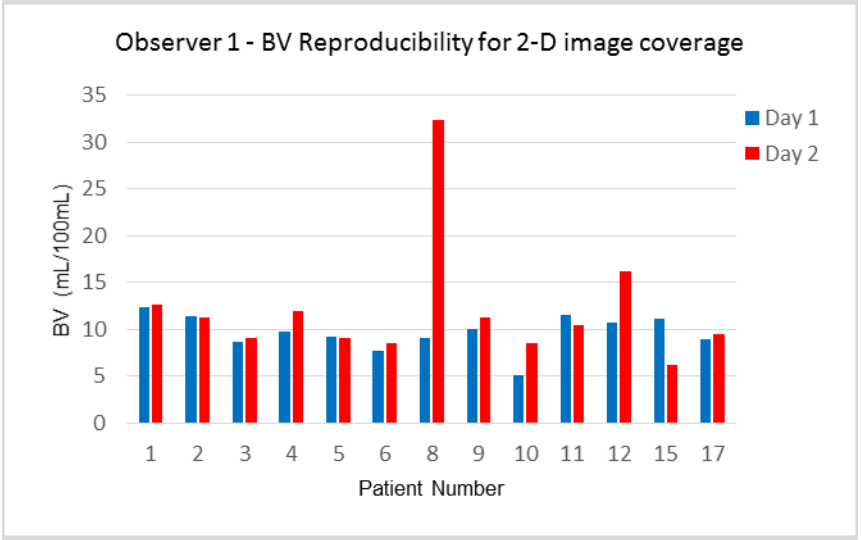

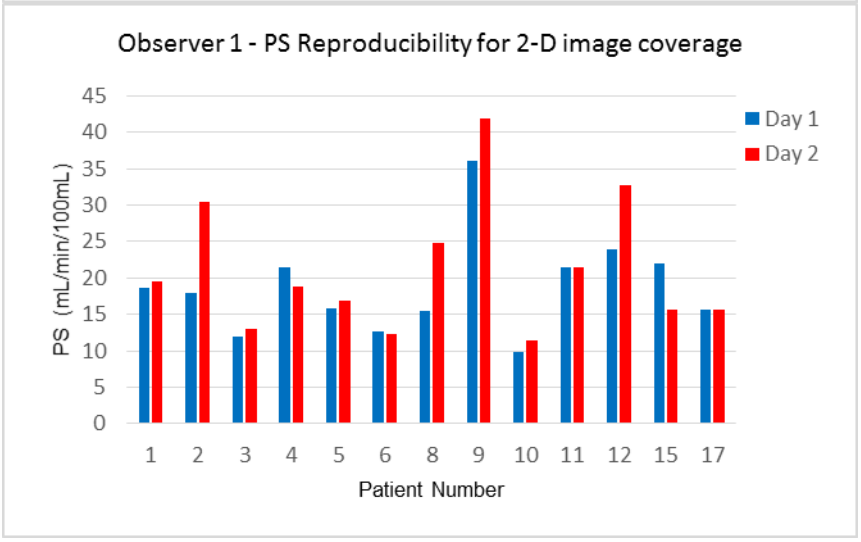

B - Observer 2

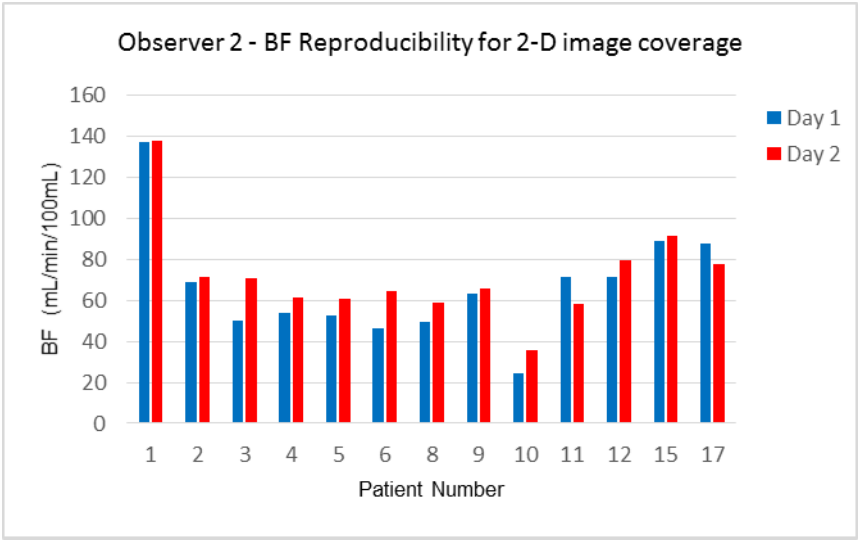
Observer 2 - BF Reproducibility for 2-D image coverage
BF (mL/min/100mL)
160
140
120
100
80
60
40
20
0
1 2 3 4 5 6 8 9 10 11 12 15 17
Patient Number
Day 1
Day 2

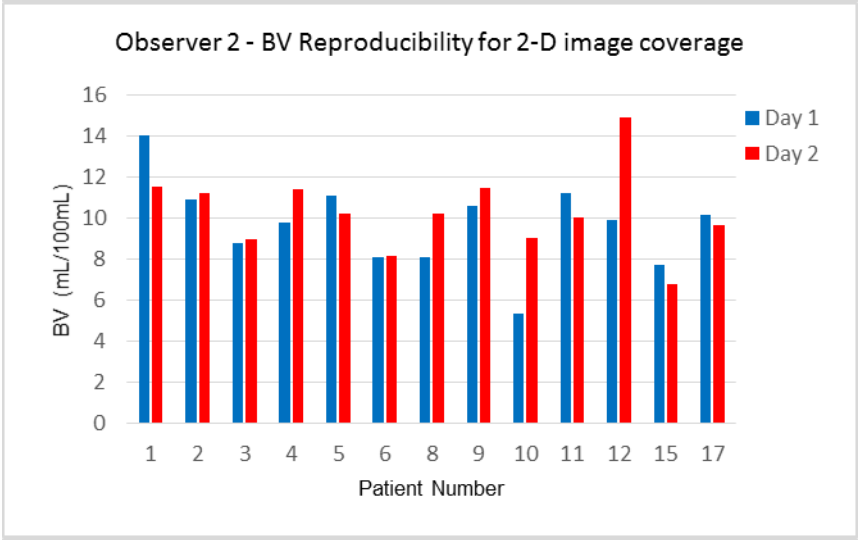
Observer 2 - BV Reproducibility for 2-D image coverage
BV (mL/100mL)
16
14
12
10
8
6
4
2
0
1 2 3 4 5 6 8 9 10 11 12 15 17
Patient Number
Day 1
Day 2

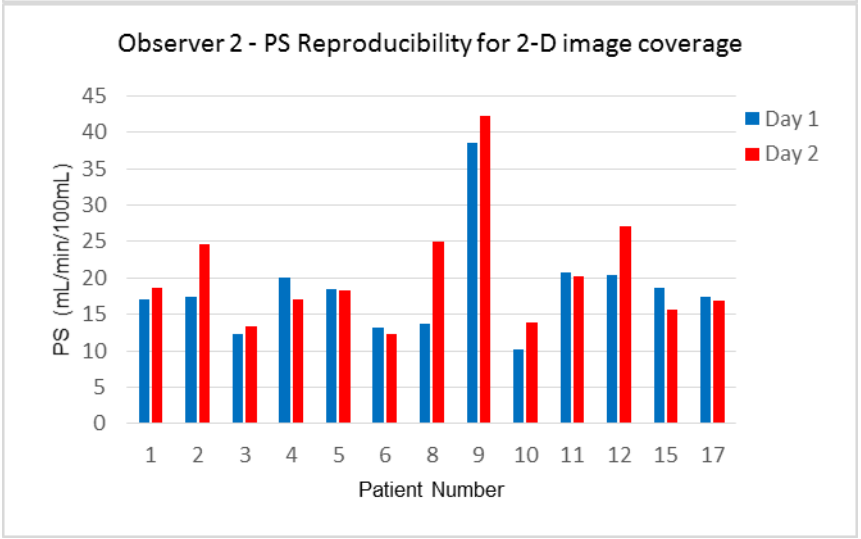
Observer 2 - PS Reproducibility for 2-D image coverage
PS (mL/min/100mL)
45
40
35
30
25
20
15
10
5
0
1 2 3 4 5 6 8 9 10 11 12 15 17
Patient Number
Day 1
Day 2

Table 6.3: Day-1:Day-2 reproducibility analysis of DCE-CT parameters obtained from 2-D image coverage for each observer

	Blood Flow (mL/min/100mL)		Blood Volume (mL/100mL)		Permeability Surface (mL/min/100mL)	
Observer	**1**	**2**	**1**	**2**	**1**	**2**
Measurements						
$T_0^{(1)}$; $T_0^{(2)}$ (mean)	60.9; 74.7	64.3; 71.7	9.37; 12.08	9.65; 10.2	18.02; 21.1	18.08; 20.3
Mean (Total)	68.33	69.13	10.88	9.98	19.90	18.91
Mean Difference	-12.85	-5.20	-2.4	-0.61	-2.47	-2.04
Wilcoxon test	0.007	0.07	0.08	0.5	0.099	0.15
Spontaneous Changes						
95% Group CI for mean difference❖	-10.38, -14.11 (*-19.2%, 9.82%*)	-4.34, -5.51 (*-16.45%, 6.02%)*	-2.93, -1.73 (*-27.66%, 22.41%)*	±1.25 (12.5%)	±3.39 (17%)	±2.75 (14.5%)
F	7.4**	19.1**	1.26	2.9	7.2**	9.9**
Repeatability						
wSD (*95% CI*)	0.179 (*0.11, 0.24*)	0.139 (*0.07, 0.19*)	0.307 (*0.17, 0.43*)	1.46 (*1.09, 2.52*)	3.97 (*2.96, 6.82*)	3.21 (*2.4, 5.53*)
r (*95% CI*)❖	0.49* (*-42.7%, 54.9%)*	0.38* (*-36%, 38.4%)*	0.85* (*-59.8%, 120.6%*)	4.06 (*3.03, 6.98*)	11.0 (*8.21, 18.90*)	8.91 (*6.65, 15.32*)
95% LoA (*Precision limits*)	*-0.54 (*-0.72, -0.35*); 0.16 (*-0.017, 0.34*)	*-0.45 (*-0.63,-0.27*); 0.23 (*0.06, 0.41*)	*-1.0 (-1.43, -0.56); 0.69 (0.25, 1.12)	-4.74 (*-6.87, -2.6*); 3.51 (*1.38, 5.65*)	-12.97 (*-18.4, -7.54*); 8.04 (*2.61, 13.47*)	-10.51 (*-14.8,-6.13*); 6.42 (*2.04, 10.79*)
Reproducibility						
ICC (*95% CI*)	0.75 (*0.37, 0.91*)	0.93 (*0.79, 0.97*)	0.031 (*-0.50, 0.55*)	0.49 (*-0.05, 0.81*)	0.78 (*0.43, 0.92*)	0.84 (0.55, 0.94)
wCV (*95% CI*)	0.19 (*0.11, 0.28*)	0.14 (*0.08, 0.22*)	0.36 (*0.19, 0.55*)	0.14 (*0.12, 0.17*)	0.17 (*0.14, 0.19*)	0.16 (0.13, 0.19)
Between- / within-subject variance components	440.8; 141.0	595.4; 48.96	0.76; 22.5	0.97; 3.18	50.1; 13.78	44.93; 12.18

*CI – confidence interval (❖as % for log transformed data); F – variance ratio; wSD – within-subject standard deviation; wCV – within-subject coefficient of variation; r – repeatability coefficient; LoA – Limits of agreement; ICC – Inter-class coefficient; *Natural Log transformed data; ** p<0.05*

Figure 6.5: Bland-Altman plots of Day-1:Day-2 reproducibility of parametric measurements obtained from 2-D image coverage

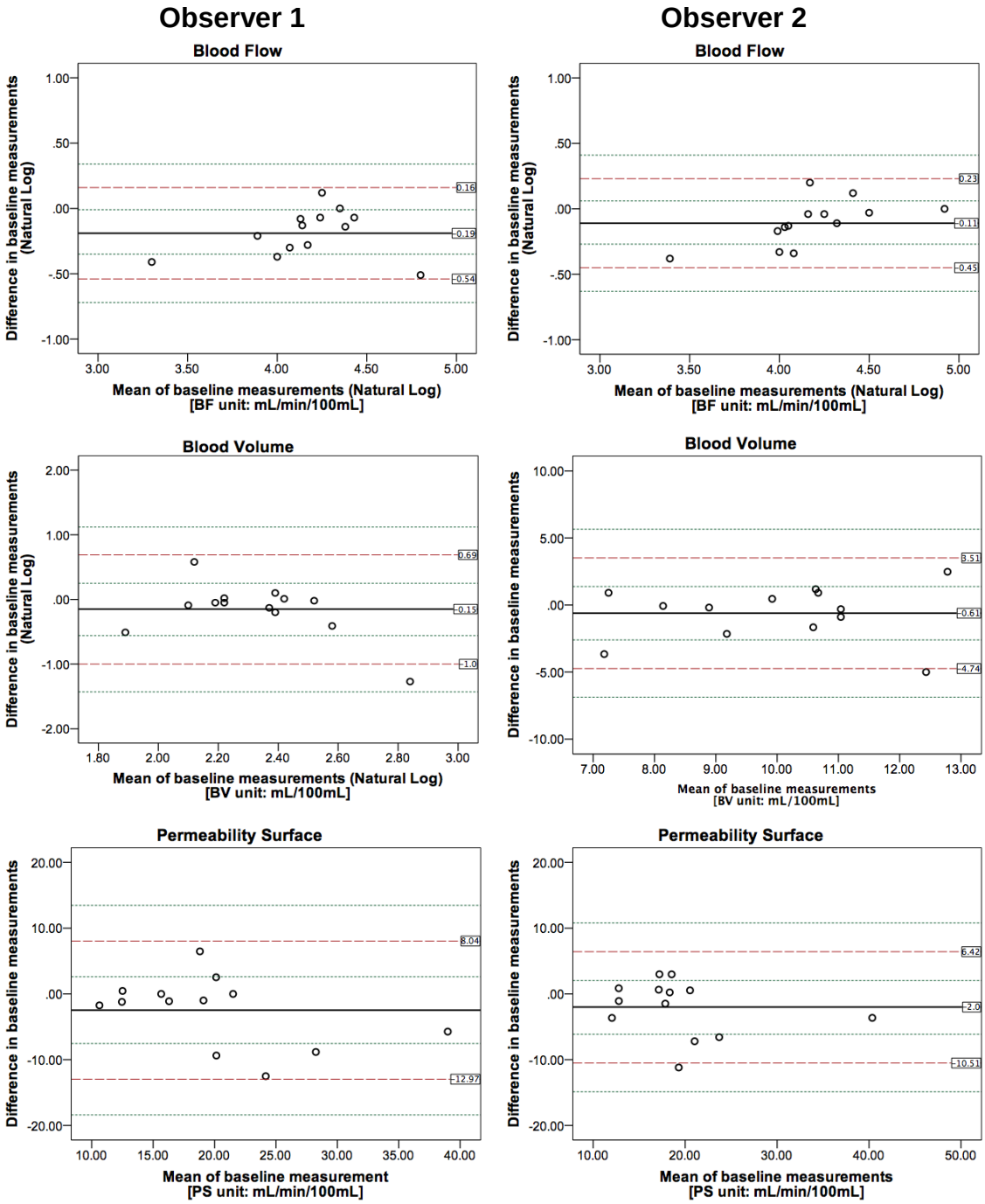

Table 6.4: Inter-observer agreement of DCE-CT parametric measurements on Day 1 obtained from 2-D image coverage

	Blood Flow (mL/min/100mL)	**Blood Volume (mL/100mL)**	**Permeability Surface (mL/min/100mL)**
Measurements			
Observer 1; 2 (mean)	60.9; 64.3	9.37; 9.65	18.02; 18.08
Mean (Total)	62.62	9.51	18.05
Mean Difference	-3.42	-0.28	-0.05
Wilcoxon test	0.40	0.37	0.87
Repeatability			
wSD (*95% CI*)	0.095 (*0.05, 0.13*)	1.08 (*0.83, 1.74*)	1.55 (*1.18, 2.49*)
r (*95% CI*)❖	0.26* (*-28.2%, 21.8%)*	3.015 (*2.3, 4.82*)	4.31 (*3.29, 6.89*)
95% LoA (*Precision limits*)	*-0.30 (-0.*43,-0.18*); 0.22 (*0.10, 0.35*)	-3.4 (*-4.8, -1.9*); 2.85 (*1.42, 4.27*)	-4.60 (*-6.6, -2.5*); 4.49 (*2.4, 6.5*)
Reproducibility			
ICC (*95% CI*)	0.92 (*0.78, 0.97*)	0.84 (0.56, 0.94)	0.97 (*0.91, 0.99*)
wCV (*95% CI*)	0.10 (*0.06, 0.14*)	0.112 (*0.09, 0.12*)	0.077 (*0.072, 0.08*)
Between-/ within-subject variance components	469.3; 67.8	4.174, 0.302	44.9; 5.38

*CI – confidence interval (❖as %of the mean for log transformed data); F – variance ratio; wSD – within-subject standard deviation; wCV – within-subject coefficient of variation; r – repeatability coefficient; LoA – Limits of agreement; ICC – Inter-class coefficient; *Natural Log transformed data; ** p<0.05*

Figure 6.6: Bland-Altman plots of Inter-observer agreement of DCE-CT parametric measurements on Day 1 obtained from 2-D image coverage

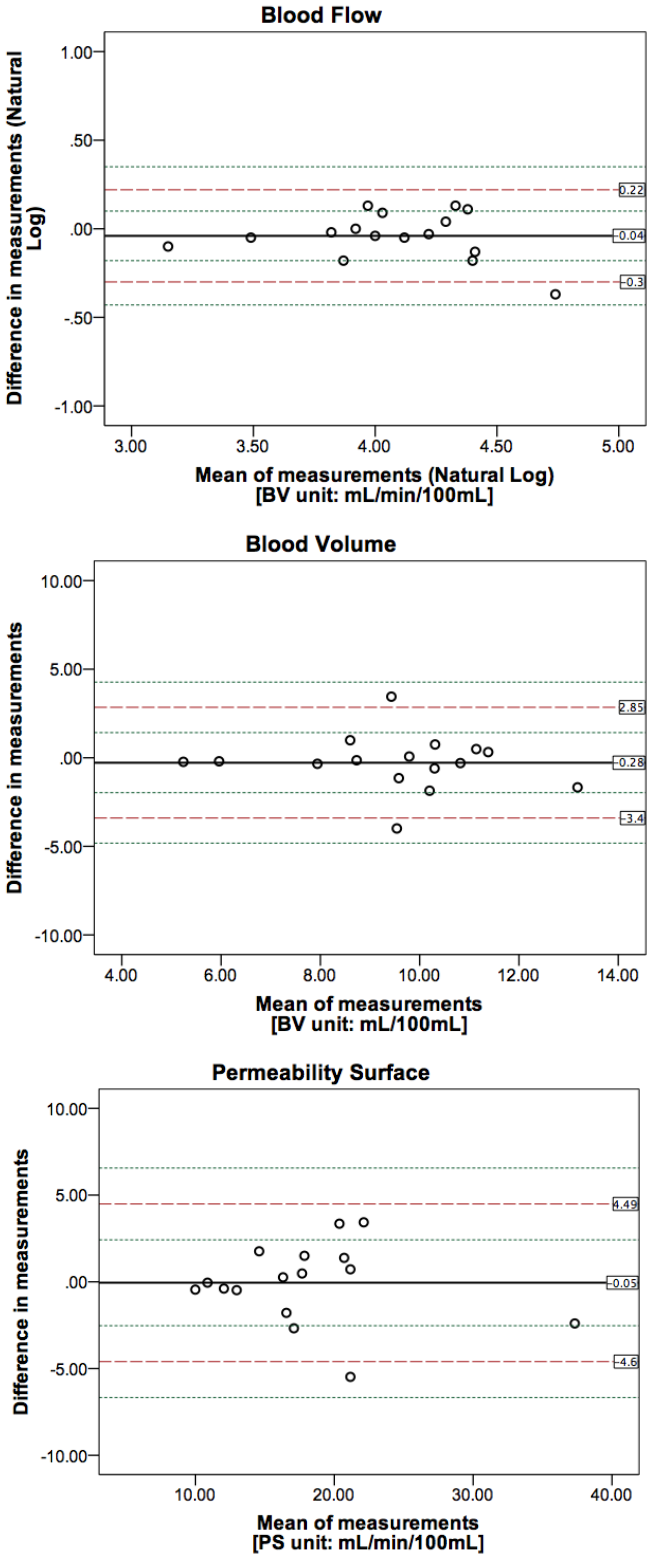

6.3.3 Baseline Day-1:Day-2 reproducibility and observer agreement of baseline DCE-CT parametric measurements obtained by 3-D image coverage of rectal cancers

The actual DCE-CT parameter measurements obtained by 3-D coverage are shown in table 6.5 and figure 6.7.The baseline Day1:Day2 reproducibility is shown in table 6.6 and figure 6.8. The inter-observer agreement for day 1 measurements is shown in table 6.7 and figure 6.9.

6.3.3.1 Summary of results

For day-1:day-2 reproducibility:

- The mean difference was least for BV and most for BF measurements for both observers
- The BV measurements were most sensitive to spontaneous change followed by PS measurements. This analysis was more pronounced for observer 2 (variance ration >8 for both BV and PS).
- The mean difference of all parametric values between observers fell below the values defined by repeatability coefficient. The Bland-Altman LoA were small for PS measurements for both observers and for BV measurements for observer 2. The Bland-Altman LoA were extremely wide for BV measurements for both observers.
- The variation in measurements between day-1:day-2 was most for BF (low wCV; low ICC and between/within-subject variance components) and least for BV. The PS measurement were also varied between two days as seen by high wCV and between/within-subject variance components for both

observers, however, observer dependent variance was least for observer 2 only (ICC=0.80).

For inter-observer analysis:

- In general, the mean difference was least for BV measurements. The maximum mean difference was seen in BF.
- The repeatability coefficient values were above the mean difference for all parametric values. The Bland-Altman LoA was narrow for BV measurement and PS measurements. In contrast, the BV measurement showed wide Bland-Altman LoA.
- The wCV was low for all parameters with corresponding high ICC and between/within-subject variance for BF and PS. The BV measurement showed relatively poor reproducibility between observers (wCV=0.244, ICC=0.50, between/within-subject variance=4.03; 2.49)

Table 6.5: The actual Day-1:Day-2 DCE-CT parametric measurements obtained from 3-D image coverage

Code		Blood Flow (mL/min/100mL)				Blood Volume (mL/100mL)				Permeability Surface (mL/min/100mL)			
		Observer 1		Observer 2		Observer 1		Observer 2		Observer 1		Observer 2	
		$T_0^{(1)}$	$T_0^{(2)}$	$T_0^{(1)}$	$T_0^{(2)}$	$T_0^{(1)}$	$T_0^{(2)}$	$T_0^{(1)}$	$T_0^{(2)}$	$T_0^{(1)}$	$T_0^{(2)}$	$T_0^{(1)}$	$T_0^{(2)}$
1	RY	106.1	167.71	106.39	153.08	13.38	14.22	13.24	13.26	19.36	19.25	20.06	19.35
2	DG	68.88	75.04	72.88	79.65	12.31	12.03	12.28	12.34	17.53	24.35	18.23	27.41
3	DJ	73.36	86.3	75.7	84.52	12.81	12.82	13.16	12.39	22.89	22.09	22.94	20.74
4	AH	60.53	96.16	69.39	89.56	9.85	11.35	11.78	11.22	14.66	14.25	16.55	13.45
5	KB	55.18	69.01	57.69	62.51	10.44	11.86	10.98	11.81	18.06	21.75	18.7	20.27
6	ED	73.14	69.61	64.01	71.06	11.67	10.58	10.01	10.2	19.3	16.59	17.89	16.84
8	JN	66.84	65.94	69.76	72.08	11.46	11.17	11.62	12.46	38.77	40.78	41.28	44.67
9	SD	53.45	62.25	57.86	63.69	8.95	10.82	9.73	11.04	14.56	25.83	15.73	26.96
10	JH	68.53	64.48	69.47	75.56	9.96	11.1	10.36	12.94	15.37	16.7	16.94	21.24
11	DP	94.68	72.28	84.61	65.1	14.1	11.98	12.85	11.21	22.09	21.04	21.71	18.84
12	GA	80.28	98.95	96.48	96.1	10.12	15.74	13.26	15.32	21.09	29.09	27.31	24.95
15	RC1	33.83	103.78	40.89	106.08	5.46	7.22	5.99	7.45	11.21	***46.68***	12.91	17.43
17	JT	72.19	70.45	90.47	83.28	9.37	9.21	11.21	10.38	15.42	16.28	18.35	18.34

Bold and italic – outlier value; $T_0^{(1)}$- Day 1 scan; $T_0^{(2)}$- Day 2 scan

Figure 6.7: Baseline DCE-CT parameter measurement reproducibility obtained from 2-D image coverage

A - Observer 1

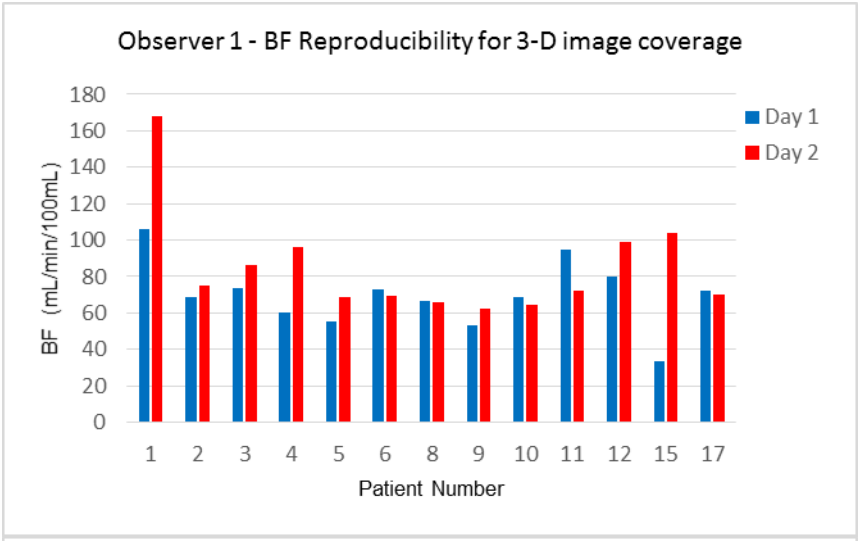

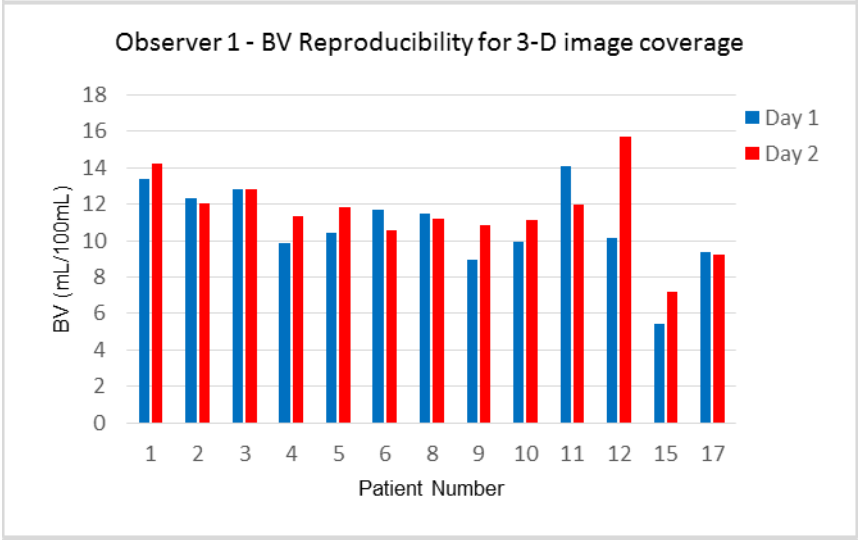

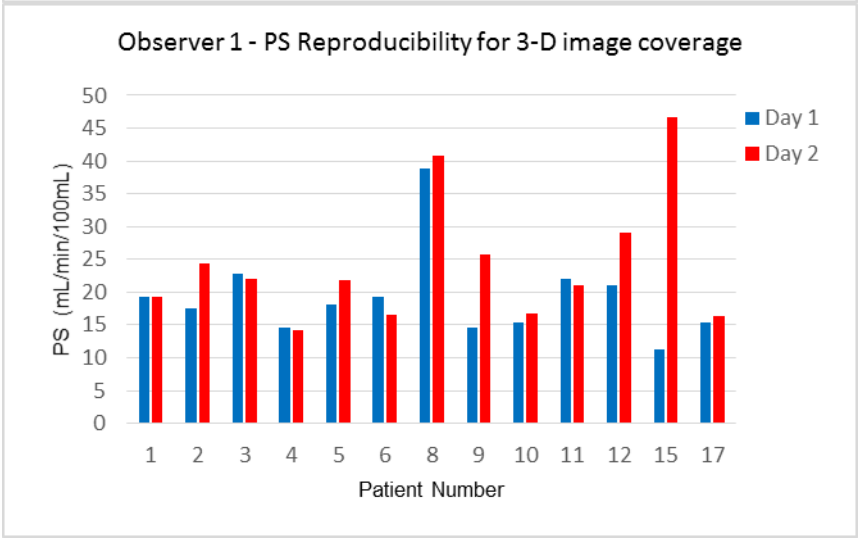

B - Observer 2

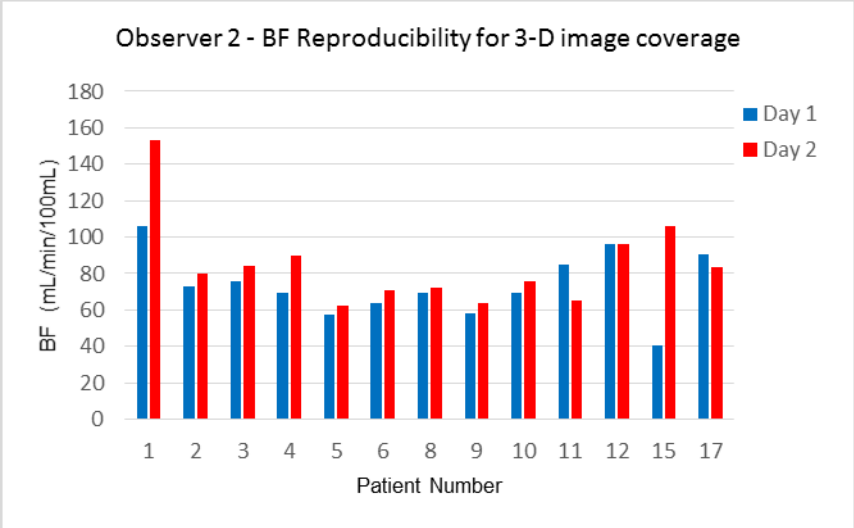
Observer 2 - BF Reproducibility for 3-D image coverage
BF (mL/min/100mL)
180
160
140
120
100
80
60
40
20
0
1 2 3 4 5 6 8 9 10 11 12 15 17
Patient Number
Day 1
Day 2

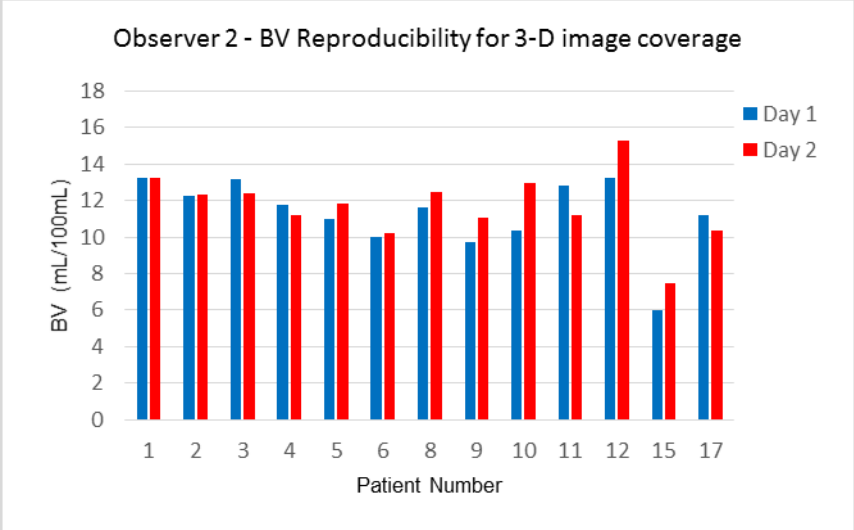
Observer 2 - BV Reproducibility for 3-D image coverage
BV (mL/100mL)
18
16
14
12
10
8
6
4
2
0
1 2 3 4 5 6 8 9 10 11 12 15 17
Patient Number
Day 1
Day 2

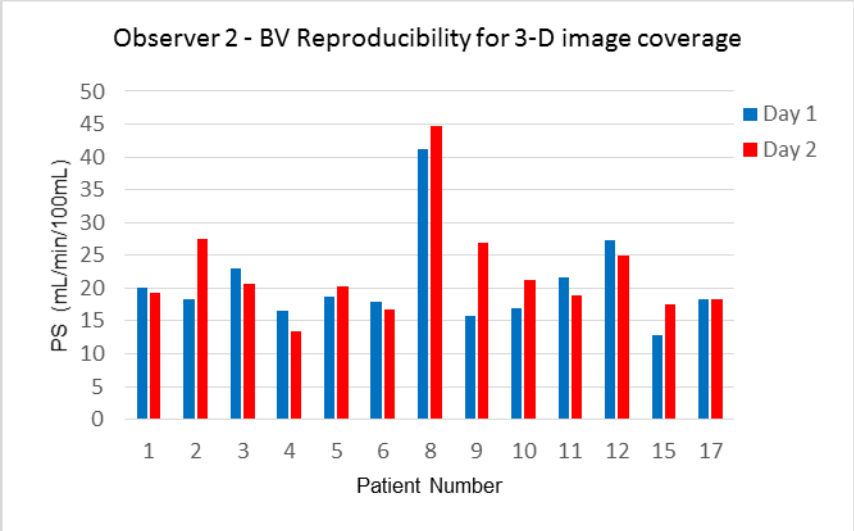
Observer 2 - BV Reproducibility for 3-D image coverage
PS (mL/min/100mL)
50
45
40
35
30
25
20
15
10
5
0
1 2 3 4 5 6 8 9 10 11 12 15 17
Patient Number
Day 1
Day 2

Table 6.6: Day-1:Day-2 reproducibility analysis of DCE-CT parameters obtained from 3-D image coverage for each observer

	Blood Flow (mL/min/100mL)		Blood Volume (mL/100mL)		Permeability Surface (mL/min/100mL)	
Observer	**1**	**2**	**1**	**2**	**1**	**2**
Measurements						
$T_0^{(1)}$; $T_0^{(2)}$ (mean)	65.3; 84.77	71.1; 84.79	10.06; 11.55	10.96; 11.69	19.25; 24.2	19.92; 22.35
Mean (Total)	77.27	79.15	11.15	11.48	21.73	21.5
Mean Difference	-14.9	-11.28	-0.79	-0.43	4.95	-1.68
Wilcoxon	0.075	0.06	0.19	0.85	0.06	0.34
Spontaneous Changes						
95% Group CI for mean difference❖	±17.82 (23%)	±14.55 (18.3%)	±1.189 (10.6%)	±0.758 (6.6%)	-3.55, -6.12 (-28.3%, 23.6%)	-1.40, -1.85 (-16.8%, 10.03%)
F	1.82	2.25	4.0	8.52**	1.52	8.9**
Repeatability						
wSD (*95% CI*)	20.85 (*15.5, 35.8*)	17.03 (*12.7, 29.2*)	1.39 (*1.03, 2.39*)	0.88 (*0.66, 1.52*)	0.319 (*0.18, 0.45*)	0.163 (0.09, 0.23)
r (*95% CI*)❖	57.75 (*43.1, 99.2*)	47.1 (*35.1, 81.0*)	3.85 (*2.87, 6.62*)	2.45 (*1.83, 4.22*)	0.88* (-61%, 127.9%)	0.45* (-39%, 50.5%)
95% LoA (*Precision limits*)	-67.85 (*-95.1, -40.5*); 37.8 (*10.55, 65.1*)	-55.5 (*-78.4, -32.6*) 33.01 (10.12, 55.9)	-4.54 (*-6.48,2.60*); 2.96 (*1.02, 4.90*)	-2.88 (*-4.14, -1.61*) 2.02 (*0.76, 3.29*)	*-1.04 (*-1.47, -0.61*); 0.61 (*0.18, 1.04*)	*-0.53 (*-0.76, -0.29*); 0.37 (*0.14, 0.61*
Reproducibility						
ICC (*95% CI*)	0.39 (*-0.18, 0.76*)	0.45 (-0.10, 0.79)	0.62 (*0.14, 0.87*)	0.79 (0.46, 0.93)	0.28 (*-0.29, 0.70*)	0.80 (0.48, 0.93)
wCV (*95% CI*)	0.253 (*0.17, 0.33*)	0.206 (*0.14, 0.26)*	0.122 (*0.107, 2.39*)	0.081 (*0.076, 0.086*)	0.376 (*0.20, 0.57*)	0.177 (0.09, 0.26)
Between / within-subject variance components	233.0; 349.2	203.9; 245.3	2.99; 1.76	2.97; 0.75	19.53; 50.26	0.098; 0.263

*CI – confidence interval (❖as % of the mean for log transformed data); F – variance ratio; wSD – within-subject standard deviation; wCV – within-subject coefficient of variation; r – repeatability coefficient; LoA – Limits of agreement; ICC – Inter-class coefficient; *Natural Log transformed data; ** p<0.05*

Figure 6.8: Bland-Altman plots of Day-1:Day-2 reproducibility of parametric measurements obtained from 3-D image coverage

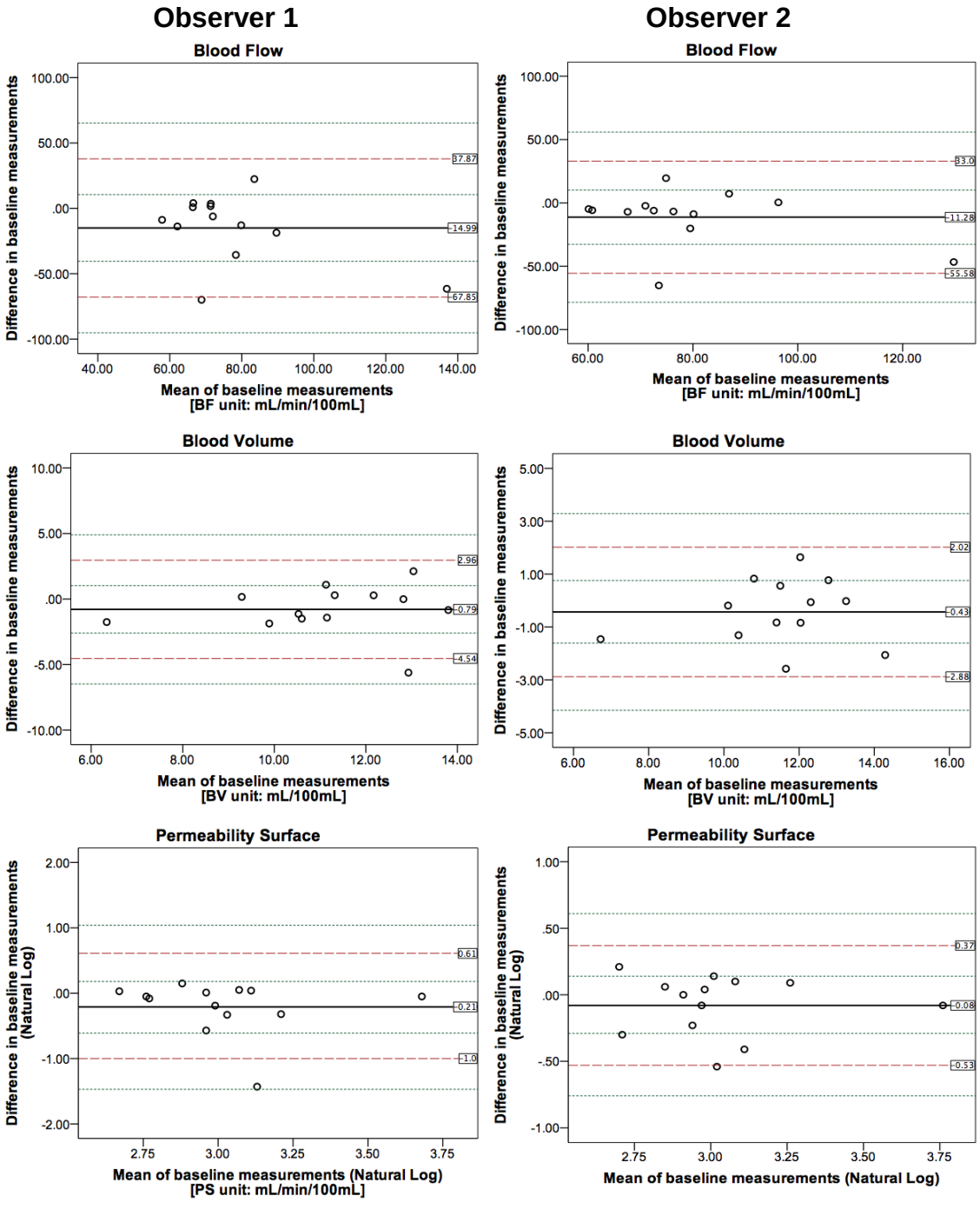

Table 6.7: Inter-observer agreement of DCE-CT parametric measurements on Day 1 obtained from 3-D image coverage

	Blood Flow (mL/min/100mL)	**Blood Volume (mL/100mL)**	**Permeability Surface (mL/min/100mL)**
Measurements			
Observer 1; 2 (mean)	65.3; 71.1	10.06; 10.96	17.9; 19.9
Mean (Total)	68.22	10.5	18.9
Mean Difference	-5.77	-0.91	-1.93
Wilcoxon test	0.12	0.17	0.06
Repeatability			
wSD (*95% CI*)	9.27 (*7.07, 14.8*)	1.65 (*1.26, 2.64*)	0.27 (*0.16, 0.37*)
r (*95% CI)*❖	25.6 (*19.6, 41.07*)	4.59 (*3.5, 7.3*)	0.75* (*-56.02%, 97.90%)*
95% LoA (*Precision limits*)	-30.1(*-41.1, -19*); 18.57 (*7.48, 29.6*)	-5.37 (*-7.4, -3.33*); 3.55 (*1.52, 5.58*)	*-0.96 (*-1.33, -0.59*); 0.66 (*0.29, 1.03*)
Reproducibility			
ICC (*95% CI*)	0.71 (*0.22, 0.89*)	0.50 (*0.35, 0.82*)	0.86 (*0.61, 0.95*)
wCV (*95% CI*)	0.24 (*0.13, 0.35*)	0.244 (*0.13, 0.35*)	0.311 (*0.18, 0.45*)
Between- / within-subject variance components	323.7; 74.06	4.03; 2.49	44.92; 5.38

*CI – confidence interval (❖as % of the mean for log transformed data); F – variance ratio; wSD – within-subject standard deviation; wCV – within-subject coefficient of variation; r – repeatability coefficient; LoA – Limits of agreement; ICC – Inter-class coefficient; *Natural Log transformed data; ** p<0.05*

Figure 6.9: Bland-Altman plots of Inter-observer agreement of DCE-CT parametric measurements on Day 1 obtained from 3-D image coverage

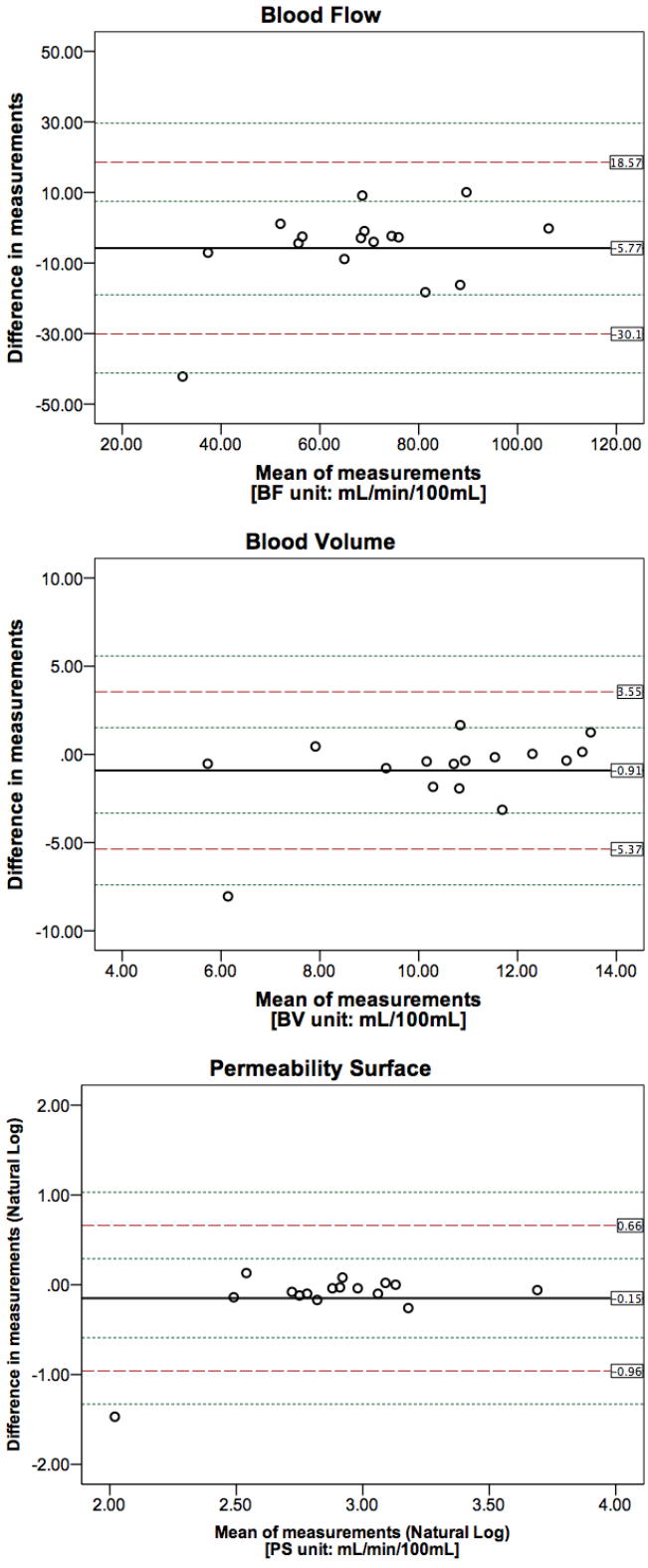

6.3.4 Alterations in DCE-CT parameters (3-D image coverage) in response to NCRT

6.3.4.1 Estimation of significant changes in parametric measurements for a cohort of patients

The mean values of all the measured DCE-CT parameters show a statistically significant decline during the interval after NCRT and surgery as shown in tables 6.8 - 6.9 and figure 6.10. The BF measurement show similar decline at 6 weeks post-NCRT (T_2) and pre-operative stage (T_3) (-41.01% and -41.08%, respectively, see table 6.9 and figure 6.10), whilst BV and PS show a continuous steady decline.

Table 6.8: Mean parametric alterations after NCRT

Parameter	n	T_0	T_1	p	n	T_0	T_2	p	n	T_0	T_3	p
		(mean)				(mean)				(mean)		
BF (mL/min/ 100mL)	14	75.75	56.07	***0.013***	12	76.51	42.70	**0.002**	12	74.12	40.77	***0.002***
BV (mL/ 100mL)	14	11.04	8.53	***0.016***	12	11.04	7.75	**0.005**	12	10.69	6.82	***0.002***
PS (mL/min/ 100mL)	14	19.41	15.75	***0.035***	12	19.50	13.42	**0.003**	12	18.77	10.96	***0.002***

Bold *– significant changes; Statistical test – Shapiro-Wilk and Q-Q plots distribution test; Wilcoxon signed rank test*

Table 6.9: Percentage parametric alterations after NCRT

Parameter	% Change at T_1 (*Cohort CI for 'n'*)	% Change at T_2 (*Cohort CI for 'n'*)	% Change at T_3 (*Cohort CI for 'n'*)
BF (mL/min/100 mL)	**-23.44%** (*-18.19%, 22.23%; n=14*)	**-42.01%** (*-16.01%,19.06%;n=12*)	**-42.08%** (*-16.01%,19.06%;n=12*)
BV (mL/ 100mL)	**-19.77%** (*-5.89%, 6.26%; n=14*)	**-27.87%** (*-6.35%, 6.78%; n=12*)	**-35.56%** (*-6.35%, 6.78%; n=12*)
PS (mL/min/100 mL)	**-17.04%** [*-11.42%, 12.89%; n=14*)	**-32.68%** (*-12.27%, 13.99%; n=12*)	**-42.30%** (*-12.27%, 13.99%; n=12*)

Bold *– significant changes; Statistical test – Shapiro-Wilk and Q-Q plots distribution test; Wilcoxon signed rank test; Cohort CI – represent the confidence interval of spontaneous change in a group of 'n' patients.*

Figure 6.10: DCE-CT parameter alteration after NCRT by percentage change

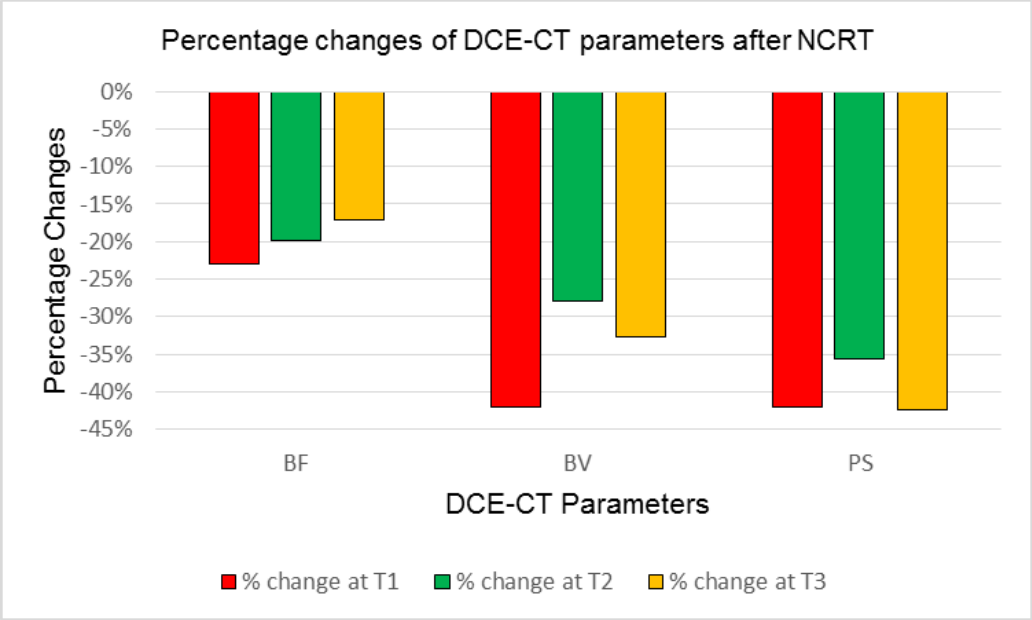

6.3.4.2 Estimation of significant changes in parametric measurements for individual patient

The parametric measurements and their percentage change from the mean of paired baseline measurements for each patient during the interval after NCRT and surgery is given in table 6.10 - 6.13 and figures 6.11 - 6.13.

In general, there was numerical decline in measurements for all parameters with statistical significance commonly seen in BV measurements for most patients. The most significant decline from baseline was seen on pre-operative stage (T_3) for all parameters indicating continual tumour devascularisation.

Table 6.10: Post-NCRT measurement of DCE parameter obtained from 3-D image coverage

Code		Blood Flow (mL/min/100mL)			Blood Volume (mL/100mL)			Permeability Surface (mL/min/100mL)		
		T_1	T_2	T_3	T_1	T_2	T_3	T_1	T_2	T_3
1	RY	55.65	52.13	36.09	8.52	8.79	6.39	15.44	14.33	10.03
2	DG	52.53	48.81	50.27	10.59	8.91	9.52	19.7	15.17	11.99
3	AH	89.93	48.57	49.68	11.29	9.73	9.6	25.54	16.79	11.86
5	KB	54.15	54.69	42.18	11.54	11.94	7.1	18.01	19.66	13.97
6	ED	51.16	-	42.62	8.86	-	4.7	16.41	-	9.7
7	AF	35.2	18.72	21.97	6.03	4.98	4.92	5.9	10.16	9.89
8	JN	59.47	53.23	54.92	12.81	9.42	10.07	19.27	16.29	17.17
10	JH	33.78	37.02	31.18	6.01	7.23	6.68	12.76	15.47	10.68
11	DP	46.44	-	-	7.98	-	-	11.61	-	-
12	GA	52.09	48.5	-	7.39	5.7	-	11.88	13.71	-
14	MM	38.56	32.64	37.24	5.9	7.83	5.29	13.49	0.71	4.88
15	RC1	***110.57***	41.48	54.34	10.39	5.86	5.43	18.97	13.21	7.85
16	RC2	59.34	54.1	41.19	6.21	8.19	7.38	14.39	16.27	13.15
17	JT	46.2	22.54	27.6	6.03	4.46	4.84	17.17	9.33	10.38

Bold italic – outlier value; T_1- Day 3 scan; T_2- Day 4 scan; T_3- Day 5 scan

Table 6.11: Blood flow measurements (mL/min/100mL) and percentage changes after NCRT (r = -45.3% to 83%)

Code		$T_{0\ (mean)}$	T_1	T_2	T_3
1	RY	129.74	**55.65 (-57%)**	**52.13 (-60%)**	**36.09 (-72%)**
2	DG	76.27	52.53 (-31%)	48.81 (-36%)	50.27 (-34%)
4	AH	80.11	89.93 (12%)	48.57 (39%)	49.68 (38%)
5	KB	60.10	54.15 (-10%)	54.69 (-9%)	42.18 (-30%)
6	ED	67.54	51.16 (-24%)	-	42.62 (-37%)
7	AF	53.32	35.2 (-34%)	18.72 (-65%)	21.97 (59%)
8	JN	60.78	59.47 (-2%)	53.23 (-12%)	54.92 (-10%)
10	JH	72.52	**33.78 (-53%)**	**37.02 (-49%)**	**31.18 (-57%)**
11	DP	74.8	46.44 (-38%)		
12	GA	96.29	**52.09 (-46%)**	**48.5 (-50%)**	-
14	MM	51.45	38.56 (-25%)	32.64 (-37%)	37.24 (28%)
15	RC1	73.49	110.57 (50%)	41.48 (-44%)	**54.34 (-26%)**
16	RC2	77.27	**59.34 (-23%)**	54.1 (-30%)	41.19 (-47%)
17	JT	86.88	**46.2 (-47%)**	**22.54 (-74%)**	**27.6 (-68%)**

*r – repeatability coefficient expressed at %; **BOLD** – significant changes; prefix '+ / -' indicates positive or negative change; T_1- Day 3 scan; T_2- Day 4 scan; T_3- Day 5 scan*

Figure 6.11 Absolute and percentage 'BF' value changes after NCRT (individual patients)

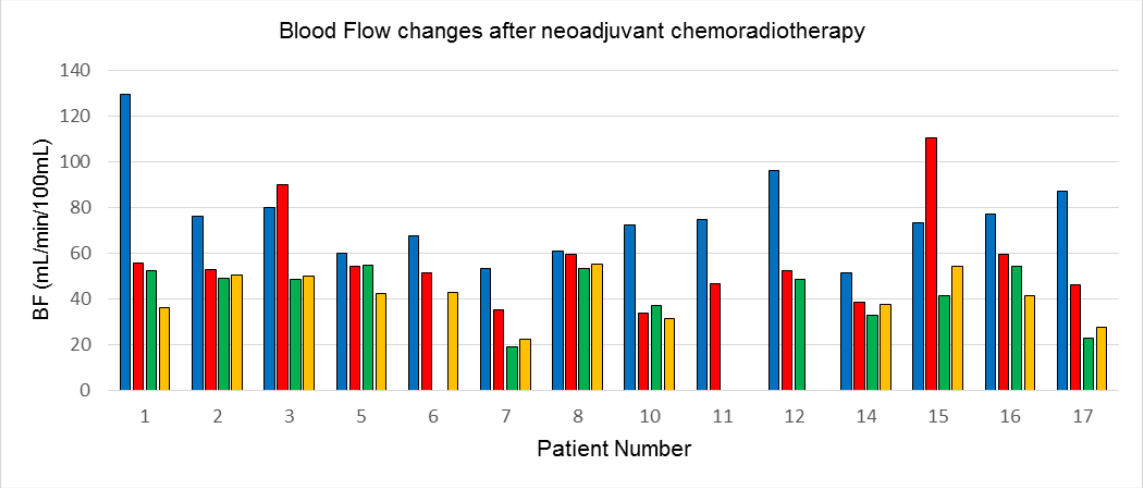

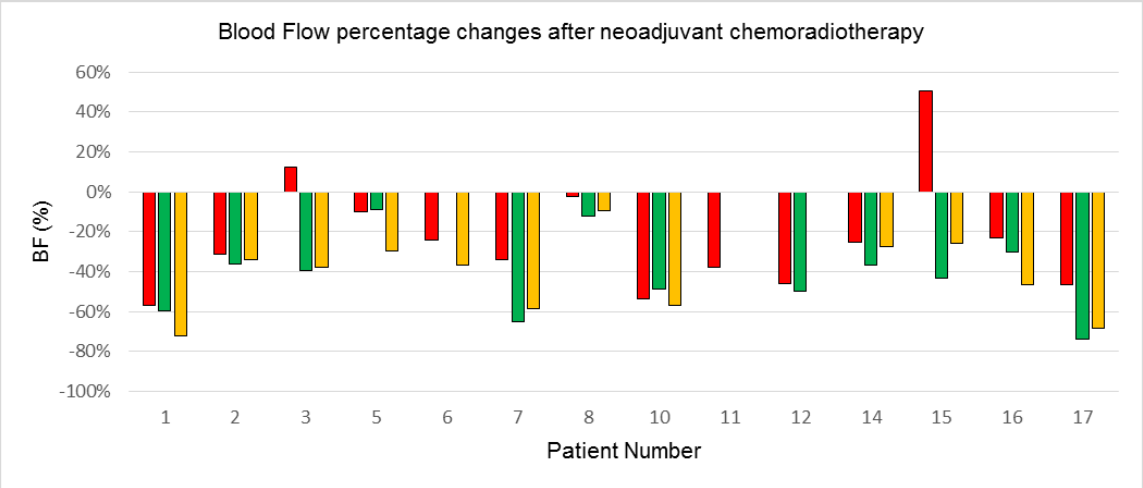

Table 6.12 Blood volume measurements (mL/100mL) and percentage changes after NCRT (r = -20.3% to 25.5%)

Code		$T_{0\ (mean)}$	T_1	T_2	T_3
1	RY	13.25	**8.52 (-38%)**	**8.79 (-34%)**	**6.39 (-52%)**
2	DG	12.31	10.59 (-14%)	**8.91 (-28%)**	**9.52 (-23%)**
4	AH	12.78	11.29 (-12%)	**9.73 (-24%)**	**9.6 (-25%)**
5	KB	11.40	11.54 (1%)	11.94 (5%)	**7.1 (-38%)**
6	ED	10.11	8.86 (-12%)	-	**4.7 (-53%)**
7	AF	10.16	6.03 (-41%)	4.98 (-51%)	4.92 (-52%)
8	JN	10.39	12.81 (23%)	9.42 (-9%)	10.07 (-3%)
10	JH	11.65	**6.01 (-48%)**	**7.23 (-38%)**	**6.68 (-43%)**
11	DP	12.03	**7.98 (-34%)**	-	-
12	GA	14.29	**7.39 (-48%)**	**5.7 (60%)**	-
14	MM	7.68	5.9 (-23%)	7.83 (2%)	5.29 (-31%)
15	RC1	6.72	10.39 (55%)	5.86 (-13%)	5.43 (-19%)
16	RC2	11.11	**6.21 (-44%)**	8.19 (-26%)	7.38 (-34%)
17	JT	10.80	**6.03 (-44%)**	**4.46 (-59%)**	**4.84 (-55%)**

r – repeatability coefficient expressed at %; ***BOLD*** *– significant changes; prefix '+ / -' indicates positive or negative change; T_1- Day 3 scan; T_2- Day 4 scan; T_3- Day 5 scan*

Figure 6.12 Absolute and percentage 'BV' value changes after NCRT (individual patients)

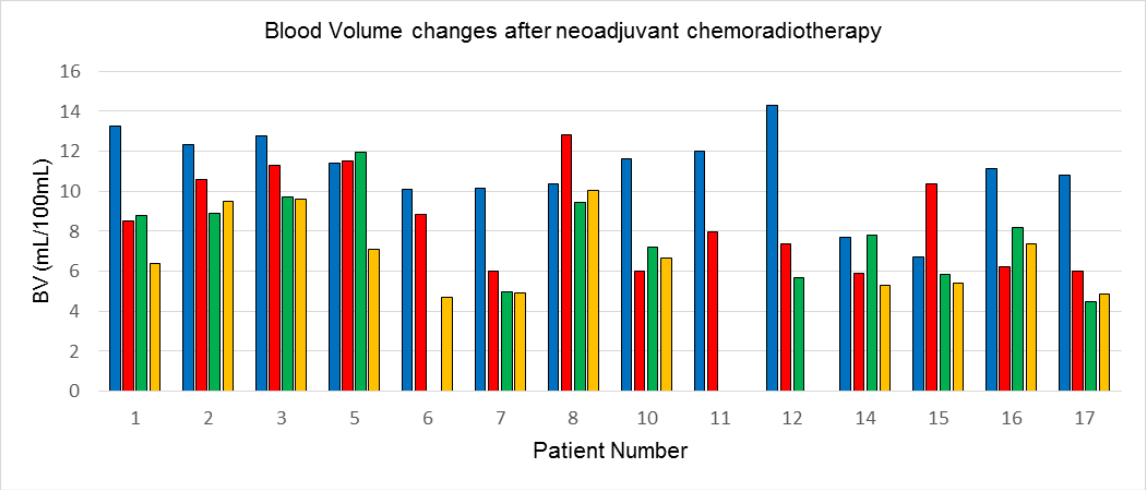

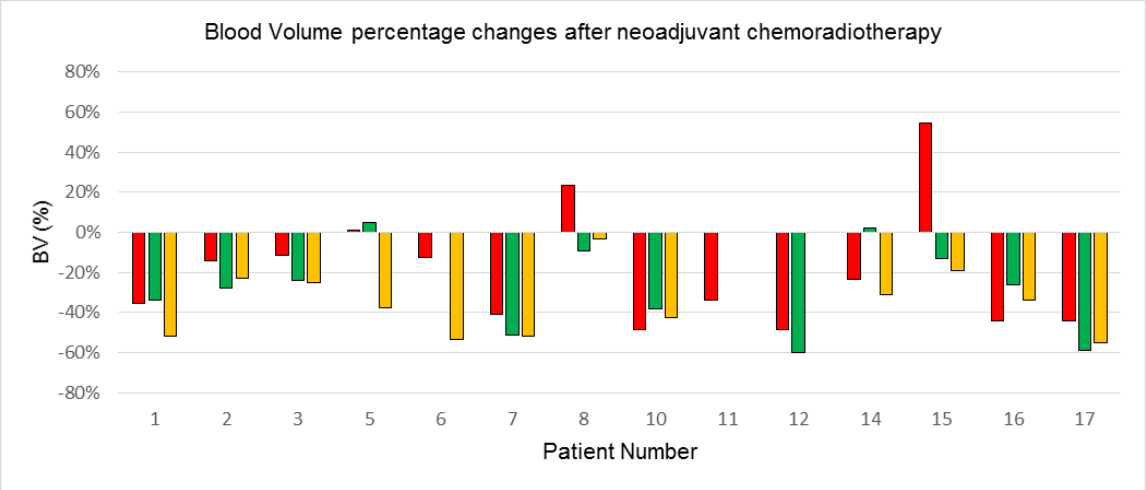

Table 6.13: Permeability surface (mL/min/100mL) and percentage changes after NCRT (r = -36.5% to 57.4%)

Code		$T_{0\ (mean)}$	T_1	T_2	T_3
1	RY	19.71	15.44 (-22%)	14.33 (-27%)	**10.03 (-49%)**
2	DG	22.82	19.7 (-14%)	15.17 (-33%)	**11.99 (-47%)**
4	AH	21.84	25.54 (17%)	16.79 (-23%)	**11.86 (-46%)**
5	KB	19.49	18.01 (-8%)	19.66 (0.9%)	13.97 (-28%)
6	ED	17.37	16.41 (-5%)	-	**9.7 (-44%)**
7	AF	15.72	**5.9 (-62%)**	10.16 (-35%)	9.89 (-35%)
8	JN	21.35	19.27 (-10%)	16.29 (-24%)	17.17 (-20%)
10	JH	19.09	12.76 (-33%)	15.47 (-19%)	**10.68 (-44%)**
11	DP	20.28	**11.61 (-43%)**	-	-
12	GA	26.13	**11.88 (-55%)**	**13.71 (-47%)**	-
14	MM	11.96	13.49 (13%)	**0.71 (-94%)**	**4.88 (-59%)**
15	RC1	15.17	18.97 (25%)	13.21 (-13%)	**7.85 (-48%)**
16	RC2	22.46	14.39 (-36%)	16.27 (-28%)	**13.15 (-41%)**
17	JT	18.35	17.17 (-6%)	**9.33 (-49%)**	**10.38 (-42%)**

r – repeatability coefficient expressed at %; **BOLD** – significant changes; prefix '+ / -' indicates positive or negative change; *T_1- Day 3 scan; T_2- Day 4 scan; T_3- Day 5 scan*

Figure 6.13 Absolute and percentage 'PS' value changes after NCRT (individual patients)

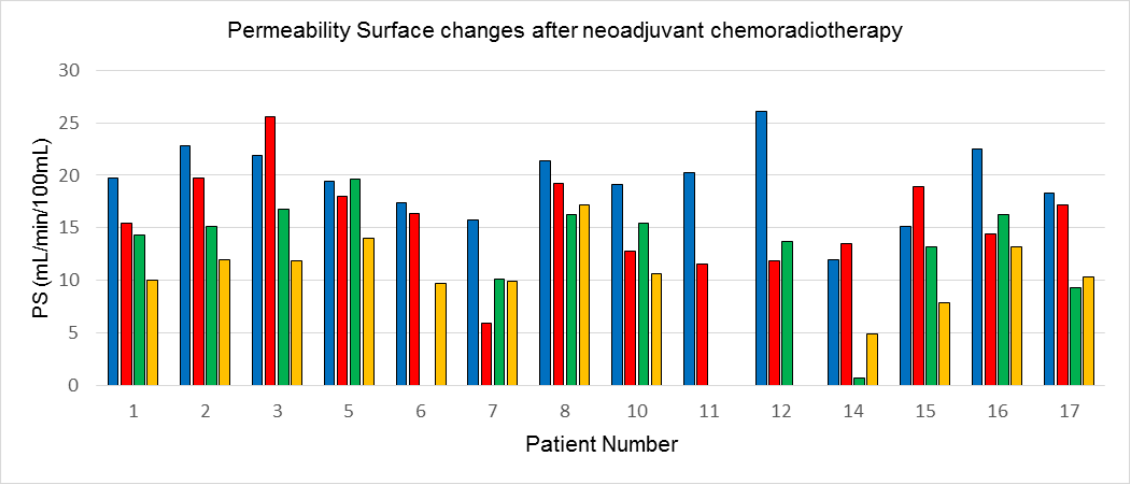

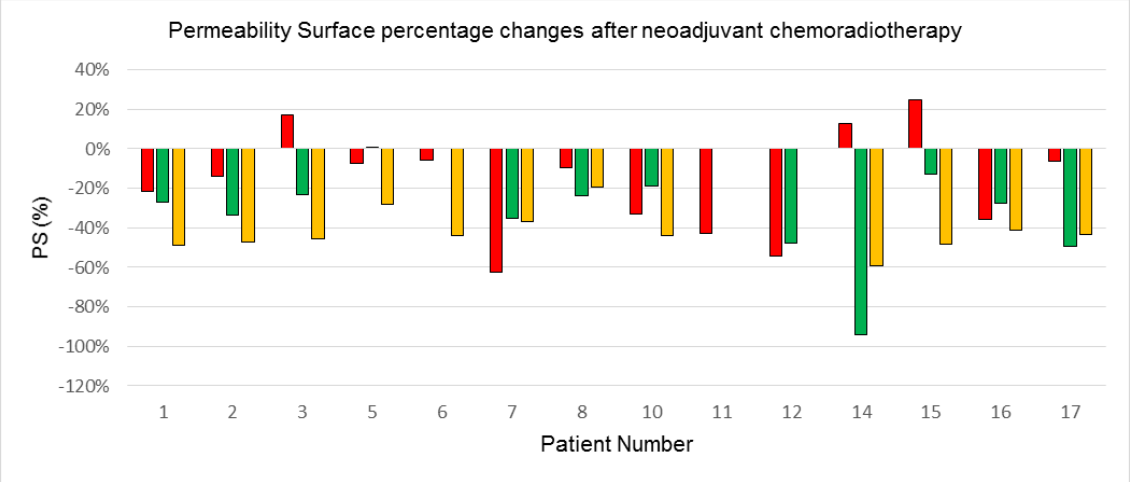

6.3.5 Relationship between DCE-CT parametric measurements (3-D image coverage) and clinicopathological markers

The correlation between DCE-CT parameters and clinical markers is shown in tables 6.14 (A-C). The difference in mean parametric values between clinical markers is given in tables 6.15. There was no difference in mean DCE-CT parametric measurements in response to NCRT (see in table 6.16) and long-term outcomes (6.17).

Summary of results:

- At the pre-treatment stage, a low BF was associated with higher clinical T-stage (ρ -0.53, p 0.03); a higher PS was associated with lower clinical T- and higher N-stage (ρ -0.53, p 0.03 and ρ 0.52, p 0.03, respectively); whilst, BV did not show any correlation with clinical markers. The results indicate poor perfusion in larger tumours with higher PS in tumours with metastatic potential
- Two weeks after NCRT, node positive tumours showed strong positive correlation with BF and BV (ρ 0.63, p 0.01 for both parameters). Tumours with high BV and PS at this stage also showed higher tumour length (ρ 0.68, p 0.007) and nodal involvement on histopathology (ρ 0.60, p 0.02; mean PS = 14.6 mL/min/100mL for pN0 vs 22.6 mL/min/100mL for pN1, p 0.01), respectively. The results indicate active angiogenesis in tumours with metastatic nodes after NCRT.
- Six weeks post-NCRT, there was no correlation between DCT-CT parameters and clinical markers.

- Pre-operatively, there was strong positive correlation between PS and tumour length on histopathology (ρ 0.58, p 0.04). Higher mean PS measurements were also seen in cT3 than cT4 tumours (11.51 mL/min/100mL vs 4.88 mL/min/100mL, p 0.03), indicating that tumors that remained large after NCRT had increased vascular leakage.

CHAPTER 6: DCE-CT: MICROCIRCULATION ANALYSIS

Table 6.14: Correlation between DCE-CT parameters and clinicopathological markers

Table 6.14 A: Blood Flow (mL/min/100mL)

BF		Clinicopathological Features							Response to NCRT				Long-term Outcomes		
		cT	cN	pT	pN	cL	nL	pL	T↓	N↓	pCR	RECIST	LR	DM	Death
T_0	ρ / r	**-0.53**	0.35	0.27	0.40	0	0.49	0.131	-0.30	-0.31	-0.017	-0.15	-0.18	0.22	0.27
	p	***0.03***	*0.17*	*0.35*	*0.15*		*0.07*	*0.65*	*0.24*	*0.23*	*0.94*	*0.57*	*0.50*	*0.41*	*0.29*
T_1	ρ / r	-0.23	**0.63**	0.11	0.40	-0.155	0.12	0.52	0.21	0.101	-0.45	0.093	0.44	-0.10	0.15
	p	*0.41*	***0.01***	*0.69*	*0.15*	*0.59*	*0.68*	*0.05*	*0.45*	*0.73*	*0.10*	*0.75*	*0.10*	*0.73*	*0.60*
T_2	ρ / r	0.177	0.248	0.004	0.45	-0.052	0.37	0.42	0.15	-0.06	-0.195	-0.41	0.30	0.06	0.36
	p	*0.58*	*0.43*	*0.99*	*0.13*	*0.87*	*0.22*	*0.16*	*0.63*	*0.84*	*0.54*	*0.18*	*0.33*	*0.84*	*0.24*
T_3	ρ / r	-0.21	0.502	0.089	0.51	-0.40❖	0.31❖	0.49❖	0.051	-0.25	0	-0.20	0.48	0.25	0.30
	p	*0.49*	*0.09*	*0.78*	*0.08*	*0.90*	*0.31*	*0.09*	*0.87*	*0.41*		*0.52*	*0.11*	*0.41*	0.33

'+' positive correlation; '-' negative correlation; prefix 'c' –Clinical; prefix 'p' – pathological; prefix 'n' – post-NCRT; suffix '↓' – downstage; T – TNM T-stage; N – TNM N-stage; L – craniocaudal tumour length; RECIST – response evaluation criteria in solid tumours; CR – complete response; LR – local recurrence; DM – Distant metastasis; Statistical test – Shapiro-Wilk test for normality; Spearman rho correlation analysis (ρ) non-parametric data, ❖Pearson correlation (r) for parametric data, p – significant value at 0.05

Table 6.14 B: Blood Volume (mL/100mL)

BV		Clinicopathological Features							Response to NCRT				Long-term Outcomes		
		cT	cN	pT	pN	cL	nL	pL	T↓	N↓	pCR	nRECIST	LR	DM	Death
T_0	ρ / r	-0.53	0.35	0.27	0.40	0	0.49	0.13	-0.30	-0.31	-0.17	-0.157	-0.18	0.227	0.278
	p	*0.03*	*0.17*	*0.35*	*0.15*		*0.07*	*0.65*	*0.24*	*0.24*	*0.94*	*0.57*	*0.50*	*0.41*	*0.29*
T_1	ρ / r	-0.23	**0.63**	0.11	0.40	-0.14	0.25	**0.68**	0.21	0.10	-0.45	0.093	0.44	-0.10	0.151
	p	*0.41*	***0.01***	*0.69*	*0.15*	*0.63*	*0.40*	***0.007***	*0.45*	*0.73*	*0.10*	*0.103*	*0.10*	*0.73*	*0.60*
T_2	ρ / r	0.177	0.24	0.004	0.45	-0.161	0.45	0.45	0.15	-0.06	-0.19	-0.41	0.306	0.065	0.36
	p	*0.58*	*0.43*	*0.99*	*0.13*	*0.61*	*0.14*	*0.14*	*0.63*	*0.84*	*0.54*	*0.18*	*0.33*	*0.84*	*0.24*
T_3	ρ / r	-0.21	0.50	0.08	0.51	0.05	0.54	0.43	0.051	-0.25	0	-0.205	0.48	0.259	0.307
	p	*0.49*	*0.09*	*0.78*	*0.08*	*0.86*	*0.06*	*0.15*	*0.87*	*0.41*		*0.52*	*0.11*	*0.41*	0.33

'+' positive correlation; '-' negative correlation; prefix 'c' –Clinical; prefix 'p' – pathological; prefix 'n' – post-NCRT; suffix '↓' – downstage; T – TNM T-stage; N – TNM N-stage; L – craniocaudal tumour length; RECIST – response evaluation criteria in solid tumours; CR – complete response; LR – local recurrence; DM – Distant metastasis; Statistical test – Shapiro-Wilk test for normality; Spearman rho correlation analysis (ρ) non-parametric data, ❖Pearson correlation (r) for parametric data, p – significant value at 0.05

Table 6.14 C: Permeability Surface (mL/min/100mL)

PS		Clinicopathological Features							Response to NCRT				Long-term Outcomes		
		cT	cN	pT	pN	cL	nL	pL	T↓	N↓	pCR	nRECIST	LR	DM	Death
T_0	ρ / r	**-0.53**	**0.52**	-0.012	0.45	-0.02	0.38	0.19	0.13	-0.15	0.122	-0.03	0.12	0.13	0.13
	p	***0.03***	***0.03***	*0.96*	*0.10*	*0.94*	*0.17*	*0.49*	*0.62*	*0.56*	*0.65*	*0.91*	*0.66*	*0.62*	*0.62*
T_1	ρ / r	0.094	0.37	0.27	**0.60**	-0.49❖	0.05❖	0.25❖	-0.11	-0.10	-0.36	0.092	0.31	0.101	0.19
	p	*0.75*	*0.19*	*0.33*	***0.02***	*0.07*	*0.85*	*0.37*	*0.68*	*0.73*	*0.197*	*0.75*	*0.28*	*0.73*	*0.50*
T_2	ρ / r	-0.23	0.39	0.03	0.32	-0.01	0.54	0.44	0.15	-0.13	-0.251	-0.307	0.30	0.13	0.41
	p	*0.45*	*0.20*	*0.91*	*0.30*	*0.97*	*0.06*	*0.15*	*0.63*	*0.68*	*0.43*	*0.33*	*0.33*	*0.68*	*0.17*
T_3	ρ / r	-0.48	0.50	0.17	0.25	0.157❖	0.21❖	**0.58**❖	-0.05	-0.19	-0.13	-0.051	0.48	0.19	0.41
	p	*0.11*	*0.09*	*0.58*	*0.41*	*0.62*	*0.49*	***0.04***	*0.87*	*0.54*	*0.68*	*0.87*	*0.11*	*0.54*	0.17

'+' positive correlation; '-' negative correlation; prefix 'c' –Clinical; prefix 'p' – pathological; prefix 'n' – post-NCRT; suffix '↓' – downstage; T – TNM T-stage; N – TNM N-stage; L – craniocaudal tumour length; RECIST – response evaluation criteria in solid tumours; CR – complete response; LR – local recurrence; DM – Distant metastasis; Statistical test – Shapiro-Wilk test for normality; Spearman rho correlation analysis (ρ) non-parametric data, ❖Pearson correlation (r) for parametric data, p – significant value at 0.05

Table 6.15: Difference in mean parametric values according to clinicopathological features

Parameter		cT				cN				pT					pN		
		cT2	**cT3**	***cT4***	***p***	**cN0**	**cN1**	**cN2**	***p***	**pT0**	**pT1**	**pT2**	**pT3**	***p***	**pN0**	**pN1**	***p***
BF (mL/min/100mL)	❖T_0	96.29	75.94	51.45	*0.11*❖	61.98	77.26	79.06	*0.29*❖	75.00	67.54	67.11	91.35	*0.37*❖	75.35	78.19	*0.36*❖
	❖T_1	52.09	57.86	38.56	*0.52*❖	36.17	56.80	67.16	*0.07*❖	49.99	51.16	65.96	47.04	*0.61*❖	53.55	71.23	*0.27*❖
	❖T_2	48.50	43.12	32.64	*0.58*❖	34.83	41.78	50.10	*0.41*❖	45.08	-	43.33	40.12	*0.87*❖	41.50	48.69	*0.66*❖
	T_3	-	41.09	37.2	*0.74*	34.21	39.53	52.30	*0.20*	39.21	42.62	44.61	36.28	*0.74*	38.93	49.97	*0.18*
BV (mL/100mL)	❖T_0	14.29	11.16	7.68	*0.11*❖	9.66	11.03	12.48	*0.37*❖	11.02	10.11	10.58	12.00	*0.46*❖	10.79	12.54	*0.14*❖
	❖T_1	7.39	8.85	5.90	*0.24*❖	5.95	8.46	10.49	*0.053*❖	6.50	8.86	10.0	7.78	*0.19*❖	8.13	10.94	*0.14*❖
	❖T_2	5.70	7.95	7.83	*0.58*❖	7.53	7.59	8.28	*0.69*❖	7.24	-	8.38	7.34	*0.56*❖	7.44	9.32	*0.13*❖
	T_3	-	6.96	5.29	*0.46*❖	5.98	6.28	9.83	*0.09*❖	6.33	4.70	7.42	6.85	*0.39*❖	6.28	9.56	*0.08*❖
PS (mL/min/100mL)	❖T_0	26.13	20.83	11.96	*0.11*❖	15.52	20.85	23.10	*0.12*❖	20.18	17.37	18.97	19.99	*0.74*❖	18.92	22.33	*0.10*❖
	T_1	11.88	16.26	13.49	*0.62*	13.12	15.28	18.89	*0.38*	13.25	16.41	16.55	16.26	*0.82*	**14.60**	**22.62**	***0.018***
	❖T_2	13.71	14.66	0.71	*0.23*❖	8.09	14.01	15.59	*0.41*❖	10.20	-	15.22	13.57	*0.45*❖	12.91	15.98	*0.28*❖
	T_3	**-**	**11.51**	**4.88**	***0.03***	7.78	10.87	14.51	*0.07*	9.01	9.70	12.14	10.77	*0.69*	10.77	11.92	*0.65*

*Prefix 'c' –Clinical; prefix 'p' – pathological; prefix 'n' – post-NCRT; suffix '🡻' – downstage; T – TNM T-stage; N – TNM N-stage; L – craniocaudal tumour length; RECIST – response evaluation criteria in solid tumours; CR – complete response; LR – local recurrence; DM – Distant metastasis; T_X – Time-point of measure; BV – blood volume; BF – blood flow; PS – permeability surface; Statistical test – Shapiro-Wilk test and Q-Q plots for normality; Spearman rho correlation analysis (ρ) (non-parametric data)***,*** **Pearson Correlation (r) (for parametric data); Means compared with ANOVA (for normally distributed data),* ❖*Kruskal-Wallis test or Mann-Whitney-U test for non-normal distribution;* ***Bold*** *– significance <0.05*

Table 6.16: Difference in mean multiparametric values according to response to NCRT

Parameter		T- downstaging			N-downstaging			Post NCRT RECIST			Post Operative NCRT			
		T↓	**T⊘**	***p***	**N↓**	**N⊘**	***p***	**PR**	**SD**	***p***	**CR**	**PR**	**SD**	***p***
BF (mL/min/ 100mL)	T_0	69.64	88.97	*0.06*	75.98	74.79	*0.90*	80.17	68.32	*0.23*	75.00	73.92	81.08	*0.33❖*
	T_1	59.69	47.04	*0.32*	58.23	43.15	*0.27*	58.02	52.57	*0.38*	49.99	57.14	62.88	*0.91❖*
	T_2	40.12	43.99	*0.61*	42.66	42.91	*0.83*	42.43	43.23	*1.0*	45.08	42.87	39.97	*0.89❖*
	T_3	43.01	36.28	*0.23*	40.78	40.72	*1.0*	41.12	40.07	*0.73*	39.21	40.47	42.51	*0.94*
BV (mL/ 100mL)	T_0	10.79	11.90	*0.23*	10.89	11.87	*0.22*	11.01	11.26	*0.55*	11.02	10.52	11.96	*0.52❖*
	T_1	8.84	7.78	*0.43*	8.57	8.30	*0.71*	8.53	8.54	*0.73*	6.50	9.16	9.30	*0.31❖*
	T_2	7.95	7.34	*0.61*	7.69	8.07	*0.83*	7.03	9.18	*0.17*	7.24	8.03	7.70	*0.80❖*
	T_3	6.81	6.85	*0.86*	6.57	8.10	*0.39*	6.65	7.16	*0.49*	6.33	6.47	7.98	*0.79❖*
PS (mL/min/ 100mL)	T_0	21.34	18.99	*0.61*	19.15	24.97	*0.54*	19.89	22.60	*0.90*	20.18	18.27	21.00	*0.35❖*
	T_1	15.54	16.26	*0.67*	15.67	16.23	*0.71*	15.45	16.28	*0.73*	13.25	15.25	20.80	*0.11*
	T_2	13.35	13.57	*0.61*	13.04	15.32	*0.66*	13.55	13.15	*0.30*	10.23	14.85	13.76	*0.69❖*
	T_3	11.05	10.77	*0.86*	10.88	11.33	*0.51*	11.27	10.34	*0.86*	11.32	11.32	11.41	*0.66*

*Prefix 'c' –Clinical; prefix 'p' – pathological; prefix 'n' – post-NCRT; suffix '↓' – downstage; T – TNM T-stage; N – TNM N-stage; L – craniocaudal tumour length; RECIST – response evaluation criteria in solid tumours; CR – complete response; LR – local recurrence; DM – Distant metastasis; T_X – Time-point of measure; BV – blood volume; BF – blood flow; PS – permeability surface; Statistical test – Shapiro-Wilk test and Q-Q plots for normality; Spearman rho correlation analysis (ρ) (non-parametric data), *Pearson Correlation (r) (for parametric data); Means compared with ANOVA (for normally distributed data), ❖Kruskal-Wallis test or Mann-Whitney-U test for non-normal distribution;* ***Bold*** *– significance <0.05*

Table 6.17: Difference in mean multiparametric values according to long-term outcomes

Parameter		Local Recurrence			Distant Metastasis			Any recurrence			Survival		
		Yes	**No**	***p***	**Yes**	**No**	***p***	**Yes**	**No**	***p***	**Yes**	**No**	***p***
BF (mL/min/ 100mL)	T_0	60.78	76.48	*0.35*	74.39	75.59	*0.86*	72.26	76.83	*0.90*	77.43	71.85	0.61
	T_1	59.47	55.81	*0.26*	43.15	58.23	*0.27*	48.59	58.11	*0.81*	58.60	46.82	0.48
	T_2	41.74	53.23	*0.311*	42.91	42.66	*0.83*	46.35	41.48	*0.64*	41.23	46.84	0.40
	T_3	54.92	39.48	*0.11*	40.72	40.78	*1.0*	45.45	39.21	*0.30*	40.62	41.21	0.92
BV (mL/ 100mL)	T_0	10.39	11.16	*0.48*	11.98	10.98	*0.39*	11.46	11.03	*0.71*	10.84	11.78	0.28
	T_1	12.81	8.21	*0.10*	8.30	8.57	*0.71*	9.80	8.19	*0.48*	8.31	9.38	0.28
	T_2	9.42	7.60	*0.31*	8.07	7.69	*0.83*	8.52	7.49	*0.40*	7.21	9.36	0.22
	T_3	10.07	6.53	*0.11*	8.10	6.57	*0.39*	8.75	6.18	*0.07*	6.51	7.76	0.30
PS (mL/min/ 100mL)	T_0	21.35	20.95	*0.64*	20.95	20.98	*0.61*	19.56	20.95	*1.0*	19.12	23.87	0.61
	T_1	19.27	15.48	*0.26*	16.23	15.67	*0.71*	17.24	15.34	*0.31*	15.46	16.82	0.48
	T_2	16.29	13.16	*0.31*	15.32	13.04	*0.66*	15.64	12.68	*0.30*	12.31	16.76	0.16
	T_3	17.17	10.39	*0.11*	11.33	10.88	*0.51*	13.28	10.19	*0.11*	10.54	12.21	0.16

*Prefix 'c' –Clinical; prefix 'p' – pathological; prefix 'n' – post-NCRT; suffix '↓' – downstage; T – TNM T-stage; N – TNM N-stage; L – craniocaudal tumour length; RECIST – response evaluation criteria in solid tumours; CR – complete response; LR – local recurrence; DM – Distant metastasis; T_X – Time-point of measure; BV – blood volume; BF – blood flow; PS – permeability surface; Statistical test – Shapiro-Wilk test and Q-Q plots for normality; Spearman rho correlation analysis (ρ) (non-parametric data)***,*** **Pearson Correlation (r) (for parametric data); Means compared with ANOVA (for normally distributed data),* ❖*Kruskal-Wallis test or Mann-Whitney-U test for non-normal distribution;* ***Bold*** *– significance <0.05*

6.3.6 Association between DCE-CT parametric alteration after NCRT (3-D image coverage) and response to therapy and long-term outcomes

The alterations trends in DCE-CT parametric measurements post-NCRT for each patient are given in table 6.18. The changes in the DCE-CT mean parametric values pre- and post NCRT for patients with and without TNM and RECIST downstaging and long-term outcome is showed in in tables 6.19 to 6.21.

Summary of results:

- In general, there was a decline in DCE-CT parametric measurements after NCRT in all patients. Significant decline was commonly seen for PS measurements.
- In tumour that showed T and N- downstaging, there was statistically significant decline in all mean parametric values at six week post-NCRT (T_2) and pre-operative stage (T_3) only. In tumour that showed N-downstaging, there was statistically significant decline in mean BF and BV values at all time-point.
- In tumours that showed downstaging by RECIST criteria, there was statistically significant decline in mean BF and BV parametric values at six week post-NCRT (T_2) and pre-operative stage (T_3) only, whilst mean PS measurements significantly declined at all time-points.
- In patients without disease recurrences and in patients who survived the study observation periods (with or without recurrence) , there was

statistically significant decline in mean BF and BV parametric values at all time-points and in mean PS measurements at six week post-NCRT (T_2) and pre-operative stage (T_3) only.

Table 6.18: DCE- CT parametric alterations after NCRT and clinical outcomes

Code		Sex	Age	cTNM	3-D Coverage			Post NCRT TNM (yp or r)	Local Recurrence	Distant Recurrence	Death
					Δ BF (mL/min /100mL)	Δ BV (mL /100mL)	Δ PS (mL/min /100mL)				
1	RY	M	59	T3N1M0	↓*	↓*	↓*	T3N0			
2	DG*	M	52	T3N1M0	↓	↓*	↓*	T3N1		✓: Lung	✓
3	DJ	M	72	T3N1M2	-	-	-	-	-	✓: Liver	✓
4	AH	M	74	T3N2M0	↓	↓*	↓*	T2N1			
5	KB	M	78	T3N1M0	↓	↓*	↓	T2N0			✓
6	ED	F	72	T3N1M0	↓	↓*	↓*	T1N0			
7	AF	F	60	T3N1M0	↓	↓	↓	T2N0			
8	JN	M	79	T3N2M0	↓	↓	↓	T2N0	✓		
9	SD**	M	71	T3N1M0	-	-	-	-			✓
10	JH	M	67	T3N0M0	↓*	↓*	↓*	T3N0		✓: Pancreas	✓
11	DP	M	58	T3N1M0	↓	↓*	↓*	T2N0			
12	GA***	M	53	T2N2M0	↓*	↓*	↓*	RCR			
13	PO	F	59	T3N2M0	-	-	-	T3N2		✓: Liver	
14	MM***	F	78	T4N0M0	↓	↓	↓*	RCR			
15	RC1	M	76	T3N1M0	↓*	↓	↓*	T2N0			
16	RC2	M	56	T3N1M0	↓	↓	↓*	PCR			
17	JT	F	79	T3N1M0	↓*	↓*	↓*	T3N0			

*Prefix 'c' –Clinical; prefix 'p' – pathological; prefix 'n' – post-NCRT; T – TNM T-stage; N – TNM N-stage; BV – blood volume; BF – blood flow; PS – permeability surface; symbol '↓' – downstage; * - significant changes*

Table 6.19: Difference in mean parametric values after NCRT between patient with and without TNM downstaging

Parameter		T_0 vs. T_1 (mean)		*p*	T_0 vs. T_2 (mean)		*p*	T_0 vs. T_3 (mean)		*p*
T↓	**BF**	69.52	59.69	*0.114*	69.10	43.99	***0.012***	65.50	43.01	***0.012***
	BV	10.66	8.84	*0.114*	10.56	7.95	***0.036***	10.04	6.81	***0.012***
	PS	19.17	15.54	*0.169*	19.26	13.35	***0.017***	18.17	11.05	***0.012***
T⊘	**BF**	91.35	47.04	*0.068*	91.35	40.12	*0.068*	91.35	36.28	*0.068*
	BV	12.00	7.78	*0.068*	12.00	7.34	*0.068*	12.00	6.85	*0.068*
	PS	19.99	16.26	*0.068*	19.99	13.57	*0.068*	19.99	10.77	*0.068*
N↓	**BF**	74.98	58.23	***0.034***	76.94	42.66	***0.005***	74.06	40.78	***0.005***
	BV	10.85	8.57	***0.034***	10.44	7.69	***0.013***	10.44	6.57	***0.005***
	PS	19.15	15.67	*0.084*	19.21	13.04	***0.007***	18.34	10.88	***0.005***
N⊘	**BF**	74.39	43.15	*0.18*	74.39	42.91	*0.18*	74.39	40.72	*0.18*
	BV	11.98	8.30	*0.18*	11.98	8.07	*0.18*	11.98	8.10	*0.18*
	PS	20.95	16.23	*0.18*	20.95	15.32	*0.18*	20.95	11.33	*0.18*

*'↓' denotes downstaging; '⊘' denotes no change Statistical Test: Paired sample T-test; *Wilcoxon Signed ranked test; Units: BF – mL/min/100mL, BV – mL/100mL, PS – mL/min/100mL*

Table 6.20: Difference in mean parametric values after NCRT between patient with and without RECIST downstaging

Parameter		T_0 vs. T_1 (mean)		*p*	T_0 vs. T_2 (mean)		*p*	T_0 vs. T_3 (mean)		*p*
RECIST↓	**BF**	80.17	58.02	*0.051*	**81.75**	**42.43**	***0.012***	**78.16**	**41.12**	***0.012***
	BV	11.01	8.53	*0.066*	**11.12**	**7.03**	***0.012***	**10.60**	**6.65**	***0.012***
	PS	**19.89**	**15.45**	***0.038***	**20.21**	**13.55**	***0.012***	**19.11**	**11.27**	***0.012***
RECIST⊘	**BF**	67.80	52.57	*0.13*	66.04	43.23	*0.068*	66.04	40.07	*0.068*
	BV	11.10	8.54	*0.08*	10.87	9.18	*0.465*	10.87	7.16	*0.068*
	PS	18.53	16.28	*0.50*	18.09	13.15	*0.14*	18.09	10.34	*0.068*

*'↓' denotes downstaging; '⊘' denotes no change Statistical Test: Paired sample T-test; *Wilcoxon Signed ranked test; Units: BF – mL/min/100mL, BV – mL/100mL, PS – mL/min/100mL*

Table 6.21: Changes after NCRT and long-term outcomes

Outcomes		T_0 vs. T_1 (mean)		*p*	T_0 vs. T_2 (mean)		*p*	T_0 vs. T_3 (mean)		*p*
Recurrence (local or distant)	**BF**	69.85	48.59	*0.10*	69.85	46.35	*0.10*	69.85	45.45	*0.10*
	BV	11.45	9.80	*0.59*	11.45	8.52	*0.10*	11.45	8.75	*0.10*
	PS	21.08	17.24	*0.10*	21.08	15.64	*0.10*	21.08	13.28	*0.10*
No Recurrence (local or distant)	**BF**	77.36	58.11	***0.041***	78.73	41.48	***0.008***	75.54	39.21	***0.008***
	BV	10.93	8.19	***0.016***	10.91	7.49	***0.021***	10.44	6.18	***0.008***
	PS	18.95	15.34	*0.110*	18.98	12.68	***0.011***	18.00	10.19	***0.008***
Alive	**BF**	77.43	58.60	***0.041***	78.81	41.32	***0.008***	75.62	40.62	***0.008***
	BV	10.84	8.31	***0.033***	10.79	7.21	***0.011***	10.33	6.51	***0.008***
	PS	19.12	15.46	*0.091*	19.18	12.31	***0.008***	18.21	10.54	***0.008***
Diseased	**BF**	69.63	46.82	*0.109*	69.63	46.84	*0.109*	69.63	41.21	*0.109*
	BV	11.78	9.38	*0.285*	11.78	9.36	*0.285*	11.78	7.76	*0.109*
	PS	20.46	16.82	*0.109*	20.46	16.76	*0.285*	20.46	12.21	*0.109*

*'🡻' denotes downstaging; '⃠' denotes no change Statistical Test: Paired sample T-test; *Wilcoxon Signed ranked test; Units: BF – mL/min/100mL, BV – mL/100mL, PS – mL/min/100mL*

6.4 Discussion

The current experiment presents result on the application of DCE-CT using volumetric techniques in patients with locally advanced rectal cancers and its association with clinical parameters and long-term prognosis. Tumour hypoxia and neoangiogenesis contribute to radioresistance and chemoresistance and hence, the evaluation of functional vascular heterogeneity will prove to be of critical value in clinical practice [497]. The ability to map spatially the vascular heterogeneity across the whole tumour may be relevant to treatment targeting as well as monitoring response.

6.4.1 Reproducibility analysis and influence of coverage volume

An appreciation of the baseline reproducibility is important in the therapeutic response setting in order to estimate the effects of treatment on parameters over and above the day-to-day variation. The study shows difference in day-to-day reproducibility of DCE-CT parameters, at baseline, between 2-D ROI and 3-D VOI coverage and also the effects of observers. Unlike previous studies of solid tumours [493, 495] overall reproducibility was much more variable: the extent and direction of change appeared to be parameter-dependent, i.e., reproducibility did not necessarily improve with greater volume coverage. This reflects the greater spatial and temporal vascular heterogeneity of rectal tumour, and the challenges presented by the relative motility of the gut, due to peristalsis, respiration, and abdominal wall motion.

Regional *blood flow* represents the delivery rate of contrast agent to the tumour (blood flow per unit volume or mass of tissue). Given the physiological regulation of regional blood flow to the needs of the tissue, and the nature of the tumour vasculature, changes in regional blood flow are expected to be high from day 1 to day 2. This was reflected on both 2-D and 3-D analysis with large mean difference. The level of day1:day2 reproducibility in the current study for the 2-D ROI was similar to previously published colorectal cancer study of a similar limited tumour volume [386]: the BF measurements were sensitive to spontaneous changes, narrow B-A limits of agreement and minimal observer variance between readings. However the current study also revealed that BF worsened with increased tumour coverage (3-D analysis) for both observers, unlike previous studies on lung [493] and renal cancer [495]. For example, the repeatability coefficient decreased from -42.6% to 54.9% around the mean to 57.7 absolute difference for observer 1, and from -36% to 38.4% around the mean to 47.1 absolute difference for observer 2 (see table 6.3). The observer variance also increased as seen by decrease in ICC from 0.75 to 0.39 for observer 1 and from 0.93 to 0.45 for observer 2. This effect of tumour volume indicates that the spatial variation in BF is considerable; this is also confirmed by poor wCV and variance component analysis.

Regional tumour *blood volume* represents the functional vascular volume. For the BV measurements, there was good day-1:day-2 reproducibility analysis independent of volume coverage; however, sensitivity to spontaneous changes was much better on 3-D volume. The poor results for observer 1 were probably due to outlier values on day 2 with 2-D coverage (see table 6.2). Hence for day 1, the inter-observer agreement was better for 2-D volumes, especially with low

observer variance (wCV 0.11 and ICC 0.84 for 2-D volume versus wCV 0.24 and ICC 0.50 for 3-D volume, see tables 6.4 and 6.7). The difference between BV and BF suggests that for blood volume the spatial variation is less than for BF, and reflected by the wCV and variance component analysis. Given that blood volume provides a 'snapshot' of the functional vascular volume, this is not unexpected from physiology.

The blood *permeability surface* product reflects the rate of transfer of the contrast agent from the intravascular to extravascular space. This is dependent both on the flow rate and flux of contrast agent into the interstitial space. With the haphazard anatomical and functional nature of the microvasculature, one might expect this to be highly variable. However, overall, the day-to-day reproducibility for the PS was consistently good for both observers with 2-D coverage and slightly worse on 3-D coverage. Between 2-D and 3-D coverage: the repeatability coefficient worsened from 11 absolute difference to -61% to 127.9% around the mean for observer 1, and from 8.91 absolute difference to -39% to 50.5% around the mean for observer 2, whilst the ICC declined from 0.78 to 0.28 and 0.84 to 0.80 for observer 1 and 2 respectively. However, the obviously poor results for observer 1 with 3-D coverage may reflect the outlier value on day-1 (see table 6.5). Similarly, the inter-observer agreement was also better on 2-D coverage with identical measurement on day one for both observers.

6.4.2 Changes in DCE-CT parameters after neoadjuvant chemoradiotherapy

During the interval between NCRT and surgery, there was a significant decline in absolute (and/or percentage) measurements for all DCE-CT parameters compared to baseline levels. This is consistent with previous studies [403, 404] and the drop in post-NCRT parametric measurements relates to progressive tumour devascularisation. All parameters show most significant decline immediately post-NCRT, thereafter, the percentage decline in BF is lower, suggesting gradual recovery with time, whereas, BV and PS show marginal recovery at 6 weeks post-NCRT followed by a further decline at pre-operative stage (see figure 6.10). These variable changes in DCE-parameters reflect partial recovery of blood network with poor function. Such effect may be due to radiotherapy induced loss of the tumour volume and fibrosis that decreases the amount of blood entering the tumour microcirculation (BV) and the rate of contrast passing through these vessels (PS). Hence, the maximal devascularisation occurs immediately after NCRT with the overall tumour functional microcirculation remaining poor till surgery.

6.4.3 The impact of DCE-CT parameters and clinical markers

There were important correlations between DCE-CT perfusion parameters and clinical markers. The rectal tumours with higher T-stage were found to have lower measurements for perfusion parameters especially when obtain by 2-D volume coverage. This correlation supports the theory that large tumours have poor functional vascularity with areas of hypoxia and collapsed vessels. In the

literature, authors have reported an association of low baseline perfusion parameters with poorly differentiated histopathology [382, 392] and potential to metastasize [498]. In contrast, tumours with higher blood volume and permeability surface showed nodal involvement. Such finding supports the pathophysiological aspect of tumour metastasis: tumours cells with readily available blood supply and leaky tumoural endothelium showed early metastasis [499]. Moreover, tumours with clinical nodal involvement showed persistent functional vascularity even after NCRT. Hence tumours with high angiogenic activity (independent of tumour size) were biologically aggressive at the time of diagnosis and also resisted vascular disruption by standard NCRT. These finding supports the theory that tumour size is not representative of its intrinsic biology and also supports the case for adding anti-vascular biological agents into NCRT regimes for locally advanced rectal cancers with nodal disease. Previously, authors have investigated the role of baseline DCE-CT parameters in predicting response to NCRT; the results are conflicting: whilst some authors have shown a low BF and high MTT in responders, others have shown lower BF in non-responders [403, 404, 500]. In the current study, there were numerical differences without statistical significance in baseline values between responders and non-responders: patients with T-downstaging showed a relatively lower baseline BF and higher PS than non-responders, whilst, patients with N-downstaging showed a relatively higher BF and lower PS than non-responder; both findings were independent of observer and coverage volume. Therefore it can be hypothesized that presence of leaky endothelium (high PS) within tumours enabled delivery of radical oxidant generated by NCRT to susceptible cancer cell load even at lower delivery rates (low BF) and,

at higher delivery rates and less leaky tumoural endothelium, the radical oxidant reached draining lymph node. There are several reasons for conflicting results on the role of baseline DCE-CT parameters in predicting response to NCRT in previous studies including different end-points to assess response, different patient selection criteria, difference in perfusion techniques and different mathematical models used to derive parameters [420, 500]. After NCRT, patients with significantly declining perfusion parameters showed tumour downstaging and remained alive without disease recurrence for the entire study period. Rectal tumour with significantly declining blood volume and permeability surface after NCRT achieved pathological complete response. In contrast, patients with persistently high blood volume and permeability surface (persistent angiogenic activity) after NCRT had tumour that remained large in size (according to RECIST criteria), had higher pathological T and N stage and suffered recurrence. The results of current study show an obvious distinction in DCE-CT parameters between patients with and without favourable prognosis and support the role of DCE-CT analysis to filter patients for tailored management regimes.

6.4.4 Benefits and limitation of current experiment

The current study adds to the literature by showing that reproducibility may vary additional due to spatial heterogeneity of vasculature; reproducibility results from a more limited coverage may not necessarily be translatable to the whole tumour; nor may whole tumour coverage improve reproducibility in all tumour types. Given the relative good inter-observer agreement, the effect of observers on reproducibility is less relevant than the spatial and temporal fluctuations in

regional perfusion. The baseline DCE-CT parameters provide an insight into tumour biology and supports previous evidence [499]. After NCRT, responsive tumours show an obvious decline is perfusion parameters, whilst aggressive tumours maintain good functional vasculature. Such finding can be utilized in clinical setting to help tailor management of rectal cancers.

There are some limitations to the current study: the sample size is small (though comparable to previous studies on reproducibility), reflecting challenges in recruiting patients for a second study that they perceive confers no additional benefit. About 50% of the patients who were originally screened to take part in the study declined due to the different components of the study, which they perceived as invasive (serial biopsies and blood sampling). On the other hand, the current experiment is the first study in literature to provide a comprehensive assessment on reproducibility of DCE-CT perfusion parameters with two different volumes in rectal cancers at baseline also provide an insight into association of these parameters with clinical markers and long-term prognosis.

6.4.5 Conclusion

The current study shows that coverage volume influences the reproducibility of DCE-CT parameters due to spatial and temporal fluctuation in vascular parameters. Whole tumour analysis may provide assessment of vascular heterogeneity in rectal cancers but may not necessarily improve reproducibility over and above smaller volume coverage. The DCE-CT parameters decline after NCRT in responsive tumours, whilst persistent BV and PS (angiogenic activity) after NCRT correlate with biologically aggressive tumours with early nodal disease and recurrence.

7 CHAPTER 7: CONCLUSIONS

The current work presented in this thesis demonstrates the first prospective report on the biological behaviour of rectal cancers to standard therapy. The experiments showed alteration in the DNA repair profiles, tumour cellularity, tumour hypoxic blood volumes, and functional vascularity in locally advance rectal cancer during the interval between neoadjuvant chemoradiotherapy and curative surgery with notable clinical correlations.

7.1 Hypothesis and results

"We believe that effects of NCRT are time-limited and aggressive rectal cancers can overcome the effects of NCRT after certain time by repairing their DNA and re-generating functional vascularity"

The primary mechanism of NCRT is cell death by DNA damage. The DNA repair analysis confirmed the effects of NCRT to be time-limited: comet assay analysis of rectal cancers showed that the DNA demonstrates poor repair profiles until six weeks post-NCRT, thereafter, the residual tumour load at pre-operative stage had comparable DNA repair properties to the baseline samples (see figure 4.4). Interestingly, all viable tumour cells harvested at different time points showed a tendency towards repair however impaired on timed-comet assay analysis (see figure 4.11). Hence, at the time of surgery, the residual tumour load had cells with intact DNA repair mechanism. These tumour cells may either represent radioresistent fraction within original tumour or a new populations of cells with enhanced DNA repair.

The oxygen radicals generated by NCRT may also disrupts tumour microvasculature. Functional imaging did not show regeneration of functional vascularity. There seems to be a steady decline in microcirculation until surgery, however, the findings do indicate rearrangement of cells around available blood supply to improve oxygenation (see below).

"We believe that after NCRT, there are functional changes in rectal cancer tissues, such as cellularity, hypoxic foci and functional vascularity, which may be detectable with functional imaging techniques."

There were many relevant changes detectable on functional imaging that appeared before morphological changes seen on conventional imaging techniques. Immediately after NCRT, there was an acute drop in blood reaching tumour cells (decreased BF) affecting the volume of blood within tumour tissue (decreased BV) and exchange of nutrients at endothelial level (drop in PS, K^{trans}/$IAUGC_{60}$ and k_{ep}), indicating vascular disruption. There were corresponding rise in ADC and v_e suggesting cell destruction and increased extracellular extravascular space. The acute increase in ADC and v_e may also represent tissue oedema after NCRT. Interestingly, there was only modest rise in tissue hypoxia (increase R_2*), indicating tumour cells around blood vessels are able to maintain oxygenation despite sharp changes in microcirculation. At sixth-week post-NCRT, the microcirculatory changes were incoherent: whilst the BF improved, there was only modest improvement in BV and PS and continued drop in K^{trans}/$IAUGC_{60}$ and k_{ep}, indicating that despite improvements in the amount of blood reaching the tumour tissue, there is poor exchange of nutrients at endothelial levels. This is further demonstrated by a rise in hypoxia levels

(increasing R_2*). The drop in ADC and v_e may at sixth-week post-NCRT may represented true level of cell destruction as tissue oedema subsides. At the pre-operative stage, the BF continues to recover, however, both BV and PS show decline similar to worsening K^{trans}/IAUGC$_{60}$ and k_{ep}, suggesting continual tumour devascularisation until surgery and formation of fibrosis. The rise is ADC also suggests further cell destruction. Interestingly, there is decline in v_e and improvement in the level of tumour hypoxia (R_2*), which may indicate concentration of residual tumour cells near blood vessels to improve survival. The improved hypoxia also indicate that surviving tumour cells are not entirely dependent on their own micro-environment.

"We believe that baseline and changes after NCRT in DNA repair properties, cellularity, hypoxic foci and functional vascularity may affect clinical outcomes"

The limited sample size means all clinical correlation present must be considered with caution. The experiments revealed interesting clinical correlations: the DNA repair analysis showed that rectal cancers with intact DNA repair on biopsy specimen also showed clinical downstaging or vice versa, hence the sample biopsied may not be representative of majority of tumour cell population, indicating tumour composition of cell populations with heterogeneous radiosensitivities. The R_2* and MRI-DCE parameter measurements provided vitals clues about tumour behaviours and aggressiveness: a pre-operative return of angiogenesis indicated higher potential for local recurrence, whereas pre-operative tumour cell hypoxia indicates higher potential for distant metastasis. The DCE-CT parameters

decline after NCRT in responsive tumours, whilst persistent angiogenic activity (stable BV and PS) after NCRT correlates with biologically aggressive tumours with early nodal disease and recurrence.

7.2 The optimal time to surgery

Based on the DNA repair analysis, the optimal time for surgery should fall between six-to-twelve weeks from completion of NCRT. This is based on the fact that NCRT mechanism of action is cell death by DNA damage with secondary disruption of microcirculation. Since the DNA repair profiles of rectal cancer show obvious impairment until six weeks after NCRT and thereafter imitates baselines values, surgical resection of tumour after six weeks would enable successful treatment.

The microcirculatory decline continues at pre-operative stage despite tumour cell regaining DNA repair mechanisms. Such observation indicate that tumour cell survival is not entirely dependent on its own micro-environment. Hence, the effect of NCRT continues on tumour microenvironment well after six weeks, but this observation would not affect timing of surgery. In theory, surviving cell fraction can potentiate tumour regrowth and re-establish their circulation with time. This is supported by studies showing higher risk of local recurrence in patients achieving pCR after NCRT who did not undergo curative surgery [501]. The microcirculatory changes do however provide vital insight into tumour biology and holds potential for future tumour staging and response assessment of novel therapeutics.

8 REFERENCES

1. *Bowel Cancer Incidence Statistics*. [Webpage] 2009 26/03/2012 [cited 2012; Available from: http://info.cancerresearchuk.org/cancerstats/types/bowel/incidence/uk-bowel-cancer-incidence-statistics.
2. Valentini, V., et al., *Multidisciplinary Rectal Cancer Management: 2nd European Rectal Cancer Consensus Conference (EURECA-CC2).* Radiother Oncol, 2009. **92**(2): p. 148-63.
3. Sauer, R., et al., *Preoperative versus postoperative chemoradiotherapy for rectal cancer.* The New England journal of medicine, 2004. **351**(17): p. 1731-40.
4. Hohenberger, P., *Locoregional recurrence of rectal cancer: biological and technical aspects of surgical failure.* Recent Results Cancer Res, 1998. **146**: p. 127-40.
5. Ghazi, S., et al., *Analysis of colorectal cancer morphology in relation to sex, age, location, and family history.* Journal of gastroenterology, 2012. **47**(6): p. 619-34.
6. Geraint T Williams, P.Q., Neil A Shepherd, *Standards and Datasets for Reporting Cancers*, T.R.C.o. Pathologists, Editor. 2007: United Kingdom.
7. Lopez-Kostner, F., et al., *Total mesorectal excision is not necessary for cancers of the upper rectum.* Surgery, 1998. **124**(4): p. 612-7; discussion 617-8.
8. Hwang, M.R., et al., *Prognostic impact of peritonealisation in rectal cancer treated with preoperative chemoradiotherapy: extraperitoneal versus intraperitoneal rectal cancer.* Radiotherapy and oncology : journal of the European Society for Therapeutic Radiology and Oncology, 2010. **94**(3): p. 353-8.
9. Chan, C.L., et al., *Local recurrence after curative resection for rectal cancer is associated with anterior position of the tumour.* The British journal of surgery, 2006. **93**(1): p. 105-12.
10. Lee, S.H., et al., *The effect of circumferential tumor location in clinical outcomes of rectal cancer patients treated with total mesorectal excision.* Dis Colon Rectum, 2005. **48**(12): p. 2249-57.
11. Wang, Z., et al., *Regional micrometastasis of low rectal cancer in mesorectum: a study utilizing HE stain on whole-mount section and ISH analyses on tissue microarray.* Cancer Invest, 2006. **24**(4): p. 374-81.
12. Jessup, J.M. and G.E. Gallick, *The biology of colorectal carcinoma.* Current problems in cancer, 1992. **16**(5): p. 261-328.
13. Topor, B., et al., *Mesorectal lymph nodes: their location and distribution within the mesorectum.* Dis Colon Rectum, 2003. **46**(6): p. 779-85.
14. Tan, K.Y., et al., *Improving prediction of lateral node spread in low rectal cancers--multivariate analysis of clinicopathological factors in 1,046 cases.* Langenbecks Arch Surg, 2010. **395**(5): p. 545-9.
15. Colombo, P.E., et al., *Clinical impact of lymph node status in rectal cancer.* Surg Oncol, 2011. **20**(4): p. e227-33.
16. Ding, P., et al., *Pulmonary recurrence predominates after combined modality therapy for rectal cancer: an original retrospective study.* Annals of surgery, 2012. **256**(1): p. 111-6.
17. Dukes, C.E., *The classification of cancer of the rectum.* The Journal of Pathology and Bacteriology, 1932. **35**(3): p. 323-332.
18. Sobin, L.H., M.K. Gospodarowicz, and C. Wittekind, *TNM classification of malignant tumours*. 7th ed. ed. 2010, Oxford: Wiley-Blackwell.

REFERENCES

19. Heald, R.J., E.M. Husband, and R.D. Ryall, *The mesorectum in rectal cancer surgery--the clue to pelvic recurrence?* Br J Surg, 1982. **69**(10): p. 613-6.

20. Daniels, I.R., et al., *Accurate staging, selective preoperative therapy and optimal surgery improves outcome in rectal cancer: a review of the recent evidence.* Colorectal Dis, 2007. **9**(4): p. 290-301.

21. Boras, Z., et al., *Prognostic factors of local recurrence and survival after curative rectal cancer surgery: a single institution experience.* Coll Antropol, 2012. **36**(4): p. 1355-61.

22. Koca, D., et al., *Prognostic factors affecting recurrence and survival in patients with locally advanced rectal cancer.* J BUON, 2012. **17**(2): p. 291-8.

23. Glasgow, S.C., et al., *Meta-analysis of histopathological features of primary colorectal cancers that predict lymph node metastases.* J Gastrointest Surg, 2012. **16**(5): p. 1019-28.

24. Burton, S., et al., *Predictive poor prognostic factors in colonic carcinoma.* Surg Oncol, 2006. **15**(2): p. 71-8.

25. Hassan, C., et al., *Histologic risk factors and clinical outcome in colorectal malignant polyp: a pooled-data analysis.* Dis Colon Rectum, 2005. **48**(8): p. 1588-96.

26. Rasheed, S., et al., *Can depth of tumour invasion predict lymph node positivity in patients undergoing resection for early rectal cancer? A comparative study between T1 and T2 cancers.* Colorectal Dis, 2008. **10**(3): p. 231-8.

27. Qiu, H.Z., et al., *Combination of differentiation and T stage can predict unresponsiveness to neoadjuvant therapy for rectal cancer.* Colorectal Dis, 2011. **13**(12): p. 1353-60.

28. Kumar, V., R.S. Cotran, and S.L. Robbins, *Robbins basic pathology*. 7th ed. ed. 2003, Philadelphia, Pa. ; London: Saunders.

29. Halvorsen, T.B. and E. Seim, *Association between invasiveness, inflammatory reaction, desmoplasia and survival in colorectal cancer.* J Clin Pathol, 1989. **42**(2): p. 162-6.

30. Compton, C.C., *Pathologic prognostic factors in the recurrence of rectal cancer.* Clin Colorectal Cancer, 2002. **2**(3): p. 149-60.

31. Zlobec, I., et al., *Tumor border configuration added to TNM staging better stratifies stage II colorectal cancer patients into prognostic subgroups.* Cancer, 2009. **115**(17): p. 4021-9.

32. Tanaka, M., et al., *Tumor budding at the invasive margin can predict patients at high risk of recurrence after curative surgery for stage II, T3 colon cancer.* Dis Colon Rectum, 2003. **46**(8): p. 1054-9.

33. Ueno, H., et al., *Tumour 'budding' as an index to estimate the potential of aggressiveness in rectal cancer.* Histopathology, 2002. **40**(2): p. 127-32.

34. Ueno, H., et al., *A new prognostic staging system for rectal cancer.* Ann Surg, 2004. **240**(5): p. 832-9.

35. Guzinska-Ustymowicz, K., *The role of tumour budding at the front of invasion and recurrence of rectal carcinoma.* Anticancer Res, 2005. **25**(2B): p. 1269-72.

36. Okuyama, T., M. Oya, and H. Ishikawa, *Budding as a risk factor for lymph node metastasis in pT1 or pT2 well-differentiated colorectal adenocarcinoma.* Dis Colon Rectum, 2002. **45**(5): p. 628-34.

37. Choi, H.J., et al., *Tumor budding as a prognostic marker in stage-III rectal carcinoma.* Int J Colorectal Dis, 2007. **22**(8): p. 863-8.

REFERENCES

38. Okuyama, T., T. Nakamura, and M. Yamaguchi, *Budding is useful to select high-risk patients in stage II well-differentiated or moderately differentiated colon adenocarcinoma.* Dis Colon Rectum, 2003. **46**(10): p. 1400-6.

39. Du, C., et al., *Morphology and prognostic value of tumor budding in rectal cancer after neoadjuvant radiotherapy.* Hum Pathol, 2012. **43**(7): p. 1061-7.

40. Jass, J.R., et al., *The grading of rectal cancer: historical perspectives and a multivariate analysis of 447 cases.* Histopathology, 1986. **10**(5): p. 437-59.

41. Katsumata, D., et al., *Depth of tumor invasion in locally advanced rectal cancer correlates with patients' prognosis: the usefulness of elastic stain for its measurement.* Surg Today, 2008. **38**(2): p. 115-22.

42. Shin, R., et al., *Depth of mesorectal extension has prognostic significance in patients with T3 rectal cancer.* Dis Colon Rectum, 2012. **55**(12): p. 1220-8.

43. Miyoshi, M., et al., *Extent of mesorectal tumor invasion as a prognostic factor after curative surgery for T3 rectal cancer patients.* Ann Surg, 2006. **243**(4): p. 492-8.

44. Merkel, S., et al., *The prognostic inhomogeneity in pT3 rectal carcinomas.* Int J Colorectal Dis, 2001. **16**(5): p. 298-304.

45. Akagi, Y., et al., *Predicting oncologic outcomes by stratifying mesorectal extension in patients with pT3 rectal cancer: a Japanese multi-institutional study.* Int J Cancer, 2012. **131**(5): p. 1220-7.

46. Nascimbeni, R.M.D.B., Lawrence J. M.D. 1; Nivatvongs, Santhat M.D. 1; Larson, Dirk R. M.S. , *Risk of Lymph Node Metastasis in T1 Carcinoma of the Colon and Rectum.* Diseases of the Colon & Rectum, 2002. **45**(2): p. 200-206.

47. Cawthorn, S.J., et al., *Extent of mesorectal spread and involvement of lateral resection margin as prognostic factors after surgery for rectal cancer.* Lancet, 1990. **335**(8697): p. 1055-9.

48. Schmoll, H.J., et al., *ESMO Consensus Guidelines for management of patients with colon and rectal cancer. a personalized approach to clinical decision making.* Ann Oncol, 2012. **23**(10): p. 2479-516.

49. Merkel, S., et al., *Prognostic subdivision of ypT3 rectal tumours according to extension beyond the muscularis propria.* Br J Surg, 2014. **101**(5): p. 566-72.

50. Quirke, P., et al., *Local recurrence of rectal adenocarcinoma due to inadequate surgical resection. Histopathological study of lateral tumour spread and surgical excision.* Lancet, 1986. **2**(8514): p. 996-9.

51. Peng, J.Y., Z.N. Li, and Y. Wang, *Risk factors for local recurrence following neoadjuvant chemoradiotherapy for rectal cancers.* World J Gastroenterol, 2013. **19**(32): p. 5227-37.

52. Wibe, A., et al., *Prognostic significance of the circumferential resection margin following total mesorectal excision for rectal cancer.* Br J Surg, 2002. **89**(3): p. 327-34.

53. Tilney, H.S., et al., *Factors affecting circumferential resection margin involvement after rectal cancer excision.* Dis Colon Rectum, 2007. **50**(1): p. 29-36.

54. den Dulk, M., et al., *The abdominoperineal resection itself is associated with an adverse outcome: the European experience based on a pooled analysis of five European randomised clinical trials on rectal cancer.* Eur J Cancer, 2009. **45**(7): p. 1175-83.

55. Battersby, N.J., et al., *MR imaging for rectal cancer: the role in staging the primary and response to neoadjuvant therapy.* Expert Rev Gastroenterol Hepatol, 2014. **8**(6): p. 703-19.

REFERENCES

56. Hall, N.R., et al., *Circumferential margin involvement after mesorectal excision of rectal cancer with curative intent. Predictor of survival but not local recurrence?* Dis Colon Rectum, 1998. **41**(8): p. 979-83.

57. Quirke, P. and M.F. Dixon, *The prediction of local recurrence in rectal adenocarcinoma by histopathological examination.* Int J Colorectal Dis, 1988. **3**(2): p. 127-31.

58. Birbeck, K.F., et al., *Rates of circumferential resection margin involvement vary between surgeons and predict outcomes in rectal cancer surgery.* Ann Surg, 2002. **235**(4): p. 449-57.

59. Adam, I.J., et al., *Role of circumferential margin involvement in the local recurrence of rectal cancer.* Lancet, 1994. **344**(8924): p. 707-11.

60. Arenas, R.B., et al., *Total mesenteric excision in the surgical treatment of rectal cancer: a prospective study.* Arch Surg, 1998. **133**(6): p. 608-11; discussion 611-2.

61. Bernstein, T.E., et al., *Circumferential resection margin as a prognostic factor in rectal cancer.* Br J Surg, 2009. **96**(11): p. 1348-57.

62. Kelly, S.B., et al., *Effect of the circumferential resection margin on survival following rectal cancer surgery.* Br J Surg, 2011. **98**(4): p. 573-81.

63. Nagtegaal, I.D. and P. Quirke, *What is the role for the circumferential margin in the modern treatment of rectal cancer?* J Clin Oncol, 2008. **26**(2): p. 303-12.

64. Kapiteijn, E., et al., *Preoperative radiotherapy combined with total mesorectal excision for resectable rectal cancer.* N Engl J Med, 2001. **345**(9): p. 638-46.

65. Nagtegaal, I.D., et al., *Circumferential margin involvement is still an important predictor of local recurrence in rectal carcinoma: not one millimeter but two millimeters is the limit.* Am J Surg Pathol, 2002. **26**(3): p. 350-7.

66. Marijnen, C.A., et al., *Radiotherapy does not compensate for positive resection margins in rectal cancer patients: report of a multicenter randomized trial.* Int J Radiat Oncol Biol Phys, 2003. **55**(5): p. 1311-20.

67. Trakarnsanga, A., et al., *What is the significance of the circumferential margin in locally advanced rectal cancer after neoadjuvant chemoradiotherapy?* Ann Surg Oncol, 2013. **20**(4): p. 1179-84.

68. Nakagoe, T., et al., *Distal intramural spread is an independent prognostic factor for distant metastasis and poor outcome in patients with rectal cancer: a multivariate analysis.* Ann Surg Oncol, 2003. **10**(2): p. 163-70.

69. Lazorthes, F., et al., *Distal intramural spread of carcinoma of the rectum correlated with lymph nodal involvement.* Surg Gynecol Obstet, 1990. **170**(1): p. 45-8.

70. Grinnell, R.S., *Distal intramural spread of carcinoma of the rectum and rectosigmoid.* Surg Gynecol Obstet, 1954. **99**(4): p. 421-30.

71. Shirouzu, K., H. Isomoto, and T. Kakegawa, *Distal spread of rectal cancer and optimal distal margin of resection for sphincter-preserving surgery.* Cancer, 1995. **76**(3): p. 388-92.

72. Mezhir, J.J., et al., *Presence of distal intramural spread after preoperative combined-modality therapy for adenocarcinoma of the rectum: what is now the appropriate distal resection margin?* Surgery, 2005. **138**(4): p. 658-63; discussion 663-4.

73. Vernava, A.M., 3rd, et al., *A prospective evaluation of distal margins in carcinoma of the rectum.* Surg Gynecol Obstet, 1992. **175**(4): p. 333-6.

74. Wang, H., et al., *Patterns of lymph node metastasis are different in colon and rectal carcinomas.* World J Gastroenterol, 2010. **16**(42): p. 5375-9.

75. Tang, R., et al., *Survival impact of lymph node metastasis in TNM stage III carcinoma of the colon and rectum.* J Am Coll Surg, 1995. **180**(6): p. 705-12.

REFERENCES

76. Brown, G., et al., *Morphologic predictors of lymph node status in rectal cancer with use of high-spatial-resolution MR imaging with histopathologic comparison.* Radiology, 2003. **227**(2): p. 371-7.

77. Eriksen, M.T., et al., *Prognostic groups in 1,676 patients with T3 rectal cancer treated without preoperative radiotherapy.* Dis Colon Rectum, 2007. **50**(2): p. 156-67.

78. Valentini, V., et al., *Does downstaging predict improved outcome after preoperative chemoradiation for extraperitoneal locally advanced rectal cancer? A long-term analysis of 165 patients.* Int J Radiat Oncol Biol Phys, 2002. **53**(3): p. 664-74.

79. Vather, R., et al., *Quantitative lymph node evaluation as an independent marker of long-term prognosis in stage III rectal cancer.* ANZ J Surg, 2011. **81**(12): p. 883-8.

80. Szynglarewicz, B., et al., *Predictive value of lymphocytic infiltration and character of invasive margin following total mesorectal excision with sphincter preservation for the high-risk carcinoma of the rectum.* Adv Med Sci, 2007. **52**: p. 159-63.

81. Habr-Gama, A., et al., *Absence of lymph nodes in the resected specimen after radical surgery for distal rectal cancer and neoadjuvant chemoradiation therapy: what does it mean?* Dis Colon Rectum, 2008. **51**(3): p. 277-83.

82. Onaitis, M.W., et al., *Neoadjuvant chemoradiation for rectal cancer: analysis of clinical outcomes from a 13-year institutional experience.* Ann Surg, 2001. **233**(6): p. 778-85.

83. Beresford, M., et al., *The reliability of lymph-node staging in rectal cancer after preoperative chemoradiotherapy.* Clin Oncol (R Coll Radiol), 2005. **17**(6): p. 448-55.

84. Tepper, J.E., et al., *Impact of number of nodes retrieved on outcome in patients with rectal cancer.* J Clin Oncol, 2001. **19**(1): p. 157-63.

85. Tranchart, H., et al., *What is the Incidence of Metastatic Lymph Node Involvement After Significant Pathologic Response of Primary Tumor Following Neoadjuvant Treatment for Locally Advanced Rectal Cancer?* Ann Surg Oncol, 2013. **20**(5): p. 1551-9.

86. Yeo, S.G., et al., *Pathologic complete response of primary tumor following preoperative chemoradiotherapy for locally advanced rectal cancer: long-term outcomes and prognostic significance of pathologic nodal status (KROG 09-01).* Ann Surg, 2010. **252**(6): p. 998-1004.

87. Talbot, I.C., et al., *The clinical significance of invasion of veins by rectal cancer.* Br J Surg, 1980. **67**(6): p. 439-42.

88. Knudsen, J.B., et al., *Venous and nerve invasion as prognostic factors in postoperative survival of patients with resectable cancer of the rectum.* Dis Colon Rectum, 1983. **26**(9): p. 613-7.

89. Gunther, K., et al., *Prediction of distant metastases after curative surgery for rectal cancer.* J Surg Res, 2002. **103**(1): p. 68-78.

90. Bayar, S., et al., *Venous invasion may predict lymph node metastasis in early rectal cancer.* Eur J Surg Oncol, 2002. **28**(4): p. 413-7.

91. Horn, A., O. Dahl, and I. Morild, *Venous and neural invasion as predictors of recurrence in rectal adenocarcinoma.* Dis Colon Rectum, 1991. **34**(9): p. 798-804.

92. Kanemitsu, Y., et al., *Prediction of residual disease or distant metastasis after resection of locally recurrent rectal cancer.* Dis Colon Rectum, 2010. **53**(5): p. 779-89.

93. Uemura, M., et al., *The features of late local recurrences following curative surgery for rectal cancer.* Hepatogastroenterology, 2012. **59**(118): p. 1800-3.

94. Dresen, R.C., et al., *Local recurrence in rectal cancer can be predicted by histopathological factors.* Eur J Surg Oncol, 2009. **35**(10): p. 1071-7.

REFERENCES

95. Sejben, I., R. Bori, and G. Cserni, *Venous invasion demonstrated by orcein staining of colorectal carcinoma specimens is associated with the development of distant metastasis.* J Clin Pathol, 2010. **63**(7): p. 575-8.

96. Bokey, E.L., et al., *Factors affecting survival after excision of the rectum for cancer: a multivariate analysis.* Dis Colon Rectum, 1997. **40**(1): p. 3-10.

97. Carrara, A., et al., *Analysis of risk factors for lymph nodal involvement in early stages of rectal cancer: when can local excision be considered an appropriate treatment? Systematic review and meta-analysis of the literature.* Int J Surg Oncol, 2012. **2012**: p. 438450.

98. Peng, J., et al., *Perineural invasion in pT3N0 rectal cancer: the incidence and its prognostic effect.* Cancer, 2011. **117**(7): p. 1415-21.

99. Kim, N.K., et al., *Factors associated with local recurrence after neoadjuvant chemoradiation with total mesorectal excision for rectal cancer.* World J Surg, 2009. **33**(8): p. 1741-9.

100. Horn, A., O. Dahl, and I. Morild, *The role of venous and neural invasion on survival in rectal adenocarcinoma.* Dis Colon Rectum, 1990. **33**(7): p. 598-601.

101. Krebs, B., et al., *Prognostic value of additional pathological variables for long-term survival after curative resection of rectal cancer.* World J Gastroenterol, 2006. **12**(28): p. 4565-8.

102. Shirouzu, K., H. Isomoto, and T. Kakegawa, *Prognostic evaluation of perineural invasion in rectal cancer.* Am J Surg, 1993. **165**(2): p. 233-7.

103. Silberfein, E.J., et al., *Long-term survival and recurrence outcomes following surgery for distal rectal cancer.* Ann Surg Oncol, 2010. **17**(11): p. 2863-9.

104. Dworak, O., L. Keilholz, and A. Hoffmann, *Pathological features of rectal cancer after preoperative radiochemotherapy.* Int J Colorectal Dis, 1997. **12**(1): p. 19-23.

105. Mandard, A.M., et al., *Pathologic assessment of tumor regression after preoperative chemoradiotherapy of esophageal carcinoma. Clinicopathologic correlations.* Cancer, 1994. **73**(11): p. 2680-6.

106. Munro, A.J., S. Lain, and D.P. Lane, *P53 abnormalities and outcomes in colorectal cancer: a systematic review.* Br J Cancer, 2005. **92**(3): p. 434-44.

107. Russo, A., et al., *The TP53 colorectal cancer international collaborative study on the prognostic and predictive significance of p53 mutation: influence of tumor site, type of mutation, and adjuvant treatment.* J Clin Oncol, 2005. **23**(30): p. 7518-28.

108. Suzuki, T., et al., *Biopsy specimens obtained 7 days after starting chemoradiotherapy (CRT) provide reliable predictors of response to CRT for rectal cancer.* Int J Radiat Oncol Biol Phys, 2013. **85**(5): p. 1232-8.

109. Komuro, Y., et al., *Evaluating the combination of molecular prognostic factors in tumor radiosensitivity in rectal cancer.* Hepatogastroenterology, 2005. **52**(63): p. 666-71.

110. Qiu, H., et al., *Molecular prognostic factors in rectal cancer treated by radiation and surgery.* Dis Colon Rectum, 2000. **43**(4): p. 451-9.

111. Edden, Y., S.D. Wexner, and M. Berho, *The use of molecular markers as a method to predict the response to neoadjuvant therapy for advanced stage rectal adenocarcinoma.* Colorectal Dis, 2012. **14**(5): p. 555-61.

112. Huerta, S., et al., *Tissue microarray constructs to predict a response to chemoradiation in rectal cancer.* Dig Liver Dis, 2010. **42**(10): p. 679-84.

113. Negri, F.V., et al., *Biological predictive factors in rectal cancer treated with preoperative radiotherapy or radiochemotherapy.* Br J Cancer, 2008. **98**(1): p. 143-7.

REFERENCES

114. Peng, J.J., et al., *Predicting prognosis of rectal cancer patients with total mesorectal excision using molecular markers.* World J Gastroenterol, 2007. **13**(21): p. 3009-15.

115. Kudrimoti, M., et al., *Genetic markers predictive of response to induction chemoradiotherapy for locally advanced rectal cancers.* J Ky Med Assoc, 2007. **105**(1): p. 18-22.

116. Ismail, H.M., et al., *Clinico-Pathological and Prognostic Significance of p53, Bcl-2 and Her-2/neu Protein Markers in Colorectal Cancer Using Tissue Microarray.* J Egypt Natl Canc Inst, 2007. **19**(1): p. 3-14.

117. Hilska, M., et al., *The significance of tumor markers for proliferation and apoptosis in predicting survival in colorectal cancer.* Dis Colon Rectum, 2005. **48**(12): p. 2197-208.

118. Saigusa, S., et al., *Gene expression profiles of tumor regression grade in locally advanced rectal cancer after neoadjuvant chemoradiotherapy.* Oncol Rep, 2012. **28**(3): p. 855-61.

119. Fucini, C., et al., *Apoptotic proteins as prognostic markers and indicators of radiochemosensitivity in stage II/III rectal cancers.* Colorectal Dis, 2012. **14**(2): p. e64-71.

120. Chang, H.J., et al., *Bax, a predictive marker for therapeutic response to preoperative chemoradiotherapy in patients with rectal carcinoma.* Hum Pathol, 2005. **36**(4): p. 364-71.

121. Nehls, O., et al., *Low BAX protein expression correlates with disease recurrence in preoperatively irradiated rectal carcinoma.* Int J Radiat Oncol Biol Phys, 2005. **61**(1): p. 85-91.

122. Ozden, S.A., et al., *Prognostic role of sensitive-to-apoptosis gene expression in rectal cancer.* World J Gastroenterol, 2011. **17**(44): p. 4905-10.

123. Contu, P.C., S.S. Contu, and L.F. Moreira, *Bcl-2 expression in rectal cancer.* Arq Gastroenterol, 2006. **43**(4): p. 284-7.

124. Cascinu, S., et al., *An analysis of p53, BAX and vascular endothelial growth factor expression in node-positive rectal cancer. Relationships with tumour recurrence and event-free survival of patients treated with adjuvant chemoradiation.* Br J Cancer, 2002. **86**(5): p. 744-9.

125. Willett, C.G., et al., *Changes in tumor proliferation of rectal cancer induced by preoperative 5-fluorouracil and irradiation.* Dis Colon Rectum, 1998. **41**(1): p. 62-7.

126. Kikuchi, M., et al., *High Ki67, Bax, and thymidylate synthase expression well correlates with response to chemoradiation therapy in locally advanced rectal cancers: proposal of a logistic model for prediction.* Br J Cancer, 2009. **101**(1): p. 116-23.

127. Yan, H., et al., *Predictive value of Smac, VEGF and Ki-67 in rectal cancer treated with neoadjuvant therapy.* Oncol Lett, 2010. **1**(4): p. 641-647.

128. Debucquoy, A., et al., *Morphological features and molecular markers in rectal cancer from 95 patients included in the European Organisation for Research and Treatment of Cancer 22921 trial: prognostic value and effects of preoperative radio (chemo) therapy.* Eur J Cancer, 2008. **44**(6): p. 791-7.

129. Terzi, C., et al., *Survivin, p53, and Ki-67 as predictors of histopathologic response in locally advanced rectal cancer treated with preoperative chemoradiotherapy.* Int J Colorectal Dis, 2008. **23**(1): p. 37-45.

130. Debucquoy, A., et al., *Molecular responses of rectal cancer to preoperative chemoradiation.* Radiother Oncol, 2006. **80**(2): p. 172-7.

REFERENCES

131. Reerink, O., et al., *Molecular prognostic factors in locally irresectable rectal cancer treated preoperatively by chemo-radiotherapy.* Anticancer Res, 2004. **24**(2C): p. 1217-21.

132. Smith, F.M., et al., *Pathological and molecular predictors of the response of rectal cancer to neoadjuvant radiochemotherapy.* Eur J Surg Oncol, 2006. **32**(1): p. 55-64.

133. Shinto, E., et al., *Pretreatment CD133 and cyclooxygenase-2 expression as the predictive markers of the pathological effect of chemoradiotherapy in rectal cancer patients.* Dis Colon Rectum, 2011. **54**(9): p. 1098-106.

134. Min, B.S., et al., *Cyclooxygenase-2 expression in pretreatment biopsy as a predictor of tumor responses after preoperative chemoradiation in rectal cancer.* Arch Surg, 2008. **143**(11): p. 1091-7; discussion 1097.

135. Kobayashi, H., et al., *Absence of cyclooxygenase-2 protein expression is a predictor of tumor regression in rectal cancer treated with preoperative short-term chemoradiotherapy.* Dis Colon Rectum, 2007. **50**(9): p. 1354-62.

136. de Heer, P., et al., *Cyclooxygenase 2 expression in rectal cancer is of prognostic significance in patients receiving preoperative radiotherapy.* Clin Cancer Res, 2007. **13**(10): p. 2955-60.

137. Kim, J.W., et al., *Molecular markers predict distant metastases after adjuvant chemoradiation for rectal cancer.* Int J Radiat Oncol Biol Phys, 2012. **84**(5): p. e577-84.

138. Yang, D., et al., *Gene expression levels of epidermal growth factor receptor, survivin, and vascular endothelial growth factor as molecular markers of lymph node involvement in patients with locally advanced rectal cancer.* Clin Colorectal Cancer, 2006. **6**(4): p. 305-11.

139. Takasu, C., et al., *Survivin expression can predict the effect of chemoradiotherapy for advanced lower rectal cancer.* Int J Clin Oncol, 2012.

140. Kim, K., et al., *High survivin expression as a predictor of poor response to preoperative chemoradiotherapy in locally advanced rectal cancer.* Int J Colorectal Dis, 2011. **26**(8): p. 1019-23.

141. Sprenger, T., et al., *Failure of downregulation of survivin following neoadjuvant radiochemotherapy in rectal cancer is associated with distant metastases and shortened survival.* Clin Cancer Res, 2011. **17**(6): p. 1623-31.

142. Knutsen, A., G. Adell, and X.F. Sun, *Survivin expression is an independent prognostic factor in rectal cancer patients with and without preoperative radiotherapy.* Int J Radiat Oncol Biol Phys, 2004. **60**(1): p. 149-55.

143. Choi, S.W. and J.B. Mason, *Folate and carcinogenesis: an integrated scheme.* J Nutr, 2000. **130**(2): p. 129-32.

144. Longley, D.B., D.P. Harkin, and P.G. Johnston, *5-fluorouracil: mechanisms of action and clinical strategies.* Nat Rev Cancer, 2003. **3**(5): p. 330-8.

145. Pullarkat, S.T., et al., *Thymidylate synthase gene polymorphism determines response and toxicity of 5-FU chemotherapy.* Pharmacogenomics J, 2001. **1**(1): p. 65-70.

146. Jakob, C., et al., *Thymidylate synthase, thymidine phosphorylase, dihydropyrimidine dehydrogenase expression, and histological tumour regression after 5-FU-based neo-adjuvant chemoradiotherapy in rectal cancer.* J Pathol, 2004. **204**(5): p. 562-8.

147. Jakob, C., et al., *Immunohistochemical analysis of thymidylate synthase, thymidine phosphorylase, and dihydropyrimidine dehydrogenase in rectal cancer (cUICC II/III): correlation with histopathologic tumor regression after 5-fluorouracil-based long-term neoadjuvant chemoradiotherapy.* Am J Surg Pathol, 2005. **29**(10): p. 1304-9.

148. Carlomagno, C., et al., *Predictive factors of complete response to neoadjuvant chemoradiotherapy in patients with rectal cancer.* Oncology, 2010. **78**(5-6): p. 369-75.

REFERENCES

149. Paez, D., et al., *Pharmacogenetic study in rectal cancer patients treated with preoperative chemoradiotherapy: polymorphisms in thymidylate synthase, epidermal growth factor receptor, GSTP1, and DNA repair genes.* Int J Radiat Oncol Biol Phys, 2011. **81**(5): p. 1319-27.

150. Tanaka, K., et al., *TS and DPD mRNA levels on formalin-fixed paraffin-embedded specimens as predictors for distant recurrence of rectal cancer treated with preoperative chemoradiotherapy.* J Surg Oncol, 2012. **105**(6): p. 529-34.

151. Conradi, L.C., et al., *Thymidylate synthase as a prognostic biomarker for locally advanced rectal cancer after multimodal treatment.* Ann Surg Oncol, 2011. **18**(9): p. 2442-52.

152. Chang, Y.Y., et al., *Mutation spectra of RAS gene family in colorectal cancer.* Am J Surg, 2016. **212**(3): p. 537-544 e3.

153. Berardi, R., et al., *Locally advanced rectal cancer: from molecular profiling to clinical practice. A literature review: Part 2.* Expert Opin Pharmacother, 2009. **10**(15): p. 2467-78.

154. Karapetis, C.S., et al., *K-ras mutations and benefit from cetuximab in advanced colorectal cancer.* N Engl J Med, 2008. **359**(17): p. 1757-65.

155. Helbling, D., et al., *Neoadjuvant chemoradiotherapy with or without panitumumab in patients with wild-type KRAS, locally advanced rectal cancer (LARC): a randomized, multicenter, phase II trial SAKK 41/07.* Ann Oncol, 2013. **24**(3): p. 718-25.

156. Lievre, A., et al., *KRAS mutation status is predictive of response to cetuximab therapy in colorectal cancer.* Cancer Res, 2006. **66**(8): p. 3992-5.

157. Demes, M., et al., *Signature of microsatellite instability, KRAS and BRAF gene mutations in German patients with locally advanced rectal adenocarcinoma before and after neoadjuvant 5-FU radiochemotherapy.* J Gastrointest Oncol, 2013. **4**(2): p. 182-92.

158. Clancy, C., J.P. Burke, and J.C. Coffey, *KRAS mutation does not predict the efficacy of neo-adjuvant chemoradiotherapy in rectal cancer: a systematic review and meta-analysis.* Surg Oncol, 2013. **22**(2): p. 105-11.

159. Bengala, C., et al., *Prognostic role of EGFR gene copy number and KRAS mutation in patients with locally advanced rectal cancer treated with preoperative chemoradiotherapy.* Br J Cancer, 2010. **103**(7): p. 1019-24.

160. Gaedcke, J., et al., *KRAS and BRAF mutations in patients with rectal cancer treated with preoperative chemoradiotherapy.* Radiother Oncol, 2010. **94**(1): p. 76-81.

161. Derbel, O., et al., *Impact of KRAS, BRAF and PI3KCA mutations in rectal carcinomas treated with neoadjuvant radiochemotherapy and surgery.* BMC Cancer, 2013. **13**: p. 200.

162. Lai, C.Y., et al., *Associations Between Genetic Polymorphisms of Epidermal Growth Factor Receptor (EGFR) and Survival of Colorectal Cancer (CRC) Patients Treated with 5-Fluorouracil-Based Chemotherapy.* Ann Surg Oncol, 2013.

163. Motlagh, A., et al., *Expression of epidermal growth factor receptor as a predictive factor for rectal cancer.* Arch Iran Med, 2007. **10**(3): p. 301-8.

164. Kim, J.S., et al., *Epidermal growth factor receptor as a predictor of tumor downstaging in locally advanced rectal cancer patients treated with preoperative chemoradiotherapy.* Int J Radiat Oncol Biol Phys, 2006. **66**(1): p. 195-200.

165. Giralt, J., et al., *The expression of epidermal growth factor receptor results in a worse prognosis for patients with rectal cancer treated with preoperative radiotherapy: a multicenter, retrospective analysis.* Radiother Oncol, 2005. **74**(2): p. 101-8.

REFERENCES

166. Ho-Pun-Cheung, A., et al., *EGFR and HER3 mRNA expression levels predict distant metastases in locally advanced rectal cancer.* Int J Cancer, 2011. **128**(12): p. 2938-46.

167. Azria, D., et al., *Prognostic impact of epidermal growth factor receptor (EGFR) expression on loco-regional recurrence after preoperative radiotherapy in rectal cancer.* BMC Cancer, 2005. **5**: p. 62.

168. Kopp, R., et al., *Reduced survival of rectal cancer patients with increased tumor epidermal growth factor receptor levels.* Dis Colon Rectum, 2003. **46**(10): p. 1391-9.

169. Bertolini, F., et al., *Prognostic and predictive value of baseline and posttreatment molecular marker expression in locally advanced rectal cancer treated with neoadjuvant chemoradiotherapy.* Int J Radiat Oncol Biol Phys, 2007. **68**(5): p. 1455-61.

170. Wagner, A.D., et al., *Anti-angiogenic therapies for metastatic colorectal cancer.* Cochrane Database Syst Rev, 2009(3): p. CD005392.

171. Folkman, J., *Tumor angiogenesis: therapeutic implications.* N Engl J Med, 1971. **285**(21): p. 1182-6.

172. Oklu, R., et al., *Angiogenesis and current antiangiogenic strategies for the treatment of cancer.* J Vasc Interv Radiol, 2010. **21**(12): p. 1791-805; quiz 1806.

173. O'Reilly, M.S., et al., *Angiostatin: a novel angiogenesis inhibitor that mediates the suppression of metastases by a Lewis lung carcinoma.* Cell, 1994. **79**(2): p. 315-28.

174. O'Reilly, M.S., et al., *Endostatin: an endogenous inhibitor of angiogenesis and tumor growth.* Cell, 1997. **88**(2): p. 277-85.

175. Bergers, G. and L.E. Benjamin, *Tumorigenesis and the angiogenic switch.* Nat Rev Cancer, 2003. **3**(6): p. 401-10.

176. Dameron, K.M., et al., *Control of angiogenesis in fibroblasts by p53 regulation of thrombospondin-1.* Science, 1994. **265**(5178): p. 1582-4.

177. Tong, R.T., et al., *Vascular normalization by vascular endothelial growth factor receptor 2 blockade induces a pressure gradient across the vasculature and improves drug penetration in tumors.* Cancer Res, 2004. **64**(11): p. 3731-6.

178. Nishida, N., et al., *Angiogenesis in cancer.* Vasc Health Risk Manag, 2006. **2**(3): p. 213-9.

179. Padera, T.P., et al., *Pathology: cancer cells compress intratumour vessels.* Nature, 2004. **427**(6976): p. 695.

180. Des Guetz, G., et al., *Microvessel density and VEGF expression are prognostic factors in colorectal cancer. Meta-analysis of the literature.* Br J Cancer, 2006. **94**(12): p. 1823-32.

181. Guedj, N., et al., *Predictors of tumor response after preoperative chemoradiotherapy for rectal adenocarcinomas.* Hum Pathol, 2011. **42**(11): p. 1702-9.

182. Sokmen, S., et al., *Prognostic significance of angiogenesis in rectal cancer: a morphometric investigation.* Anticancer Res, 2001. **21**(6B): p. 4341-8.

183. Saclarides, T.J., et al., *Tumor angiogenesis and rectal carcinoma.* Dis Colon Rectum, 1994. **37**(9): p. 921-6.

184. Takebayashi, Y., et al., *Angiogenesis as an unfavorable prognostic factor in human colorectal carcinoma.* Cancer, 1996. **78**(2): p. 226-31.

185. Vaupel, P., F. Kallinowski, and P. Okunieff, *Blood flow, oxygen and nutrient supply, and metabolic microenvironment of human tumors: a review.* Cancer Res, 1989. **49**(23): p. 6449-65.

REFERENCES

186. Jain, R.K., *Determinants of tumor blood flow: a review.* Cancer Res, 1988. **48**(10): p. 2641-58.

187. Skinner, S.A., G.M. Frydman, and P.E. O'Brien, *Microvascular structure of benign and malignant tumors of the colon in humans.* Dig Dis Sci, 1995. **40**(2): p. 373-84.

188. Hinganu, M.V., D. Hinganu, and L.L. Francu, *Microanatomic aspects of arterial blood supply in rectal carcinomas--predictive models.* Rom J Morphol Embryol, 2013. **54**(3): p. 561-5.

189. Hlatky, L., P. Hahnfeldt, and J. Folkman, *Clinical application of antiangiogenic therapy: microvessel density, what it does and doesn't tell us.* J Natl Cancer Inst, 2002. **94**(12): p. 883-93.

190. Kim, Y.E., et al., *Perfusion parameters of dynamic contrast-enhanced magnetic resonance imaging in patients with rectal cancer: correlation with microvascular density and vascular endothelial growth factor expression.* Korean J Radiol, 2013. **14**(6): p. 878-85.

191. Atkin, G., et al., *Dynamic contrast-enhanced magnetic resonance imaging is a poor measure of rectal cancer angiogenesis.* Br J Surg, 2006. **93**(8): p. 992-1000.

192. Ahn, S.J., et al., *Correlations of 3T DCE-MRI quantitative parameters with microvessel density in a human-colorectal-cancer xenograft mouse model.* Korean J Radiol, 2011. **12**(6): p. 722-30.

193. Rau, B., et al., *Accuracy of endorectal ultrasound after preoperative radiochemotherapy in locally advanced rectal cancer.* Surg Endosc, 1999. **13**(10): p. 980-4.

194. Ashraf, S., et al., *A critical appraisal of endorectal ultrasound and transanal endoscopic microsurgery and decision-making in early rectal cancer.* Colorectal Dis, 2012. **14**(7): p. 821-6.

195. Brown, G., et al., *Preoperative assessment of prognostic factors in rectal cancer using high-resolution magnetic resonance imaging.* Br J Surg, 2003. **90**(3): p. 355-64.

196. Group, M.S., *Extramural depth of tumor invasion at thin-section MR in patients with rectal cancer: results of the MERCURY study.* Radiology, 2007. **243**(1): p. 132-9.

197. Group, M.S., *Diagnostic accuracy of preoperative magnetic resonance imaging in predicting curative resection of rectal cancer: prospective observational study.* BMJ, 2006. **333**(7572): p. 779.

198. Smith, N.J., et al., *Prognostic significance of magnetic resonance imaging-detected extramural vascular invasion in rectal cancer.* Br J Surg, 2008. **95**(2): p. 229-36.

199. Koh, D.M., et al., *The Relationship Between MR Demonstration of Extramural Venous Invasion and Nodal Disease in Rectal Cancer.* Clin Med Oncol, 2008. **2**: p. 267-73.

200. Yu, S.K., et al., *MRI predictive factors for tumor response in rectal cancer following neoadjuvant chemoradiation therapy--implications for induction chemotherapy?* Int J Radiat Oncol Biol Phys, 2013. **87**(3): p. 505-11.

201. Das, P., et al., *Predictors of tumor response and downstaging in patients who receive preoperative chemoradiation for rectal cancer.* Cancer, 2007. **109**(9): p. 1750-5.

202. Salerno, G.V., et al., *Magnetic resonance imaging prediction of an involved surgical resection margin in low rectal cancer.* Dis Colon Rectum, 2009. **52**(4): p. 632-9.

203. Chen, C.C., et al., *How accurate is magnetic resonance imaging in restaging rectal cancer in patients receiving preoperative combined chemoradiotherapy?* Dis Colon Rectum, 2005. **48**(4): p. 722-8.

204. Allen, S.D., et al., *Rectal carcinoma: MRI with histologic correlation before and after chemoradiation therapy.* AJR Am J Roentgenol, 2007. **188**(2): p. 442-51.

REFERENCES

205. Barbaro, B., et al., *Locally advanced rectal cancer: MR imaging in prediction of response after preoperative chemotherapy and radiation therapy.* Radiology, 2009. **250**(3): p. 730-9.

206. Eisenhauer, E.A., et al., *New response evaluation criteria in solid tumours: revised RECIST guideline (version 1.1).* Eur J Cancer, 2009. **45**(2): p. 228-47.

207. Patel, U.B., et al., *Magnetic resonance imaging-detected tumor response for locally advanced rectal cancer predicts survival outcomes: MERCURY experience.* J Clin Oncol, 2011. **29**(28): p. 3753-60.

208. *Improved survival with preoperative radiotherapy in resectable rectal cancer. Swedish Rectal Cancer Trial.* N Engl J Med, 1997. **336**(14): p. 980-7.

209. Folkesson, J., et al., *Swedish Rectal Cancer Trial: long lasting benefits from radiotherapy on survival and local recurrence rate.* J Clin Oncol, 2005. **23**(24): p. 5644-50.

210. Peeters, K.C., et al., *The TME trial after a median follow-up of 6 years: increased local control but no survival benefit in irradiated patients with resectable rectal carcinoma.* Ann Surg, 2007. **246**(5): p. 693-701.

211. van Gijn, W., et al., *Preoperative radiotherapy combined with total mesorectal excision for resectable rectal cancer: 12-year follow-up of the multicentre, randomised controlled TME trial.* Lancet Oncol, 2011. **12**(6): p. 575-82.

212. Sebag-Montefiore, D., et al., *Preoperative radiotherapy versus selective postoperative chemoradiotherapy in patients with rectal cancer (MRC CR07 and NCIC-CTG C016): a multicentre, randomised trial.* Lancet, 2009. **373**(9666): p. 811-20.

213. Frykholm, G.J., B. Glimelius, and L. Pahlman, *Preoperative or postoperative irradiation in adenocarcinoma of the rectum: final treatment results of a randomized trial and an evaluation of late secondary effects.* Dis Colon Rectum, 1993. **36**(6): p. 564-72.

214. Bosset, J.F., et al., *Chemotherapy with preoperative radiotherapy in rectal cancer.* N Engl J Med, 2006. **355**(11): p. 1114-23.

215. Bosset, J.F., et al., *Fluorouracil-based adjuvant chemotherapy after preoperative chemoradiotherapy in rectal cancer: long-term results of the EORTC 22921 randomised study.* Lancet Oncol, 2014. **15**(2): p. 184-90.

216. Gerard, J.P., et al., *Preoperative radiotherapy with or without concurrent fluorouracil and leucovorin in T3-4 rectal cancers: results of FFCD 9203.* J Clin Oncol, 2006. **24**(28): p. 4620-5.

217. Sauer, R., et al., *Preoperative versus postoperative chemoradiotherapy for rectal cancer.* N Engl J Med, 2004. **351**(17): p. 1731-40.

218. Bujko, K., et al., *Sphincter preservation following preoperative radiotherapy for rectal cancer: report of a randomised trial comparing short-term radiotherapy vs. conventionally fractionated radiochemotherapy.* Radiother Oncol, 2004. **72**(1): p. 15-24.

219. Bujko, K., et al., *Long-term results of a randomized trial comparing preoperative short-course radiotherapy with preoperative conventionally fractionated chemoradiation for rectal cancer.* Br J Surg, 2006. **93**(10): p. 1215-23.

220. Ngan, S.Y., et al., *Randomized trial of short-course radiotherapy versus long-course chemoradiation comparing rates of local recurrence in patients with T3 rectal cancer: Trans-Tasman Radiation Oncology Group trial 01.04.* J Clin Oncol, 2012. **30**(31): p. 3827-33.

REFERENCES

221. Wong, R.K., et al., *Pre-operative radiotherapy and curative surgery for the management of localized rectal carcinoma.* Cochrane Database Syst Rev, 2007(2): p. CD002102.

222. Glimelius, B., et al., *A systematic overview of radiation therapy effects in rectal cancer.* Acta Oncol, 2003. **42**(5-6): p. 476-92.

223. Munro, A.J. and A.H.M. Bentley, *Adjuvant radiotherapy in operable rectal cancer: A systematic review.* Seminars in Colon and Rectal Surgery. **13**(1): p. 31-42.

224. Camma, C., et al., *Preoperative radiotherapy for resectable rectal cancer: A meta-analysis.* JAMA, 2000. **284**(8): p. 1008-15.

225. Colorectal Cancer Collaborative, G., *Adjuvant radiotherapy for rectal cancer: a systematic overview of 8,507 patients from 22 randomised trials.* Lancet, 2001. **358**(9290): p. 1291-304.

226. Francois, Y., et al., *Influence of the interval between preoperative radiation therapy and surgery on downstaging and on the rate of sphincter-sparing surgery for rectal cancer: the Lyon R90-01 randomized trial.* J Clin Oncol, 1999. **17**(8): p. 2396.

227. Glehen, O., et al., *Long-term results of the Lyons R90-01 randomized trial of preoperative radiotherapy with delayed surgery and its effect on sphincter-saving surgery in rectal cancer.* Br J Surg, 2003. **90**(8): p. 996-8.

228. Pettersson, D., et al., *Tumour regression in the randomized Stockholm III Trial of radiotherapy regimens for rectal cancer.* Br J Surg, 2015. **102**(8): p. 972-8; discussion 978.

229. Latkauskas, T., et al., *Initial results of a randomized controlled trial comparing clinical and pathological downstaging of rectal cancer after preoperative short-course radiotherapy or long-term chemoradiotherapy, both with delayed surgery.* Colorectal Dis, 2012. **14**(3): p. 294-8.

230. Heald, R.J. and R.D. Ryall, *Recurrence and survival after total mesorectal excision for rectal cancer.* Lancet, 1986. **1**(8496): p. 1479-82.

231. Wang, Z., et al., *Microscopic spread of low rectal cancer in regions of mesorectum: pathologic assessment with whole-mount sections.* World J Gastroenterol, 2004. **10**(20): p. 2949-53.

232. Bernstein, T.E., et al., *Improved local control of rectal cancer reduces distant metastases.* Colorectal Dis, 2012. **14**(10): p. e668-78.

233. Martling, A., et al., *The surgeon as a prognostic factor after the introduction of total mesorectal excision in the treatment of rectal cancer.* Br J Surg, 2002. **89**(8): p. 1008-13.

234. Tekkis, P.P., et al., *Comparison of circumferential margin involvement between restorative and nonrestorative resections for rectal cancer.* Colorectal Dis, 2005. **7**(4): p. 369-74.

235. Marr, R., et al., *The modern abdominoperineal excision: the next challenge after total mesorectal excision.* Ann Surg, 2005. **242**(1): p. 74-82.

236. West, N.P., et al., *Multicentre experience with extralevator abdominoperineal excision for low rectal cancer.* Br J Surg, 2010. **97**(4): p. 588-99.

237. Phillips, R.K.S.e.o.c. and S.M.D.e.o.c. Clark, *Colorectal surgery*. Fifth edition. ed.

238. Rodel, C., et al., *Prognostic significance of tumor regression after preoperative chemoradiotherapy for rectal cancer.* J Clin Oncol, 2005. **23**(34): p. 8688-96.

239. Foster, J.D., et al., *Timing of surgery after long-course neoadjuvant chemoradiotherapy for rectal cancer: a systematic review of the literature.* Dis Colon Rectum, 2013. **56**(7): p. 921-30.

REFERENCES

240. Kim, J.J. and I.F. Tannock, *Repopulation of cancer cells during therapy: an important cause of treatment failure.* Nat Rev Cancer, 2005. **5**(7): p. 516-25.

241. Hlushchuk, R., et al., *Tumor recovery by angiogenic switch from sprouting to intussusceptive angiogenesis after treatment with PTK787/ZK222584 or ionizing radiation.* Am J Pathol, 2008. **173**(4): p. 1173-85.

242. Coffey, J.C., et al., *Excisional surgery for cancer cure: therapy at a cost.* Lancet Oncol, 2003. **4**(12): p. 760-8.

243. Ajithkumar, T.V., *Oncology*. 2011, Oxford: Oxford University Press.

244. Mathews, L.A., S.M. Cabarcas, and E.M. Hurt, *DNA repair of cancer stem cells*. 2013, Dordrecht: Springer.

245. Helleday, T., et al., *DNA double-strand break repair: from mechanistic understanding to cancer treatment.* DNA Repair (Amst), 2007. **6**(7): p. 923-35.

246. Collins, A.R., *The comet assay for DNA damage and repair: principles, applications, and limitations.* Mol Biotechnol, 2004. **26**(3): p. 249-61.

247. Ostling, O. and K.J. Johanson, *Microelectrophoretic study of radiation-induced DNA damages in individual mammalian cells.* Biochem Biophys Res Commun, 1984. **123**(1): p. 291-8.

248. Singh, N.P., et al., *A simple technique for quantitation of low levels of DNA damage in individual cells.* Exp Cell Res, 1988. **175**(1): p. 184-91.

249. Olive, P.L., J.P. Banath, and R.E. Durand, *Heterogeneity in radiation-induced DNA damage and repair in tumor and normal cells measured using the "comet" assay.* Radiat Res, 1990. **122**(1): p. 86-94.

250. Moller, P., *The alkaline comet assay: towards validation in biomonitoring of DNA damaging exposures.* Basic Clin Pharmacol Toxicol, 2006. **98**(4): p. 336-45.

251. Moller, P., et al., *Assessment and reduction of comet assay variation in relation to DNA damage: studies from the European Comet Assay Validation Group.* Mutagenesis, 2010. **25**(2): p. 109-11.

252. Sasaki, Y.F., et al., *The comet assay with multiple mouse organs: comparison of comet assay results and carcinogenicity with 208 chemicals selected from the IARC monographs and U.S. NTP Carcinogenicity Database.* Crit Rev Toxicol, 2000. **30**(6): p. 629-799.

253. Olliver, J.R., et al., *Risk factors, DNA damage, and disease progression in Barrett's esophagus.* Cancer Epidemiol Biomarkers Prev, 2005. **14**(3): p. 620-5.

254. Schabath, M.B., et al., *Dietary carotenoids and genetic instability modify bladder cancer risk.* J Nutr, 2004. **134**(12): p. 3362-9.

255. Smith, T.R., et al., *DNA damage and breast cancer risk.* Carcinogenesis, 2003. **24**(5): p. 883-9.

256. Sigurdson, A.J., et al., *DNA damage among thyroid cancer and multiple cancer cases, controls, and long-lived individuals.* Mutat Res, 2005. **586**(2): p. 173-88.

257. West, C.M., et al., *The independence of intrinsic radiosensitivity as a prognostic factor for patient response to radiotherapy of carcinoma of the cervix.* Br J Cancer, 1997. **76**(9): p. 1184-90.

258. Bjork-Eriksson, T., et al., *Tumor radiosensitivity (SF2) is a prognostic factor for local control in head and neck cancers.* Int J Radiat Oncol Biol Phys, 2000. **46**(1): p. 13-9.

259. Price, M.E., et al., *Induction and rejoining of DNA double-strand breaks in bladder tumor cells.* Radiat Res, 2000. **153**(6): p. 788-94.

REFERENCES

260. Marples, B., et al., *The ratio of initial/residual DNA damage predicts intrinsic radiosensitivity in seven cervix carcinoma cell lines.* Br J Cancer, 1998. **77**(7): p. 1108-14.

261. McKeown, S.R., et al., *Potential use of the alkaline comet assay as a predictor of bladder tumour response to radiation.* Br J Cancer, 2003. **89**(12): p. 2264-70.

262. Moneef, M.A., et al., *Measurements using the alkaline comet assay predict bladder cancer cell radiosensitivity.* Br J Cancer, 2003. **89**(12): p. 2271-6.

263. Dunne, A.L., et al., *Relationship between clonogenic radiosensitivity, radiation-induced apoptosis and DNA damage/repair in human colon cancer cells.* Br J Cancer, 2003. **89**(12): p. 2277-83.

264. Puzanov, I., et al., *Phase I pharmacokinetic and pharmacodynamic study of SJG-136, a novel DNA sequence selective minor groove cross-linking agent, in advanced solid tumors.* Clin Cancer Res, 2011. **17**(11): p. 3794-802.

265. Anthoney, D.A., et al., *Phase I study of TP300 in patients with advanced solid tumors with pharmacokinetic, pharmacogenetic and pharmacodynamic analyses.* BMC Cancer, 2012. **12**: p. 536.

266. Olive, P.L., et al., *Gel electrophoresis of individual cells to quantify hypoxic fraction in human breast cancers.* Cancer Res, 1993. **53**(4): p. 733-6.

267. Dorie, M.J., et al., *DNA damage measured by the comet assay in head and neck cancer patients treated with tirapazamine.* Neoplasia, 1999. **1**(5): p. 461-7.

268. Olive, P.L., et al., *The comet assay in clinical practice.* Acta Oncol, 1999. **38**(7): p. 839-44.

269. Webley, S.D., et al., *Measurement of the critical DNA lesions produced by antibody-directed enzyme prodrug therapy (ADEPT) in vitro, in vivo and in clinical material.* Br J Cancer, 2001. **84**(12): p. 1671-6.

270. Baltaci, V., et al., *Assessment of cytogenetic aberrations and comet assay in colorectal adenocarcinomas.* Tumori, 2003. **89**(3): p. 305-10.

271. Pool-Zobel, B.L., et al., *Analysis of DNA strand breaks, oxidized bases, and glutathione S-transferase P1 in human colon cells from biopsies.* Cancer Epidemiol Biomarkers Prev, 1999. **8**(7): p. 609-14.

272. McGlynn, A.P., et al., *Detection of replicative integrity in small colonic biopsies using the BrdUrd comet assay.* Br J Cancer, 2003. **88**(6): p. 895-901.

273. Pool-Zobel, B.L., et al., *Genetic damage and repair in human rectal cells for biomonitoring: sex differences, effects of alcohol exposure, and susceptibilities in comparison to peripheral blood lymphocytes.* Mutat Res, 2004. **551**(1-2): p. 127-34.

274. Muller, W.U., et al., *Does radiotherapy affect the outcome of the comet assay?* Br J Radiol, 2002. **75**(895): p. 608-14.

275. Garcia, O., et al., *Sensitivity and variability of visual scoring in the comet assay. Results of an inter-laboratory scoring exercise with the use of silver staining.* Mutat Res, 2004. **556**(1-2): p. 25-34.

276. Moller, P., et al., *Intra-laboratory comet assay sample scoring exercise for determination of formamidopyrimidine DNA glycosylase sites in human mononuclear blood cell DNA.* Free Radic Res, 2004. **38**(11): p. 1207-14.

277. Morgan, B., et al., *Dynamic contrast-enhanced magnetic resonance imaging as a biomarker for the pharmacological response of PTK787/ZK 222584, an inhibitor of the vascular endothelial growth factor receptor tyrosine kinases, in patients with advanced colorectal cancer and liver metastases: results from two phase I studies.* J Clin Oncol, 2003. **21**(21): p. 3955-64.

REFERENCES

278. Schaefer, N.G., et al., *Hodgkin disease: diagnostic value of FDG PET/CT after first-line therapy--is biopsy of FDG-avid lesions still needed?* Radiology, 2007. **244**(1): p. 257-62.

279. Al-Ibraheem, A., et al., *Clinical Applications of FDG PET and PET/CT in Head and Neck Cancer.* J Oncol, 2009. **2009**: p. 208725.

280. Hu, L.S., et al., *Relative cerebral blood volume values to differentiate high-grade glioma recurrence from posttreatment radiation effect: direct correlation between image-guided tissue histopathology and localized dynamic susceptibility-weighted contrast-enhanced perfusion MR imaging measurements.* AJNR Am J Neuroradiol, 2009. **30**(3): p. 552-8.

281. Li, S.P., A.R. Padhani, and A. Makris, *Dynamic contrast-enhanced magnetic resonance imaging and blood oxygenation level-dependent magnetic resonance imaging for the assessment of changes in tumor biology with treatment.* J Natl Cancer Inst Monogr, 2011. **2011**(43): p. 103-7.

282. Koh, D.M. and D.J. Collins, *Diffusion-weighted MRI in the body: applications and challenges in oncology.* AJR Am J Roentgenol, 2007. **188**(6): p. 1622-35.

283. Patterson, D.M., A.R. Padhani, and D.J. Collins, *Technology insight: water diffusion MRI--a potential new biomarker of response to cancer therapy.* Nat Clin Pract Oncol, 2008. **5**(4): p. 220-33.

284. Padhani, A.R., et al., *Diffusion-weighted magnetic resonance imaging as a cancer biomarker: consensus and recommendations.* Neoplasia, 2009. **11**(2): p. 102-25.

285. Stejskal, E.O. and J.E. Tanner, *Spin Diffusion Measurements: Spin Echoes in the Presence of a Time - Dependent Field Gradient.* The Journal of Chemical Physics, 1965. **42**(1): p. 288-292.

286. Le Bihan, D., et al., *Separation of diffusion and perfusion in intravoxel incoherent motion MR imaging.* Radiology, 1988. **168**(2): p. 497-505.

287. Niendorf, T., et al., *Biexponential diffusion attenuation in various states of brain tissue: implications for diffusion-weighted imaging.* Magn Reson Med, 1996. **36**(6): p. 847-57.

288. Taouli, B., et al., *Evaluation of liver diffusion isotropy and characterization of focal hepatic lesions with two single-shot echo-planar MR imaging sequences: prospective study in 66 patients.* Radiology, 2003. **226**(1): p. 71-8.

289. Koh, D.M., et al., *Detection of colorectal hepatic metastases using MnDPDP MR imaging and diffusion-weighted imaging (DWI) alone and in combination.* Eur Radiol, 2008. **18**(5): p. 903-10.

290. Parikh, T., et al., *Focal liver lesion detection and characterization with diffusion-weighted MR imaging: comparison with standard breath-hold T2-weighted imaging.* Radiology, 2008. **246**(3): p. 812-22.

291. Sumi, M., et al., *Discrimination of metastatic cervical lymph nodes with diffusion-weighted MR imaging in patients with head and neck cancer.* AJNR Am J Neuroradiol, 2003. **24**(8): p. 1627-34.

292. Yoshikawa, M.I., et al., *Relation between cancer cellularity and apparent diffusion coefficient values using diffusion-weighted magnetic resonance imaging in breast cancer.* Radiat Med, 2008. **26**(4): p. 222-6.

293. Manenti, G., et al., *Malignant renal neoplasms: correlation between ADC values and cellularity in diffusion weighted magnetic resonance imaging at 3 T.* Radiol Med, 2008. **113**(2): p. 199-213.

294. Hayashida, Y., et al., *Diffusion-weighted imaging of metastatic brain tumors: comparison with histologic type and tumor cellularity.* AJNR Am J Neuroradiol, 2006. **27**(7): p. 1419-25.

REFERENCES

295. Humphries, P.D., et al., *Tumors in pediatric patients at diffusion-weighted MR imaging: apparent diffusion coefficient and tumor cellularity.* Radiology, 2007. **245**(3): p. 848-54.

296. Zelhof, B., et al., *Correlation of diffusion-weighted magnetic resonance data with cellularity in prostate cancer.* BJU Int, 2009. **103**(7): p. 883-8.

297. Liu, Y., et al., *Diffusion-weighted magnetic resonance imaging of uterine cervical cancer.* J Comput Assist Tomogr, 2009. **33**(6): p. 858-62.

298. Lyng, H., O. Haraldseth, and E.K. Rofstad, *Measurement of cell density and necrotic fraction in human melanoma xenografts by diffusion weighted magnetic resonance imaging.* Magn Reson Med, 2000. **43**(6): p. 828-36.

299. Wang, X.Z., et al., *Diffusion-weighted imaging of prostate cancer: correlation between apparent diffusion coefficient values and tumor proliferation.* J Magn Reson Imaging, 2009. **29**(6): p. 1360-6.

300. Calvar, J.A., et al., *Characterization of brain tumors by MRS, DWI and Ki-67 labeling index.* J Neurooncol, 2005. **72**(3): p. 273-80.

301. Arvinda, H.R., et al., *Glioma grading: sensitivity, specificity, positive and negative predictive values of diffusion and perfusion imaging.* J Neurooncol, 2009. **94**(1): p. 87-96.

302. Geschwind, J.F., et al., *Chemoembolization of liver tumor in a rabbit model: assessment of tumor cell death with diffusion-weighted MR imaging and histologic analysis.* J Vasc Interv Radiol, 2000. **11**(10): p. 1245-55.

303. Liimatainen, T., et al., *Monitoring of gliomas in vivo by diffusion MRI and (1)H MRS during gene therapy-induced apoptosis: interrelationships between water diffusion and mobile lipids.* NMR Biomed, 2009. **22**(3): p. 272-9.

304. Kim, H., et al., *Breast tumor xenografts: diffusion-weighted MR imaging to assess early therapy with novel apoptosis-inducing anti-DR5 antibody.* Radiology, 2008. **248**(3): p. 844-51.

305. Hamstra, D.A., et al., *Diffusion magnetic resonance imaging: an imaging treatment response biomarker to chemoradiotherapy in a mouse model of squamous cell cancer of the head and neck.* Transl Oncol, 2008. **1**(4): p. 187-94.

306. Pickles, M.D., et al., *Diffusion changes precede size reduction in neoadjuvant treatment of breast cancer.* Magn Reson Imaging, 2006. **24**(7): p. 843-7.

307. Yankeelov, T.E., et al., *Integration of quantitative DCE-MRI and ADC mapping to monitor treatment response in human breast cancer: initial results.* Magn Reson Imaging, 2007. **25**(1): p. 1-13.

308. Theilmann, R.J., et al., *Changes in water mobility measured by diffusion MRI predict response of metastatic breast cancer to chemotherapy.* Neoplasia, 2004. **6**(6): p. 831-7.

309. Kamel, I.R., et al., *Functional MR imaging assessment of tumor response after 90Y microsphere treatment in patients with unresectable hepatocellular carcinoma.* J Vasc Interv Radiol, 2007. **18**(1 Pt 1): p. 49-56.

310. Cui, Y., et al., *Apparent diffusion coefficient: potential imaging biomarker for prediction and early detection of response to chemotherapy in hepatic metastases.* Radiology, 2008. **248**(3): p. 894-900.

311. Hayashida, Y., et al., *Monitoring therapeutic responses of primary bone tumors by diffusion-weighted image: Initial results.* Eur Radiol, 2006. **16**(12): p. 2637-43.

312. Uhl, M., et al., *Osteosarcoma: preliminary results of in vivo assessment of tumor necrosis after chemotherapy with diffusion- and perfusion-weighted magnetic resonance imaging.* Invest Radiol, 2006. **41**(8): p. 618-23.

REFERENCES

313. Moffat, B.A., et al., *Functional diffusion map: a noninvasive MRI biomarker for early stratification of clinical brain tumor response.* Proc Natl Acad Sci U S A, 2005. **102**(15): p. 5524-9.

314. Mardor, Y., et al., *Early detection of response to radiation therapy in patients with brain malignancies using conventional and high b-value diffusion-weighted magnetic resonance imaging.* J Clin Oncol, 2003. **21**(6): p. 1094-100.

315. Hamstra, D.A., et al., *Functional diffusion map as an early imaging biomarker for high-grade glioma: correlation with conventional radiologic response and overall survival.* J Clin Oncol, 2008. **26**(20): p. 3387-94.

316. Song, I., et al., *Value of diffusion-weighted imaging in the detection of viable tumour after neoadjuvant chemoradiation therapy in patients with locally advanced rectal cancer: comparison with T2 weighted and PET/CT imaging.* Br J Radiol, 2012. **85**(1013): p. 577-86.

317. Batchelor, T.T., et al., *AZD2171, a pan-VEGF receptor tyrosine kinase inhibitor, normalizes tumor vasculature and alleviates edema in glioblastoma patients.* Cancer Cell, 2007. **11**(1): p. 83-95.

318. Schaefer, P.W., P.E. Grant, and R.G. Gonzalez, *Diffusion-weighted MR imaging of the brain.* Radiology, 2000. **217**(2): p. 331-45.

319. Ries, M., et al., *Diffusion tensor MRI of the human kidney.* J Magn Reson Imaging, 2001. **14**(1): p. 42-9.

320. Parker, G.J., *Analysis of MR diffusion weighted images.* Br J Radiol, 2004. **77 Spec No 2**: p. S176-85.

321. Westbrook, C., C.K. Roth, and J.M. Talbot, *MRI in practice*. 4th ed. / Catherine Westbrook, Carolyn Kaut Roth and John Talbot. ed. 2011, Oxford: Wiley-Blackwell.

322. Toth, V., et al., *MR-based hypoxia measures in human glioma.* J Neurooncol, 2013. **115**(2): p. 197-207.

323. Chopra, S., et al., *Comparing oxygen-sensitive MRI (BOLD R2*) with oxygen electrode measurements: a pilot study in men with prostate cancer.* Int J Radiat Biol, 2009. **85**(9): p. 805-13.

324. Taylor, N.J., et al., *BOLD MRI of human tumor oxygenation during carbogen breathing.* J Magn Reson Imaging, 2001. **14**(2): p. 156-63.

325. Diergarten, T., et al., *Functional characterization of prostate cancer by integrated magnetic resonance imaging and oxygenation changes during carbogen breathing.* Invest Radiol, 2005. **40**(2): p. 102-9.

326. Alonzi, R., et al., *Carbogen breathing increases prostate cancer oxygenation: a translational MRI study in murine xenografts and humans.* Br J Cancer, 2009. **100**(4): p. 644-8.

327. Rijpkema, M., et al., *Effects of breathing a hyperoxic hypercapnic gas mixture on blood oxygenation and vascularity of head-and-neck tumors as measured by magnetic resonance imaging.* Int J Radiat Oncol Biol Phys, 2002. **53**(5): p. 1185-91.

328. Muller, A., et al., *Analysing the response in R2* relaxation rate of intracranial tumours to hyperoxic and hypercapnic respiratory challenges: initial results.* Eur Radiol, 2011. **21**(4): p. 786-98.

329. Hallac, R.R., et al., *Oxygenation in cervical cancer and normal uterine cervix assessed using blood oxygenation level-dependent (BOLD) MRI at 3T.* NMR Biomed, 2012. **25**(12): p. 1321-30.

330. Robinson, S.P., F.A. Howe, and J.R. Griffiths, *Noninvasive monitoring of carbogen-induced changes in tumor blood flow and oxygenation by functional magnetic resonance imaging.* Int J Radiat Oncol Biol Phys, 1995. **33**(4): p. 855-9.

REFERENCES

331. Baudelet, C. and B. Gallez, *How does blood oxygen level-dependent (BOLD) contrast correlate with oxygen partial pressure (pO2) inside tumors?* Magn Reson Med, 2002. **48**(6): p. 980-6.

332. Robinson, S.P., et al., *Tumor vascular architecture and function evaluated by non-invasive susceptibility MRI methods and immunohistochemistry.* J Magn Reson Imaging, 2003. **17**(4): p. 445-54.

333. Neeman, M., et al., *In vivo BOLD contrast MRI mapping of subcutaneous vascular function and maturation: validation by intravital microscopy.* Magn Reson Med, 2001. **45**(5): p. 887-98.

334. Rodrigues, L.M., et al., *Tumor R2* is a prognostic indicator of acute radiotherapeutic response in rodent tumors.* J Magn Reson Imaging, 2004. **19**(4): p. 482-8.

335. Choi, J.W., et al., *Blood oxygen level-dependent MRI for evaluation of early response of liver tumors to chemoembolization: an animal study.* Anticancer Res, 2013. **33**(5): p. 1887-92.

336. Hallac, R.R., et al., *Correlations of noninvasive BOLD and TOLD MRI with pO2 and relevance to tumor radiation response.* Magn Reson Med, 2014. **71**(5): p. 1863-73.

337. Hoskin, P.J., et al., *Hypoxia in prostate cancer: correlation of BOLD-MRI with pimonidazole immunohistochemistry-initial observations.* Int J Radiat Oncol Biol Phys, 2007. **68**(4): p. 1065-71.

338. Jiang, L., et al., *Blood oxygenation level-dependent (BOLD) contrast magnetic resonance imaging (MRI) for prediction of breast cancer chemotherapy response: a pilot study.* J Magn Reson Imaging, 2013. **37**(5): p. 1083-92.

339. Kim, C.K., et al., *Blood oxygenation level-dependent MR imaging as a predictor of therapeutic response to concurrent chemoradiotherapy in cervical cancer: a preliminary experience.* Eur Radiol, 2014.

340. Dunn, J.F., et al., *Changes in oxygenation of intracranial tumors with carbogen: a BOLD MRI and EPR oximetry study.* J Magn Reson Imaging, 2002. **16**(5): p. 511-21.

341. Kostourou, V., et al., *Overexpression of dimethylarginine dimethylaminohydrolase enhances tumor hypoxia: an insight into the relationship of hypoxia and angiogenesis in vivo.* Neoplasia, 2004. **6**(4): p. 401-11.

342. Al-Hallaq, H.A., et al., *Spectrally inhomogeneous BOLD contrast changes detected in rodent tumors with high spectral and spatial resolution MRI.* NMR Biomed, 2002. **15**(1): p. 28-36.

343. Parker, G.J., et al., *Probing tumor microvascularity by measurement, analysis and display of contrast agent uptake kinetics.* J Magn Reson Imaging, 1997. **7**(3): p. 564-74.

344. Padhani, A.R. and A. Dzik-Jurasz, *Perfusion MR imaging of extracranial tumor angiogenesis.* Top Magn Reson Imaging, 2004. **15**(1): p. 41-57.

345. Schlemmer, H.P., et al., *Can pre-operative contrast-enhanced dynamic MR imaging for prostate cancer predict microvessel density in prostatectomy specimens?* Eur Radiol, 2004. **14**(2): p. 309-17.

346. Ferrier, M.C., et al., *Validation of dynamic contrast-enhanced magnetic resonance imaging-derived vascular permeability measurements using quantitative autoradiography in the RG2 rat brain tumor model.* Neoplasia, 2007. **9**(7): p. 546-55.

347. Lankester, K.J., et al., *Dynamic MRI for imaging tumor microvasculature: comparison of susceptibility and relaxivity techniques in pelvic tumors.* J Magn Reson Imaging, 2007. **25**(4): p. 796-805.

348. Eby, P.R., et al., *Metabolic and vascular features of dynamic contrast-enhanced breast magnetic resonance imaging and (15)O-water positron emission tomography blood flow in breast cancer.* Acad Radiol, 2008. **15**(10): p. 1246-54.

REFERENCES

349. Niermann, K.J., et al., *Measuring tumor perfusion in control and treated murine tumors: correlation of microbubble contrast-enhanced sonography to dynamic contrast-enhanced magnetic resonance imaging and fluorodeoxyglucose positron emission tomography.* J Ultrasound Med, 2007. **26**(6): p. 749-56.

350. Wilkinson, I.D., et al., *Dexamethasone and enhancing solitary cerebral mass lesions: alterations in perfusion and blood-tumor barrier kinetics shown by magnetic resonance imaging.* Neurosurgery, 2006. **58**(4): p. 640-6; discussion 640-6.

351. George, M.L., et al., *Non-invasive methods of assessing angiogenesis and their value in predicting response to treatment in colorectal cancer.* Br J Surg, 2001. **88**(12): p. 1628-36.

352. Barentsz, J.O., et al., *Evaluation of chemotherapy in advanced urinary bladder cancer with fast dynamic contrast-enhanced MR imaging.* Radiology, 1998. **207**(3): p. 791-7.

353. Ah-See, M.L., et al., *Early changes in functional dynamic magnetic resonance imaging predict for pathologic response to neoadjuvant chemotherapy in primary breast cancer.* Clin Cancer Res, 2008. **14**(20): p. 6580-9.

354. Padhani, A.R., et al., *Prediction of clinicopathologic response of breast cancer to primary chemotherapy at contrast-enhanced MR imaging: initial clinical results.* Radiology, 2006. **239**(2): p. 361-74.

355. Reddick, W.E., J.S. Taylor, and B.D. Fletcher, *Dynamic MR imaging (DEMRI) of microcirculation in bone sarcoma.* J Magn Reson Imaging, 1999. **10**(3): p. 277-85.

356. de Lussanet, Q.G., et al., *Dynamic contrast-enhanced magnetic resonance imaging of radiation therapy-induced microcirculation changes in rectal cancer.* Int J Radiat Oncol Biol Phys, 2005. **63**(5): p. 1309-15.

357. Zahra, M.A., et al., *Semiquantitative and quantitative dynamic contrast-enhanced magnetic resonance imaging measurements predict radiation response in cervix cancer.* Int J Radiat Oncol Biol Phys, 2009. **74**(3): p. 766-73.

358. Padhani, A.R., et al., *Effects of androgen deprivation on prostatic morphology and vascular permeability evaluated with mr imaging.* Radiology, 2001. **218**(2): p. 365-74.

359. Li, W., et al., *Semiquantitative assessment of uterine perfusion using first pass dynamic contrast-enhanced MR imaging for patients treated with uterine fibroid embolization.* J Magn Reson Imaging, 2000. **12**(6): p. 1004-8.

360. O'Connor, J.P., et al., *DCE-MRI biomarkers in the clinical evaluation of antiangiogenic and vascular disrupting agents.* Br J Cancer, 2007. **96**(2): p. 189-95.

361. Jain, R.K., *Normalizing tumor vasculature with anti-angiogenic therapy: a new paradigm for combination therapy.* Nat Med, 2001. **7**(9): p. 987-9.

362. Kamoun, W.S., et al., *Edema control by cediranib, a vascular endothelial growth factor receptor-targeted kinase inhibitor, prolongs survival despite persistent brain tumor growth in mice.* J Clin Oncol, 2009. **27**(15): p. 2542-52.

363. Weinmann, H.J., M. Laniado, and W. Mutzel, *Pharmacokinetics of GdDTPA/dimeglumine after intravenous injection into healthy volunteers.* Physiol Chem Phys Med NMR, 1984. **16**(2): p. 167-72.

364. Tofts, P.S., *Modeling tracer kinetics in dynamic Gd-DTPA MR imaging.* J Magn Reson Imaging, 1997. **7**(1): p. 91-101.

365. Buckley, D.L., *Uncertainty in the analysis of tracer kinetics using dynamic contrast-enhanced T1-weighted MRI.* Magn Reson Med, 2002. **47**(3): p. 601-6.

366. Landis, C.S., et al., *Determination of the MRI contrast agent concentration time course in vivo following bolus injection: effect of equilibrium transcytolemmal water exchange.* Magn Reson Med, 2000. **44**(4): p. 563-74.

REFERENCES

367. Buckley, D.L., *Transcytolemmal water exchange and its affect on the determination of contrast agent concentration in vivo.* Magn Reson Med, 2002. **47**(2): p. 420-4.

368. Miles, K.A., et al., *Current status and guidelines for the assessment of tumour vascular support with dynamic contrast-enhanced computed tomography.* Eur Radiol, 2012. **22**(7): p. 1430-41.

369. Miles, K.A., *Tumour angiogenesis and its relation to contrast enhancement on computed tomography: a review.* Eur J Radiol, 1999. **30**(3): p. 198-205.

370. Garcia-Figueiras, R., et al., *CT perfusion in oncologic imaging: a useful tool?* AJR Am J Roentgenol, 2013. **200**(1): p. 8-19.

371. Petralia, G., et al., *CT perfusion in oncology: how to do it.* Cancer Imaging, 2010. **10**: p. 8-19.

372. Kambadakone, A.R. and D.V. Sahani, *Body perfusion CT: technique, clinical applications, and advances.* Radiol Clin North Am, 2009. **47**(1): p. 161-78.

373. Miles, K.A., *Perfusion CT for the assessment of tumour vascularity: which protocol?* Br J Radiol, 2003. **76 Spec No 1**: p. S36-42.

374. Furukawa, M., et al., *Evaluation of cerebral perfusion parameters measured by perfusion CT in chronic cerebral ischemia: comparison with xenon CT.* J Comput Assist Tomogr, 2002. **26**(2): p. 272-8.

375. Ng, C.S., et al., *Tumor blood flow measured by perfusion computed tomography and 15O-labeled water positron emission tomography: a comparison study.* J Comput Assist Tomogr, 2009. **33**(3): p. 460-5.

376. Ling, S., et al., *Correlations between CT perfusion parameters and vascular endothelial growth factor expression and microvessel density in implanted VX2 lung tumors.* Cell Biochem Biophys, 2014. **70**(1): p. 629-33.

377. Spira, D., et al., *Assessment of tumor vascularity in lung cancer using volume perfusion CT (VPCT) with histopathologic comparison: a further step toward an individualized tumor characterization.* J Comput Assist Tomogr, 2013. **37**(1): p. 15-21.

378. Osimani, M., et al., *Perfusion MDCT of prostate cancer: correlation of perfusion CT parameters and immunohistochemical markers of angiogenesis.* AJR Am J Roentgenol, 2012. **199**(5): p. 1042-8.

379. Chen, T.W., et al., *Quantitative assessment of first-pass perfusion using a low-dose method at multidetector CT in oesophageal squamous cell carcinoma: correlation with VEGF expression.* Clin Radiol, 2012. **67**(8): p. 746-53.

380. Xing, N., et al., *The Use of CT Perfusion to Determine Microvessel Density in Lung Cancer: Comparison with FDG-PET and Pathology.* Chin J Cancer Res, 2011. **23**(2): p. 118-22.

381. Dighe, S., et al., *Perfusion CT vascular parameters do not correlate with immunohistochemically derived microvessel density count in colorectal tumors.* Radiology, 2013. **268**(2): p. 400-10.

382. Kim, J.W., et al., *Perfusion CT in colorectal cancer: comparison of perfusion parameters with tumor grade and microvessel density.* Korean J Radiol, 2012. **13 Suppl 1**: p. S89-97.

383. Li, Z.P., et al., *Tumor angiogenesis and dynamic CT in colorectal carcinoma: radiologic-pathologic correlation.* World J Gastroenterol, 2005. **11**(9): p. 1287-91.

384. Goh, V., et al., *Colorectal tumor vascularity: quantitative assessment with multidetector CT--do tumor perfusion measurements reflect angiogenesis?* Radiology, 2008. **249**(2): p. 510-7.

REFERENCES

385. Cenic, A., et al., *A CT method to measure hemodynamics in brain tumors: validation and application of cerebral blood flow maps.* AJNR Am J Neuroradiol, 2000. **21**(3): p. 462-70.

386. Goh, V., et al., *Quantitative assessment of colorectal cancer perfusion using MDCT: inter- and intraobserver agreement.* AJR Am J Roentgenol, 2005. **185**(1): p. 225-31.

387. Goh, V., et al., *Quantitative assessment of tissue perfusion using MDCT: comparison of colorectal cancer and skeletal muscle measurement reproducibility.* AJR Am J Roentgenol, 2006. **187**(1): p. 164-9.

388. Sahani, D.V., et al., *Advanced hepatocellular carcinoma: CT perfusion of liver and tumor tissue--initial experience.* Radiology, 2007. **243**(3): p. 736-43.

389. Qin, H.Y., et al., *Correlation between CT perfusion parameters and microvessel density and vascular endothelial growth factor in adrenal tumors.* PLoS One, 2013. **8**(11): p. e79911.

390. Shi, J., et al., *Dynamic volume perfusion CT in patients with lung cancer: baseline perfusion characteristics of different histological subtypes.* Eur J Radiol, 2013. **82**(12): p. e894-900.

391. Ellika, S.K., et al., *Role of perfusion CT in glioma grading and comparison with conventional MR imaging features.* AJNR Am J Neuroradiol, 2007. **28**(10): p. 1981-7.

392. Sun, H., et al., *Assessment of tumor grade and angiogenesis in colorectal cancer: whole-volume perfusion CT.* Acad Radiol, 2014. **21**(6): p. 750-7.

393. Shan, F., et al., *Differentiation between malignant and benign solitary pulmonary nodules: use of volume first-pass perfusion and combined with routine computed tomography.* Eur J Radiol, 2012. **81**(11): p. 3598-605.

394. Liu, Y., et al., *Accuracy of computed tomography perfusion in assessing metastatic involvement of enlarged axillary lymph nodes in patients with breast cancer.* Breast Cancer Res, 2007. **9**(4): p. R40.

395. Trojanowska, A., et al., *Squamous cell cancer of hypopharynx and larynx - evaluation of metastatic nodal disease based on computed tomography perfusion studies.* Eur J Radiol, 2012. **81**(5): p. 1034-9.

396. Chen, Y.W., et al., *Assessment of blood flow in hepatocellular carcinoma: correlations of computed tomography perfusion imaging and circulating angiogenic factors.* Int J Mol Sci, 2013. **14**(9): p. 17536-52.

397. Satoh, A., et al., *Role of perfusion CT in assessing tumor blood flow and malignancy level of gastric cancer.* Dig Surg, 2010. **27**(4): p. 253-60.

398. Hayano, K., et al., *Quantitative measurement of blood flow using perfusion CT for assessing clinicopathologic features and prognosis in patients with rectal cancer.* Dis Colon Rectum, 2009. **52**(9): p. 1624-9.

399. Hermans, R., et al., *Tumor perfusion rate determined noninvasively by dynamic computed tomography predicts outcome in head-and-neck cancer after radiotherapy.* Int J Radiat Oncol Biol Phys, 2003. **57**(5): p. 1351-6.

400. Fraioli, F., et al., *Whole-tumour CT-perfusion of unresectable lung cancer for the monitoring of anti-angiogenetic chemotherapy effects.* Br J Radiol, 2013. **86**(1029): p. 20120174.

401. Hayano, K., et al., *Perfusion CT can predict the response to chemoradiation therapy and survival in esophageal squamous cell carcinoma: initial clinical results.* Oncol Rep, 2007. **18**(4): p. 901-8.

402. Kim, D.H., et al., *Intermodality comparison between 3D perfusion CT and 18F-FDG PET/CT imaging for predicting early tumor response in patients with liver metastasis after chemotherapy: preliminary results of a prospective study.* Eur J Radiol, 2012. **81**(11): p. 3542-50.

REFERENCES

403. Sahani, D.V., et al., *Assessing tumor perfusion and treatment response in rectal cancer with multisection CT: initial observations.* Radiology, 2005. **234**(3): p. 785-92.

404. Bellomi, M., et al., *CT perfusion for the monitoring of neoadjuvant chemotherapy and radiation therapy in rectal carcinoma: initial experience.* Radiology, 2007. **244**(2): p. 486-93.

405. Willett, C.G., et al., *Direct evidence that the VEGF-specific antibody bevacizumab has antivascular effects in human rectal cancer.* Nat Med, 2004. **10**(2): p. 145-7.

406. Baeten, C.I., et al., *Effects of radiotherapy and chemotherapy on angiogenesis and leukocyte infiltration in rectal cancer.* Int J Radiat Oncol Biol Phys, 2006. **66**(4): p. 1219-27.

407. Janssen, M.H., et al., *Tumor perfusion increases during hypofractionated short-course radiotherapy in rectal cancer: sequential perfusion-CT findings.* Radiother Oncol, 2010. **94**(2): p. 156-60.

408. Eisa, F., et al., *Dynamic contrast-enhanced micro-CT on mice with mammary carcinoma for the assessment of antiangiogenic therapy response.* Eur Radiol, 2012. **22**(4): p. 900-7.

409. Tai, J.H., et al., *Assessment of acute antivascular effects of vandetanib with high-resolution dynamic contrast-enhanced computed tomographic imaging in a human colon tumor xenograft model in the nude rat.* Neoplasia, 2010. **12**(9): p. 697-707.

410. Lim, W.T., et al., *A Phase II study of pazopanib in Asian patients with recurrent/metastatic nasopharyngeal carcinoma.* Clin Cancer Res, 2011. **17**(16): p. 5481-9.

411. Sacco, R., et al., *Assessment of response to sorafenib in advanced hepatocellular carcinoma using perfusion computed tomography: results of a pilot study.* Dig Liver Dis, 2013. **45**(9): p. 776-81.

412. Zhu, A.X., et al., *Early antiangiogenic activity of bevacizumab evaluated by computed tomography perfusion scan in patients with advanced hepatocellular carcinoma.* Oncologist, 2008. **13**(2): p. 120-5.

413. Han, K.S., et al., *Pretreatment assessment of tumor enhancement on contrast-enhanced computed tomography as a potential predictor of treatment outcome in metastatic renal cell carcinoma patients receiving antiangiogenic therapy.* Cancer, 2010. **116**(10): p. 2332-42.

414. Messiou, C., et al., *Advanced solid tumors treated with cediranib: comparison of dynamic contrast-enhanced MR imaging and CT as markers of vascular activity.* Radiology, 2012. **265**(2): p. 426-36.

415. Faria, S.C., et al., *CT quantification of effects of thalidomide in patients with metastatic renal cell carcinoma.* AJR Am J Roentgenol, 2007. **189**(2): p. 378-85.

416. Tacelli, N., et al., *Perfusion CT allows prediction of therapy response in non-small cell lung cancer treated with conventional and anti-angiogenic chemotherapy.* Eur Radiol, 2013. **23**(8): p. 2127-36.

417. Frampas, E., et al., *Advanced Hepatocellular Carcinoma: early evaluation of response to targeted therapy and prognostic value of Perfusion CT and Dynamic Contrast Enhanced-Ultrasound. Preliminary results.* Eur J Radiol, 2013. **82**(5): p. e205-11.

418. Jain, R.K., *Normalization of tumor vasculature: an emerging concept in antiangiogenic therapy.* Science, 2005. **307**(5706): p. 58-62.

419. Ng, Q.S., et al., *Tumor antivascular effects of radiotherapy combined with combretastatin a4 phosphate in human non-small-cell lung cancer.* Int J Radiat Oncol Biol Phys, 2007. **67**(5): p. 1375-80.

REFERENCES

420. Koh, T.S., et al., *Primary colorectal cancer: use of kinetic modeling of dynamic contrast-enhanced CT data to predict clinical outcome.* Radiology, 2013. **267**(1): p. 145-54.

421. Goh, V., S. Halligan, and C.I. Bartram, *Quantitative tumor perfusion assessment with multidetector CT: are measurements from two commercial software packages interchangeable?* Radiology, 2007. **242**(3): p. 777-82.

422. Djuric-Stefanovic, A., et al., *Comparison between the deconvolution and maximum slope 64-MDCT perfusion analysis of the esophageal cancer: is conversion possible?* Eur J Radiol, 2013. **82**(10): p. 1716-23.

423. Tofts, P.S., et al., *Estimating kinetic parameters from dynamic contrast-enhanced T(1)-weighted MRI of a diffusable tracer: standardized quantities and symbols.* J Magn Reson Imaging, 1999. **10**(3): p. 223-32.

424. Capirci, C., et al., *Prognostic value of pathologic complete response after neoadjuvant therapy in locally advanced rectal cancer: long-term analysis of 566 ypCR patients.* Int J Radiat Oncol Biol Phys, 2008. **72**(1): p. 99-107.

425. Vecchio, F.M., et al., *The relationship of pathologic tumor regression grade (TRG) and outcomes after preoperative therapy in rectal cancer.* Int J Radiat Oncol Biol Phys, 2005. **62**(3): p. 752-60.

426. Hartley J, S.V., Hartley J. , *Single Cell Gel Electrophoresis (Comet) Assay (SB).* Document No. COMET/Strand breaks/Research/001/Version1, 2008.

427. Thoms, J. and R.G. Bristow, *DNA repair targeting and radiotherapy: a focus on the therapeutic ratio.* Semin Radiat Oncol, 2010. **20**(4): p. 217-22.

428. Eriksson, D. and T. Stigbrand, *Radiation-induced cell death mechanisms.* Tumour Biol, 2010. **31**(4): p. 363-72.

429. Dovedi, S.J., et al., *Acquired Resistance to Fractionated Radiotherapy Can Be Overcome by Concurrent PD-L1 Blockade.* Cancer Res, 2014. **74**(19): p. 5458-68.

430. Brown, J.M. and W.R. Wilson, *Exploiting tumour hypoxia in cancer treatment.* Nat Rev Cancer, 2004. **4**(6): p. 437-47.

431. Kandioler, D., et al., *TP53 genotype but not p53 immunohistochemical result predicts response to preoperative short-term radiotherapy in rectal cancer.* Ann Surg, 2002. **235**(4): p. 493-8.

432. Shimura, T., et al., *Acquired radioresistance of human tumor cells by DNA-PK/AKT/GSK3beta-mediated cyclin D1 overexpression.* Oncogene, 2010. **29**(34): p. 4826-37.

433. Li, J.Y., et al., *ABT-737 reverses the acquired radioresistance of breast cancer cells by targeting Bcl-2 and Bcl-xL.* J Exp Clin Cancer Res, 2012. **31**: p. 102.

434. Klein, T.J. and P.M. Glazer, *The tumor microenvironment and DNA repair.* Semin Radiat Oncol, 2010. **20**(4): p. 282-7.

435. Buchynska, L., et al., *DNA repair deficiency in peripheral blood lymphocytes of endometrial cancer patients with a family history of cancer.* BMC Cancer, 2014. **14**(1): p. 765.

436. Santos, R.A., et al., *Basal levels of DNA damage detected by micronuclei and comet assays in untreated breast cancer patients and healthy women.* Clin Exp Med, 2010. **10**(2): p. 87-92.

437. Lim, S.B., et al., *Optimal surgery time after preoperative chemoradiotherapy for locally advanced rectal cancers.* Ann Surg, 2008. **248**(2): p. 243-51.

438. Petrelli, F., et al., *Increasing the Interval Between Neoadjuvant Chemoradiotherapy and Surgery in Rectal Cancer: A Meta-Analysis of Published Studies.* Ann Surg, 2013.

REFERENCES

439. d'Arcy, J.A., et al., *Informatics in Radiology (infoRAD): Magnetic Resonance Imaging Workbench: analysis and visualization of dynamic contrast-enhanced MR imaging data.* Radiographics, 2006. **26**(2): p. 621-32.

440. Parker, G.J., et al., *Experimentally-derived functional form for a population-averaged high-temporal-resolution arterial input function for dynamic contrast-enhanced MRI.* Magn Reson Med, 2006. **56**(5): p. 993-1000.

441. Bland, J.M. and D.G. Altman, *Statistical methods for assessing agreement between two methods of clinical measurement.* Lancet, 1986. **1**(8476): p. 307-10.

442. Bland, J.M. and D.G. Altman, *Measuring agreement in method comparison studies.* Stat Methods Med Res, 1999. **8**(2): p. 135-60.

443. Galbraith, S.M., et al., *Reproducibility of dynamic contrast-enhanced MRI in human muscle and tumours: comparison of quantitative and semi-quantitative analysis.* NMR Biomed, 2002. **15**(2): p. 132-42.

444. Bland, J.M. and D.G. Altman, *Measurement error.* BMJ, 1996. **312**(7047): p. 1654.

445. Bland, J.M. and D.G. Altman, *Measurement error proportional to the mean.* BMJ, 1996. **313**(7049): p. 106.

446. Curvo-Semedo, L., *Usefulness of diffusion-weighted MRI in the characterization and assessment of response to neoadjuvant therapy in rectal cancer.* Imaging in Medicine, 2014. **6**(1): p. 75-87.

447. Koh, D.M., et al., *Reproducibility and changes in the apparent diffusion coefficients of solid tumours treated with combretastatin A4 phosphate and bevacizumab in a two-centre phase I clinical trial.* Eur Radiol, 2009. **19**(11): p. 2728-38.

448. Intven, M., O. Reerink, and M.E. Philippens, *Repeatability of diffusion-weighted imaging in rectal cancer.* J Magn Reson Imaging, 2014. **40**(1): p. 146-50.

449. Curvo-Semedo, L., et al., *Diffusion-weighted MRI in rectal cancer: apparent diffusion coefficient as a potential noninvasive marker of tumor aggressiveness.* J Magn Reson Imaging, 2012. **35**(6): p. 1365-71.

450. Tong, T., et al., *Extramural depth of tumor invasion at thin-section MR in rectal cancer: Associating with prognostic factors and ADC value.* J Magn Reson Imaging, 2013.

451. Akashi, M., et al., *Assessment of aggressiveness of rectal cancer using 3-T MRI: correlation between the apparent diffusion coefficient as a potential imaging biomarker and histologic prognostic factors.* Acta Radiol, 2013. **55**(5): p. 524-531.

452. Unterberger, M.J., et al., *A new approach to model cross-linked actin networks: multi-scale continuum formulation and computational analysis.* J Mech Behav Biomed Mater, 2013. **22**: p. 95-114.

453. Cho, E.Y., et al., *Apparent diffusion coefficient for discriminating metastatic from non-metastatic lymph nodes in primary rectal cancer.* Eur J Radiol, 2013. **82**(11): p. e662-8.

454. Heijnen, L.A., et al., *Diffusion-weighted MR imaging in primary rectal cancer staging demonstrates but does not characterise lymph nodes.* Eur Radiol, 2013. **23**(12): p. 3354-60.

455. Park, M.J., et al., *Locally advanced rectal cancer: added value of diffusion-weighted MR imaging for predicting tumor clearance of the mesorectal fascia after neoadjuvant chemotherapy and radiation therapy.* Radiology, 2011. **260**(3): p. 771-80.

456. de Gramont, A., et al., *Bevacizumab plus oxaliplatin-based chemotherapy as adjuvant treatment for colon cancer (AVANT): a phase 3 randomised controlled trial.* Lancet Oncol, 2012. **13**(12): p. 1225-33.

REFERENCES

457. Barbaro, B., et al., *Diffusion-weighted magnetic resonance imaging in monitoring rectal cancer response to neoadjuvant chemoradiotherapy.* Int J Radiat Oncol Biol Phys, 2012. **83**(2): p. 594-9.

458. Intven, M., O. Reerink, and M.E. Philippens, *Diffusion-weighted MRI in locally advanced rectal cancer : pathological response prediction after neo-adjuvant radiochemotherapy.* Strahlenther Onkol, 2013. **189**(2): p. 117-22.

459. Kim, S.H., et al., *Apparent diffusion coefficient for evaluating tumour response to neoadjuvant chemoradiation therapy for locally advanced rectal cancer.* Eur Radiol, 2011. **21**(5): p. 987-95.

460. Sun, Y.S., et al., *Locally advanced rectal carcinoma treated with preoperative chemotherapy and radiation therapy: preliminary analysis of diffusion-weighted MR imaging for early detection of tumor histopathologic downstaging.* Radiology, 2010. **254**(1): p. 170-8.

461. Genovesi, D., et al., *Diffusion-weighted magnetic resonance for prediction of response after neoadjuvant chemoradiation therapy for locally advanced rectal cancer: preliminary results of a monoinstitutional prospective study.* Eur J Surg Oncol, 2013. **39**(10): p. 1071-8.

462. Lambrecht, M., et al., *Value of diffusion-weighted magnetic resonance imaging for prediction and early assessment of response to neoadjuvant radiochemotherapy in rectal cancer: preliminary results.* Int J Radiat Oncol Biol Phys, 2012. **82**(2): p. 863-70.

463. Elmi, A., et al., *Apparent diffusion coefficient as a non-invasive predictor of treatment response and recurrence in locally advanced rectal cancer.* Clin Radiol, 2013. **68**(10): p. e524-31.

464. Monguzzi, L., et al., *Locally advanced rectal cancer: value of ADC mapping in prediction of tumor response to radiochemotherapy.* Eur J Radiol, 2013. **82**(2): p. 234-40.

465. Ha, H.I., et al., *Locally advanced rectal cancer: diffusion-weighted MR tumour volumetry and the apparent diffusion coefficient for evaluating complete remission after preoperative chemoradiation therapy.* Eur Radiol, 2013. **23**(12): p. 3345-53.

466. Kim, S.H., et al., *Locally advanced rectal cancer: added value of diffusion-weighted MR imaging in the evaluation of tumor response to neoadjuvant chemo- and radiation therapy.* Radiology, 2009. **253**(1): p. 116-25.

467. Cai, G., et al., *Diffusion-weighted magnetic resonance imaging for predicting the response of rectal cancer to neoadjuvant concurrent chemoradiation.* World J Gastroenterol, 2013. **19**(33): p. 5520-7.

468. DeVries, A.F., et al., *Tumor microcirculation and diffusion predict therapy outcome for primary rectal carcinoma.* Int J Radiat Oncol Biol Phys, 2003. **56**(4): p. 958-65.

469. Curvo-Semedo, L., et al., *Rectal cancer: assessment of complete response to preoperative combined radiation therapy with chemotherapy--conventional MR volumetry versus diffusion-weighted MR imaging.* Radiology, 2011. **260**(3): p. 734-43.

470. Engin, G., et al., *Can diffusion-weighted MRI determine complete responders after neoadjuvant chemoradiation for locally advanced rectal cancer?* Diagn Interv Radiol, 2012. **18**(6): p. 574-81.

471. Attenberger, U.I., et al., *Multi-parametric MRI of rectal cancer - do quantitative functional MR measurements correlate with radiologic and pathologic tumor stages?* Eur J Radiol, 2014. **83**(7): p. 1036-43.

472. Lambregts, D.M., et al., *Tumour ADC measurements in rectal cancer: effect of ROI methods on ADC values and interobserver variability.* Eur Radiol, 2011. **21**(12): p. 2567-74.

REFERENCES

473. Alonzi, R., et al., *Reproducibility and correlation between quantitative and semiquantitative dynamic and intrinsic susceptibility-weighted MRI parameters in the benign and malignant human prostate.* J Magn Reson Imaging, 2010. **32**(1): p. 155-64.

474. Li, S.P., et al., *Primary human breast adenocarcinoma: imaging and histologic correlates of intrinsic susceptibility-weighted MR imaging before and during chemotherapy.* Radiology, 2010. **257**(3): p. 643-52.

475. Wendling, P., et al., *Heterogeneous oxygenation of rectal carcinomas in humans: a critical parameter for preoperative irradiation?* Adv Exp Med Biol, 1984. **180**: p. 293-300.

476. Dietz, D.W., et al., *Tumor hypoxia detected by positron emission tomography with 60Cu-ATSM as a predictor of response and survival in patients undergoing Neoadjuvant chemoradiotherapy for rectal carcinoma: a pilot study.* Dis Colon Rectum, 2008. **51**(11): p. 1641-8.

477. Havelund, B.M., et al., *Tumour hypoxia imaging with 18F-fluoroazomycinarabinofuranoside PET/CT in patients with locally advanced rectal cancer.* Nucl Med Commun, 2013. **34**(2): p. 155-61.

478. Theodoropoulos, G.E., et al., *Hypoxia, angiogenesis and apoptosis markers in locally advanced rectal cancer.* Int J Colorectal Dis, 2006. **21**(3): p. 248-57.

479. Lu, X.G., et al., *Clinical significance of immunohistochemical expression of hypoxia-inducible factor-1alpha as a prognostic marker in rectal adenocarcinoma.* Clin Colorectal Cancer, 2006. **5**(5): p. 350-3.

480. Lollert, A., et al., *Rectal cancer: dynamic contrast-enhanced MRI correlates with lymph node status and epidermal growth factor receptor expression.* J Magn Reson Imaging, 2014. **39**(6): p. 1436-42.

481. Yeo, D.-M., et al., *Correlation of dynamic contrast-enhanced MRI perfusion parameters with angiogenesis and biologic aggressiveness of rectal cancer: Preliminary results.* Journal of Magnetic Resonance Imaging, 2015. **41**(2): p. 474-480.

482. Oberholzer, K., et al., *Rectal cancer: assessment of response to neoadjuvant chemoradiation by dynamic contrast-enhanced MRI.* J Magn Reson Imaging, 2013. **38**(1): p. 119-26.

483. Kremser, C., et al., *Dynamic T(1) mapping predicts outcome of chemoradiation therapy in primary rectal carcinoma: sequence implementation and data analysis.* J Magn Reson Imaging, 2007. **26**(3): p. 662-71.

484. Lim, J.S., et al., *Perfusion MRI for the prediction of treatment response after preoperative chemoradiotherapy in locally advanced rectal cancer.* Eur Radiol, 2012. **22**(8): p. 1693-700.

485. Gollub, M.J., et al., *Dynamic contrast enhanced-MRI for the detection of pathological complete response to neoadjuvant chemotherapy for locally advanced rectal cancer.* Eur Radiol, 2012. **22**(4): p. 821-31.

486. Kim, S.H., et al., *Dynamic contrast-enhanced MRI to evaluate the therapeutic response to neoadjuvant chemoradiation therapy in locally advanced rectal cancer.* J Magn Reson Imaging, 2014. **40**(3): p. 730-7.

487. Dinter, D.J., et al., *Can dynamic MR imaging predict response in patients with rectal cancer undergoing cetuximab-based neoadjuvant chemoradiation?* Onkologie, 2009. **32**(3): p. 86-93.

488. Lind, J.S., et al., *Dynamic contrast-enhanced CT in patients treated with sorafenib and erlotinib for non-small cell lung cancer: a new method of monitoring treatment?* Eur Radiol, 2010. **20**(12): p. 2890-8.

REFERENCES

489. Cao, N., et al., *Monitoring the effects of anti-angiogenesis on the radiation sensitivity of pancreatic cancer xenografts using dynamic contrast-enhanced computed tomography.* Int J Radiat Oncol Biol Phys, 2014. **88**(2): p. 412-8.

490. Truong, M.T., et al., *Prediction of locoregional control in head and neck squamous cell carcinoma with serial CT perfusion during radiotherapy.* AJNR Am J Neuroradiol, 2011. **32**(7): p. 1195-201.

491. Hennedige, T. and S.K. Venkatesh, *Imaging of hepatocellular carcinoma: diagnosis, staging and treatment monitoring.* Cancer Imaging, 2013. **12**: p. 530-47.

492. Chaplin, D.J. and S.A. Hill, *Temporal heterogeneity in microregional erythrocyte flux in experimental solid tumours.* Br J Cancer, 1995. **71**(6): p. 1210-3.

493. Ng, Q.S., et al., *Lung cancer perfusion at multi-detector row CT: reproducibility of whole tumor quantitative measurements.* Radiology, 2006. **239**(2): p. 547-53.

494. Larici, A.R., et al., *First-pass perfusion of non-small-cell lung cancer (NSCLC) with 64-detector-row CT: a study of technique repeatability and intra- and interobserver variability.* Radiol Med, 2014. **119**(1): p. 4-12.

495. Reiner, C.S., et al., *CT perfusion of renal cell carcinoma: impact of volume coverage on quantitative analysis.* Invest Radiol, 2012. **47**(1): p. 33-40.

496. Goh, V., et al., *Quantitative colorectal cancer perfusion measurement by multidetector-row CT: does greater tumour coverage improve measurement reproducibility?* Br J Radiol, 2006. **79**(943): p. 578-83.

497. Bernier, J., E.J. Hall, and A. Giaccia, *Radiation oncology: a century of achievements.* Nat Rev Cancer, 2004. **4**(9): p. 737-47.

498. Goh, V., et al., *Can perfusion CT assessment of primary colorectal adenocarcinoma blood flow at staging predict for subsequent metastatic disease? A pilot study.* Eur Radiol, 2009. **19**(1): p. 79-89.

499. Milburn Jessup, J. and G.E. Gallich, *The biology of colorectal carcinoma.* Current Problems in Cancer. **16**(5): p. 265-328.

500. Curvo-Semedo, L., et al., *Usefulness of perfusion CT to assess response to neoadjuvant combined chemoradiotherapy in patients with locally advanced rectal cancer.* Acad Radiol, 2012. **19**(2): p. 203-13.

501. Li, J., et al., *Wait-and-see treatment strategies for rectal cancer patients with clinical complete response after neoadjuvant chemoradiotherapy: a systematic review and meta-analysis.* Oncotarget, 2016. **7**(28): p. 44857-44870.

502. Howe, F.A., et al., *Issues in flow and oxygenation dependent contrast (FLOOD) imaging of tumours.* NMR Biomed, 2001. **14**(7-8): p. 497-506.

503. Padhani, A., *Science to practice: what does MR oxygenation imaging tell us about human breast cancer hypoxia?* Radiology, 2010. **254**(1): p. 1-3.

504. Padhani, A.R., et al., *Imaging oxygenation of human tumours.* Eur Radiol, 2007. **17**(4): p. 861-72.

505. Chavhan, G.B., et al., *Principles, techniques, and applications of T2*-based MR imaging and its special applications.* Radiographics, 2009. **29**(5): p. 1433-49.

506. Fernandez-Seara, M.A. and F.W. Wehrli, *Postprocessing technique to correct for background gradients in image-based R*(2) measurements.* Magn Reson Med, 2000. **44**(3): p. 358-66.

507. Cuenod, C.A. and D. Balvay, *Perfusion and vascular permeability: basic concepts and measurement in DCE-CT and DCE-MRI.* Diagn Interv Imaging, 2013. **94**(12): p. 1187-204.

REFERENCES

508. Calamante, F., D.G. Gadian, and A. Connelly, *Delay and dispersion effects in dynamic susceptibility contrast MRI: simulations using singular value decomposition.* Magn Reson Med, 2000. **44**(3): p. 466-73.

509. Wang, Y., et al., *Feasibility of using limited-population-based arterial input function for pharmacokinetic modeling of osteosarcoma dynamic contrast-enhanced MRI data.* Magn Reson Med, 2008. **59**(5): p. 1183-9.

510. Kim, S.M., et al., *A method for patient dose reduction in dynamic contrast enhanced CT study.* Med Phys, 2011. **38**(9): p. 5094-103.

511. Schnall, M.D., et al., *Diagnostic architectural and dynamic features at breast MR imaging: multicenter study.* Radiology, 2006. **238**(1): p. 42-53.

512. Thomassin-Naggara, I., et al., *Dynamic contrast-enhanced magnetic resonance imaging: a useful tool for characterizing ovarian epithelial tumors.* J Magn Reson Imaging, 2008. **28**(1): p. 111-20.

513. Tofts, P.S. and A.G. Kermode, *Measurement of the blood-brain barrier permeability and leakage space using dynamic MR imaging. 1. Fundamental concepts.* Magn Reson Med, 1991. **17**(2): p. 357-67.

514. Kety, S.S., *The theory and applications of the exchange of inert gas at the lungs and tissues.* Pharmacol Rev, 1951. **3**(1): p. 1-41.

515. O'Connor, J.P., et al., *Quantifying antivascular effects of monoclonal antibodies to vascular endothelial growth factor: insights from imaging.* Clin Cancer Res, 2009. **15**(21): p. 6674-82.

516. Dellas, K., et al., *Phase II trial of preoperative radiochemotherapy with concurrent bevacizumab, capecitabine and oxaliplatin in patients with locally advanced rectal cancer.* Radiat Oncol, 2013. **8**(1): p. 90.

517. Miles, K.A., et al., *Application of CT in the investigation of angiogenesis in oncology.* Acad Radiol, 2000. **7**(10): p. 840-50.

518. Kanda, T., et al., *CT hepatic perfusion measurement: comparison of three analytic methods.* Eur J Radiol, 2012. **81**(9): p. 2075-9.

APPENDIX

APPENDIX I

I Colorectal Cancer Staging

American Joint Committee on Cancer

Colon and Rectum Cancer Staging

7th EDITION

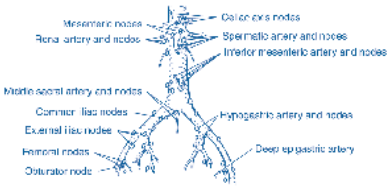

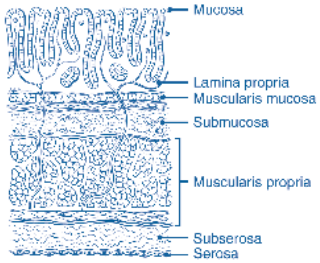

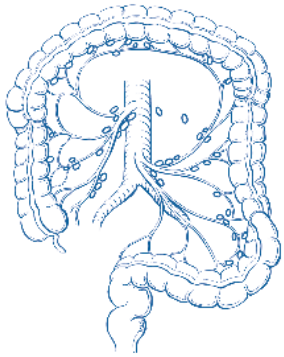

Definitions

Primary Tumor (T)

- **TX** Primary tumor cannot be assessed
- **T0** No evidence of primary tumor
- **Tis** Carcinoma in situ: intraepithelial or invasion of lamina propria[1]
- **T1** Tumor invades submucosa
- **T2** Tumor invades muscularis propria
- **T3** Tumor invades through the muscularis propria into pericolorectal tissues
- **T4a** Tumor penetrates to the surface of the visceral peritoneum[2]
- **T4b** Tumor directly invades or is adherent to other organs or structures[2,3]

Regional Lymph Nodes (N)[4]

- **NX** Regional lymph nodes cannot be assessed
- **N0** No regional lymph node metastasis
- **N1** Metastasis in 1–3 regional lymph nodes
- **N1a** Metastasis in one regional lymph node
- **N1b** Metastasis in 2–3 regional lymph nodes
- **N1c** Tumor deposit(s) in the subserosa, mesentery, or nonperitonealized pericolic or perirectal tissues without regional nodal metastasis
- **N2** Metastasis in 4 or more regional lymph nodes
- **N2a** Metastasis in 4–6 regional lymph nodes
- **N2b** Metastasis in 7 or more regional lymph nodes

Distant Metastasis (M)

- **M0** No distant metastasis
- **M1** Distant metastasis
- **M1a** Metastasis confined to one organ or site (for example, liver, lung, ovary, nonregional node)
- **M1b** Metastases in more than one organ/site or the peritoneum

ANATOMIC STAGE/PROGNOSTIC GROUPS

Stage	T	N	M	Dukes*	MAC*
0	Tis	N0	M0	–	–
I	T1	N0	M0	A	A
	T2	N0	M0	A	B1
IIA	T3	N0	M0	B	B2
IIB	T4a	N0	M0	B	B2
IIC	T4b	N0	M0	B	B3
IIIA	T1–T2	N1/N1c	M0	C	C1
	T1	N2a	M0	C	C1
IIIB	T3–T4a	N1/N1c	M0	C	C2
	T2–T3	N2a	M0	C	C1/C2
	T1–T2	N2b	M0	C	C1
IIIC	T4a	N2a	M0	C	C2
	T3–T4a	N2b	M0	C	C2
	T4b	N1–N2	M0	C	C3
IVA	Any T	Any N	M1a	–	–
IVB	Any T	Any N	M1b	–	–

NOTE: cTNM is the clinical classification, pTNM is the pathologic classification. The y prefix is used for those cancers that are classified after neoadjuvant pretreatment (for example, ypTNM). Patients who have a complete pathologic response are ypT0N0cM0 that may be similar to Stage Group 0 or I. The r prefix is to be used for those cancers that have recurred after a disease-free interval (rTNM).
* Dukes B is a composite of better (T3 N0 M0) and worse (T4 N0 M0) prognostic groups, as is Dukes C (any TN1 M0 and Any T N2 M0). MAC is the modified Astler-Coller classification.

ajcc

American Cancer Society

Financial support for AJCC 7th Edition Staging Posters provided by the American Cancer Society

Notes

[1] Tis includes cancer cells confined within the glandular basement membrane (intraepithelial) or mucosal lamina propria (intramucosal) with no extension through the muscularis mucosae into the submucosa.

[2] Direct invasion in T4 includes invasion of other organs or other segments of the colorectum as a result of direct extension through the serosa, as confirmed on microscopic examination (for example, invasion of the sigmoid colon by a carcinoma of the cecum) or, for cancers in a retroperitoneal or subperitoneal location, direct invasion of other organs or structures by virtue of extension beyond the muscularis propria (that is, a tumor on the posterior wall of the descending colon invading the left kidney or lateral abdominal wall; or a mid or distal rectal cancer with invasion of prostate, seminal vesicles, cervix, or vagina).

[3] Tumor that is adherent to other organs or structures, grossly, is classified cT4b. However, if no tumor is present in the adhesion, microscopically, the classification should be pT1-4a depending on the anatomical depth of wall invasion. The V and L classifications should be used to identify the presence or absence of vascular or lymphatic invasion, whereas the PN site-specific factor should be used for perineural invasion.

[4] A satellite peritumoral nodule in the pericolorectal adipose tissue of a primary carcinoma without histologic evidence of residual lymph node in the nodule may represent discontinuous spread, venous invasion with extravascular spread (V1/2), or a totally replaced lymph node (N1/2). Replaced nodes should be counted separately as positive nodes in the N category, whereas discontinuous spread or venous invasion should be classified and counted in the Site-Specific Factor category Tumor Deposits (TD).

APPENDIX II

II Mathematical principals of ISW-MRI:

The deoxygenated haemoglobin increases the transverse relaxation rate (R_2*) of water in blood and in the tissue surrounding blood vessels, represented as:

$$R_2^* = \frac{1}{T_2^*}$$

Thus ISW-MRI is sensitive to pO_2 within and in tissues adjacent to perfused vessels [502]. It has been suggested that fast R_2* rate may be directly indicative of tumour hypoxia (extensive deoxyhaemoglobin) [503]. However R_2* is also highly dependent on intrinsic tissue properties which can have static and dynamic component. The static components includes tissue iron content (for example, myoglobin found in muscle), presence of fibrous structure or ligamentous structures, calcification, vascular structure and/or quantity (blood volume) and dynamic components include the velocity of blood circulation (blood flow), local haematocrit, haemorrhage or red blood cells in the tissue [504]. Other factors affecting R_2* include B_0 field inhomogeneity at tissue interfaces [504-506]. Also, the amount of deoxyhaemoglobin at a particular region of the tumour is not only dependent on blood oxygenation but also tumour blood flow. A high tumour blood flow reduces the extraction of oxygen from blood, thereby decreasing deoxyhaemoglobin levels. In order to separate the effects of flow from deoxyhaemoglobin and static components it is necessary to measure the T_2* relaxation rates. Gradient-recalled-echo (GRE) sequence with increasing echo times (TE; usually spanning 5–65 ms) are used to display T_2* effects

[321]; the series of images obtained have T_2* susceptibility effects with increasing TE. The rate of signal intensity decay is dependent on intrinsic T_2* relaxation (local structures), deoxyhaemoglobin and local blood flow as mentioned above. Synthetic R_2* images are created by plotting the natural logarithm (ln) of the signal intensity against the TE. R_2* map reflects on the structure of the tissues and local deoxyhaemoglobin but inflow effects are minimised; however, R_2* maps retain sensitivity to pO_2 changes caused by alterations in blood flow [504]. The contribution of blood deoxyhaemoglobin to R_2* relaxation rate of the surrounding tissue can be written as:

$$R_2^* = R_{2\,tissue}^* + R_{2\,blood}^*$$

where, $R_2^*{}_{tissue}$ is assumed to be the static component, $R_2^*{}_{blood}$ is related to blood volume and tumour blood oxygenation saturation and can be expressed as:

$$R_{2\,blood}^* = k.V\,(1 - Y)$$

where, k is constant, V is the blood volume, and Y is the tumour blood oxygenation saturation, or

$$R_{2\,blood}^* = k'[dHb]$$

where, [dHb] is the concentration of deoxyhaemoglobin in the tissue, therefore

$$R_2^* = R_{2\,tissue}^* + k'[dHb]$$

Thus R2* contains a component that depends on the tumour tissue deoxyhaemoglobin content [dHb], which is a function of the vascular volume of the tumour actively perfused by erythrocytes.

APPENDIX II

So it can be deduced that ISW-MRI images are more likely to reflect on acute tissue hypoxia as hypoxic areas extend to the level of the blood vessels (whereas, in chronic hypoxia the red cells in the vessels are too distant from area of hypoxia) and red blood cells have to be delivered to the tissue in order to assess its oxygenation status. It should also be noted that perfusion in tumour tissue is heterogeneous, the red cell perfusion is not simply related to the absence/presence of vessels; plenty of tumour vessels may be present but perfusion by red cell may not occur [332]. Hence R_2* does not measure tissue pO_2 directly and therefore, the distribution of blood volume in tissue has to be determined in order to be able to correctly interpret R_2* images in order to infer oxygenation status [504]; this hypothesis is supported by preclinical and clinical data [341]

Many studies have reported that changes in R_2* are temporally correlated with changes in tissue pO_2 in response to vasomodulation with hyperoxic gas challenge, for example carbogen (95%CO2: 2% O2) inhalation. The changes in tumour vascular oxygenation as revealed by changes in R_2* are represented as:

$$\Delta R_2^* = \Delta R_{2\,tissue}^* + \Delta R_{2\,blood}^* = k'\Delta[dHb]$$

where, Δ [dHb] is the change is tissue deoxyhaemoglobin concentration caused by challenge with carbogen. Thus ΔR_2* is sensitive to blood volume, haematocrit, and oxygenation. Hence ΔR_2* can provide vital information about the potential to enhance oxygen delivery to the tumour [333].

APPENDIX III

III Mathematical principals of Dynamic Contrast Enhanced Imaging (CT and MRI)

Dynamic contrast enhanced imaging (DCEI) offer measurement of tissue microcirculation including details on capillary networks, exchanges between blood and extravascular space, and vascular permeability. DCEI provides vital insight in to tumour pathophysiology before morphological changes are obvious. Advancements in both CT and MRI technology and availability of commercial software has made it possible to obtain high temporal and spatial resolution images and enabled imaging of microcirculation with morphological imaging. The most popular method of analysing microcirculation by cross-sectional imaging is the analysis of the kinetics of passage of contrast agent through the tissue after a bolus intravenous injection.

Physiological parameters of microcirculation

Microcirculatory parameters are generally expressed for a given mass or volume of tissue so that different tissues can be compared. As in cross-sectional imaging voxel represents one volume element of tissue, the parameters of the microcirculation are expressed per unit of volume. In DCEI, blood flow in large vessels is measured by flow rate Q which is quantity or volume of blood passing through a tube of given surface area expressed as volume of blood per unit time (unit: mL/min), whereas, blood flow in tissue is measured by ‘flow per tissue volume’, expressed as volume of blood per unit time and per unit volume of tissue (unit: mL/min/100mL). Flow and volume parameters can be measured as a function of plasma rather than blood. The

APPENDIX III

correspondence between the parameters expressed for plasma and those expressed for blood involves the haematocrit.

Main parameters of the microcirculation (Adopted from Cuenod et al [507])

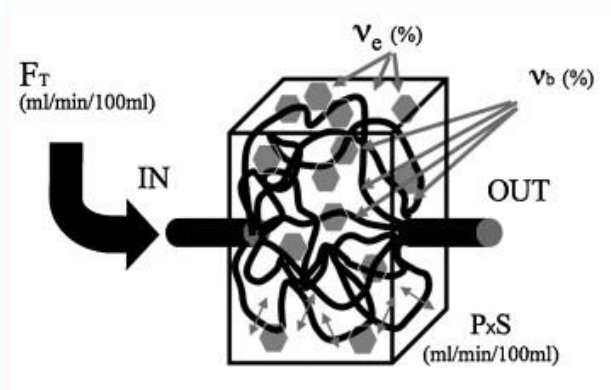

Physiology Marker	Definition and units
Tissue blood flow (BF)	Blood flow entering (and exiting) a volume of tissue (unit: mL of blood/min/100 mL tissue) Can be expressed as tissue plasma flow (unit: mL of plasma/min/100 mL of tissue)
Tissue blood volume (BV)	Volume of capillary blood contained in a certain volume of tissue. (unit: mL blood/100 mL of tissue OR %) Can be expressed as tissue plasma volume (unit: mL plasma/100 mL of tissue OR %)
Mean Transit Time	Mean time taken by blood to pass through capillary network (unit: seconds)
Permeability –surface area product (PS)	Rate of flow of molecules through the capillary membranes in a certain volume of tissue (unit: mL/min/100mL tissue) PS depends on characteristics of both capillary wall and contrast agent
Transfer constant (K^{trans})	Part of molecules the flow into the interstitium
Extravascular and extracellular volume fraction (v_e)	Tissue interstitial volume in which contrast may accumulate if they cross the endothelial barrier (unit: mL of extracellular volume/100mL of tissue OR %). The distribution volume is often called the extravascular extracellular space (ESS)

APPENDIX III

Principals of tissue kinetics of contrast agents

After injection of contrast agent, it enters the tissue capillary network from surrounding arterial network, thereafter, depending on endothelial permeability, it may pass into the interstitium, followed by passage into venous network and finally eliminated by kidneys. The temporal kinetics of enhancement depends on general (cardiac output) and local circulatory systems (endothelial permeability), the mode of injection (injection rate, dose, concentration of contrast) and type of contrast. After injection of contrast, two phenomenon occur simultaneously:

(i) Perfusion in the microcirculatory network and accumulation in the interstitium (depending on capillary permeability), followed by

(ii) Release from the interstitium due to capillary leakage.

The time course and kinetics of these two phenomenon are different but they overlap. Figures below illustrate contrast kinetics and image enhancement seen according to the type of capillary network.

APPENDIX III

Contrast kinetic in tissue not permeable to contrast agent (e.g. Brain)

In tissue where contrast remains confined in the microvascular network (for example in brain due to blood brain barrier), the and if it is completely eliminated by the kidney is the first passage, tissue enhancement would show a rapid rise after arrival of the bolus, followed by rapid exponential decay to a values close to the initial value before the injection.

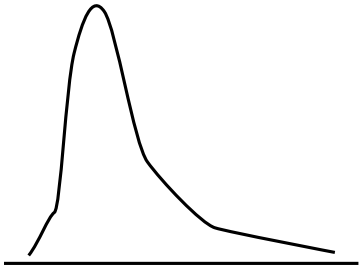

If the contrast is not eliminated in first pass, the second pass (blue line) is visible as a second peak, which is much lower than first peak.

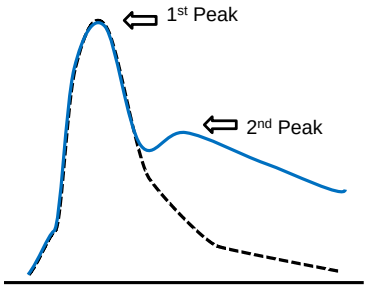

Contrast kinetic in tissue not permeable to contrast agent (e.g. Brain)

Permeable capillary endothelium allows contrast agent accumulation in the interstitium, which is eliminated later once the concentration of contrast in plasma becomes lower than interstitium

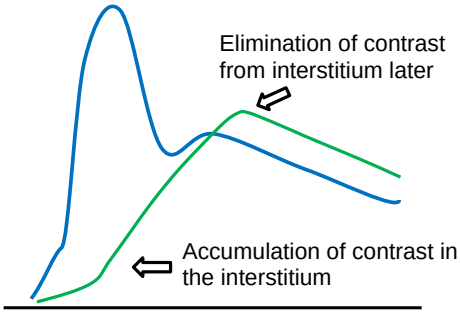

The tissue enhancement seen on DCEI is the product of contrast agent in capillary network and the interstitium

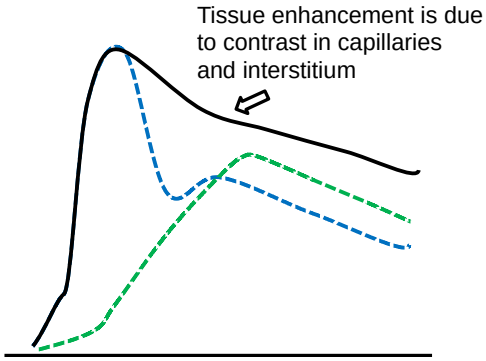

APPENDIX III

Measurement of tissue kinetic of contrast agents by DCEI

The passage of contrast through capillary network is very fast (in order of seconds). Also the capillary networks spread over few millimetres only. Therefore, DCEI involves scanning sequence with high temporal (fast image acquisition) and spatial (think slices) resolution. Hence, DCEI involves repeated acquisition of images on the same or several slices after injection of contrast agent to obtain signal enhancement kinetics in the tissues (see figure below).

Sequential acquisition for DCEI and tissue enhancement curve (Adopted from Cuenod et al [507])

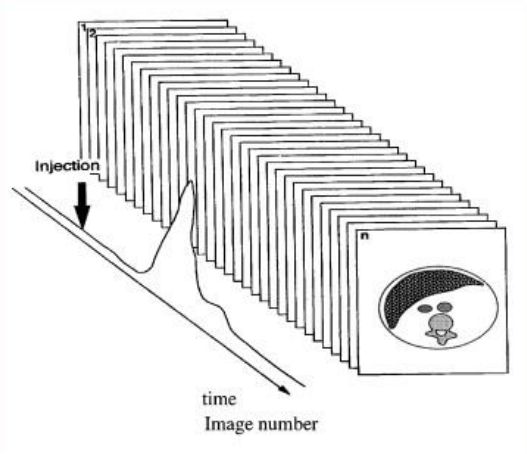

The tissue enhancement by passage of contrast agent can be divided into 4 phases:

1. The arrival of contrast into the capillary network. There is rapid increment of contrast into capillary network and very fast image acquisition speed is required to record tissue enhancement. This phase depends on tissue perfusion flow rate.

APPENDIX III

2. The first peak occurs when maximum contrast (in plasma) volume is in the capillary network (blue line); thereafter, the volume of contrast in capillaries decline due to passage into the interstitium and venous system for elimination by kidneys. This phase depends on tissue blood volume.
3. The leakage of contrast into the interstitium (green line) causes a sustained enhancement on DCEI. This phase depends on capillary endothelial permeability and surface area.
4. A second peak (slow) occurs as the contrast reaches maximum concentration within interstitium (more than plasma in capillaries); thereafter, the contrast passes back in to capillaries to be eliminated by kidneys. This phase depends on tissue interstitial volume

Components of tissue enhancement curve. (Adopted from Cuenod et al [507])

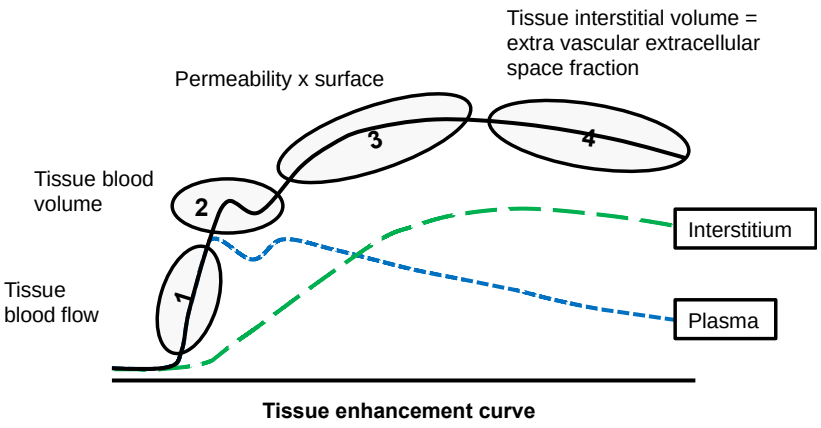

APPENDIX III

Measuring DCEI parameters of tissue microvascular circulation.

The derivation of DCEI parameters of tissue microvascular circulation involves the following steps:

1) Conversion of tissue enhancement signal into contrast concentration
2) Measurement of arterial input function
3) Application of mathematical tracer-kinetic models to derive DCEI parameters

Conversion of tissue signal enhancement into contrast concentration

All DCE methods are based on the standard tracer kinetic theory of linear and stationary systems. Linearity in this case means that the tissue response is assumed proportional to the injected dose, stationary means that the response is independent from the time of injection. If this is the case, then time-dependent tissue concentration $c_t(t)$ is related to the time-dependent concentration $c_a(t)$ in a supplying blood vessel by the convolution with a residue function $R(t)$:

$$c_t(t) = F_p . R(t) \otimes c_a(t)$$

where, F_p is the plasma flow that's carries contrast agent, $\otimes$ denotes convolution, $c_a(t)$ is the arterial input function and $R(t)$ is the tissue characteristic time course which reflects the distribution of contrast transit times through the tissue.

For DCE-CT, the tissue signal enhancement (unit: Hounsfield) has linear relationship to contrast concentration. This can be expressed as:

APPENDIX III

$$c(t) = k.(S(t) - S_0)$$

where, *k* is proportionality constant, *S(t)* is time dependent signal enhancement and S_0 is the pre-contrast signal.

However, for DCE-MRI, the tissue signal enhancement is not directly proportional to contrast concentration. The tissue signal enhancement is weighted with specific physical and chemical parameters such as longitudinal and transverse relaxation times or the tissue proton density. The signal also depends on various parameters of the imaging sequence. Therefore, different approximations are applied with different limitation in accuracy, precision and practical convenience for measurement of dynamic parameters. These include:

1) **Relative signal enhancement:** this method normalises signal change to baseline value. It uses relative signal enhancement as an approximation to the concentration:

$$c(t) = \frac{R_{10}}{r^1} \frac{S(t) - S_0}{S_0}$$

where, R_{10} is the pre-contrast relaxivity rate and r^1 is the relaxivity of contrast agent (independent of tissue type; calculated from phantom data)

2) **Absolute MR units:** this approach involves converting DCE-MRI signal in to functions $R_1(t)$ which measures the relaxation rate as a function of time. The $R_1(t)$ has linear relation with concentration, expressed as:

APPENDIX III

$$c(t) = \frac{R_1(t) - R_{10}}{r_1}$$

The conversion of *S(t)* to *R1(t)* results in significant sacrifice of temporal resolution.

Arterial Input Function

All physiological models require measurement of contrast kinetics in the artery supplying the capillary beds in tissue of interest. The AIF ($c_t(t)$) can be derived in the same was as tissue concentration. By taking the arterial supply into account, it is possible to obtain representative quantitative parameters that can be compared from one patient to another or for the same patient between two examinations. There are three methods of obtaining AIF:

1. AIF measured in a large artery: for example for DCEI of intra-abdominal viscera. Due to time-delay between passage of bolus in the large artery where AIF is measured and its arrival in capillary beds in tissue of interest, a Bolus Arrive Time (BAT) must be added to the model. A bolus dispersion between AIF measure site and capillary bed can also lead to error in parametric calculations [508].
2. AIF measured in a small artery: for examples for DCEI of brain. Care should be taken to minimise partial volume effects and motion artefacts.
3. Population AIF: a mean AIF corresponding to average values obtained in a population is used when no vessel is available. This technique is conventionally used in Tofts model. The technique does not take into account individual variability between patients [509].

APPENDIX III

An intermediate approach is to use population AIF and to correct these using individual values measured in a small artery [510].

Mathematical calculations of DCEI parameters – tracer kinetic models

Mathematical models help dissect out the components of microcirculation that constitute the tissue contrast enhancement curve. The derived parameters represent kinetics of contrast agent through the capillary network, which provide vital insight into microcirculatory physiology. There are three modes used to derive physiological parameters from tissue enhancement curve:

1. **Qualitative (visual) analysis:** Each tissue has exclusive enhancement curve. This method focuses on shape of the curve to distinguish between benign and malignant lesions [511].
2. **Semi-quantitative analysis:** This method derives heuristics parameters from tissue enhancement curve (see figure below). The most commonly used semi-quantitative parameters used in ‘Area Under the Curve (AUC)’. Mathematical models have been applied to this mode to provide precise definition of the parameters [512]
3. **Quantitative analysis** (with physiological model). The parameters derived by model-based analysis of tissue enhancement curve are relatively close to actual tissue physiology. The models take in to account exchanges between arterial blood, the plasma and the interstitial space.

APPENDIX III

Qualitative and Semi-quantitative analysis (Adopted from Cuenod et al [507])

Qualitative analysis: A rapid peak (wash-in) and descent (wash-out) of malignant lesion compared to slow peak and wash-out plateau of malignant lesion.

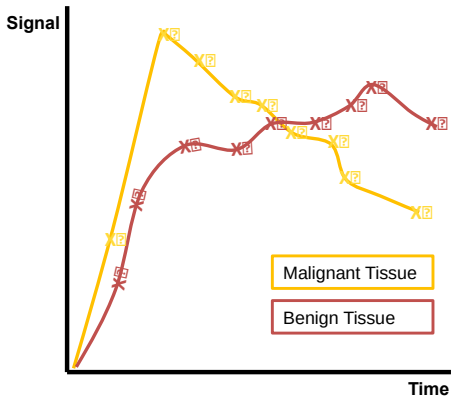

Semi-Quantitative analysis: Two tissues are compared. This analysis is useful when internal reference is available. For example distinguishing between normal (Tissue 1) and ischaemic tissue (Tissue 2).

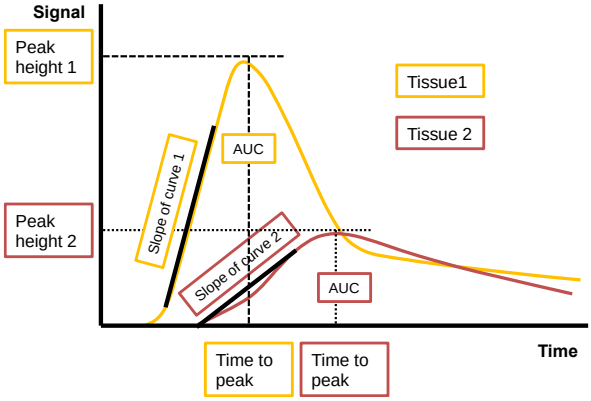

APPENDIX III

Modes of tissue contrast enhancement curves

Mode	Types	Measurements/Models
Qualitative	n/a	Wash-in – filling phase; Peak – peak intensity; Wash-out – elimination phase,
Semi-Quantitative	*Without mathematical model*	Peak height, time to peak, slop of curve, Area under the curve (AUC), etc.
	With mathematical model	Various. (see ref. [512])
Quantitative	*Tissue perfusion models*	Deconvolution; Axel; Ostergaard - Sorensen
	Permeability model	Neglecting Blood Volume: Toft-Kety ; Brix; Larsson; Patel With blood volume but without return: Patlak; Miles; Shames-Brash With blood volume return: Extended Kety or Toft General Kinetic Model; Larsson
	Complete model with exchanges	Without return: Cuenod-Pradel-de Bazelaire With return: Adiabatic approximation of tissue homogeneity; St Lawrence and Lee; Two-compartment exchange; Brix2; Comprehensive model (Cuenod-Balvay); 2CX Sourbron-Buckley; Larsson; Distributed parameter model; Koh-Dennis Cheong – Bisdas; Physiologically based pharmokinetic modelling; Brochot-Bios

APPENDIX IV

IV Pharmacokinetic Models

DCE-MRI

Pharmacokinetic analysis of DCE-MRI is the most widely used method of measuring vessel permeability changes, analyses typically being derived from variations of the Tofts' two-compartment kinetic model [513] (mathematically equivalent to Kety's dynamic model [514]), see figure below. It consists of a plasma volume connected to a large extracellular space throughout most body and also connected to a lesion through a leaky membrane. The lesion compartment is small enough not to influence the overall plasma concentration. The kidneys drains the contrast from plasma, and hence from extracellular space. The model is based on following assumptions:

- There is fast mixing of contrast in plasma after bolus injection
- The contrast agent concentration in a given compartment is uniformly distributed (that is capillary flow in the lesion must be high enough to prevent plasma concentration from being locally depleted).
- Inter-compartmental flux is linearly proportional to the concentration in each compartment
- Parameters have not changed during data acquisition
- Relaxivity of gadolinium contrast agent is directly proportional to its concentration

APPENDIX IV

Toft's two compartmental model

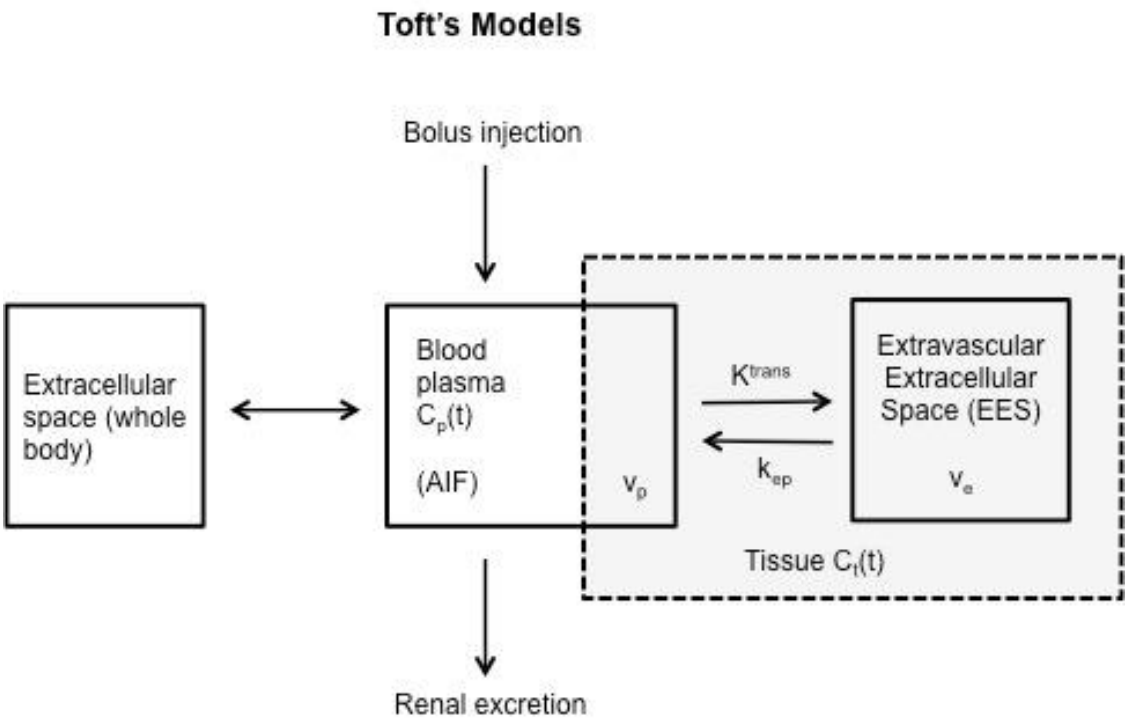

$C_p(t)$- time-varying blood plasma concentration, AIF – arterial input function, V_p – total blood plasma volume, K^{trans} – volume constant transfer, k_{ep}- rate constant, v_e – volume of extravascular extracellular space, $C_t(t)$ – time-varying tracer concentration in tissue.

The compartmental model is used to obtain three principal parameters [423]: the transfer constant (K^{trans}), the extravascular extracellular space (EES) fractional volume (v_e), and the rate constant (k_{ep}). The transfer constant and the EES relate to the fundamental physiology, whereas the rate constant is the ratio of the transfer constant to the EES, described by following formula:

$$k_{ep} = \frac{K^{trans}}{v_e}$$

APPENDIX IV

The total Gd concentration in a voxel or region of interest (ROI) is the sum of the EES contribution (which usually dominates, since $v_e \approx 10 – 60\%$) and the intravascular contribution which is always small and can be ignored ($v_p \approx 1$-10%) [364].

In this model, the bolus of injected contrast agent (Gd- chelates) gives time varying blood plasma concentration ($C_p(t)$ or AIF) which can be measured in each subject, or else a population mean can be used. Following the work of Tofts and Kermode [513], the input function ($C_p(t)$) was approximated by a bi-exponential function that was scaled according to the administered dose of Gd-DTPA:

$$C_p(t) = D[a_1 \exp(-m_1 t) + a_2 \exp(-m_2 t)$$

where, D is the dose of Gd-DTPA (mmol/kg body weight), a_1 and a_2 are the amplitudes of the components and m_1 and m_2 are their rate constants. The fast component (a_1,m_1) corresponds to equilibrium between plasma and extracellular space (which is relatively well connected; (a_2,m_2) corresponds to emptying of these two well coupled compartments to the kidneys.

From the capillaries, the contrast diffuses into the extravascular extracellular space and assessments of tissue perfusion and permeability can be derived from the shape of the observed wash-in and wash-out curves. The transfer constant K^{trans} (often called wash-in rate) characterises the diffusive transport of low-molecular-weight Gd chelates across capillary epithelium [423] and hence represents a constant of proportionality. Depending on vascular

permeability, the compartmental model can be modified to accommodate the following variations in physiology:

1. **High permeability (Flow-Limited model):** For blood vessels where diffusion is rapid (that is when extraction fraction during the first pass of the contrast agent is high, as typically found in tumours), perfusion will determine contrast agent distribution and K^{trans} approximates to tissue blood flow per unit volume [423]. The relationship between tissue concentration (C_t) and arterial concentration of contrast can be mathematically expressed as:

$$\frac{dC_t}{dt} = F\rho(1 - Hct)(\frac{C_p - C_t}{v_e})$$

where, F is perfusion of whole blood per unit mass of tissue, ρ is tissue density, Hct is haematocrit and v_e is total EES volume.

2. **Low permeability (PS-limited model):** There are circumstances where transport out of the vasculature does not significantly deplete intravascular contrast medium concentration (that is, tissue with a lower first pass extraction fraction). The blood plasma can be considered as a single pool, with equal arterial and venous concentration. This is typically found in some brain tumours, which have a largely intact blood-brain barrier, but also occurs in extracranial tumours after treatment with chemotherapy and/or late after radiotherapy, and in fibrotic lesions and in some normal tissues. The rate of uptake (K^{trans}) approximates to the product of permeability and the surface area (permeability surface area product, PS) [350, 515]. The transport equation is:

APPENDIX IV

$$\frac{dC_t}{dt} = PS\rho(\frac{C_p - C_t}{v_e})$$

3. **Mixed permeability (flow and perfusion-limited models):** The contrast uptake may be limited by both blood flow and permeability. This is represented as

$$\frac{dC_t}{dt} = EF\rho(1 - Hct)(\frac{C_p - C_t}{v_e})$$

where, E is the initial extraction ratio [516]; it is the fractional reduction in capillary blood concentration as it passes through tissue. In a flow-limited case, the extraction is complete (E=1) and the transport equation reduces to 'flow limited equation'. In permeability-limited case, there is limited extraction (E = PS/F (1-Hct)) and the transport equation reduces to 'permeability limited equation'.

4. **Clearance model:** After a variable time, the contrast agent diffuses back into the vasculature (described by the wash-out rate constant or k_{ep}) from where it is excreted usually by the kidneys. Washout of contrast medium is faster when capillary permeability is very high, due to a typically rapid return of contrast medium into the blood. Hence the distribution clearance (CL_d) can be defined for two connected compartments. This is mathematically expressed as:

$$\frac{dC_t}{dt} = \frac{CL_d}{V_t}(\frac{C_p - C_t}{v_e})$$

where CL_d /V_t defines clearance per unit volume.

The transfer constant can be physically interpreted as follows: K^{trans} = Fρ (1-Hct) under flow limited conditions, K^{trans} = PSρ under permeability limited

conditions, K^{trans} = EFρ (1 – Hct) under mixed permeability conditions and $K^{trans} = CL_d / V_t$ under clearance paradigm. Hence

$$\frac{dC_t}{dt} = K^{trans}(\frac{C_p - C_t}{v_e})$$

or

$$\frac{dC_t}{dt} = K^{trans}C_p - k_{ep}C_t$$

Therefore, in summary, the time-varying concentration of contrast in tissue at a unit time (dC_t/dt) is determined by blood plasma concentration and two additional parameters, the transfer constant (K^{trans}) and the EES fractional volume (v_e), (or alternatively, K^{trans} and the rate constant $k_{ep)}$. The time course of the contrast agent in the tissue can be described by the following equation:

$$C_t(t) = K^{trans} \times [C_p(t) \otimes \exp(-k_{ep} \times t)$$

where, C_t (t) represents Gd concentration in tissue at time t; C_p(t) represents the Gd concentration in arterial blood plasma at time t; K^{trans} is the transfer constant for transport of plasma to EES; k_{ep} represents the arte constant for the transport from EES to plasma; and ⊗ denotes convolution.

Other quantitative kinetic parameters that can be derived from pharmacokinetic modelling of DCE-MRI data include the fraction plasma volume (v_p) and the fractional extravascular, extracellular space (v_e, or simply leakage space).

APPENDIX IV

A model simulation using typical K^{trans} values for tumors [513]

1) The initial slope depends on $K^{trans,}$ and is independent of v_e. The graph show effects of increasing K^{trans} with fixed v_e =10%

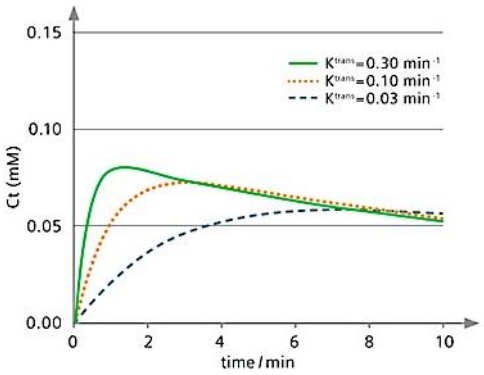

2) The final peak value depends on v_e. Tumours with large v_e take longer to reach their peak. The graph shows effect of increasing v_e with fixed K^{trans} =0.1 min^{-1}

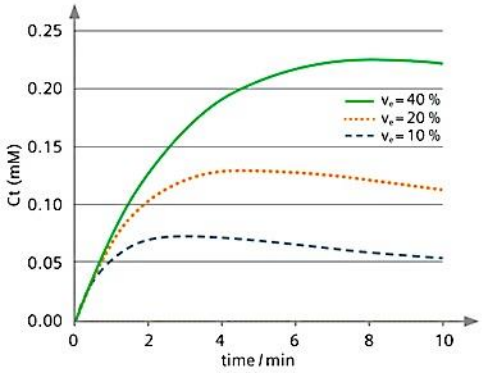

3) The shape of the curve is determined by k_{ep}, and if K^{trans} is increased whilst keeping k_{ep} fixed, the curve increases in amplitude but retains the same shape. (Constant k_{ep} = 2 min^{-1})

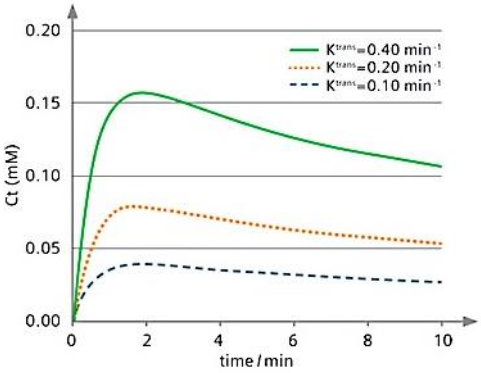

APPENDIX IV

DCE-CT

Compartmental Analysis

Compartmental analysis can be either single compartment or double-compartment method. The single compartment method is based on Fick's principals and assumes that intravascular and extravascular spaces are single compartment [373]. The perfusion parameters are calculated using the maximum slope or peak height of the tissue contrast enhancement curve normalised to the arterial input function. This method ignores venous outflow at the time of initial maximum slope, which may lead to underestimation of BF [373, 517]. The double-compartment model is based on Patlak analysis; it assumes intravascular and extravascular spaces to be separate compartments. The rate of contrast passage from intravascular to extravascular compartments is characterised by rate constant 'K'; the exchange from extravascular back into intravascular compartment is quantified by rate constant K/v_e. The model allows calculation of BV and capillary permeability. The compartmental models require only three images: baselines, immediately before and after the maximal tissue contrast enhancement. Although, analysis of only three images can help reduce motion artefacts, however, any image noise can lead to miscalculation of parameters estimates. The compartmental model is used for organs with complex circulation (for example spleen, liver, kidney)[517, 518].

APPENDIX IV

Deconvolution Analysis:

This model is based on the use of arterial and tissue time-concentration curves to calculate impulse residue function (IRF), which represents the fraction of contrast that remains in the tissue as time evolves after a bolus of injection into the arterial input. This model assumes that the concentration of contrast material in tissue is linearly dependent on the input arterial concentration when the BF is constant and ignores any leakage into the interstitial space. The height of the IRF curve reflects the tissue perfusion and area under the curve provides the relative BV estimation [517]. For the estimation of capillary permeability, a distributed model (Jonson Wilson model) is used. The deconvolution method requires inclusion of complete time series of images for calculation. Therefore, this method is resistant to image noise, but liable to motion artefact. Deconvolution analysis is particularly useful to measure organs with lower perfusion (<20mL/min per 100 mL) or lower perfusion values seen in tumour after treatment response [517].

APPENDIX IV

Mathematical Models for DCE CT parametric analysis (adopted from Garcia-Figueiras et al [370])

Model	Measure	Assumptions	Acquisition	Advantages and Disadvantages
Single Compartment (Ficks): maximal slope or peak height of tissue concentration curve normalised to arterial input function	BF	No venous flow	45s (length), <2 s intervals	Less sensitive to movement
Double-Compartment (Patlak): quantifies passage of contrast from intravascular into extravascular space	EF, BV	Well-mixed compartments; one-way transfer only	<2 min (length), <5 s intervals	Better for organs having complex microcirculation (kidney, spleen)
Deconvolution (Johnson Wilson distributed parameters): use of arterial and tissue time concentration curves to calculate impulse residue function for tissue	BF, BV, EF	Constrained impulse residue function	<2.5 min (length), < 2 s interval in first pass, < 15 s interval in delayed phase	Less sensitive to noise, uses lower tube current, higher temporal resolution

APPENDIX IV

Glossary of terms used commonly used in DCE (perfusion) CT (adopted from Kambadakone et al [372])

Perfusion parameter	Definition	Marker	Units
Blood Flow (BF) or Perfusion	Flow rate from vasculature in tissue region	Tumour vascularity; Tumour grade	mL per 100 g/min
Blood Volume (BV)	Volume of flowing blood within a vasculature in tissue region	Tumour vascularity	mL per 100 g
Mean Transit Time (MTT)	Average time taken to travel from artery to vein	Perfusion pressure	Seconds
Permeability-Surface area product (PS)	Total flux from plasma to interstitial space	Immature leaky vessels	mL per 100 g/min
Time To Peak (TTP)	Time of arrival of contrast in major arterial vessels to the peak enhancement	Perfusion pressure	seconds
Peak Enhancement intensity (PEI)	Maximum increase in tissue density after contrast injection	Tissue blood volume	HU

APPENDIX V

V Units of Measure

The unit volume of tissue is expressed per 100 mL rather than grams as cross-sectional imaging devices provide data on tissue volumes. The use of mL overcomes the problem of conversion by density (ρ), which may be unknown for the tissue of interest (lung parenchyma, bone, etc.). (Adopted from Toft et al.[423])

Quantity	Definition	Unit
Cab	Tracer concentration in the arterial blood	mM
Cap	Tracer concentration in the arterial plasma	mM
Ctp	Tracer concentration in the tissue plasma	mM
Cvp	Tracer concentration in the venous plasma	mM
Ce	Tracer concentration in the interstitium	mM
Ct	Tracer concentration in the tissue	mM
Cvb	Tracer concentration in the venous blood	mM
Cvp	Tracer concentration in the venous plasma	mM
E	Initial extraction fraction	None (%)
Hct	Hematocrit: Ca = (1-Hct)Cp	None (%)
Ft	Perfusion or blood flow rate per unit volume of tissue	mL/min/100 mL
Ftp	Perfusion or plasma flow rate per unit volume of tissue	mL/min/100 mL

APPENDIX V

P	Permeability per unit surface area of capillary wall	cm/min
S	Surface area of capillary wall per unit volume of tissue	cm2/100 mL
P x S	Permeability-surface area product per unit volume of tissue	mL/min/100 mL
Ktrans or EFp	Constant volume transfer or extraction fraction Ã— or plasma perfusion rate	mL/min/100 mL
Vb	Total volume of blood	mL
Ve	Total volume of interstitium	mL
Vp	Total volume of plasma	mL
v_s	Blood volume fraction per volume of tissue	None (%)
v_p	Plasma volume fraction per volume of tissue	None ()
v_e	Interstitial volume fraction per volume of tissue	None (%)
MTT	Mean transit time	s
HPI	Hepatic perfusion index: arterial infusion/total infusion	%

s:second